IMR – Ion-Molecule Reactions

Introduction

Ion Molecule reactions

$A^+ + B \rightarrow C^+ + D$

$A^+ + MO \rightarrow X^+ + Y$

$A^+ + B \rightarrow AB^+$

H_3^+

$$H_3^+ + CH_4 \rightarrow CH_5^+ + H_2$$

Proton transfer

The Privilege of Being a Physicist

Victor F. Weisskopf

There are certain obvious privileges that a physicist enjoys in our society. He is reasonably paid; he is given instruments, laboratories, complicated and expensive machines, and he is asked not to make money with these tools, like most other people, but to spend money. Furthermore, he is supposed to do what he himself finds most interesting, and he accounts for what he spends to the money givers in the form of progress reports and scientific papers that are much too specialized to be understood or evaluated by those who give the money—the federal authorities and, in the last analysis, the taxpayer. Still, we believe that the pursuit of science by the physicist is important and should be supported by the public. In order to prove this point, we will have to look deeper into the question of the relevance of science to society as a whole. We will not restrict ourselves to physics only; we will consider the relevance of all the natural sciences, but we will focus our attention on basic sciences, that is, to those scientific activities that are performed without a clear practical application in mind.

IMR – Ion-Molecule Reactions

H_3^+

Introduction

Ion Molecule reactions

$A^+ + B \rightarrow C^+ + D$

$A^+ + MO \rightarrow X^+ + Y$

$A^+ + B \rightarrow AB^+$

$$H_3^+ + CH_4 \rightarrow CH_5^+ + H_2$$

Proton transfer

The Privilege of Being a Physicist

Victor F. Weisskopf

There are certain obvious privileges that a physicist enjoys in our society. He is reasonably paid; he is given instruments, laboratories, complicated and expensive machines, and he is asked not to make money with these tools, like most other people, but to spend money. Furthermore, he is supposed to do what he himself finds most interesting, and he accounts for what he spends to the money givers in the form of progress reports and scientific papers that are much too specialized to be understood or evaluated by those who give the money—the federal authorities and, in the last analysis, the taxpayer. Still, we believe that the pursuit of science by the
ported by the p
have to look dee
ence to society a
physics only; we
ral sciences, bu
ences, that is,
formed without

"Intelligent play with simple, natural phenomena, the joys of discovery of unexpected experiences, are much better ways of learning to think than any teaching by rote."


© Roberta Weir
$\Omega_0>1$
$\Omega_0<1$
$\Omega_0=1$
Gerlich (80 K)
Johnsen (300 K)
Johnsen (135-160 K)
11 K
binary rate coefficient (10^{-10} cm^3 s^{-1})
concentration of H_2 (10^{13} cm^{-3})

Paestum

600 - 400 BC

1348

600 - 400 BC

MFF UK
22-pole trap

2009 - ….

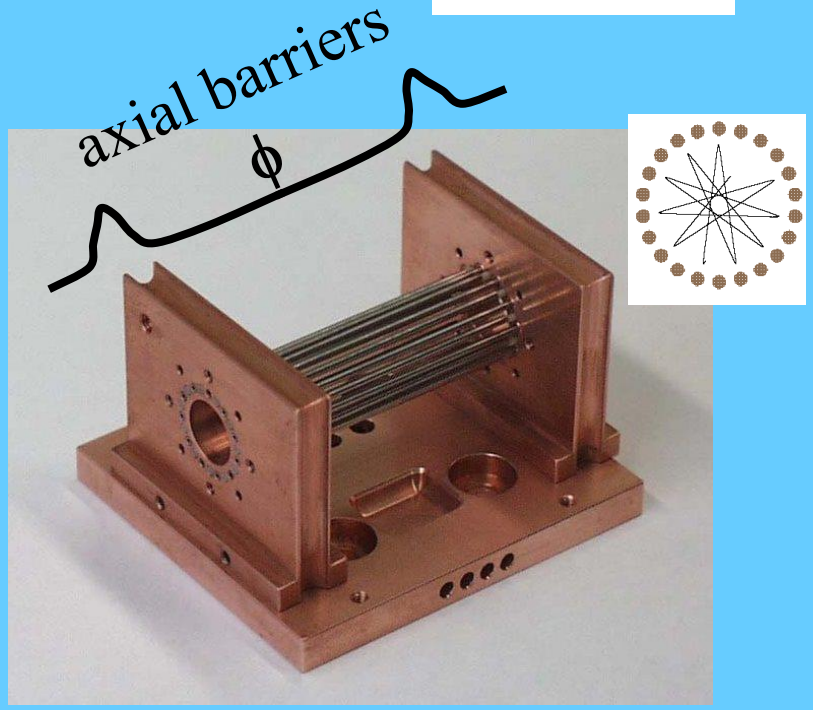

The Supernova of 1604

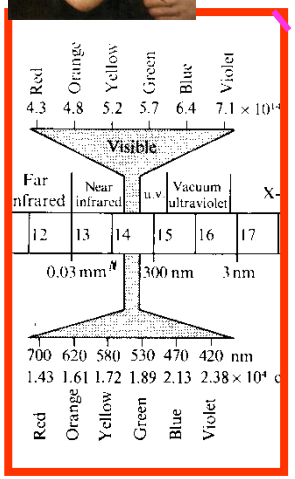

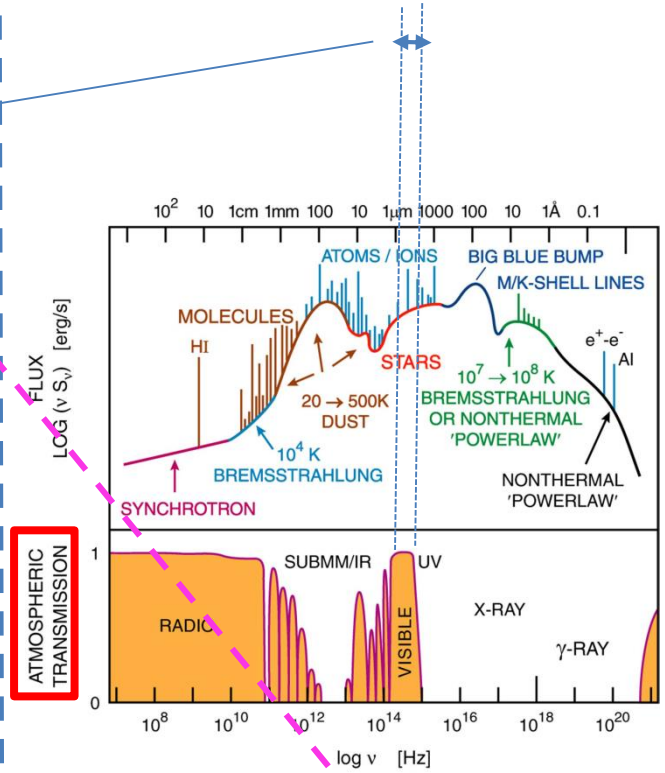

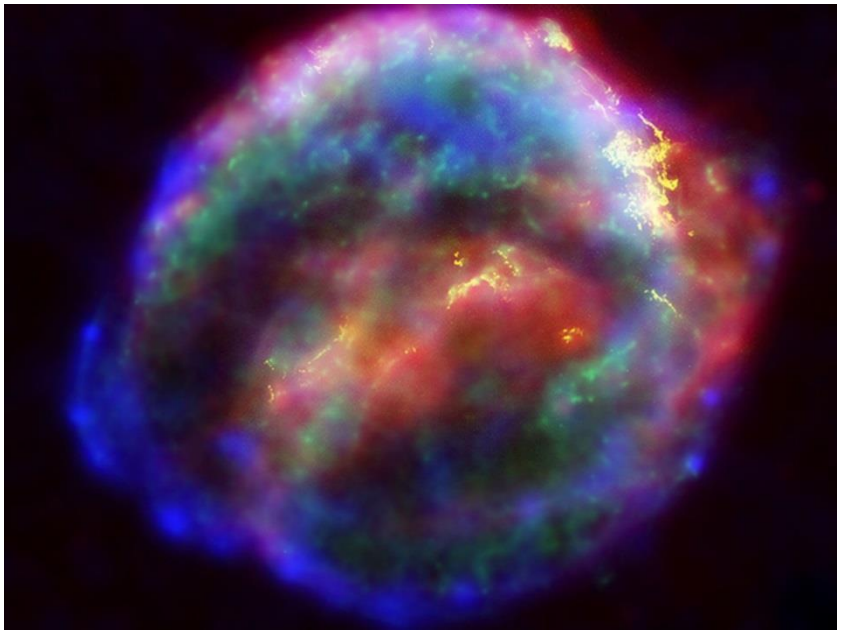

The first recorded observation was in northern Italy on October 9, 1604.[2] Johannes Kepler began observing the luminous display while working at the imperial court in Prague for Emperor Rudolf II on October 17.[3] It was subsequently named after him because his observations tracked the object for an entire year and because of his book on the subject, entitled *De Stella nova in pede Serpentarii* ("On the new star in Ophiuchus's foot", Prague 1606).[*citation needed*]

It was the second supernova to be observed in a generation (after SN 1572 seen by Tycho Brahe in Cassiopeia). No further supernovae have since been observed with certainty in the Milky Way, though many others outside our galaxy have been seen since S Andromedae[*citation needed*] and SN 1987A in the Large Magellanic Cloud was visible to the naked eye.

Why today

Mikuláš Koperník (1473-1543)

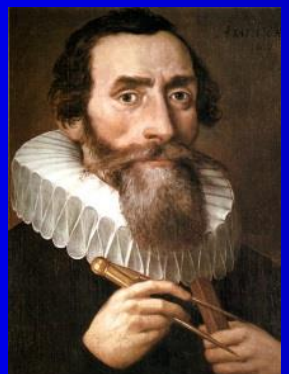

Johannes Kepler

12.4.1961

Vostok 1
9:07 moskevského času (6:07 UTC)
kosmodromu Bajkonur.

Klementinum a astronomie. Astronomická věž

Klementinum and astronomy.

Astronomická věž

Věž byla dokončena v roce 1722. Na vrcholu věže stojí socha Atlanta (olověná socha s železnou vnitřní konstrukcí, váha asi 600 kg, výška 2,4 m). Atlas nese nebeskou sféru (průměr asi 1,6 m, váha asi 150 kg) s korouhví.

(Pravděpodobně

Matyáš Braun)

Obr. 5 Areál Klementina s vyznačením současné polohy meteorologické stanice

Crab Nebula

Scio me nihil scire **I know that I know nothing**

ISM

Hydrogen only??

Ions chemistry

Electron – ion interactions

Negative ions ??

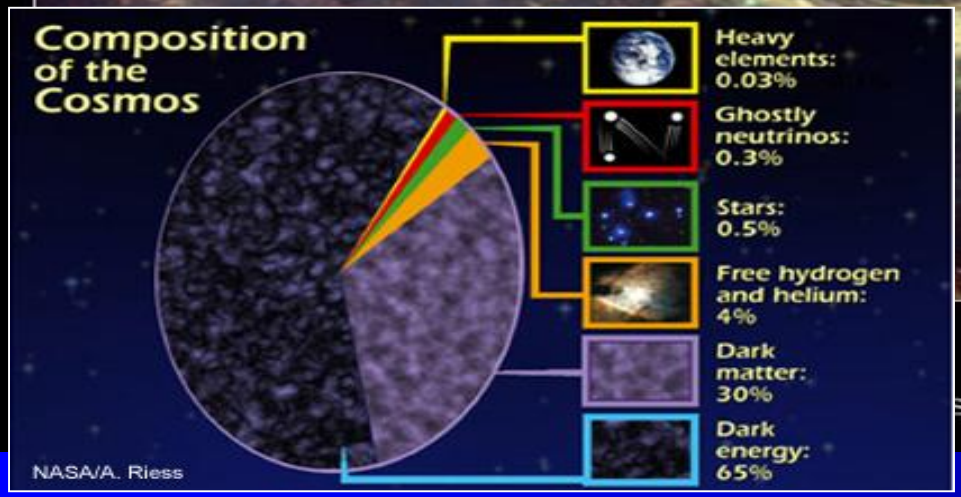

Hubble Heritage

SA and The Hubble Heritage Team (STScI/AURA)

Interstellar medium

92.1% of nucleons in the universe are protons
7.8% are helium nuclei !
0.1%……C,N,O,S,Si….

Cosmic abundance

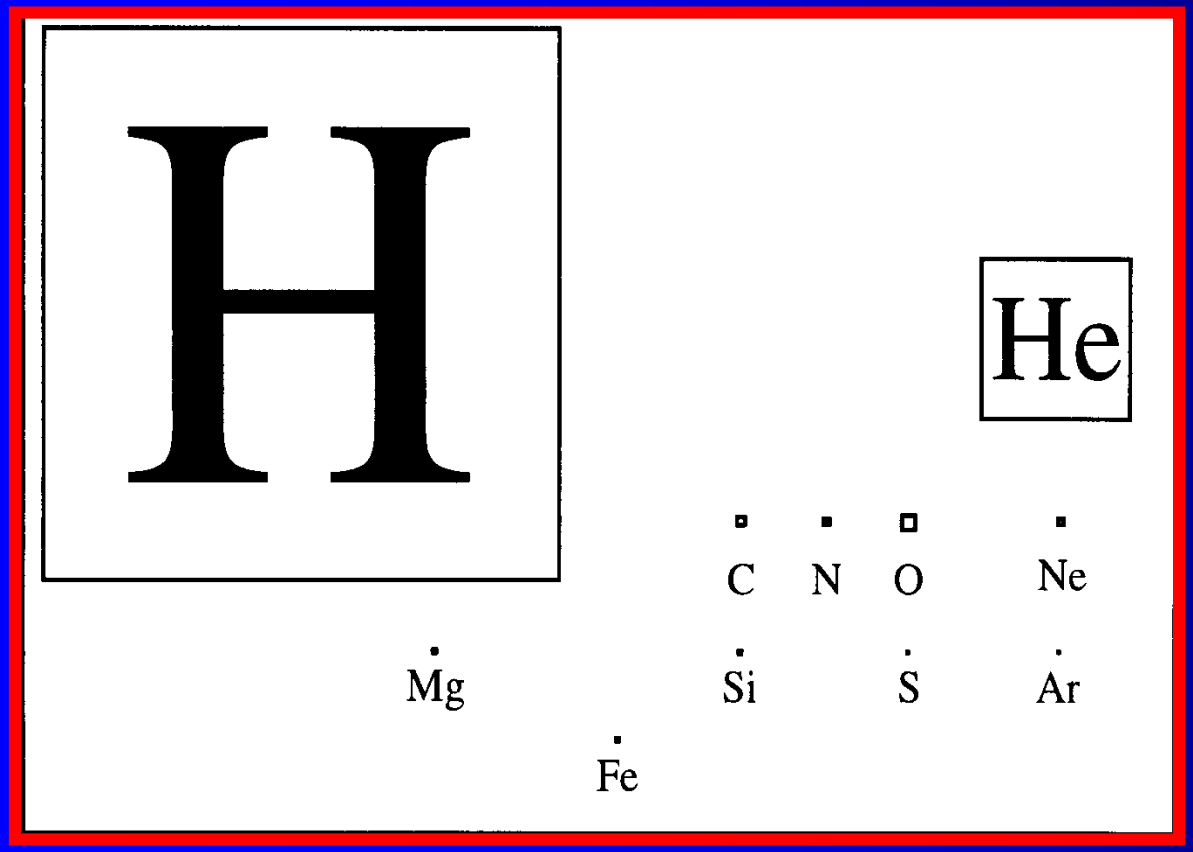

~0.005%……D

Importance of Interstellar Hydrogen

H

He

C N O Ne

Mg Si S Ar

Fe

Subaru Telescope
Mauna Kea, Hawaii

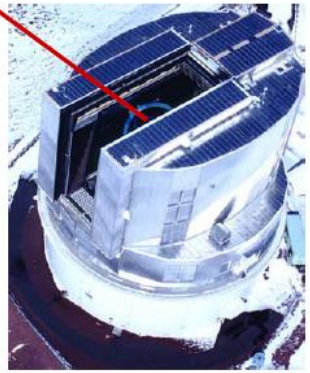

Integrated area of absorption lines

United Kingdom Infrared Telescope
Mauna Kea, Hawaii

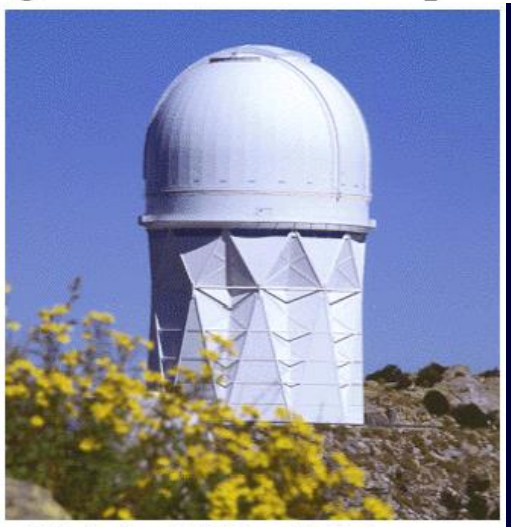

Nicholas U. Mayall Telescope
Kitt Peak, AZ

Motivations

- **H_3^+ is the cornerstone of ion-molecule reactions in the interstellar medium (ISM)**
- **Simple chemistry allows for the inference of various physical parameters (density, temperature, ionization rate, cloud size)**

Table 1 Classification of Interstellar Cloud Types

	Diffuse Atomic	Diffuse Molecular	Translucent	Dense Molecular
Defining Characteristic	$f^n_{H_2} < 0.1$	$f^n_{H_2} > 0.1$ $f^n_{C+} > 0.5$	$f^n_{C+} < 0.5$ $f^n_{CO} < 0.9$	$f^n_{CO} > 0.9$
A_V (min.)	0	~0.2	~1–2	~5–10
Typ. n_H (cm^{-3})	10–100	100–500	500–5000?	$>10^4$
Typ. T (K)	30–100	30–100	15–50?	10–50
Observational Techniques	UV/Vis H I 21-cm	UV/Vis IR abs mm abs	Vis (UV?) IR abs mm abs/em	IR abs mm em

Dense Interstellar Cloud Cores

10 K

10(4) cm-3

H2
dominant

Molecules seen in IR absorption and radio emission

sites of star formation

Cosmic rays create weak plasma

Fractional ionization < 10(-7)

"Intelligent play with simple, natural phenomena, the joys of discovery of unexpected experiences, are much better ways of learning to think than any teaching by rote."

The "Black Cloud" B68
(VLT ANTU + FORS1)

ESO PR Photo 20a/99 (30 April 1999)

Cosmic Elemental Abundances

- H = 1
- He = 6.3(-2)
- O = 7.4(-4) 1.8(-4)
- C = 4.0(-4) 7.3(-5)
- N = 9.3(-5) 2.1(-5)
- S = 2.6(-5) 8.0(-8)
- Si = 3.5(-5) 8.0(-9)
- Fe = 3.2(-5) 3.0(-9)

- Dust/gas = 1% by mass
- Gas-phase abundances of heavy elements in clouds reduced.

Some Fractional Abundances in TMC-1

- CO 1(-4)
- HCN 2(-8)
- C4H 9(-8)
- HCO+ 8(-9)
- c-C3H2 1(-8)
- HC9N 5(-10)

- OH 2(-7)
- NH3 2(-8)
- HC3N 2(-8)
- N2H+ 4(-10)
- HNC 2(-8)
- O2 < 8(-8)

Characteristics of some astrophysical sources

Table 2. Characteristics of important molecular astrophysical sources

Parameter	Object			
	TMC-1	IRC +10216	OMC-1	Sgr B2
Classification	Cold dense cloud	Outflowing C-rich circum-stellar envelope	Warm molecular cloud/star-forming region	Giant molecular cloud
Constellation	Taurus	Leo	Orion	Sagittarius
Distance/pc	140	150	460	10,000
Temperature/K	10–20	$1000 \rightarrow 10$	50–300	100
n/cm^{-3}	10^4	$10^7 \rightarrow 10^3$	10^5–10^7+	10^6–10^{10}
Representative trace constituents	HNC, c-C_3H_2, polyacetylenic compounds	Cyanopolyynes, polycarbon sulfides, metal cyanides, silicon compounds	Methylated organics	Alcohols, ethers, esters, carboxylic acids, amino acids (?)

Molecules in interstellar space

3	4	5	6	7	8	9	10	11	13
H_2	C_3	c-C_3H	C_5	C_5H	C_6H	CH_3C_3N	CH_3C_4H	CH_3C_5N?	HC_9N	$HC_{11}N$
AlF	C_2H	l-C_3H	C_4H	l-H_2C_4	CH_2CHCN	$HCOOCH_3$	CH_3CH_2CN	$(CH_3)_2CO$		
AlCl	C_2O	C_3N	C_4Si	C_2H_4	CH_3C_2H	CH_3COOH?	$(CH_3)_2O$	NH_2CH_2COOH?		
C_2	C_2S	C_3O	l-C_3H_2	CH_3CN	HC_5N	C_7H	CH_3CH_2OH			
CH	CH_2	C_3S	c-C_3H_2	CH_3NC	$HCOCH_3$	H_2C_6	HC_7N			
CH^+	HCN	C_2H_2	CH_2CN	CH_3OH	NH_2CH_3	CH_2OHCHO	C_8H			
CN	HCO	**CH_2D^+?**	CH_4	CH_3SH	c-C_2H_4O					
CO	**HCO^+**	HCCN	HC_3N	**HC_3NH^+**	CH_2CHOH					
CO^+	**HCS^+**	**$HCNH^+$**	HC2NC	HC_2CHO						
CP	**HOC^+**	HNCO	HCOOH	NH_2CHO						
CSi	H_2O	HNCS	H2CHN	C_5N						
HCl	H_2S	**$HOCO^+$**	H_2C_2O							
KCl	HNC	H_2CO	H_2NCN							
NH	HNO	H2CN	HNC_3							
NO	MgCN	H_2CS	SiH_4							
NS	MgNC	**H_3O^+**	**H_2COH^+**							
NaCl	**N_2H^+**	NH_3								
OH	N_2O	SiC_3								
PN	NaCN									
SO	OCS									
SO^+	SO_2									
SiN	c-SiC_2									
SiO	CO_2									
SiS	NH_2									
CS	**H_3^+**									
HF	SiCN									
SH	AlNC									
FeO?										

16 JULY 2015 | VOL 523 | NATURE | 323

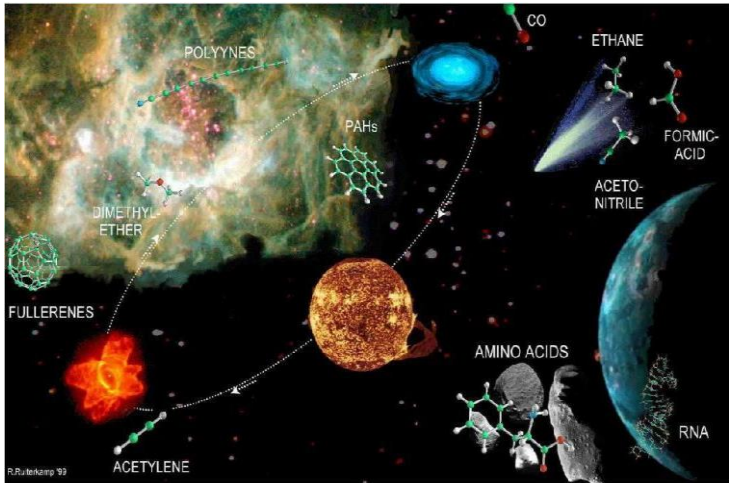

Molecules in interstellar space

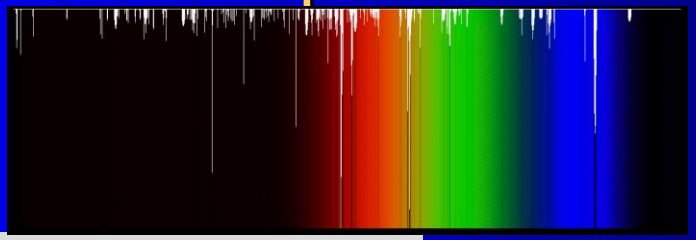

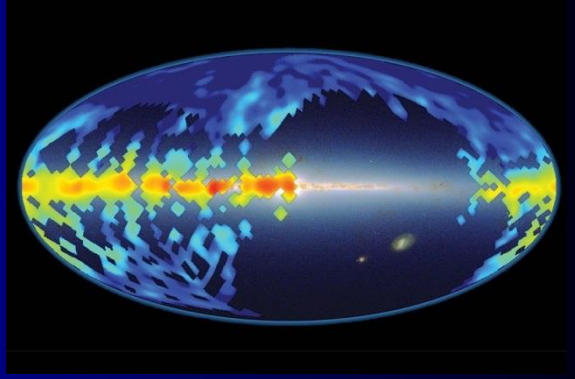

1919-1922 Heger discovers the DIBs

Nearly 100 years ago Mary Lea Heger discovered diffuse bands in the spectra of stars due to some sort of material maybe molecules in the space between stars and Earth. A map of the data from the Sloan Digital Sky Survey, by a team from Johns Hopkins produced this map. Red indicates areas with the most abundant DIB molecules, blue the least.

16 JULY 2015 | VOL 523 | NATURE | 323

LETTER

2015

Laboratory confirmation of C_{60}^+ as the carrier of two diffuse interstellar bands

E. K. Campbell[1], M. Holz[1], D. Gerlich[2] & J. P. Maier[1]

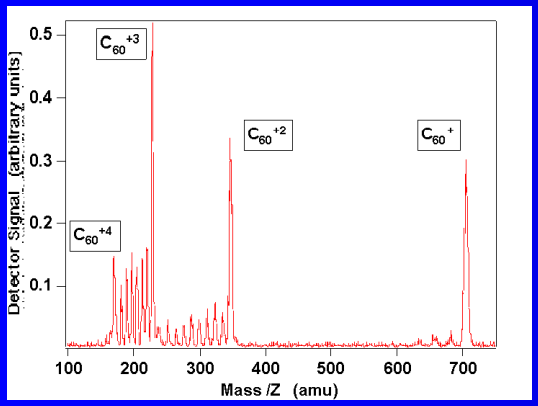

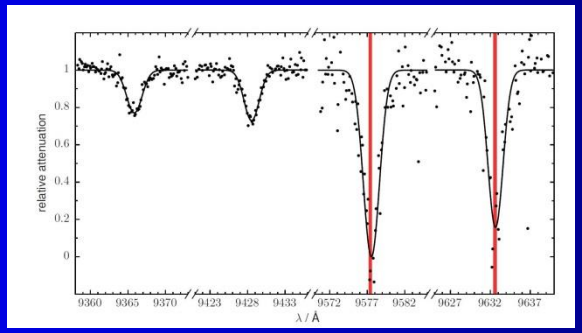

RESEARCH NEWS & VIEWS

ASTROCHEMISTRY

Fullerene solves an interstellar puzzle

Laboratory measurements confirm that a 'buckyball' ion is responsible for two near-infrared absorption features found in spectra of the interstellar medium, casting light on a century-old astrochemical mystery. SEE LETTER P.322

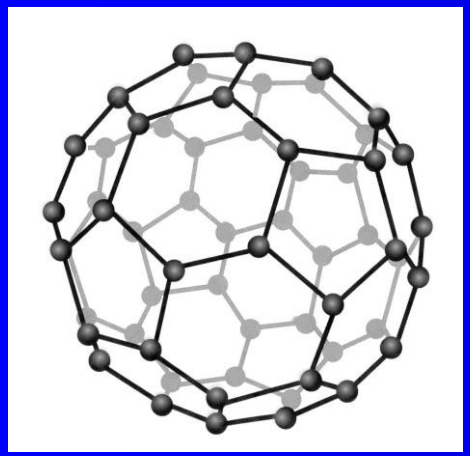

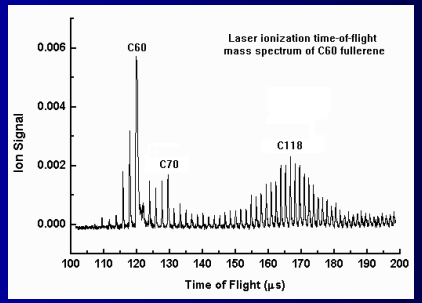

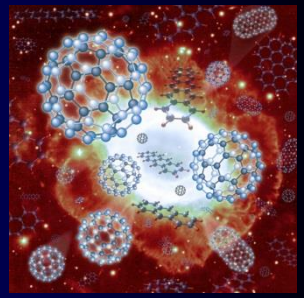

Motivation:

$e^-, H^+, H, H^-, H_2^+, H_2, \ldots . H_3^+$

Just for pleasure.

$$\psi(x) \propto \sum_n A_n e^{ip_n x/\hbar},$$

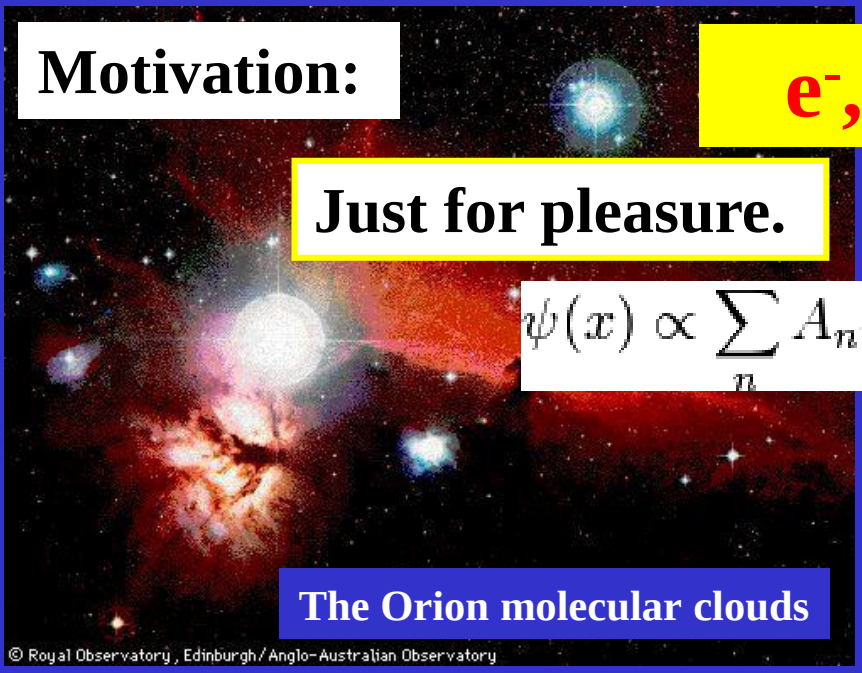

The Orion molecular clouds

92.1% of nucleons in the universe are protons
7.8% are helium nuclei !

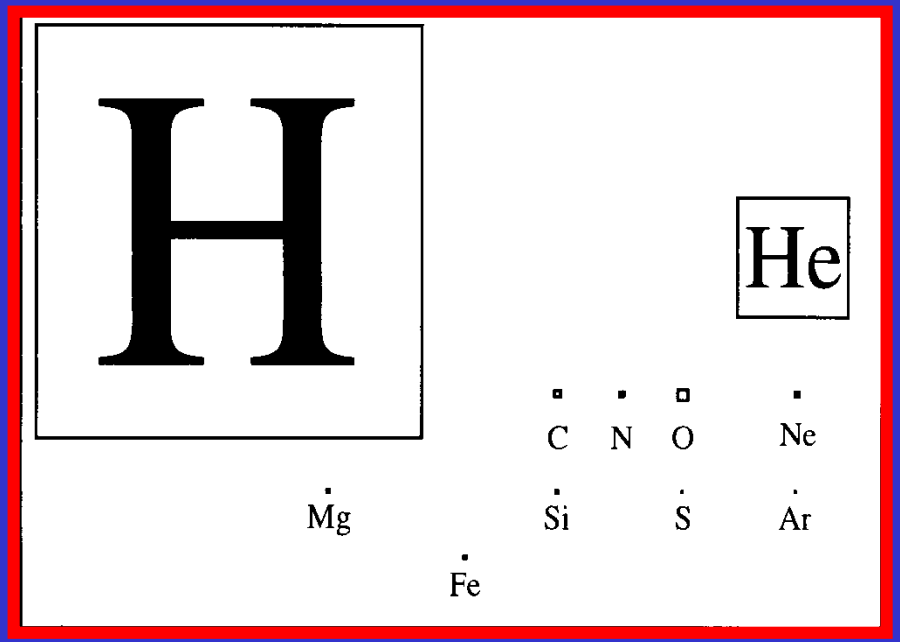

Cosmic Abundance of some elements

Element	Abundance
hydrogen (H)	1.000.000
helium	80.147
oxygen	739
carbon	445
neon	138
nitrogen	91
magnesium	40
Silcon	37
Sulfur	19

"Intelligent play with simple, natural phenomena, the joys of discovery of unexpected experiences, are much better ways of learning to think than any teaching by rote."

$$H_3^+ + CH_4 \rightarrow CH_5^+ + H_2$$

$$H_5^+ + H_2 \rightarrow H_3^+ + H_2 + H_2$$

$$H_3^+ + H_2 + H_2 \rightarrow H_5^+ + H_2$$

Top Curr Chem (2003) 225: 37–75
DOI 10.1007/b10469

2003

Mass Spectrometric Approaches to Interstellar Chemistry

Simon Petrie[1] · Diethard K. Bohme[2]

[1] Department of Chemistry, the Faculties, Australian National University, Canberra ACT 0200, Australia. *E-mail: spetrie@rsc.anu.edu.au*
[2] Department of Chemistry, Centre for Research in Mass Spectrometry, Centre for Research in Earth and Space Science, York University, Toronto, ON, Canada M3J 1P3
E-mail: dkbohme@yorku.ca

THE ASTROPHYSICAL JOURNAL, 787:44 (10pp), 2014 May 20

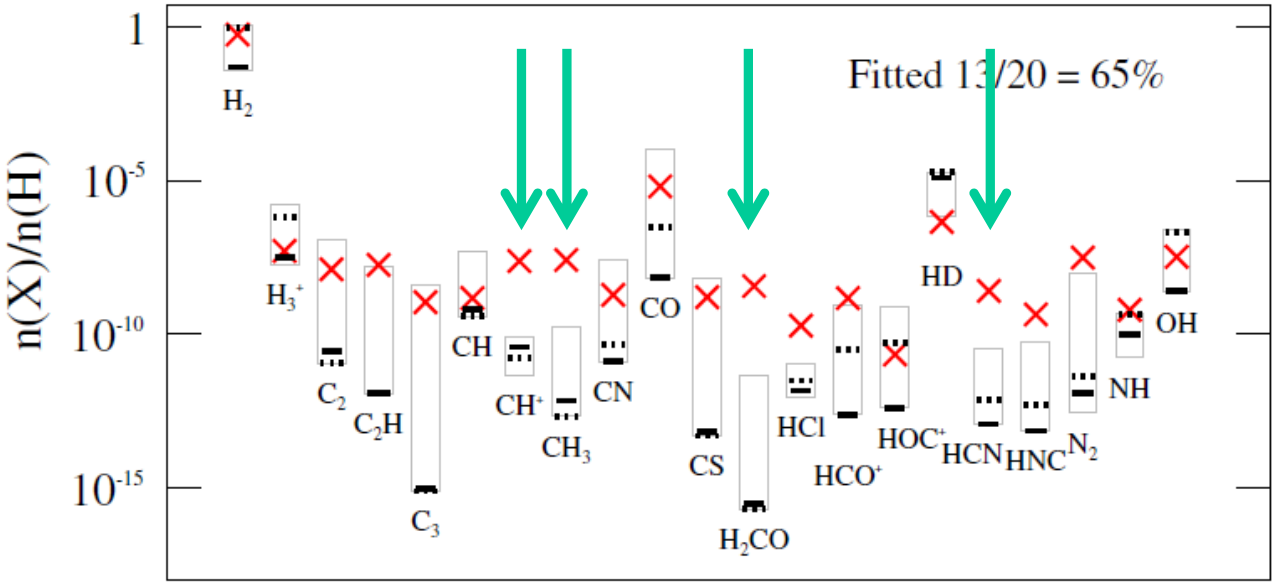

Figure 6. Comparison of observed abundances (red crosses) to modeled values of key species in diffuse clouds. Gray boxes show the range of abundances calculated from the considered models (Table 2) and black lines show abundances from the best-fit model "2X+C15" (30 K, solid line, and 90 K, dotted line).

THE ASTROPHYSICAL JOURNAL, 787:44 (10pp), 2014 May 20
doi:10.1088/0004-637X

2014

FIRST TIME-DEPENDENT STUDY OF H_2 AND H_3^+ *ORTHO–PARA* CHEMISTRY IN THE DIFFUSE INTERSTELLAR MEDIUM: OBSERVATIONS MEET THEORETICAL PREDICTIONS*

T. ALBERTSSON[1], N. INDRIOLO[2], H. KRECKEL[3], D. SEMENOV[1], K. N. CRABTREE[4], AND TH. HENNING[1]

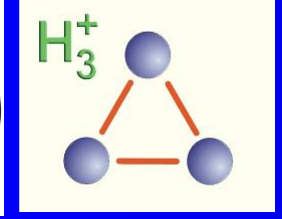

Nevyžiadaná reklama

H_2 and H_3^+ Story

(H_3^+ IMR & Recombination)

motto

If you understand hydrogen, you understand all that can be understood. V. Weisskopf (Taken from G. Herzberg).

Motivace ?... $$$? ....

…užívajte sveta …. blíži sa kometa ….

Massive Gas Cloud Speeding Toward Collision With Milky Way

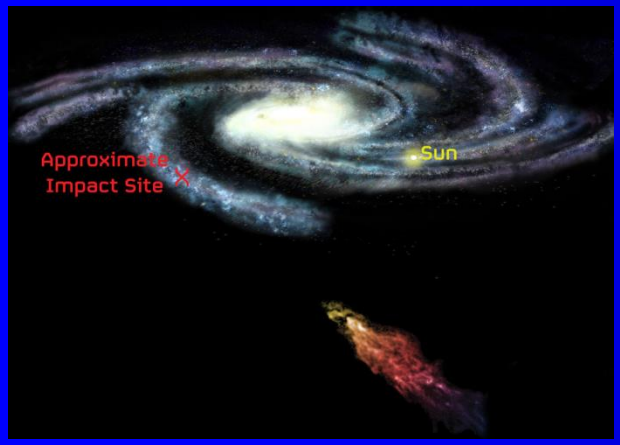

1963

The leading edge of this cloud is already interacting with gas from our Galaxy

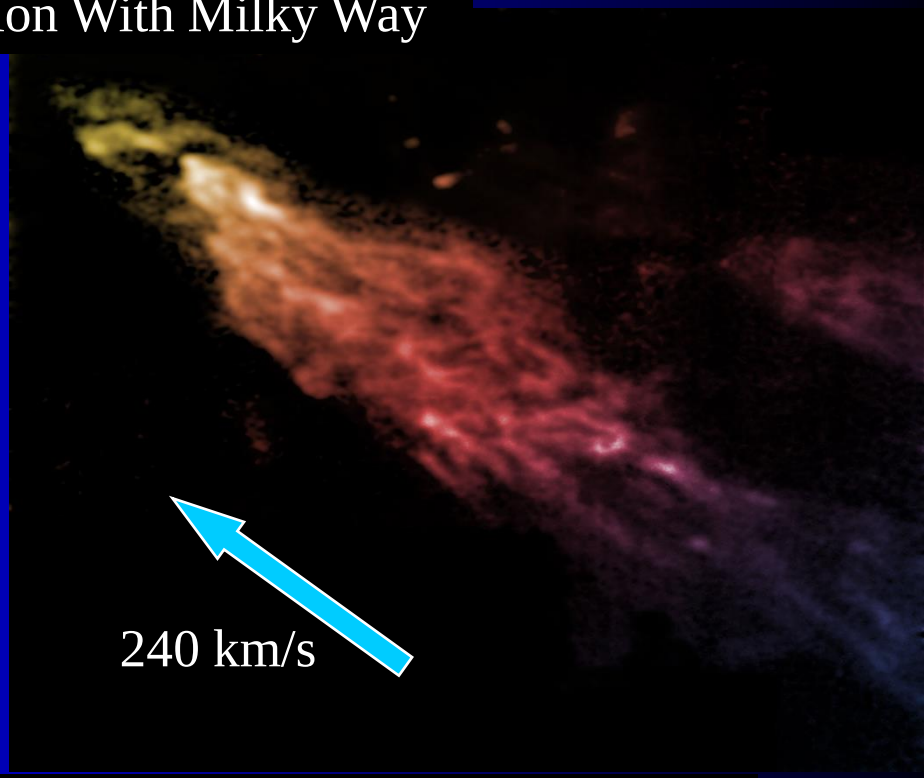

The cloud, called Smith's Cloud, after the astronomer who discovered it in 1963, contains enough hydrogen to make a million stars like the Sun. Eleven thousand light-years long and 2,500 light-years wide, it is only 8,000 light-years from our Galaxy's disk. It is careening toward our Galaxy at more than 150 miles per second, aimed to strike the Milky Way's disk at an angle of about 45 degrees.

Lockman and his colleagues used the Green Bank Telescope GBT to make an extremely detailed study of hydrogen in Smith's Cloud. Smith's Cloud is about 15 degrees long in the sky, 30 times the width of the full moon.

Its shape, somewhat similar to that of a comet, indicates that it's already hitting gas in our Galaxy's outskirts. It is also feeling a tidal force from the gravity of the Milky Way and may be in the process of being torn apart.

…. What about energy…

Our Galaxy will get a rain of gas from this cloud, then in about 20 to 40 million years, the cloud's core will smash into the Milky Way's plane," The cloud will likely strike a region somewhat farther from the Galactic center than our Solar System and about 90 degrees ahead of us in the Milky Way disk. The collision may trigger a period of rapid star formation fueled by the new gas and the shock from the collision. Some theories say that the ring of bright stars near the Sun, called Gould's Belt, was created by just such a collision event.

contains enough hydrogen to make a million stars like the Sun

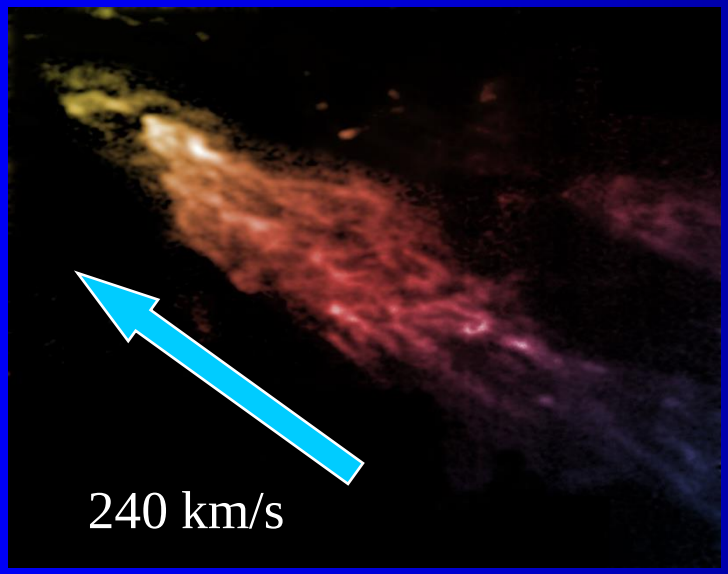

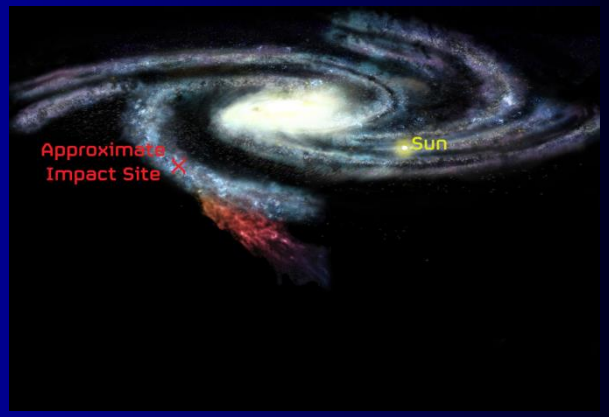

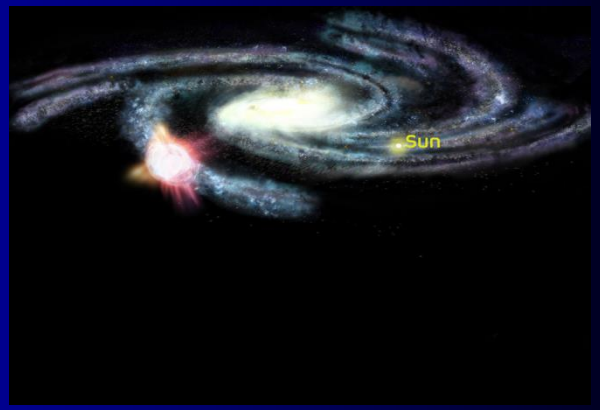

…. blíži sa …..

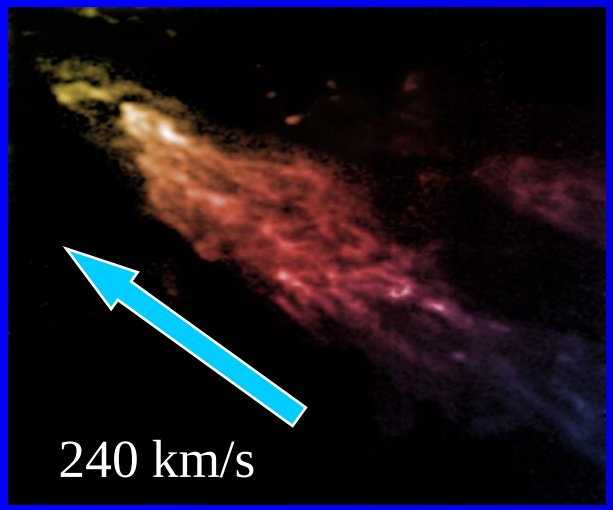

contains enough hydrogen to make a million stars like the Sun

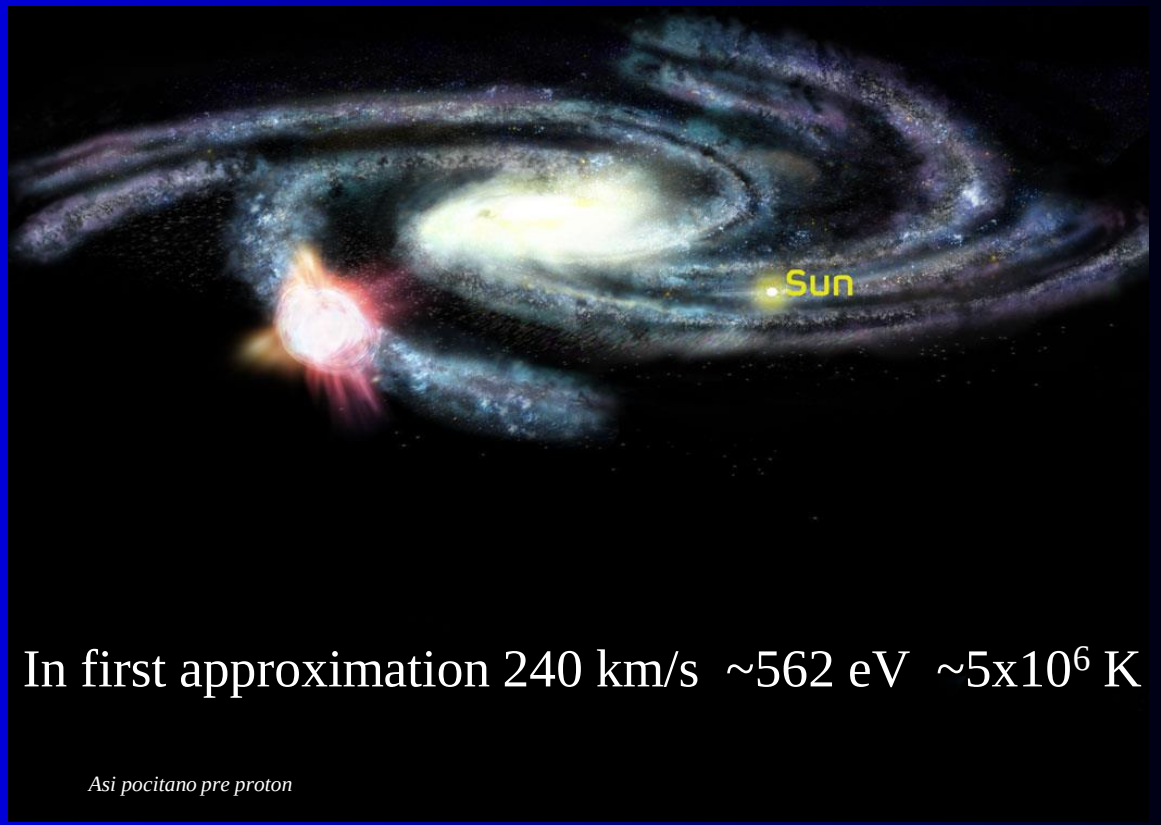

In first approximation 240 km/s ~562 eV ~5×10^6 K

Asi pocitano pre proton

Plasma is everywhere, but where is truth

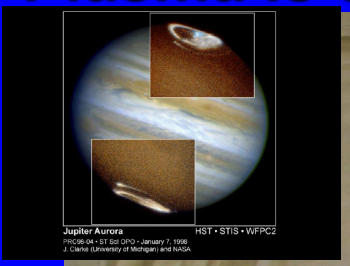

H_3^+

Πλασμα

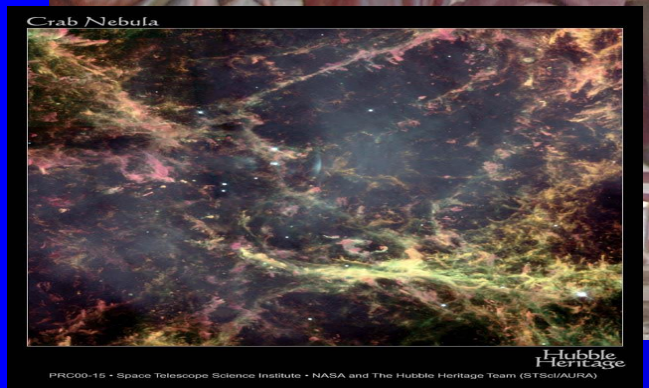

Scio me nihil scire

Sokrates, Platon

“School of Athens” Rafael, Vatican

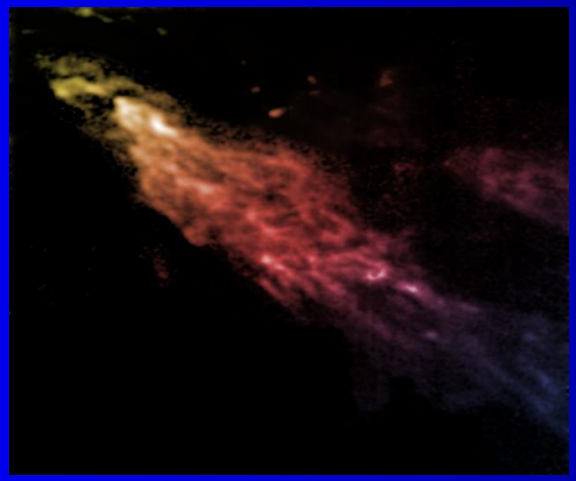

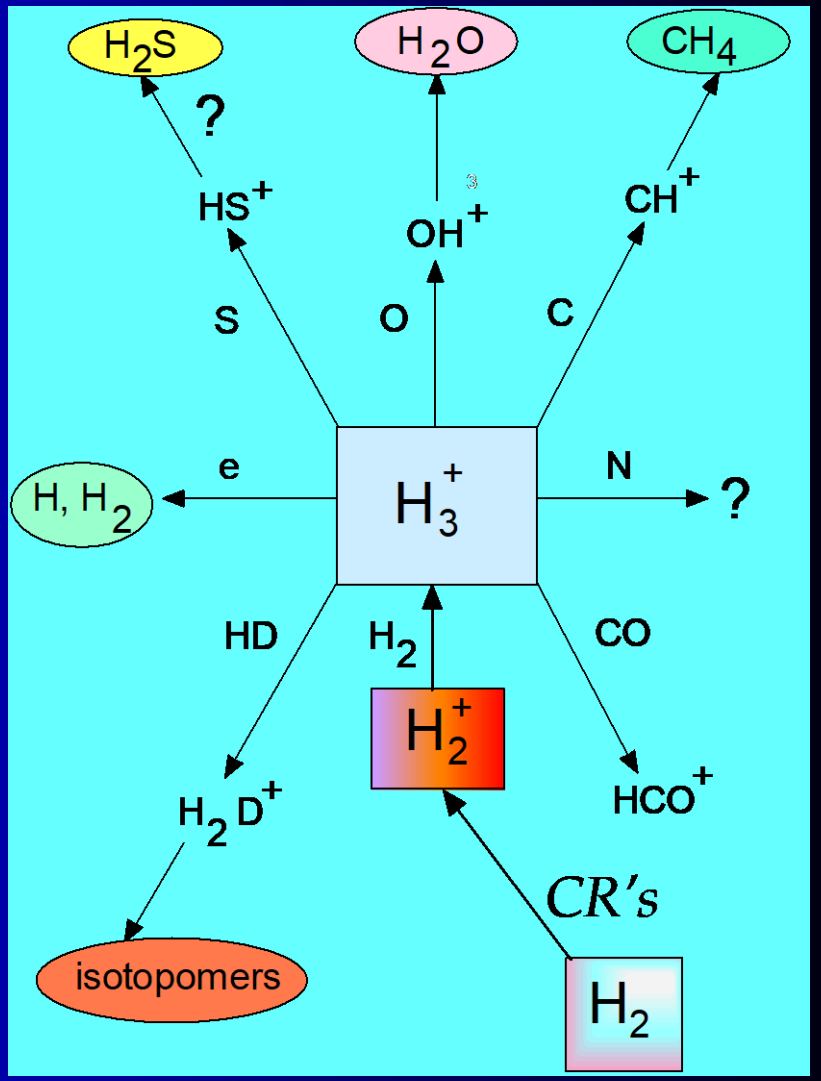

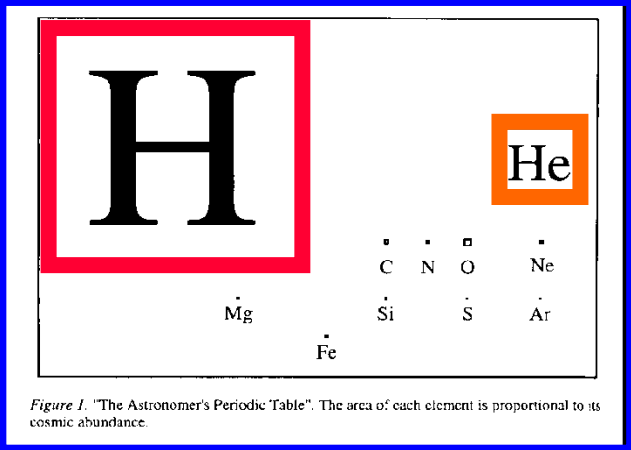

Figure 1. "The Astronomer's Periodic Table". The area of each element is proportional to its cosmic abundance.

H_3^+ in Interstellar space

Interstellar H_3^+

1961

ON THE POSSIBLE OCCURRENCE OF H_3^+ IN INTERSTELLAR SPACE

The possibilities for detection of the molecular ion H_2^+ by radio-astronomical techniques have recently received considerable attention, and theoretical predictions of the spectrum have been made by Mizushima (1961) and by Burke (1961). Recent work on ion-molecule reactions indicates that the molecular ion H_3^+ may also be expected in interstellar space. In fact, with the presence of quantities of molecular hydrogen, H_2^+ will react to form H_3^+.

Formation of H_3^+ through the reaction $H_2^+ + H_2 \rightarrow H_3^+$ has been observed independently by Stevenson and Schissler (1958) and by Barnes, Martin, and McDaniel (1961). The cross-section for this reaction has been found to have a remarkably large value of the order of 10^{-14} cm^2 at normal thermal energies. This is much greater than the gas-kinetic cross-section for neutral hydrogen molecules. The cross-section for H_3^+ formation by this reaction varies inversely with the relative velocity of the H_2^+ ion and the hydrogen molecule (Stevenson and Schissler 1958; Lampe and Field 1959). The experimental work of Barnes, Martin, and McDaniel furthermore shows that H_3^+ ions persist over very many subsequent collisions with hydrogen molecules. The H_3^+ ion is stable against spontaneous dissociation. Its binding energy of 4.18 ev (Varney 1960) exceeds that of H_2^+ (2.65 ev), so the formation reaction is exoergic (Hirschfelder, Curtiss, and Bird 1954).

Thus it may be expected that H_2^+ will be converted to H_3^+ upon encounter with a hydrgoen molecule, and the population of H_2^+ will be very strongly influenced by the density of neutral molecular hydrogen. It now appears desirable to consider the possibilities for detecting H_3^+ because this molecular ion may be present under some circumstances to the virtual exclusion of H_2^+.

D. W. MARTIN
E. W. MCDANIEL
M. L. MEEKS

June 13, 1961
GEORGIA INSTITUTE OF TECHNOLOGY
ATLANTA, GEORGIA

Martin, McDaniel, & Meeks,
Astrophys. J. 134, 1012 (1961)

H_3^+ in Interstellar space

Interstellar Chemistry

1973

Another important subclass of reactions are those involving H_3^+. This ion is produced by the well-studied reaction

$$4. \quad H_2 + H_2^+ \rightarrow H_3^+ + H\,,$$

and then reacts with many neutral species according to the general formula

$$H_3^+ + X \rightarrow XH^+ + H_2\,, \qquad (4)$$

where X = CO, N_2, H_2O, NH_3, etc. These reactions have been studied by Burt *et al.*

E. Herbst & W. Klemperer, Astrophys. J. 185, 505 (1973)

also: W. D. Watson Astrophys. J. 183, L17 (1973)

- H_3^+ "universal protonator"
  - $H_3^+ + O \rightarrow H_2 + OH^+$
  - $OH^+ + H_2 \rightarrow H + H_2O^+$
  - $H_2O^+ + H_2 \rightarrow H + H_3O^+$
  - $H_3O^+ + e^- \rightarrow H_2O + H$
- Origin of Earth's water (?)

History of H_3^+

J. J. Thomson 1912

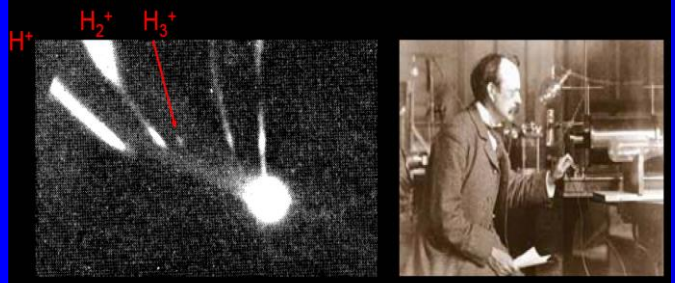

Existence of H_3.—On several plates taken when the discharge-tube contains hydrogen, the existence of a primary line for which $m/e = 3$ has been detected. There can, I think, be little doubt that this line is due to H_3. The existence of this substance is interesting from a chemical point of view, as it is not possible to reconcile its existence with the ordinary conceptions about valency, if hydrogen is regarded as always monovalent. The polymeric modification of hydrogen seems to require special conditions for its formation, for it cannot be detected on many of the plates taken with hydrogen in the tube.

J. J. Thomson, Phil. Mag. 24, 209 (1912)

m=3

Arthur J. Dempster 1916

- Discovered ^{235}U
- Physics Prof. at U. Chicago
- Principal American authority on positive rays

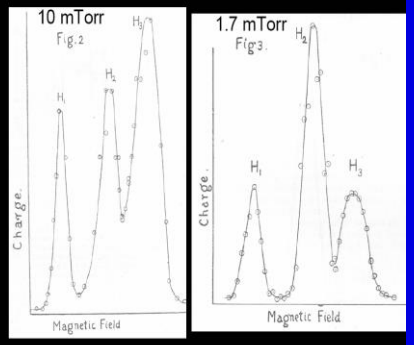

→ H_3^+ formed in secondary reaction

A. J. Dempster, Phil. Mag. 31, 438 (1916)

$H_2^+ + H_2 \rightarrow H_3^+ + H$

1935 Charles A. Coulson

- First Ph.D. student of Lennard-Jones
- First ab initio calculation on a polyatomic molecule
- "It appears that the ion H_3^+ should exist in stable equilateral form with a nuclear distance about 0.85 Å, and that all excited levels are unstable."
- Prediction not accepted by Eyring, Hirschfelder, and others
- With advent of computers, prediction was confirmed (Christoffersen, Hagstrom, & Prosser 1964, Conroy 1964)

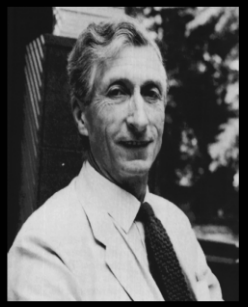

C. A. Coulson, Proc. Camb. Phil. Soc. 31, 244 (1935)

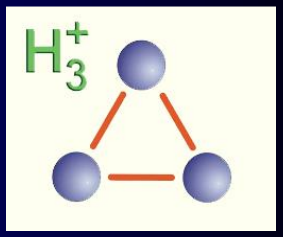

- No excited electronic state
- No dipole moment in ground state
  - → no pure rotational spectrum
- ν_1 symetric stretch - infrared inactive
- ν_2 vibration fundamental band feasible freq. ~2700 cm^{-1}

Intensive laboratory search for H_3^+ spectra

1912 1920 1930 ……. 1970 1980

Search for H_3^+ in laboratory

Oka's Search for H_3^+

Positive Column Discharge

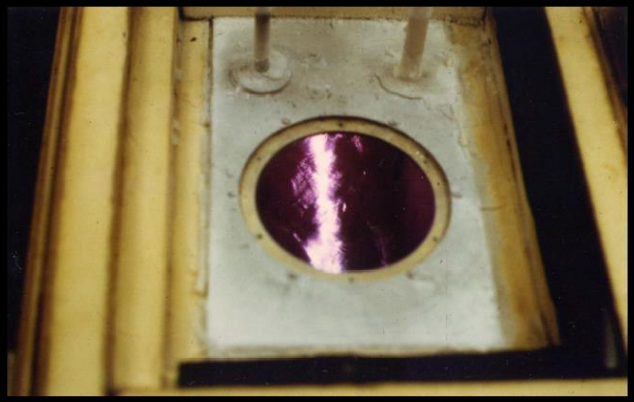

Every morning, he transferred six 50 liter cans of liquid nitrogen to the laboratory!

The Long Search

- Four and a half years. Much of it assembling the DF system and discharge cell.
- Scanned from:
  - 6/12-8/3 (1978)
  - 12/18-1/26 (1978-79)
  - 4/24-12/18 (1980)
- R(1,0) April 25, 1980.
  - Oka and Allen Karabonik in lab
  - Keiko came in at 10 pm
- Watson assigned it overnight

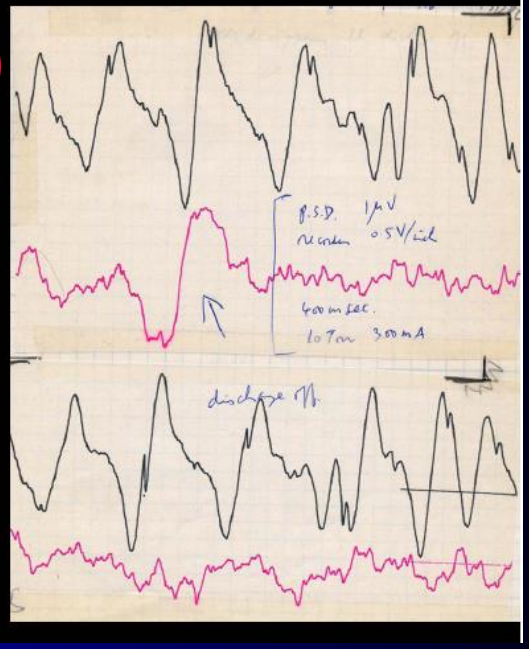

25. 4. 1980

Aastrophysical – Observations of H_3^+(v=0)

1912 .. 1916 … 1935 …….. 1980

1980 - Laboratory

T. Oka -IR Spectroscopy Observation of H_3^+

Oka, T. 1980 *Phys. Rev. Lett* **45**, 531.

1980

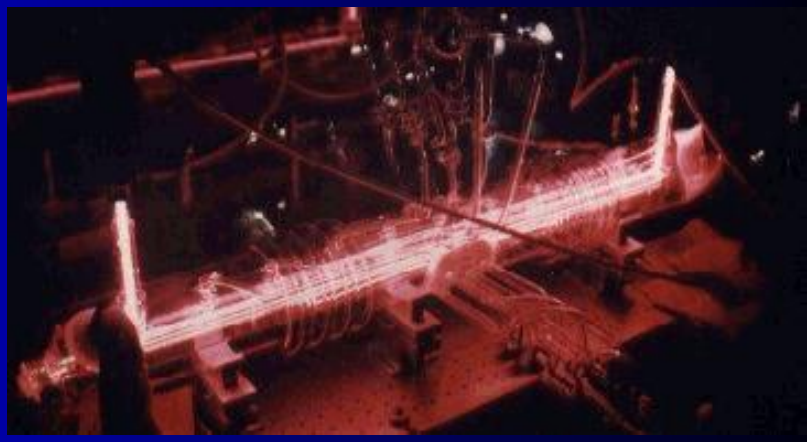

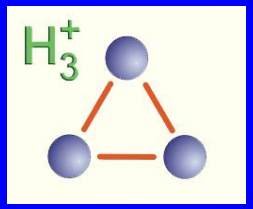

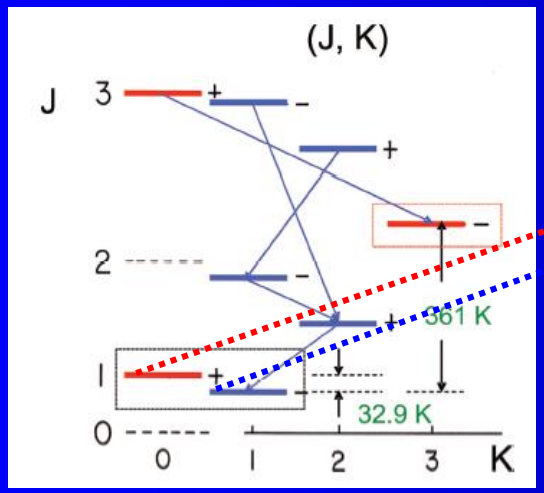

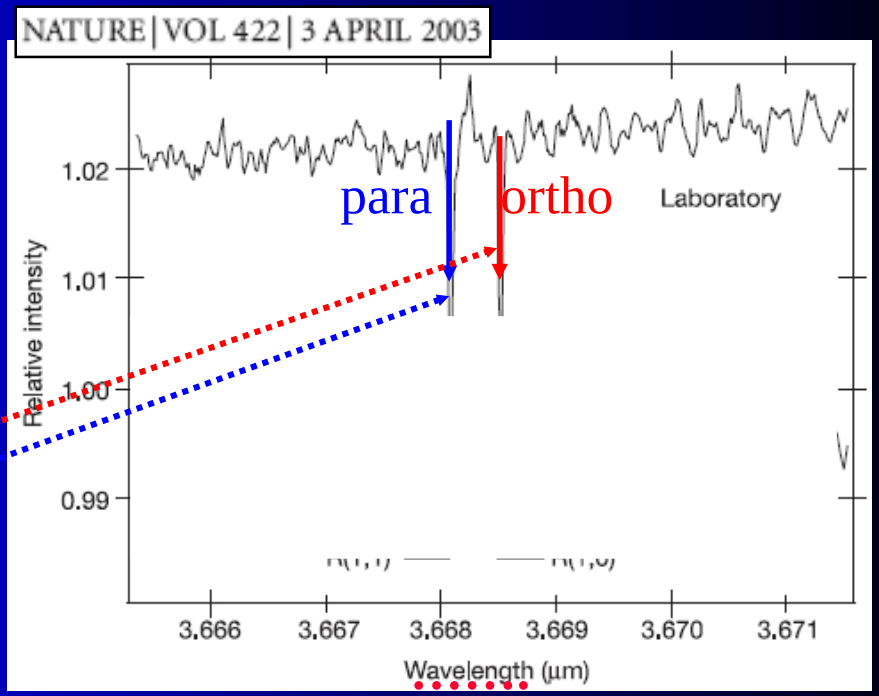

R(1,1)u originates from the lowest para level (J = 1, K = 1), while R(1,0) comes from the lowest ortho level (J = 1,K = 0). Note that the (J = K = 0) level is forbidden by the Pauli principle.

Back to the Interstellar Search

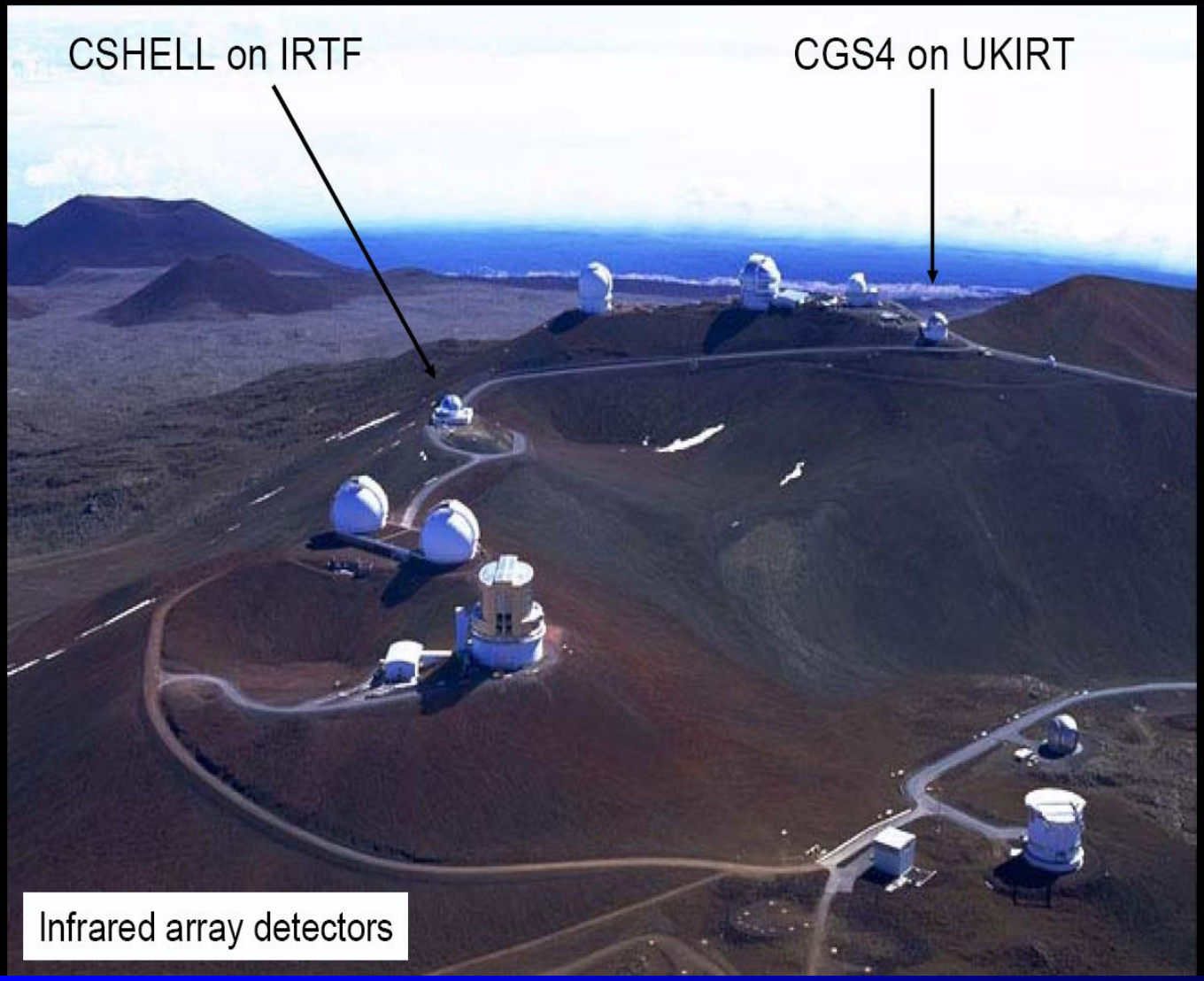

Environments with H_3^+

Jupiter

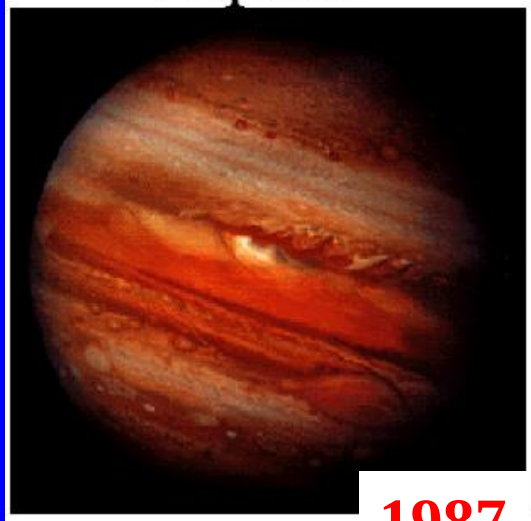

1987

Saturn

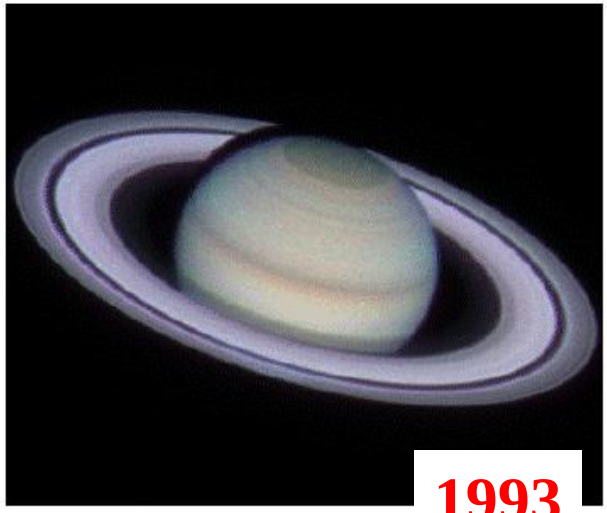

1993

Uranus

1993

Observation of H_3^+:

Ionosphere of large planets:

Jupiter (1987), Saturn (1993), Uran(1993)

Search for H_3^+ - Interstellar space

First detection!

LETTERS TO NATURE

Detection of H_3^+ in interstellar space

T. R. Geballe* & T. Oka†

* Joint Astronomy Centre, University Park, Hilo, Hawaii 96720, USA
† Department of Astronomy and Astrophysics, Department of Chemistry and the Enrico Fermi Institute, The University of Chicago, Chicago, Illinois 60637-1403, USA

1996

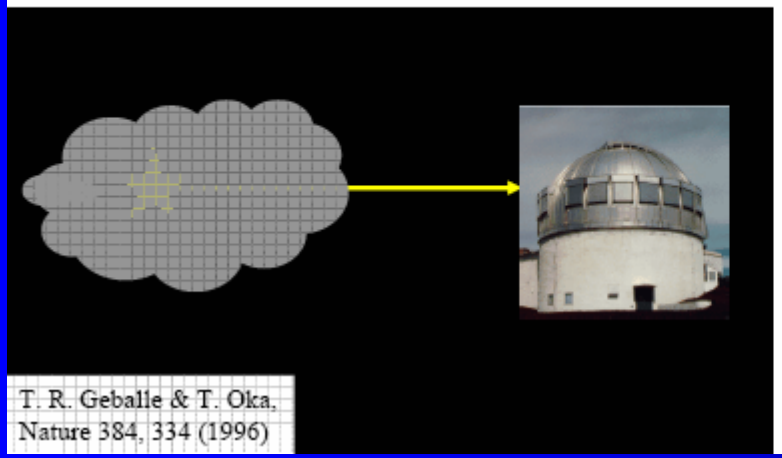

T. R. Geballe & T. Oka, Nature 384, 334 (1996)

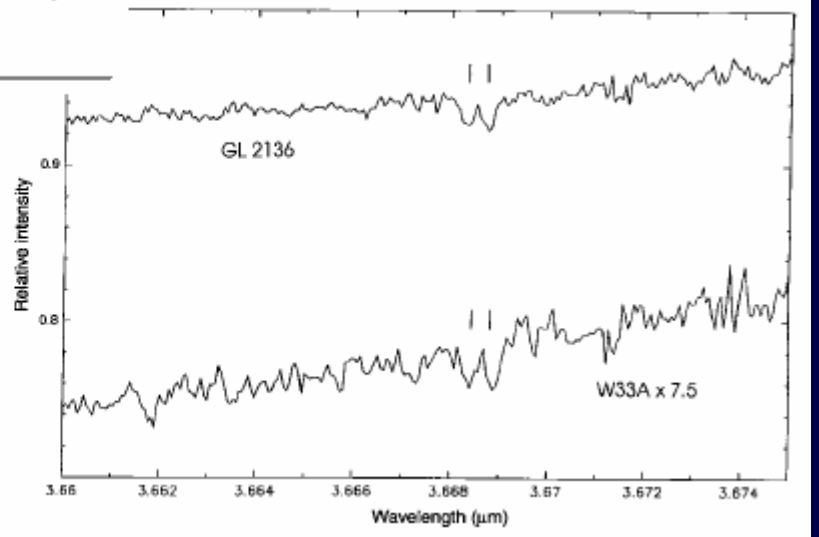

Search for H_3^+ - Interstellar space

Confirmed by Doppler Shift

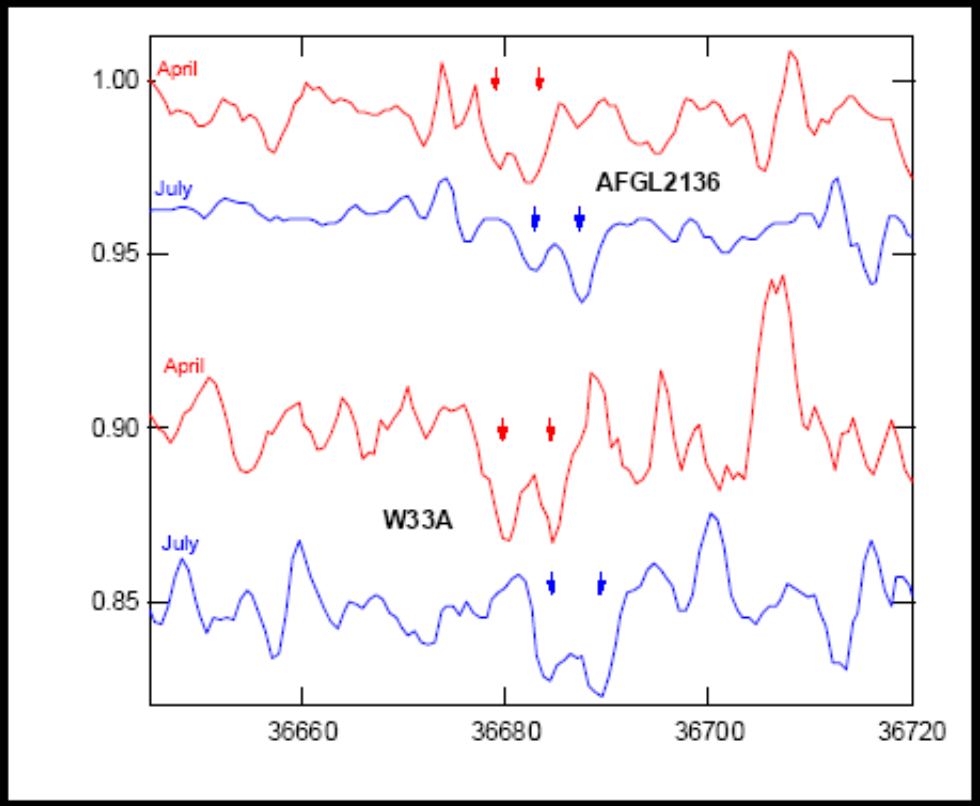

reprocessed

↓

Doppler shift confirms interstellar origin

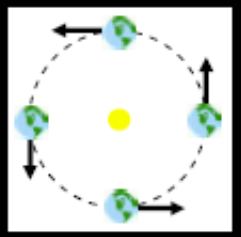

B. J. McCall, T. R. Geballe, K. H. Hinkle & T. Oka, Astrophys. J. 522, 338 (1999)

1999

Conditions in ISM

T. R. Geballe & T. Oka
Nature 384, 334 (1996)

1996

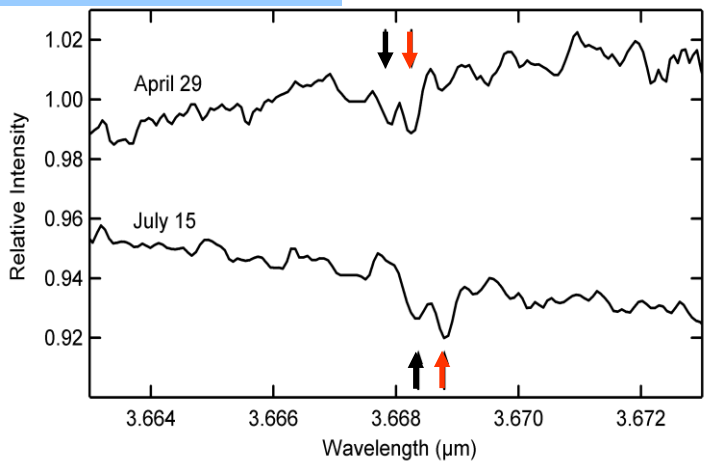

Dark Clouds:

- **T ~ 10K**
- **H_2 density ~ $10^4 cm^{-3}$**

The Orion molecular clouds

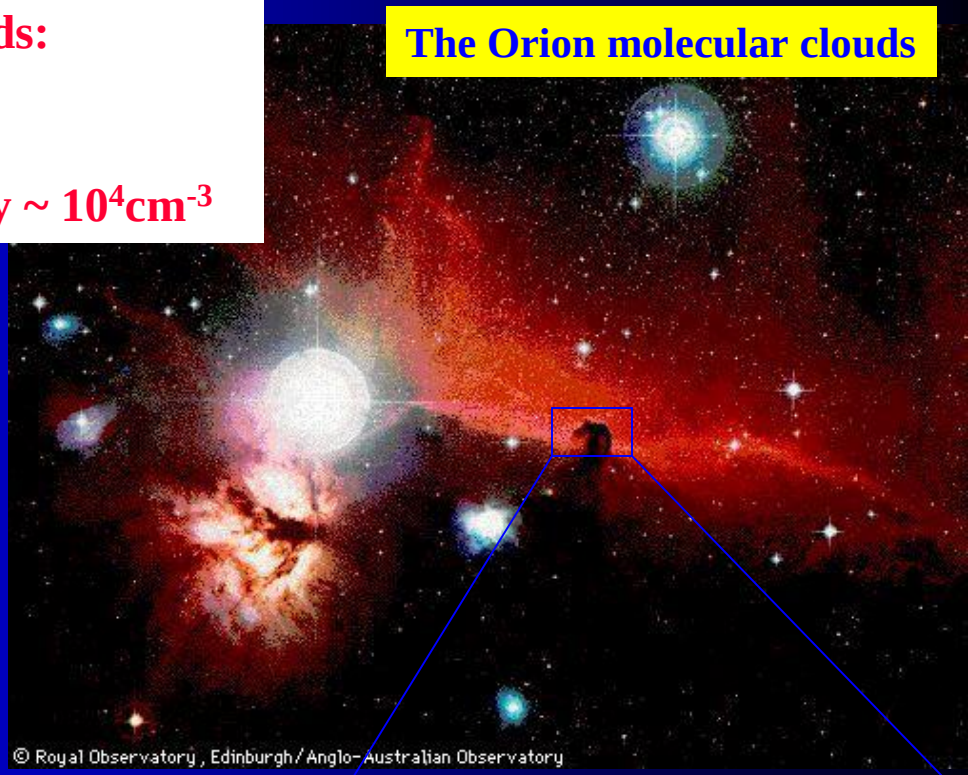

N_{para} = 4.0(9) × 10^{14} cm^{-2}

N_{ortho} = 3.0(6) × 10^{14} cm^{-2} (ΔE~32.9K)

Molecular Cloud GL2136.
The first detection of interstellar H_3^+
CGS4 spectrometer at UKIRT

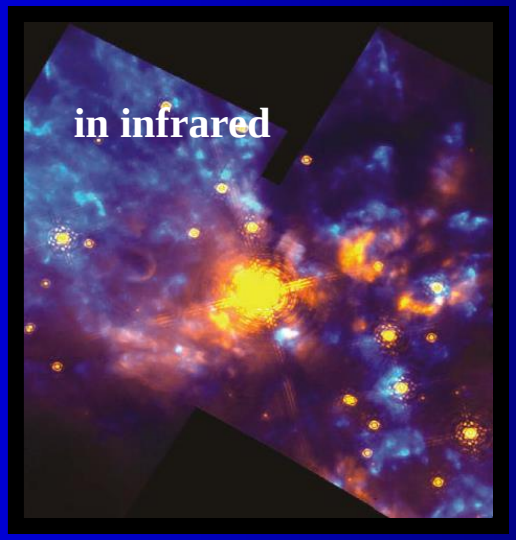

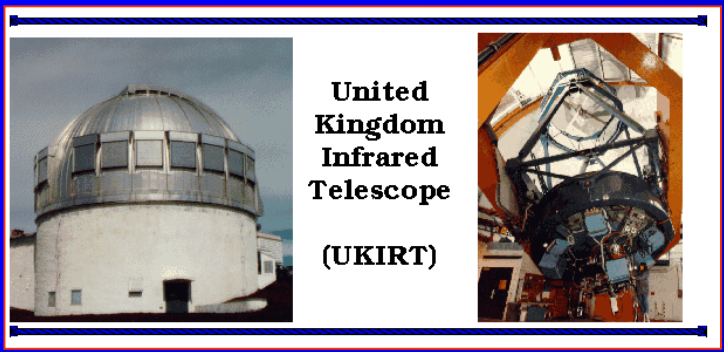

United Kingdom Infrared Telescope

(UKIRT)

Aastrophysical – Observations OF H_3^+(v=0)

1987 – 1999 - ….

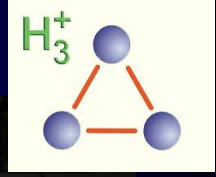

1980 - Laboratory

T. Oka -IR Spectroscopy Observation of H_3^+

Oka, T. 1980 *Phys. Rev. Lett* **45**, 531.

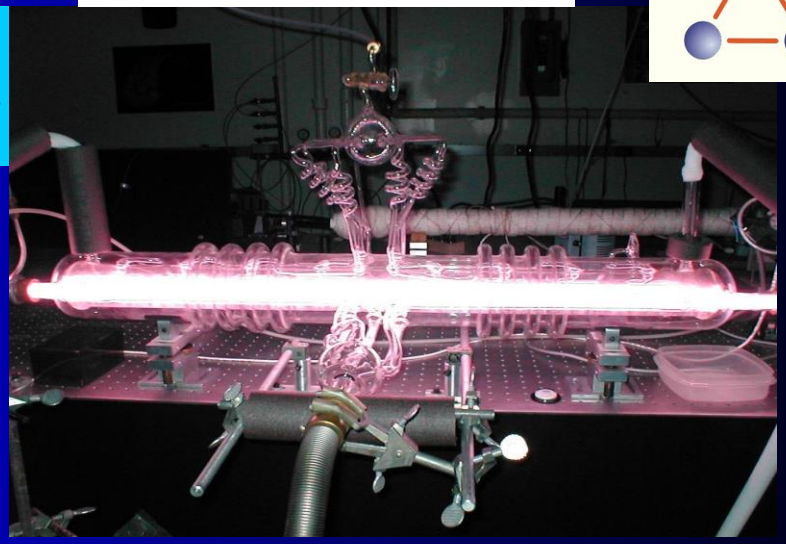

1987 -2006; Observation of H_3^+:

Supernova 1987A

Interstellar clouds (1998….)

Centre of Galaxy (1999)

Ionosphere of large planets:

Jupiter (1987), Saturn (1993), Uran(1993)

Geballe, T. R. & Oka, T. 1996 *Nature* **384**, 334.

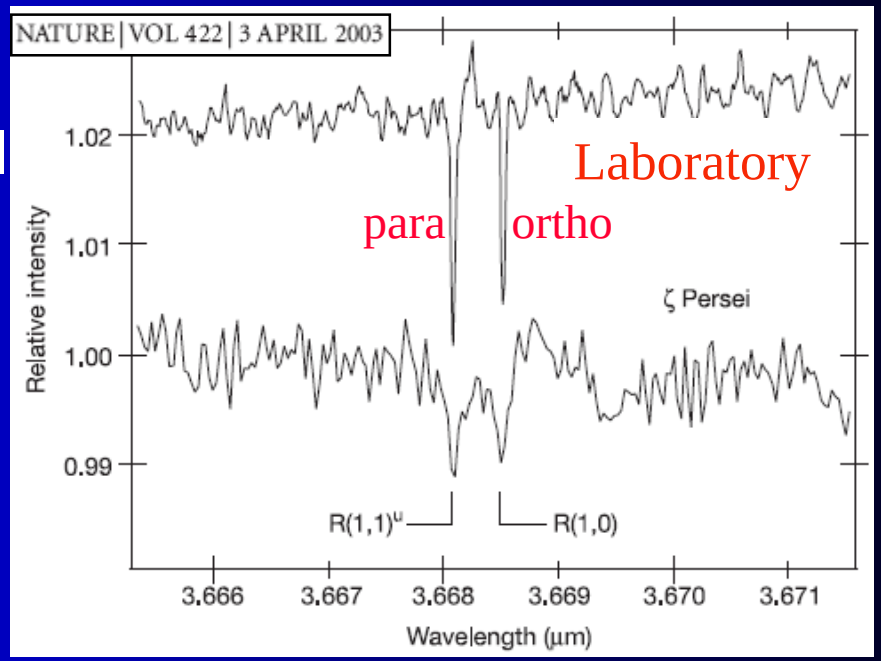

Jupiter

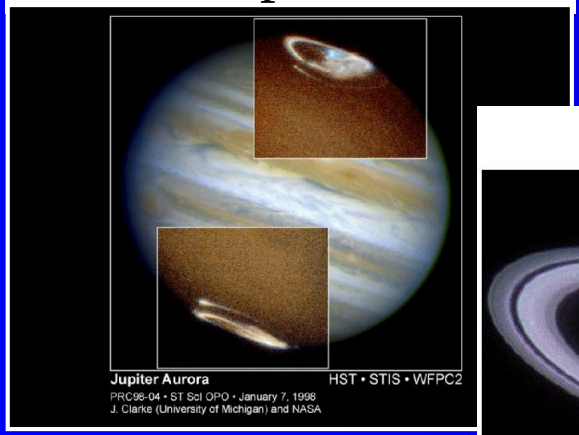

Saturn

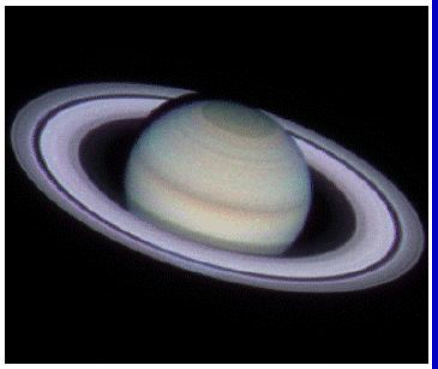

R(1,1)u originates from the lowest para level (J = 1, K = 1), while R(1,0) comes from the lowest ortho level (J = 1,K = 0). Note that the (J = K = 0) level is forbidden by the Pauli principle.

Environments with H3+

Jupiter

Saturn

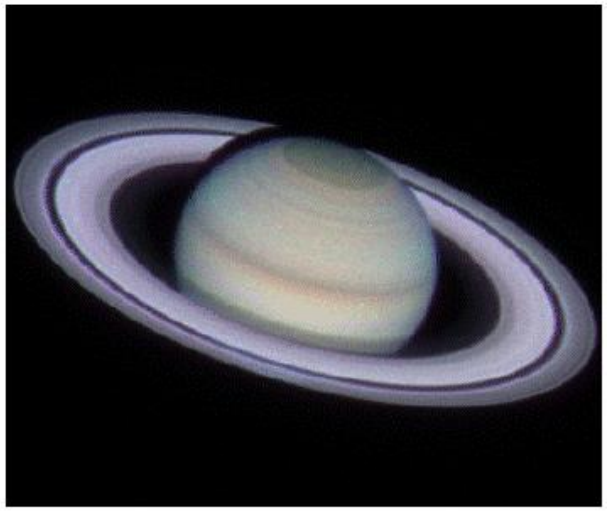

Uranus

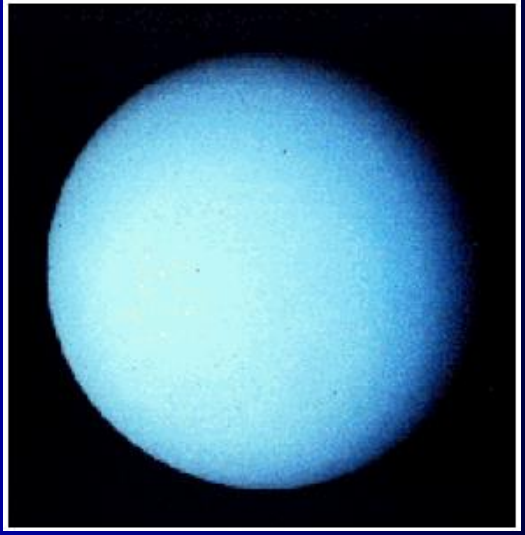

Dense Clouds

Barnard 68 (João Alves)

Diffuse Clouds

Cygnus OB2 (POSS)

Galactic Center

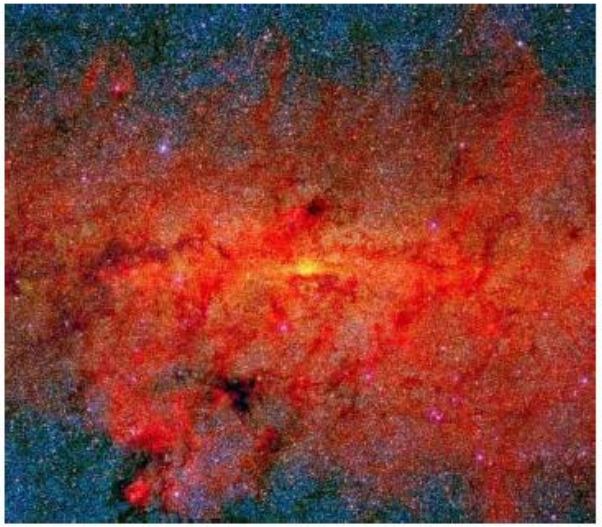

Galactic Center (2MASS/MSX)

Plasma.

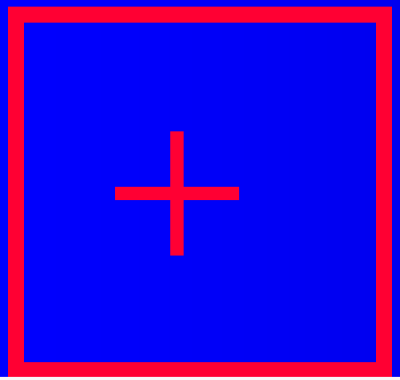

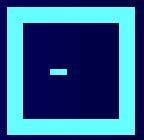

Hydrogen containing molecules

H_2 H_3^+

Hydrogen + carbon containing molecules

CH	CH^+	CH_2	C_2	C_2H	C_3	C_2H_2	l - C_3H	c-C_3H
*CH_4	H_2CCC	c-C_3H_2	C_4H	*C_5	*C_2H_4	*C_5H	C_4H_2	l - H_2C_4
*C_6H	CH_3C_2H	*C_7H	C_6H_2	l - H_2C_6	*C_8H	CH_3C_4H	c-C_6H_6	

Hydrogen + oxygen + carbon containing molecules

OH	CO	CO^+	H_2O	HCO	HCO^+	HOC^+	C_2O	CO_2
H_3O^+	$HOCO^+$	H_2CO	C_3O	CH_2CO	HCOOH	H_2COH^+	CH_3OH	C_5O
HC_2CHO	CH_3CHO	c-CH_2OCH_2	CH_2CHOH	CH_3COOH	$HCOOCH_3$	C_2H_5OH	$H_2COHCHO$	CH_3OCH_3
CH_3CH_2OH	$(CH_3)_2CO$	$CH_3OC_2H_5$	$(C_2H_5)_2O$	$(CH_2OH)_2$				

Hydrogen + nitrogen + carbon containing molecules

NH	CN	N_2	HCN	HNC	N_2H^+	NH_2	NH_3	$HCNH^+$
H_2CN	HCCN	C_3N	CH_2NH	HC_2CN	HC_2NC	HNCCC	NH_2CN	CH_2CN
CH_3CN	CH_3NC	HC_3NH^+	CH_3NH_2	C_5N	CH_2CHCN	HC_4CN	CH_3C_2CN	CH_3CH_2CN
HC_6CN	HC_7CN	$HC_{10}CN$						

Hydrogen + nitrogen + oxygen + carbon containing molecules

NO	HNO	N_2O	HNCO	NH_2CHO

Other species

CS	SO	SO^+	SN	*SiC	SiN	SiO	SiS	HCl
HF	*CP	*NaCl	*AlCl	*KCl	*AlF	PN	C_2S	SO_2
OCS	HCS^+	H_2S	c-SiC_2	H_2CS	HNCS	C_3S	*$HSiC_2$?	SiC_3
*SiH_4	*SiC_4	C_5S	CH_3SH	*NaCN	*MgCN	*MgNC	SiCN	c-CH_2SCH_2

Motivations

- H_3^+ is the cornerstone of ion-molecule reactions in the interstellar medium (ISM)
- Simple chemistry allows for the inference of various physical parameters (density, temperature, ionization rate, cloud size)

Table 1 Classification of Interstellar Cloud Types

	Diffuse Atomic	Diffuse Molecular	Translucent	Dense Molecular
Defining Characteristic	$f^n_{H_2} < 0.1$	$f^n_{H_2} > 0.1$ $f^n_{C+} > 0.5$	$f^n_{C+} < 0.5$ $f^n_{CO} < 0.9$	$f^n_{CO} > 0.9$
A_V (min.)	0	~0.2	~1–2	~5–10
Typ. n_H (cm^{-3})	10–100	100–500	500–5000?	$>10^4$
Typ. T (K)	30–100	30–100	15–50?	10–50
Observational Techniques	UV/Vis H I 21-cm	UV/Vis IR abs mm abs	Vis (UV?) IR abs mm abs/em	IR abs mm em

Importance of Interstellar H_3^+

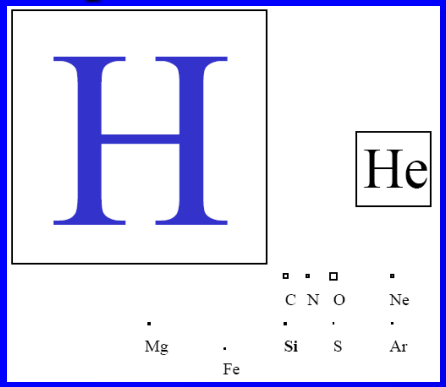

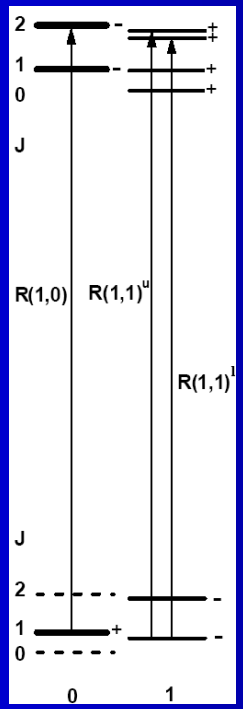

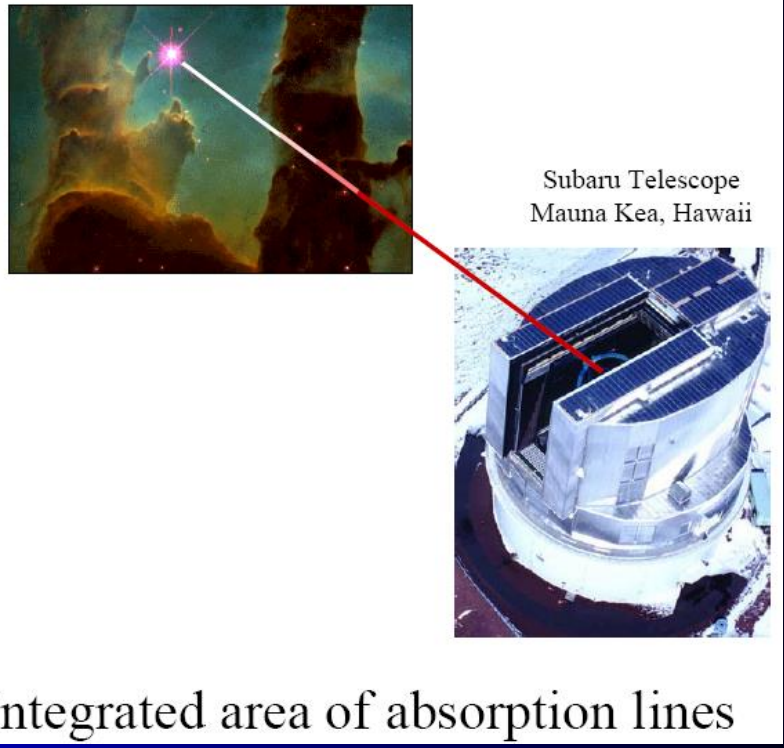

Table 2 Molecules detected in diffuse molecular clouds

Weight	Species	Method	Target	$N(X)/N_H$	Reference
2	H_2	UV	ζ Oph	0.56	1
3	HD	UV	ζ Oph	4.5 (−7)	2
3	H_3^+	IR	ζ Per	5.1 (−8)	3
13	CH	Optical	ζ Oph	1.5 (−9)	4
13	CH^+	Optical	ζ Oph	2.4 (−8)	5
14	$^{13}CH^+$	Optical	ζ Oph	3.5 (−10)	6
15	NH	Optical	ζ Oph	6.2 (−10)	7
17	OH	UV	ζ Oph	3.3 (−8)	8
24	C_2	Optical	ζ Oph	1.3 (−8)	9
25	C_2H	mm abs.	BL Lac	1.8 (−8)	10
26	CN	Optical	ζ Oph	1.9 (−9)	11
27	HCN	mm abs.	BL Lac	2.6 (−9)	12
27	HNC	mm abs.	BL Lac	4.4 (−10)	12
28	N_2	UV	HD 124314	3.1 (−8)	13
28	CO	UV	X Per	6.4 (−6)	14
29	HCO^+	mm abs.	BL Lac	1.5 (−9)	15
29	HOC^+	mm abs.	BL Lac	2.2 (−11)	15
29	^{13}CO	UV	X Per	8.9 (−8)	16
29	$C^{17}O$	UV	X Per	7.4 (−10):	16
30	$C^{18}O$	UV	X Per	2.1 (−9):	16
30	H_2CO	mm abs.	BL Lac	3.7 (−9)	17
36	C_3	Optical	ζ Oph	1.1 (−9)	18
36	HCl	UV	ζ Oph	1.9 (−10)	19
38	C_3H_2	mm abs.	BL Lac	6.4 (−10)	10
44	CS	mm abs.	BL Lac	1.6 (−9)	20
64	SO_2	mm abs.	BL Lac	≤8.2 (−10)	20

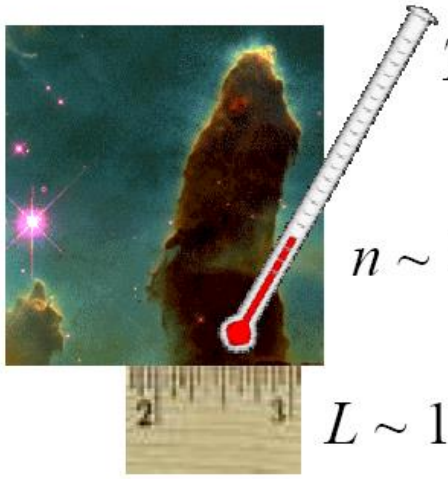

Balance in ISM

Cosmic-ray ionisation rate $\gamma \sim 3 \times 10^{-17} s^{-1}$

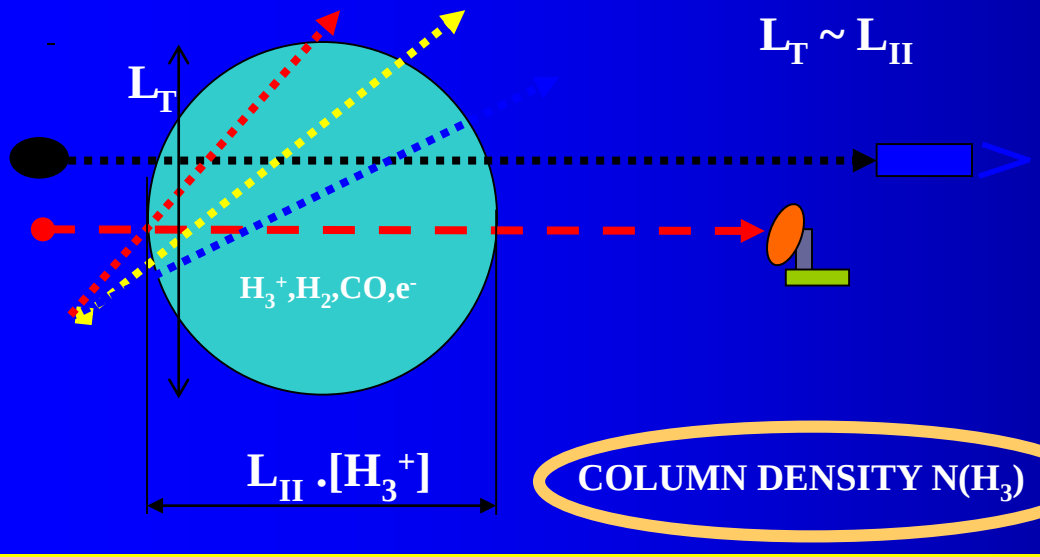

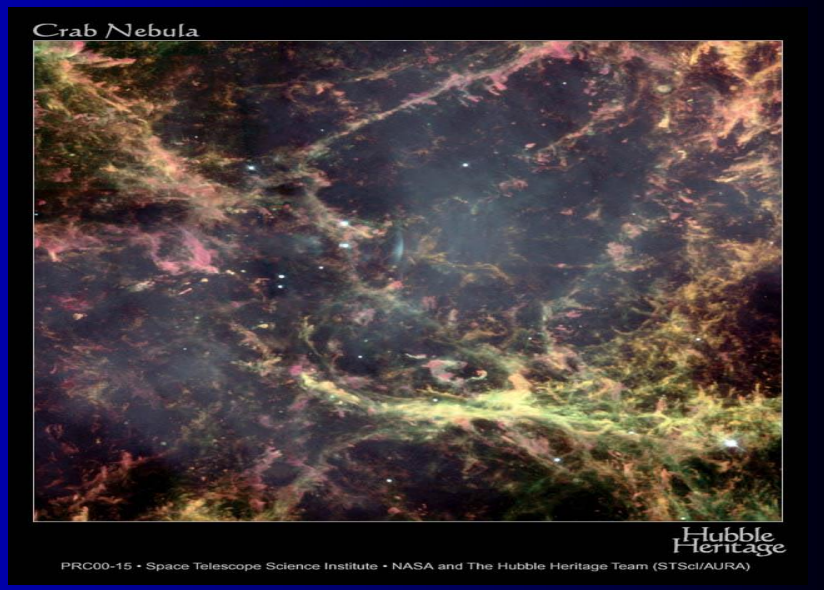

COLUMN DENSITY $N(H_3)$

PRODUCTION: $H_2 \xrightarrow{h\nu} H_2^+ \xrightarrow{H_2} H_3^+$ $\quad d[H_3^+]/dt \sim \gamma . [H_2]$

a) DENSE CLOUDS: DESTRUCTION:

$H_3^+ + CO \rightarrow HCO^+ + H_2$

$k_{CO} = 2 \times 10^{-9} cm^3 s^{-1}$

$d[H_3^+]/dt \sim -k_{CO} x [H_3^+] x [CO]$

$[H_3^+] = \gamma / k_{CO} . [H_2]/[CO] = \sim 1 \times 10^{-4} cm^{-3}$

~OK with observation

b) DIFFUSE CLOUDS: DESTRUCTION: $H_3^+ + e^-$

$d[H_3^+]/dt \sim - \alpha_{DR} [H_3^+][e^-]$

$[e^-] \sim [C]$

$\alpha_{DR} = 2 \times 10^{--7} cm^3 s^{-1} x (T/300)^{-0.65}$?

$[H_3^+] = \gamma / \alpha_{DR} . [H_2]/[C] = \sim 1 \times 10^{-7} cm^{-3}$

~ NO with observation

b) DIFFUSE CLOUDS: DESTRUCTION: $H_3^+ + e^-$

$d[H_3^+]/dt \sim - \alpha_{DR} [H_3^+][e^-]$

$[e^-] \sim [C]$

$\alpha_{DR} = 2 \times 10^{--7} cm^3 s^{-1} \times (T/300)^{-0.65}$?

$[H_3^+] = \gamma / \alpha_{DR} \cdot [H_2]/[C] = \sim 1 \times 10^{-7} cm^{-3}$

~ NO with observation

??????????

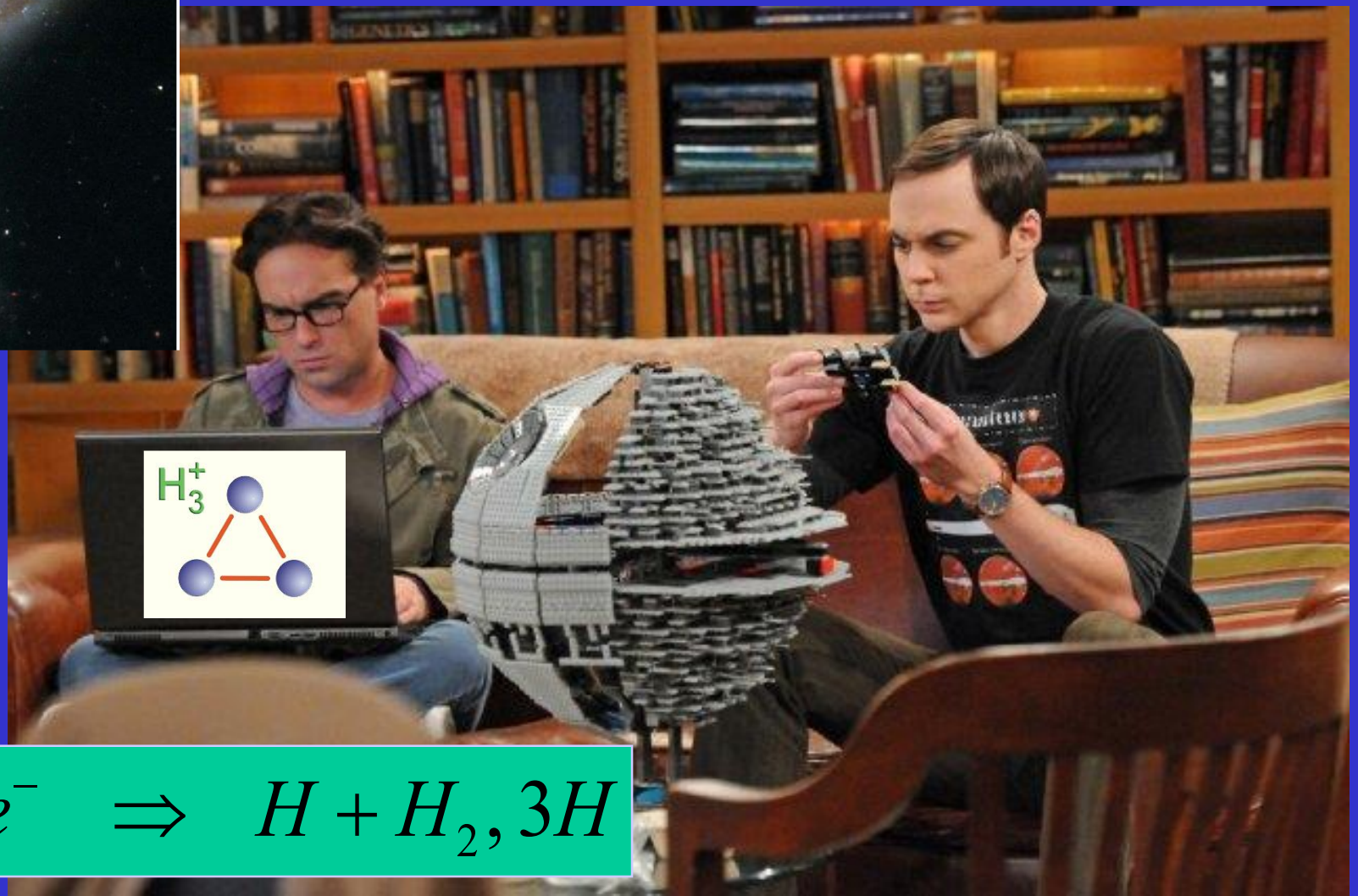

$$H_3^+ + e^- \Rightarrow H + H_2, 3H$$

Interstellar medium

92.1% of nucleons in the universe are protons
7.8% are helium nuclei !
0.1%……C,N,O,S,Si….

Cosmic abundance

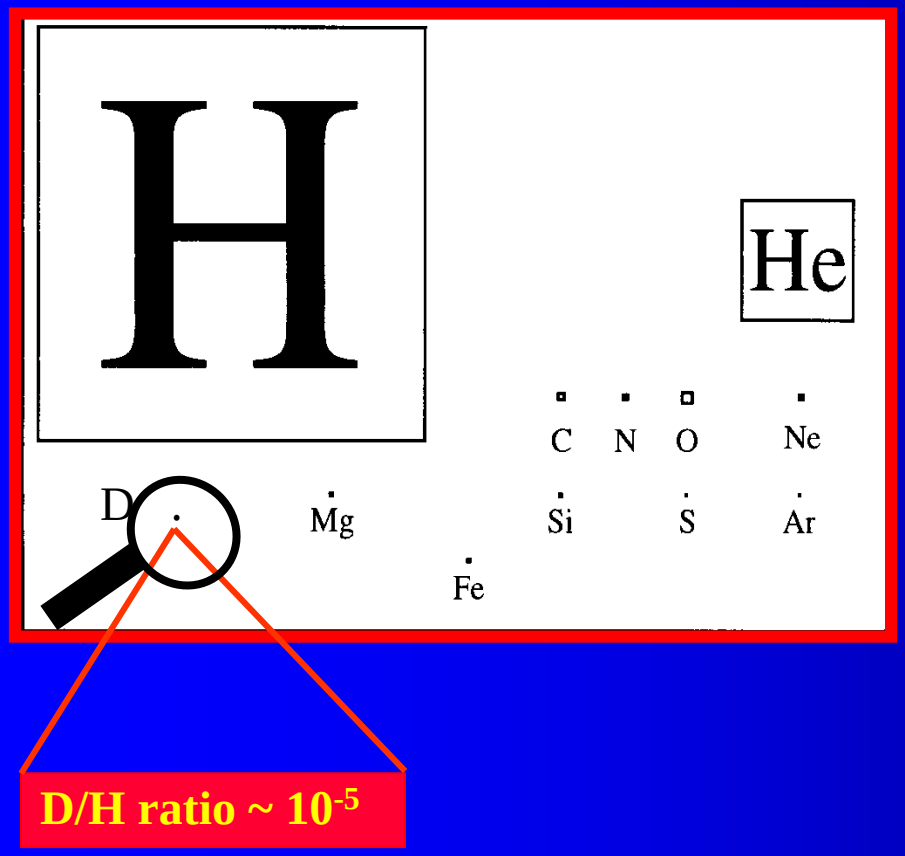

D/H ratio ~ 10^{-5}

@ 10-50K

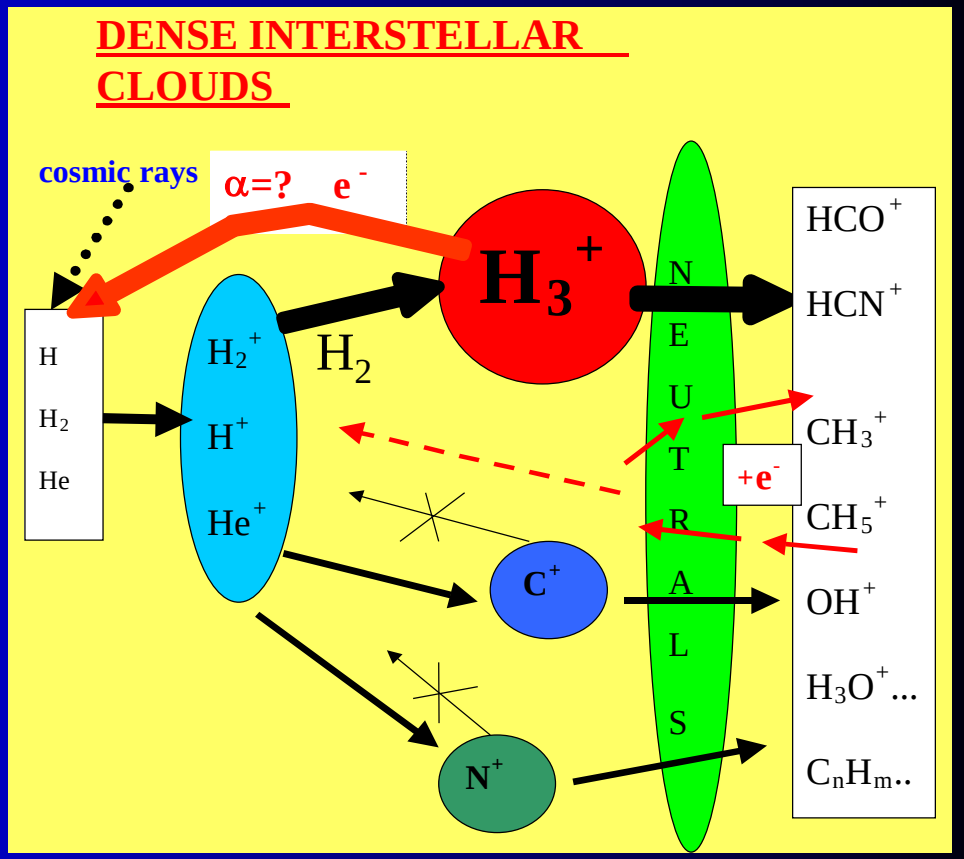

$$H_3^+ + e^- \xrightarrow{\alpha} neutral\ products$$

α (10 K) = ????

Interstellar medium, HD role

@ 10-50K

92.1% of nucleons in the universe are protons
7.8% are helium nuclei !
0.1%……C,N,O,S,Si….

Cosmic abundance

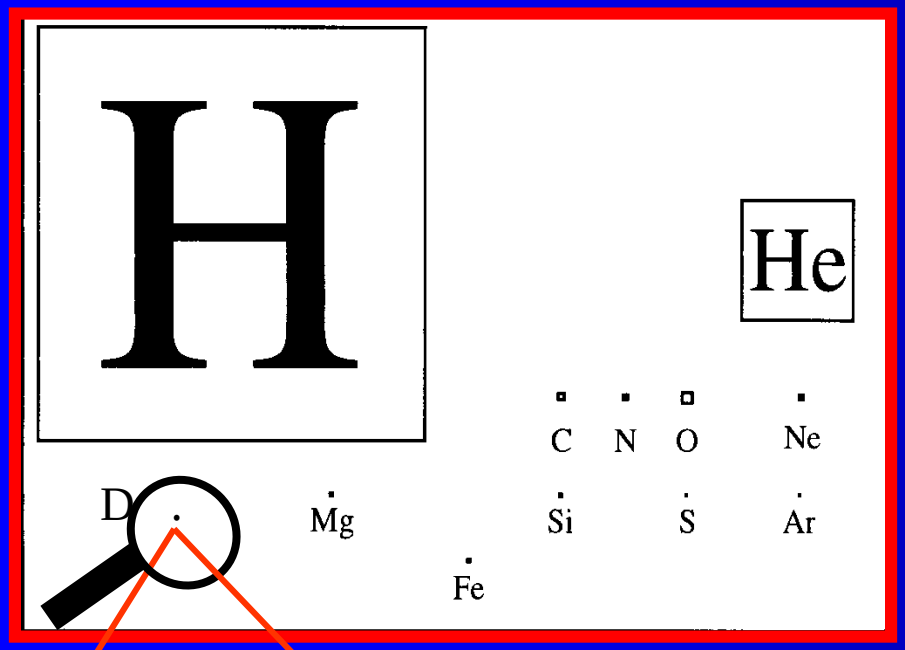

D/H ratio ~ 10^{-5}

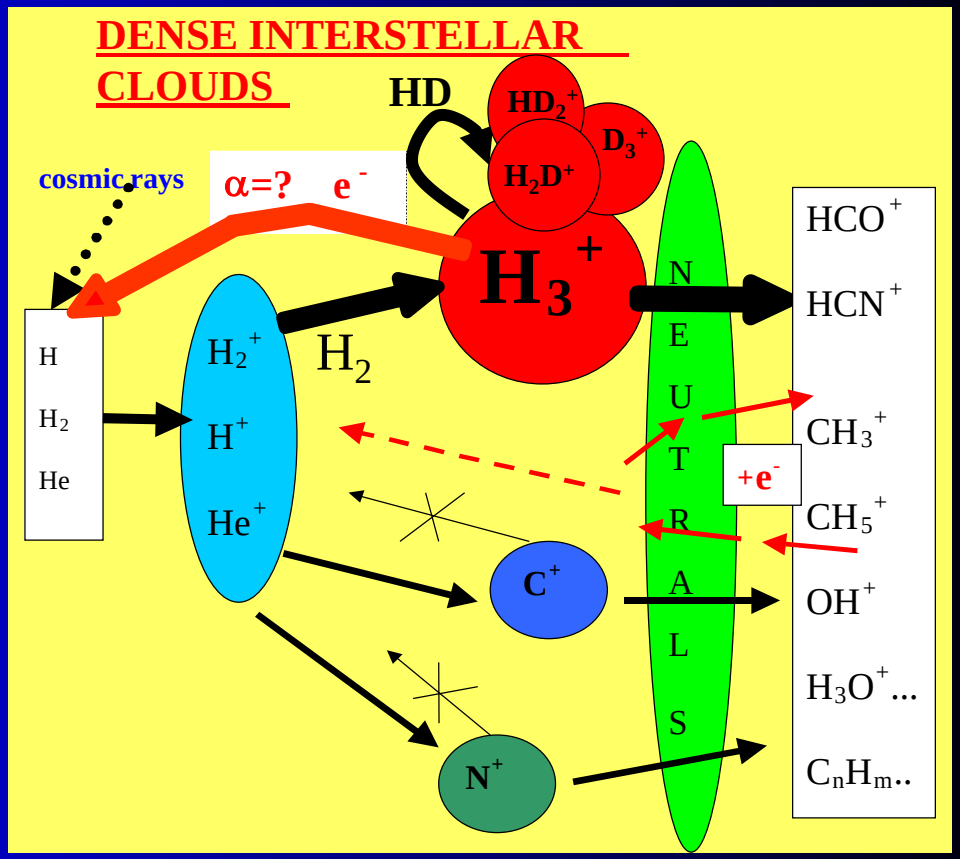

$$H_3^+ + e^- \xrightarrow{\alpha} \text{neutral products}$$

α (10 K) = ???? **k (10 K) = ????**

$$H_3^+ \xrightarrow{HD} H_2D^+ \xrightarrow{HD} HD_2^+ \xrightarrow{HD} D_3^+$$

Emotional history of experiments

–"time evolution" of $\alpha(H_3^+)$, $\alpha(D_3^+)$

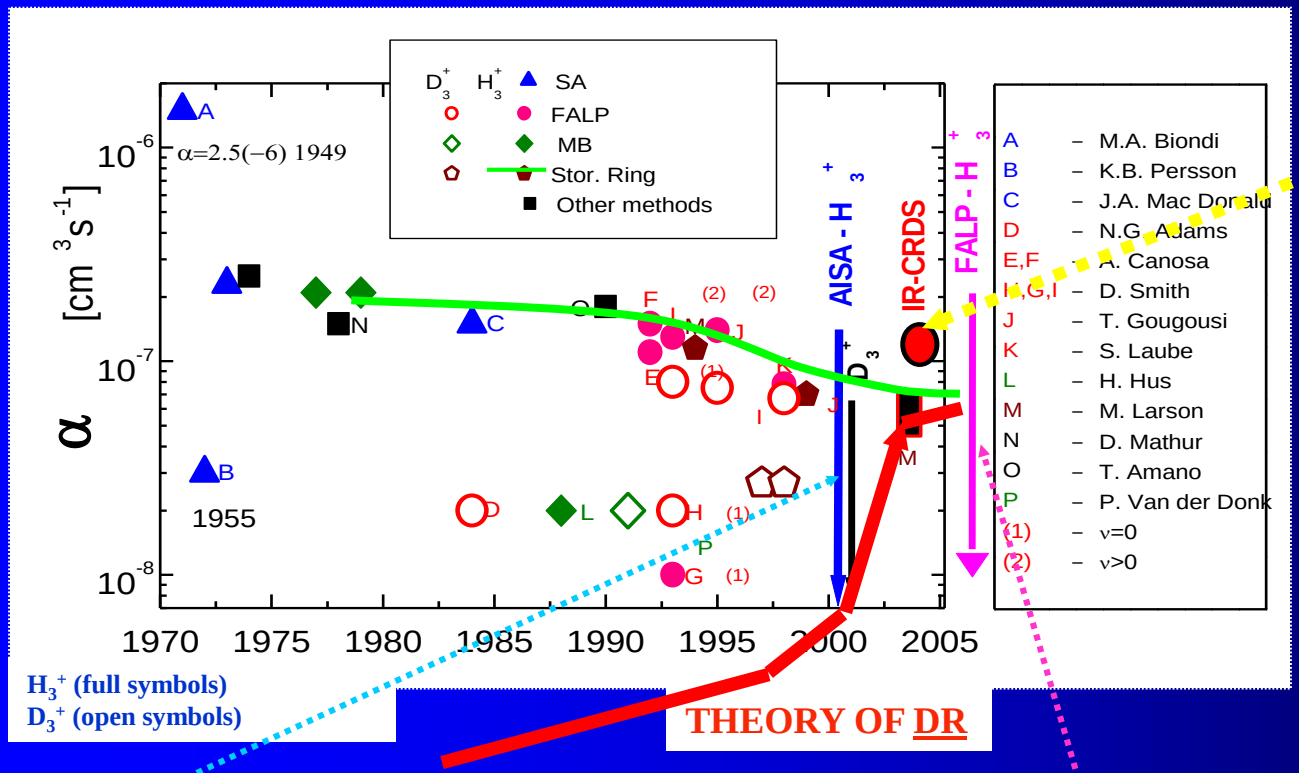

H_3^+ (full symbols)
D_3^+ (open symbols)

THEORY OF DR

CRDS

μw discharge cell

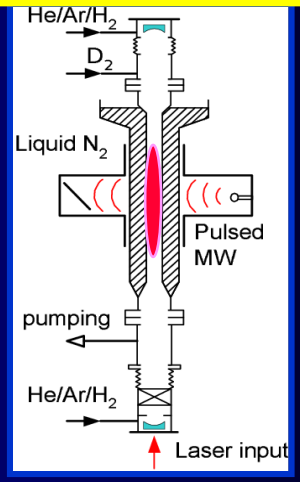

IR spectroscopy

AISA

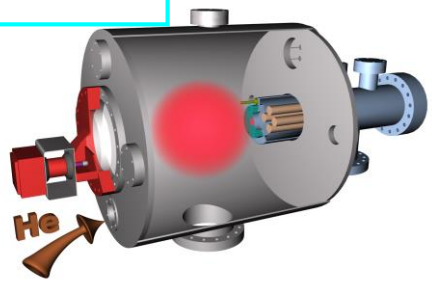

FALP

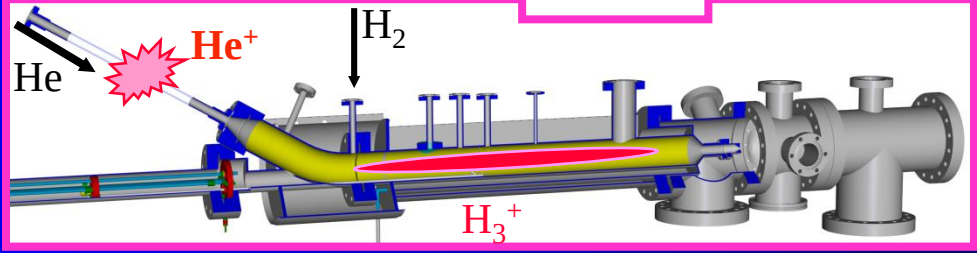

Small problems and post consonance studies

During 2000-6
The theory and well defined storage ring experiments (internally cold ions)
obtained agreement : **$\alpha(T=300\ K) = 7x10^{-8}\ cm^3s^{-1}$**

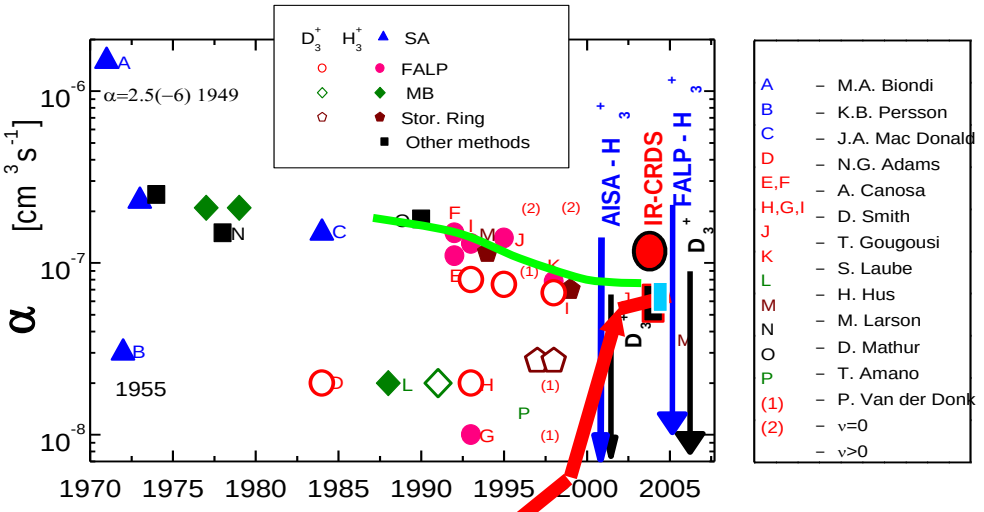

THEORY OF DR

Small problems:

-Disagreement with some Afterglow experiments
N. Adams & D. Smith; D. Smith & P. Spanel;….
R. Johnsen, Amanno

-Observation of Rydberg H_3 in plasma
- Merged-beam experiment in which the deflection field used to separate product neutrals from the ions in the post-collision region was varied It was found that the measured DR product signal increased by a factor of five (approaching that obtained in ISR experiments) when the field strength in that region was reduced from 3000 V/cm to 200 V/cm. (**R. Johnsen Mosbach)**

RYDBERG STATES **H_3**

Herzberg: in emission from a hollow cathode discharge of H_2 (Herzberg *et al* 1979-82,Dabrowski & Herzberg 1980;

Helm: Fast-neutral-beam photoionization spectra of H_3 were observed (1986); high-n Rydberg states were identified. Cosby & Helm (1988) and Helm (1988) further measured the ionization potential and investigated the photodissociation processes.

Figger and co-workers (Figger *et al* . 1989; Ketterle *et al* . 1989) also observed the emission spectra by neutralizing the parent H_3^+ ion, and obtained the lifetimes of the Rydberg states.

Bjerre *et al* . (1991) performed high-resolution laser spectroscopy of a fast neutral beam of H_3 and observed the spin-splittings in the 3d states.
Amanno (2000) … $D_3^+ + D_2 \rightarrow D_5^+ + e \rightarrow D_3^* + \ldots$.
Etc.

The most direct observation that indicates production of H_3^{**} molecules from H_3^+ recombination comes from the merged-beam experiments of Mitchell [49]. He found that the apparent H_3^+ recombination cross-sections increased by a factor of about 5 when a "deflection field" (used to deflect unrecombined ions out of the beam before they strike the detector) was reduced in magnitude. This would suggest that the majority of $H_3^+ + e^-$ "recombination" events produces long-lived H_3^{**} Rydberg molecules. The role of electric

v=??cm/ns c=30cm/ns

80 % have life time few ns ???

Small problems or post consonance studies

During 2000-6
The theory and well defined storage ring experiments (internally cold ions)
obtained agreement : **$\alpha(T=300\ K) = 7x10^{-8}\ cm^3s^{-1}$**

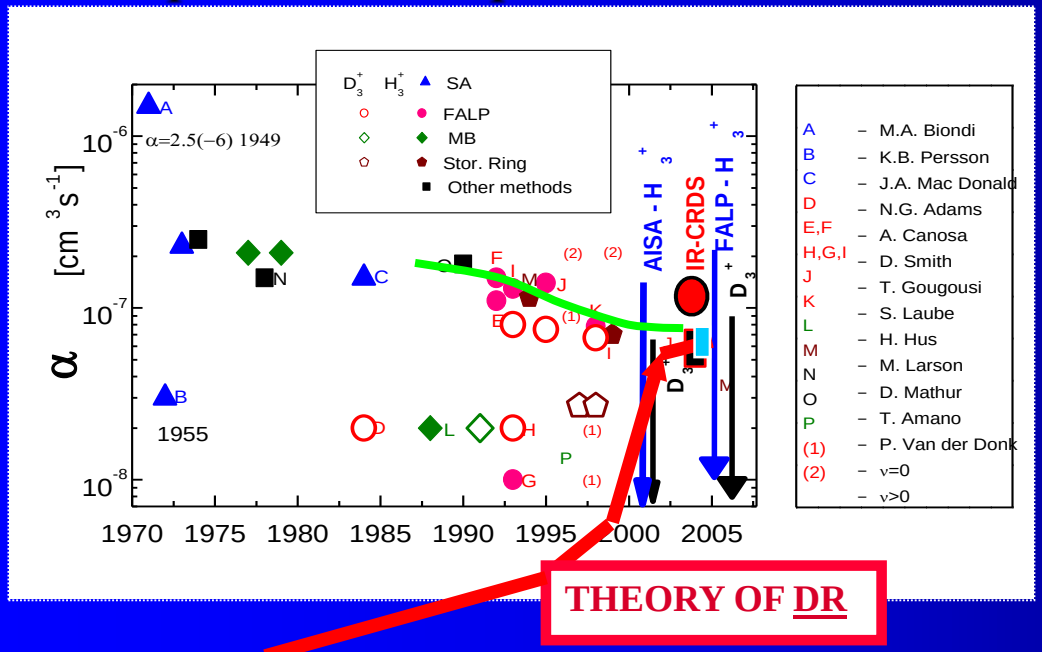

THEORY OF DR

Small problems:

-Disagreement with some Afterglow experiments
N. Adams & D. Smith; D. Smith & P. Spanel;….
R. Johnsen, Amanno

-Observation of Rydberg H_3 in plasma
- Merged-beam experiment in which the deflection field used to separate product neutrals from the ions in the post-collision region was varied It was found that the measured DR product signal increased by a factor of five (approaching that obtained in ISR experiments) when the field strength in that region was reduced from 3000 V/cm to 200 V/cm. (**R. Johnsen Mosbach)**

RYDBERG STATES **H_3**

Herzberg: in emission from a hollow cathode discharge of H_2 (Herzberg *et al* 1979-82,Dabrowski & Herzberg 1980;

Helm: Fast-neutral-beam photoionization spectra of H_3 were observed (1986); high-n Rydberg states were identified. Cosby & Helm (1988) and Helm (1988) further measured the ionization potential and investigated the photodissociation processes.

Figger and co-workers (Figger *et al* . 1989; Ketterle *et al* . 1989) also observed the emission spectra by neutralizing the parent H_3^+ ion, and obtained the lifetimes of the Rydberg states.

Bjerre *et al* . (1991) performed high-resolution laser spectroscopy of a fast neutral beam of H_3 and observed the spin-splittings in the 3d states.
Amanno (2000) … $D_3^+ + D_2 \rightarrow D_5^+ + e \rightarrow D_3^* + \ldots$.
Etc.

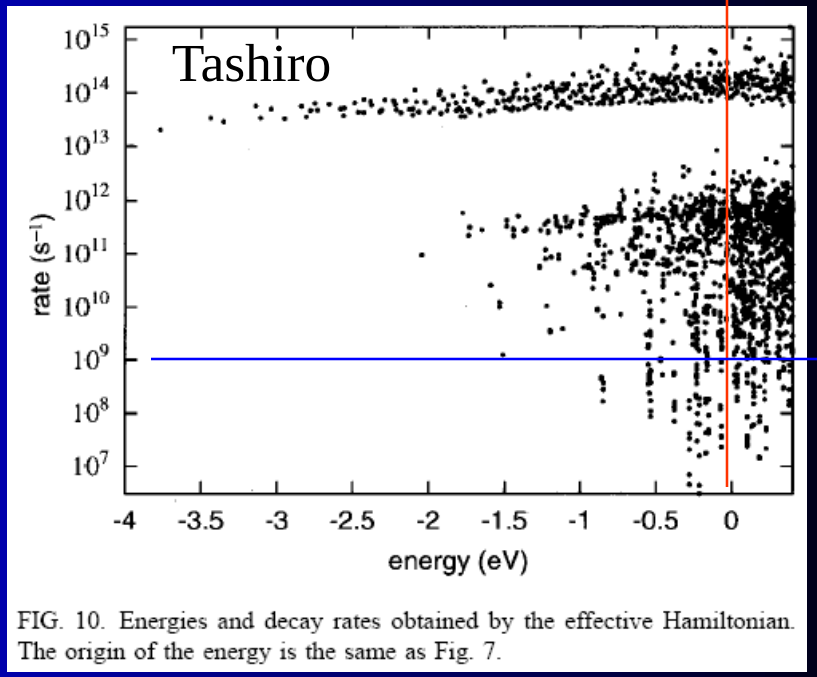

FIG. 10. Energies and decay rates obtained by the effective Hamiltonian. The origin of the energy is the same as Fig. 7.

Quo vadis ???

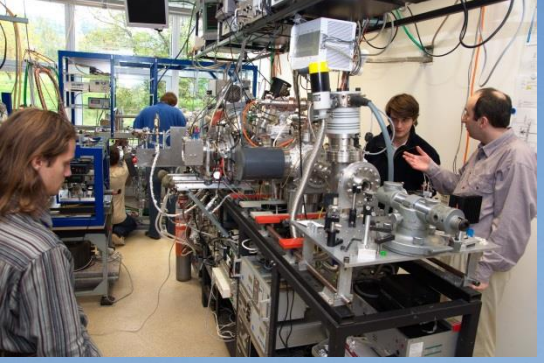

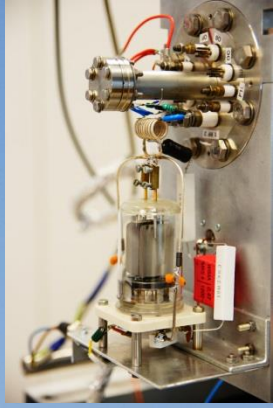

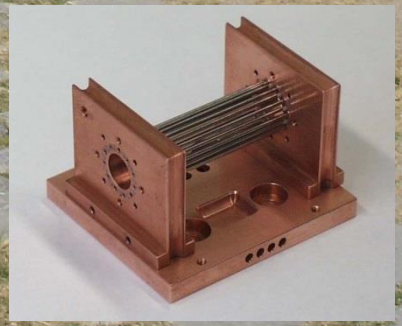

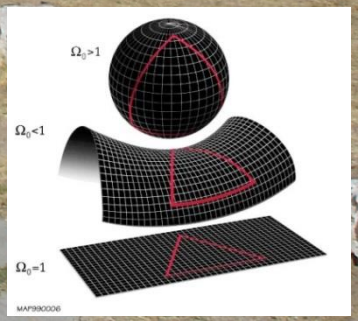

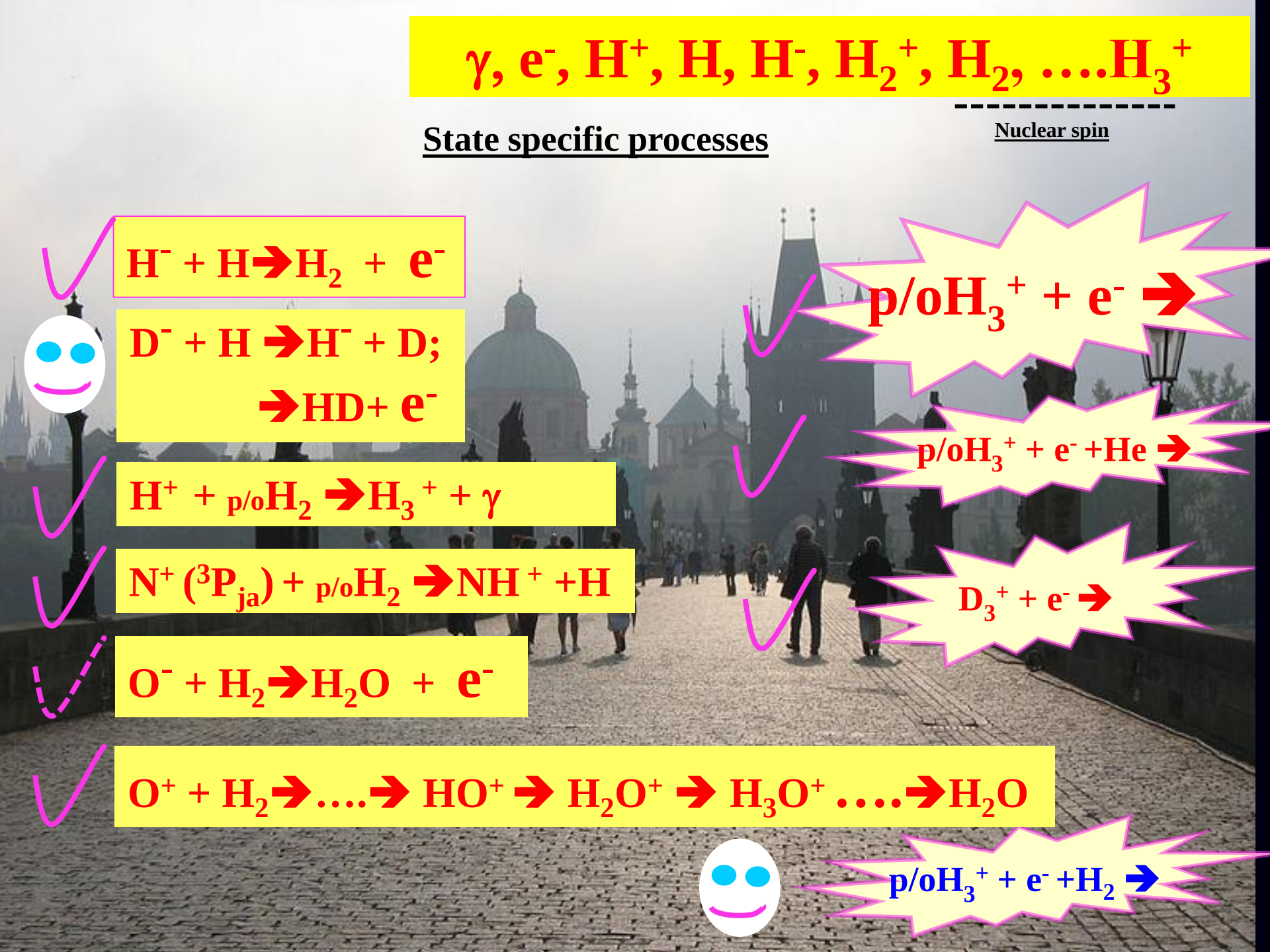
γ, e⁻, H⁺, H, H⁻, H₂⁺, H₂, ….H₃⁺
Nuclear spin
State specific processes
H⁻ + H→H₂ + e⁻
D⁻ + H →H⁻ + D;
→HD+ e⁻
H⁺ + p/oH₂ →H₃⁺ + γ
N⁺ (³P_ja) + p/oH₂ →NH⁺ +H
O⁻ + H₂→H₂O + e⁻
O⁺ + H₂→….→ HO⁺ → H₂O⁺ → H₃O⁺ ….→H₂O
p/oH₃⁺ + e⁻ →
p/oH₃⁺ + e⁻ +He →
D₃⁺ + e⁻ →
p/oH₃⁺ + e⁻ +H₂ →

Energies experiments

E/k←→T
1eV ~ 11 400 K
1K ~ 9x10^{-5}eV

Elekt. excitace
Vibrace
Rotace
Ionization
Kinetic energy

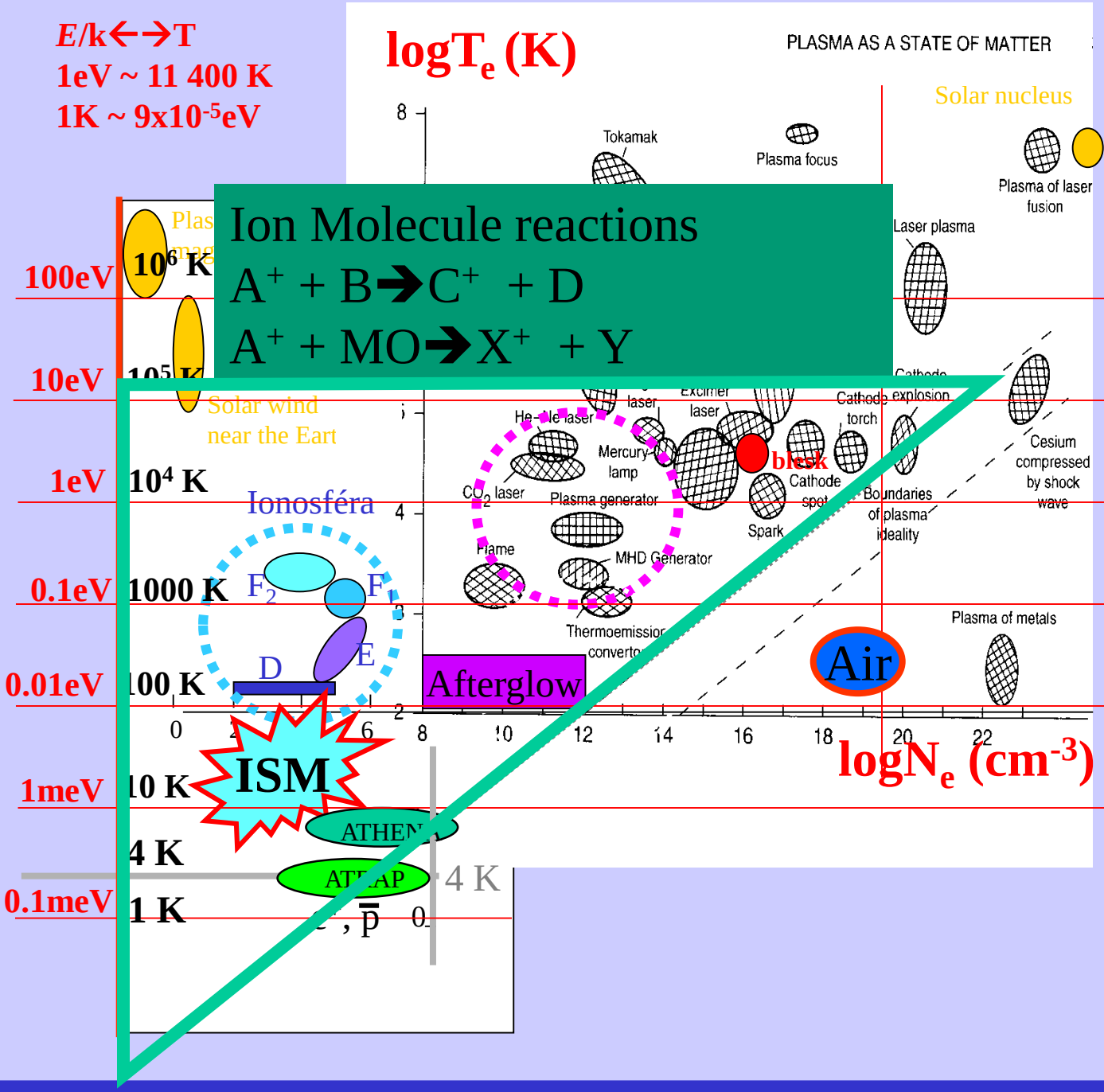

Energies experiments

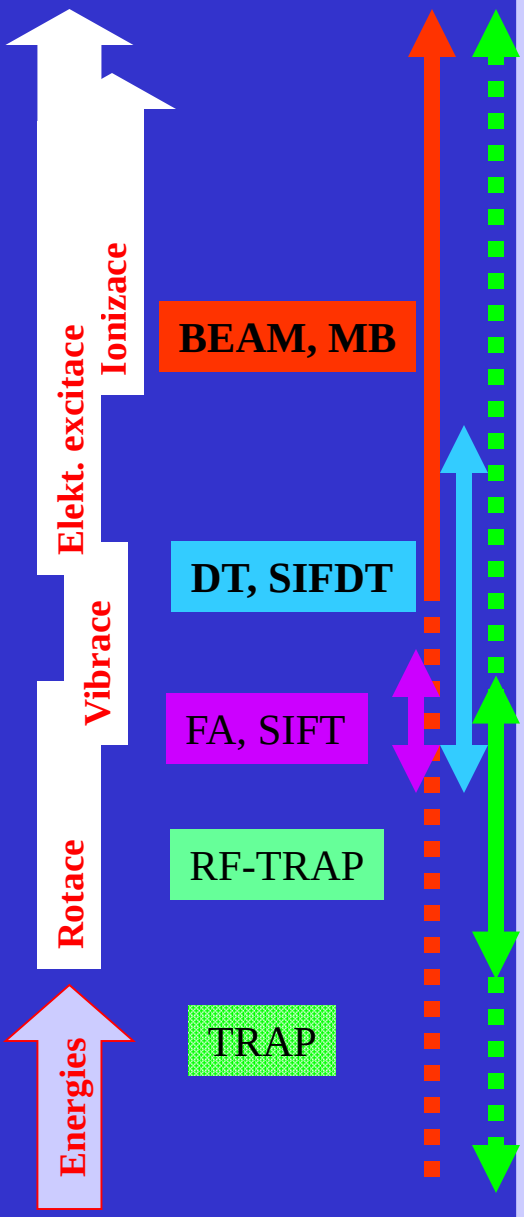

E/k←→T
1eV ~ 11 400 K
1K ~ 9x10^{-5}eV

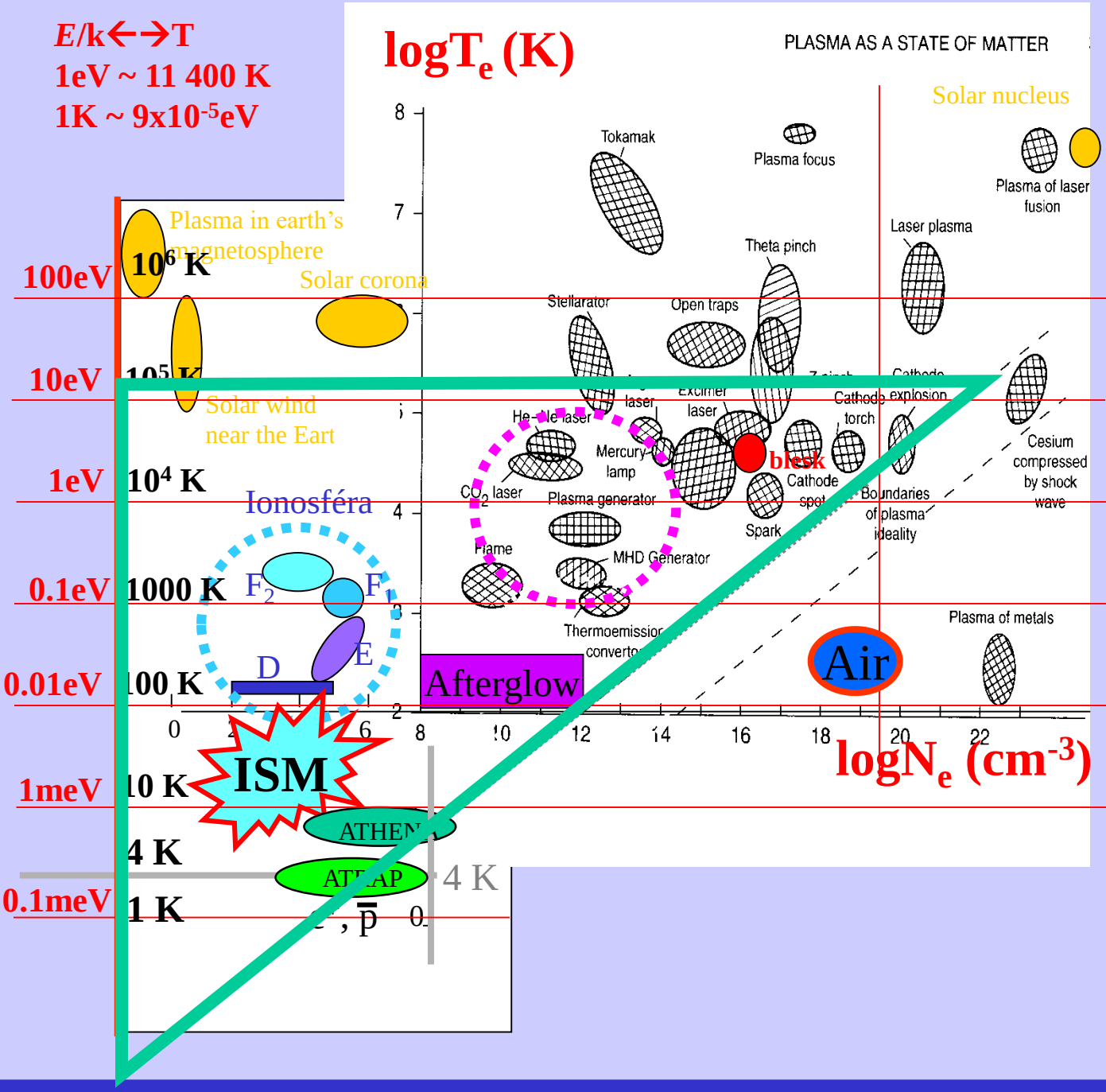

Binary reactions Reaction rate coefficient

$$A^+ + B \rightarrow C^+ + D$$

$$\frac{dA^+}{dt} = -k_{BIN} A^+ B$$

$$[k_{BIN}] = cm^3 s^{-1}$$

$$A^+ + B \rightarrow A_1^+ + C$$

$$\rightarrow A_2^+ + D$$

k (T) reaction rate coefficient

k_{coll}(T) collision rate coefficient

Single collision

$$H_2^+ + Ar \quad \Rightarrow \quad ArH^+ + H$$

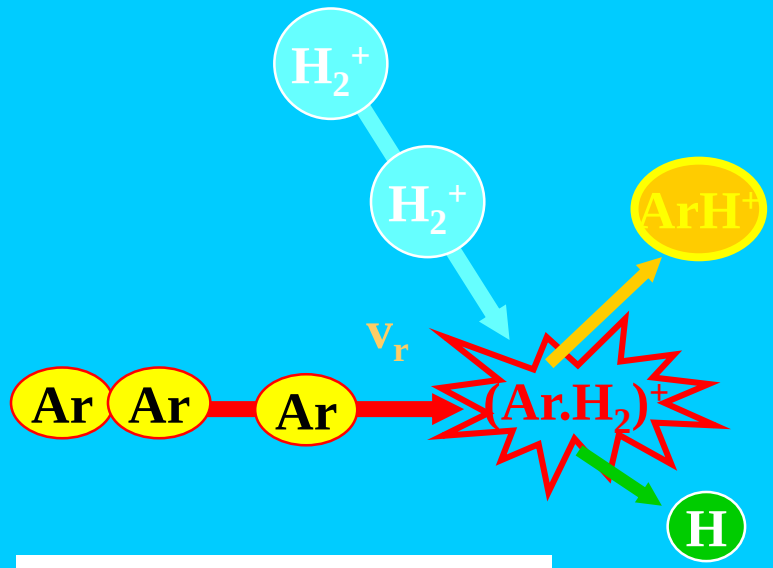

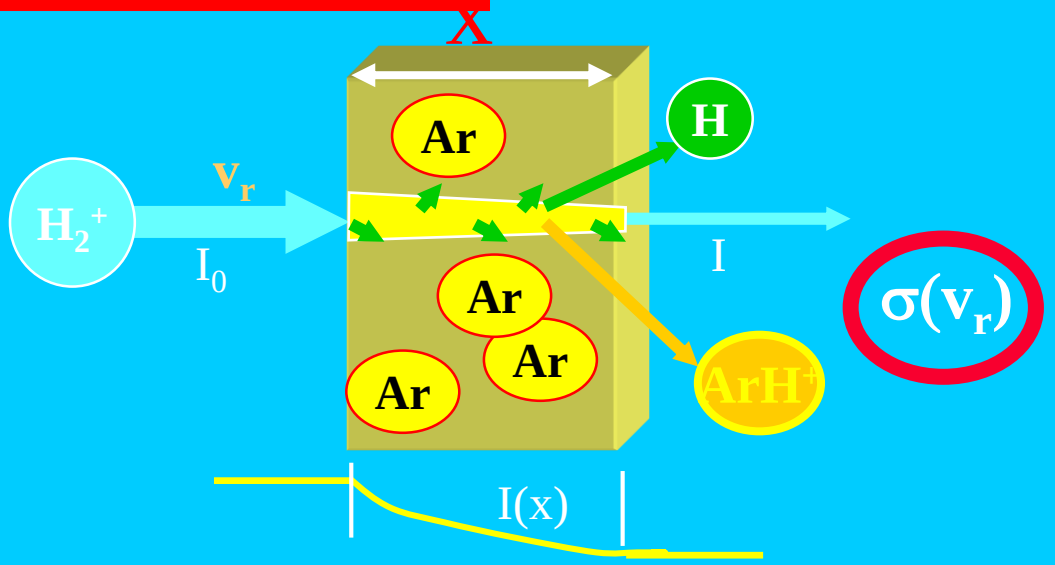

reaction cross section

$$I = I_0 \exp(-\sigma n_{Ar} x)$$

Proportionality factor

$$\frac{dI}{dx} \sim -IN \qquad \frac{dI}{dx} = -\sigma IN$$

$$\frac{dI}{Idx} = \frac{d\ln(I)}{dx} = -\sigma N$$

$$I(x) = I_0 \exp(-\sigma N x)$$

Single collision

$$H_2^+ + Ar \Rightarrow ArH^+ + H$$

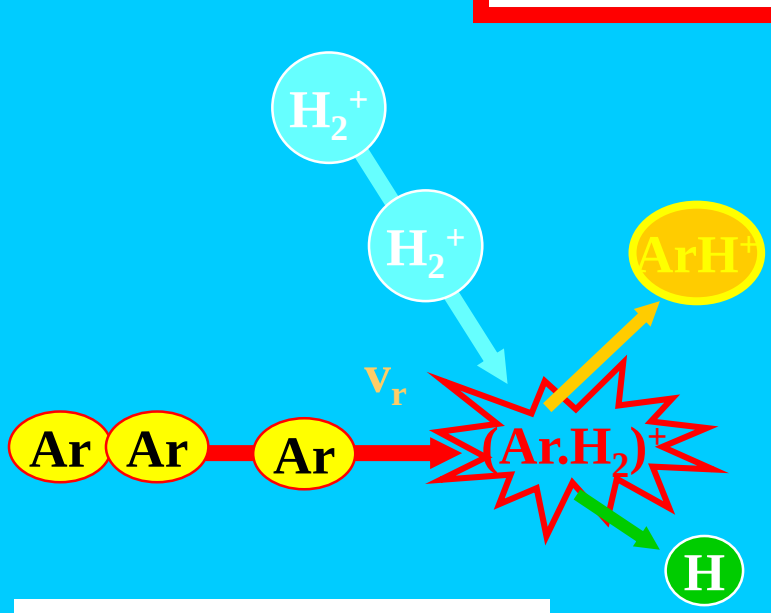

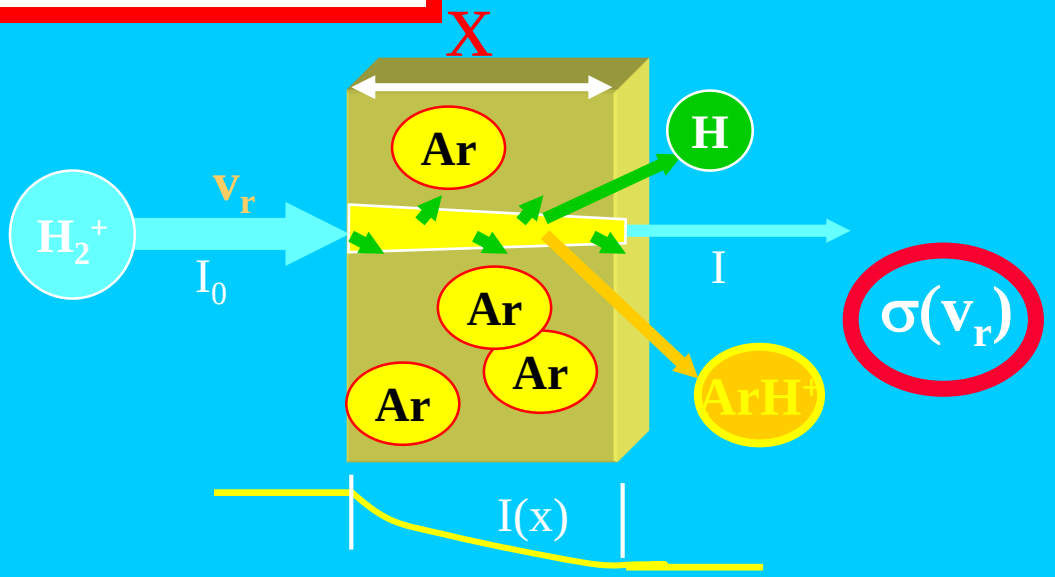

reaction cross section

$I=I_0\exp(-\sigma n_{Ar} x)$

$$\nu_{coll} = nV_{rel} = n\nu S = n\nu\pi\delta^2 = n\nu\sigma$$

$$\boldsymbol{\nu_{coll} = n\nu\sigma}$$

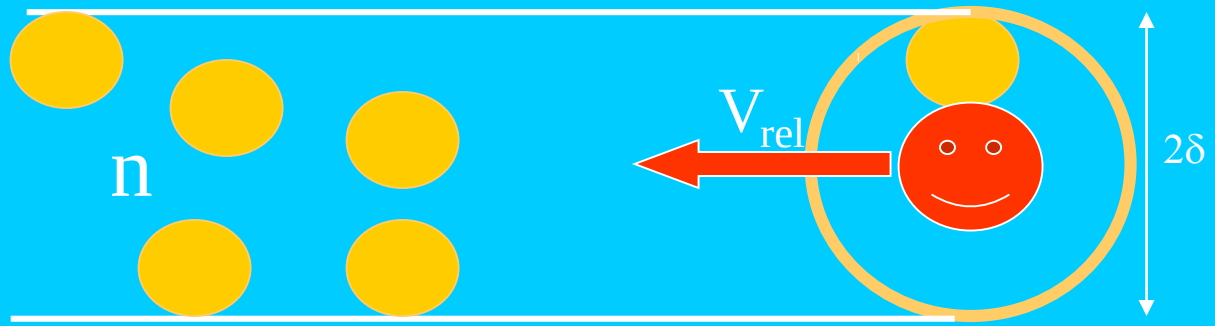

$$\frac{dI}{dt} = -\frac{I}{\tau_{coll}} = -I\nu_{coll}$$

$$I(t) = I_0 \exp(-\nu_{coll} t) = I_0 \exp(-\sigma n \nu_{rel} t)$$

Simple picture of ion – molecule interaction

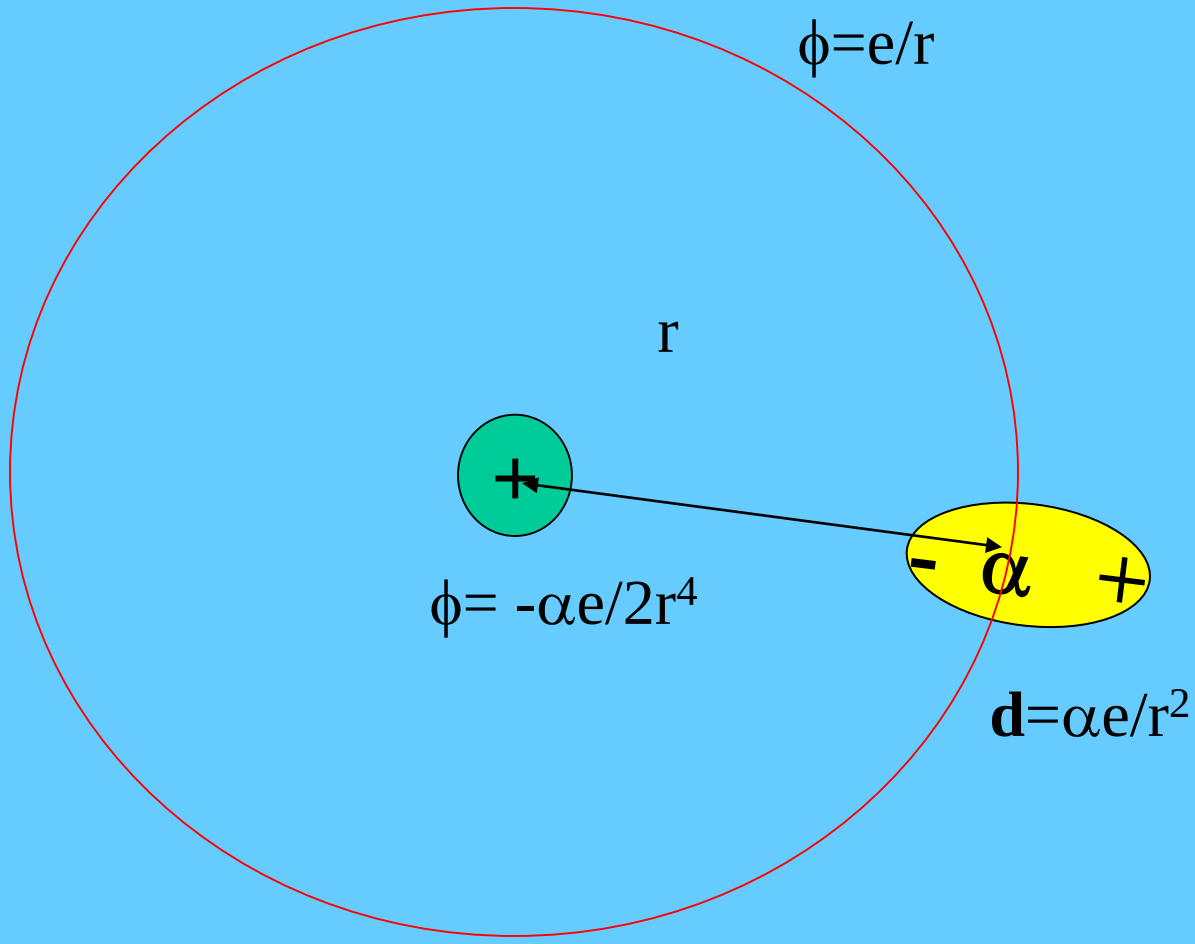

$E(ion) = 2d/r^3 = 2\alpha e/r^5$

$F(ion) = 2\alpha e^2/r^5$

α - polarisability

$U(pot) = -\alpha e^2/2r^4$

Two particles interaction

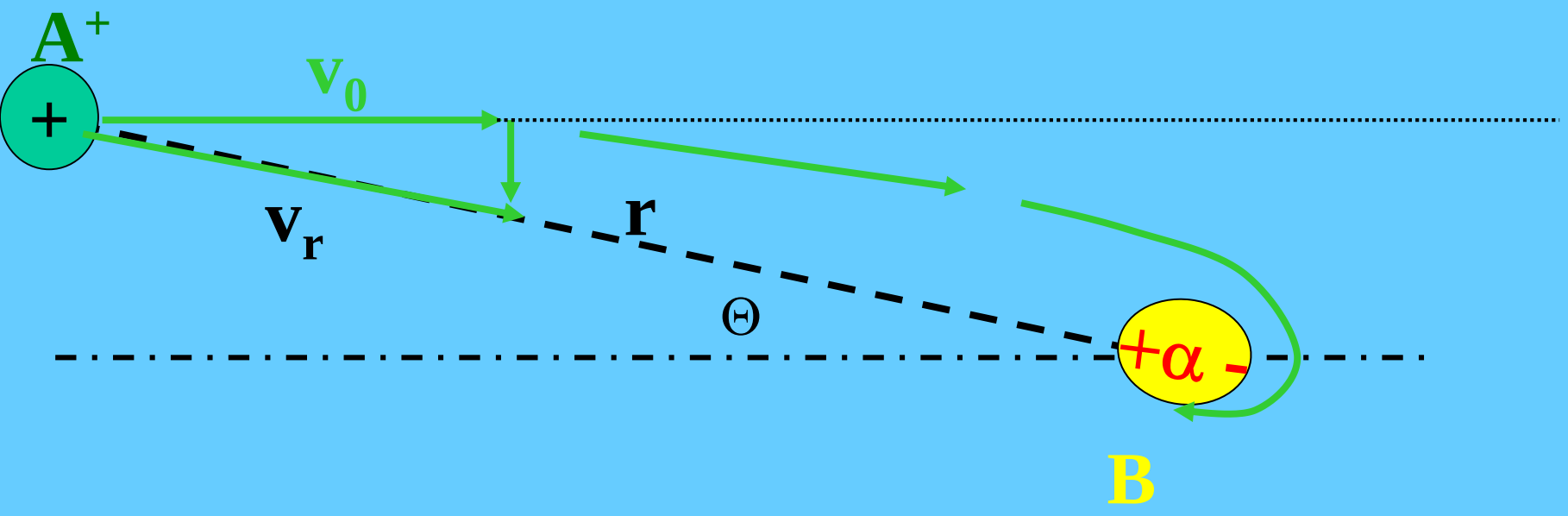

Simple picture

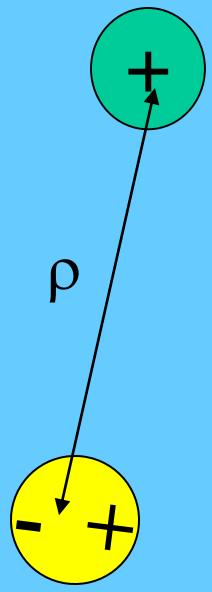

$F(\rho) \sim 2\alpha e^2/\rho^5$

$U(pot) = -\alpha e^2/2r^4$

$U(kin) = \mu v_0/2$

For U(pot) < U(kin) we have capture ➔

Capture is for $r<\rho$ where $U(\rho, pot) = U(\rho, kin)$

➔ $\mu v_0^2/2 = \alpha e^2/2\rho^4$

➔ $\sigma \sim \pi\rho^2 = \{\pi^2\alpha e^2/2\,(\mu v_0^2/2)\}^{1/2}$

➔ $\sigma \sim \pi e/v_0\,\{\alpha/\mu\}^{1/2}$

Using SI units: $$\sigma_0 = \pi\rho_0^2 = \frac{2\pi e}{v_0(4\pi\varepsilon_0)}\sqrt{\frac{\alpha}{\mu}}$$

Collision rate coefficient -Langevin rate coefficient

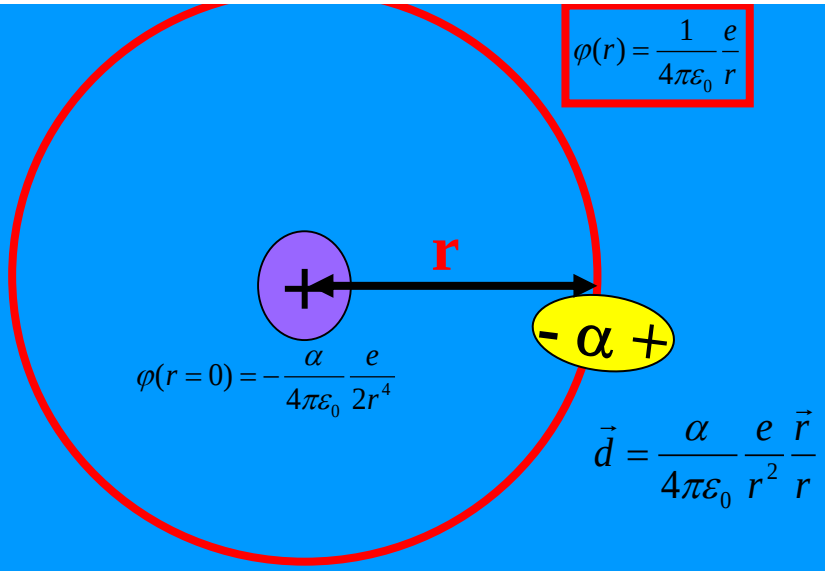

$$\varphi(r) = \frac{1}{4\pi\varepsilon_0}\frac{e}{r}$$

$$\varphi(r=0) = -\frac{\alpha}{4\pi\varepsilon_0}\frac{e}{2r^4}$$

$$\vec{d} = \frac{\alpha}{4\pi\varepsilon_0}\frac{e}{r^2}\frac{\vec{r}}{r}$$

α - polarizability

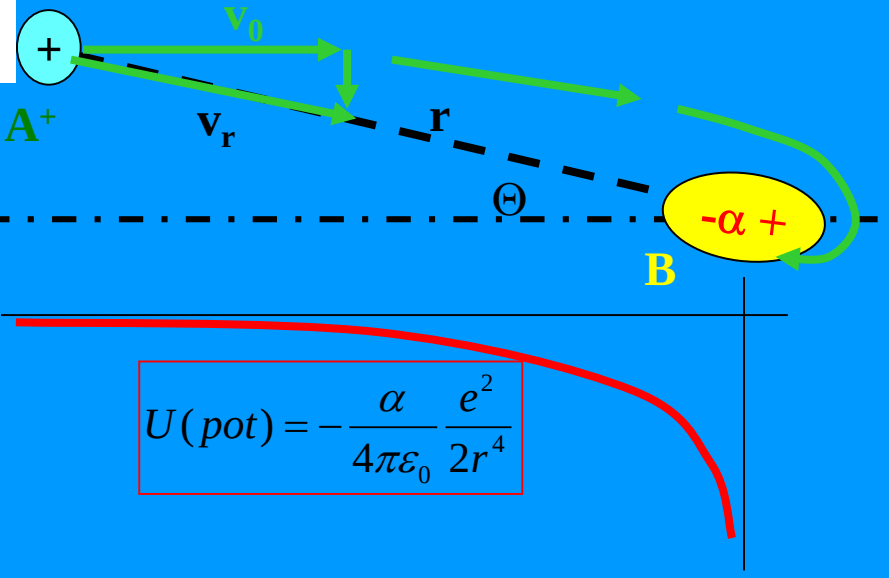

$$U(pot) = -\frac{\alpha}{4\pi\varepsilon_0}\frac{e^2}{2r^4}$$

pro U(pot) < U(kin) je záchyt ➔
Záchyt pro r<ρ kde U(ρ, pot) = U(ρ, kin)

$$\frac{\mu v_0^2}{2} = \frac{\alpha}{4\pi\varepsilon_0}\frac{e^2}{2r^4}$$

Ion-molecule interaction

Collision cross section of IMR

Langevin cross section of IMR

$$\sigma = \pi\rho_0^2 = \frac{2\pi e}{v_0}\sqrt{\frac{\alpha}{4\pi\varepsilon_0\mu}}$$

$k_{coll}(T)$ collision rate coefficient

Langevin rate coefficient

$$\sigma = \pi\rho_0^2 \sim \frac{1}{v_0}\sqrt{\frac{\alpha}{\mu}} \sim \frac{1}{\sqrt{E}}$$

Collision cross section of IMR

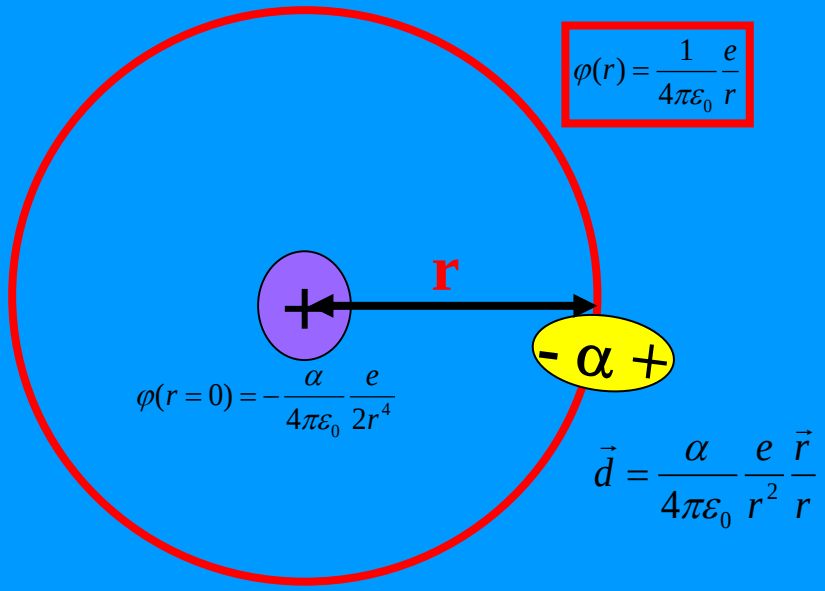

$$\varphi(r) = \frac{1}{4\pi\varepsilon_0}\frac{e}{r}$$

$$\varphi(r=0) = -\frac{\alpha}{4\pi\varepsilon_0}\frac{e}{2r^4}$$

$$\vec{d} = \frac{\alpha}{4\pi\varepsilon_0}\frac{e}{r^2}\frac{\vec{r}}{r}$$

α - polarizovatelnost

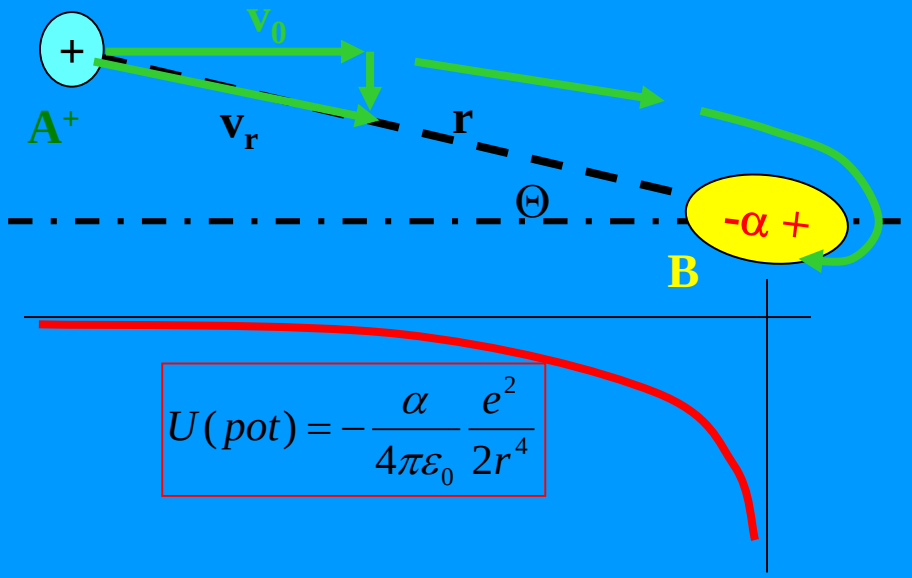

$$U(pot) = -\frac{\alpha}{4\pi\varepsilon_0}\frac{e^2}{2r^4}$$

pro U(pot) < U(kin) je záchyt ➔
Záchyt pro r<ρ kde U(ρ, pot) = U(ρ, kin)

$$\frac{\mu v_0^2}{2} = \frac{\alpha}{4\pi\varepsilon_0}\frac{e^2}{2r^4}$$

$$\sigma = \pi\rho_0^2 = \frac{2\pi e}{v_0(4\pi\varepsilon_0)}\sqrt{\frac{\alpha}{\mu}}$$

$$\sigma = \pi\rho_0^2 \sim \frac{1}{v_0}\sqrt{\frac{\alpha}{\mu}} \sim \frac{1}{\sqrt{E}}$$

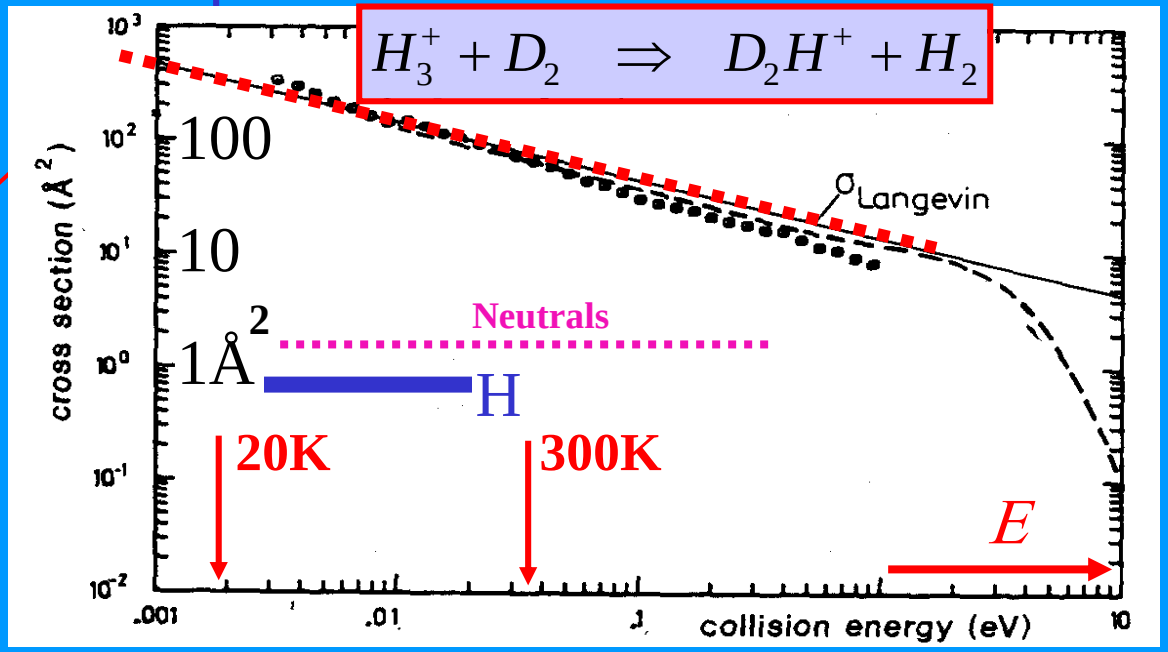

Simple picture

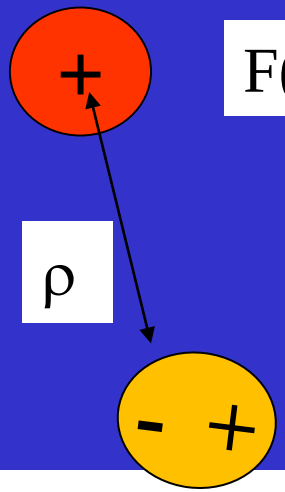

$F(\rho) \sim 2\alpha e^2/\rho^5$

$U(pot) = -\alpha e^2/2r^4$

$U(kin) = \mu v_0/2$

For U(pot) < U(kin) we have capture ➔

Capture is for $r<\rho$ where $U(\rho, pot) = U(\rho, kin)$

➔ $\mu v_0^2/2 = \alpha e^2/2\rho^4$

➔ $\sigma \sim \pi\rho^2 = \{\pi^2\alpha e^2/2\,(\mu v_0^2/2)\}^{1/2}$

➔ $\boldsymbol{\sigma \sim \pi e/v_0\,\{\alpha/\mu\}^{1/2}}$

Using SI units:

$$\sigma_0 = \pi\rho_0^2 = \frac{2\pi e}{v_0(4\pi\varepsilon_0)}\sqrt{\frac{\alpha}{\mu}}$$

Ion induced dipole interaction

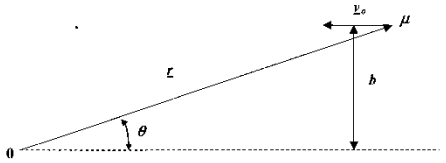

Figure 1
The coordinates for an ion–molecule collision in the scattering center system. The vector **r** with polar coordinate r and θ indicates the position of a particle of reduced mass μ relative to the stationary scattering center at the origin. The vector $\mathbf{v}_0$ indicates the initial relative velocity and b the impact parameter.

$$E = (1/2)\mu v_0^2$$

$$E = (1/2)\mu(\dot{r}^2 + r^2\dot{\theta}^2) + V(r)$$

$$L = \mu v_0 b = \mu r^2 \dot{\theta}$$

$$E = (1/2)\mu\dot{r}^2 + (1/2)\mu r^2\dot{\theta}^2 + V(r)$$

$$U(r) = (1/2)\mu r^2\dot{\theta}^2 + V(r)$$

$$U(r) = \frac{Eb^2}{r^2} + V(r)$$

$$E = (1/2)\mu\dot{r}^2 + U(r)$$

metastabile orbit

$$(1/2)\mu\dot{r}^2 = 0 \quad \Rightarrow E = U(r_0)$$

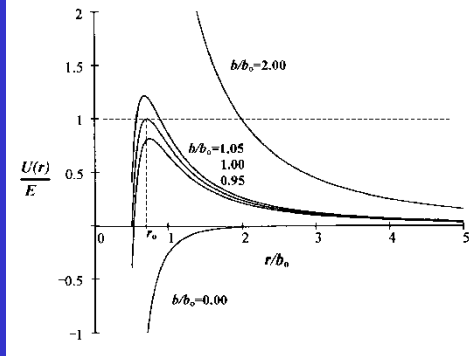

Figure 3
Plots of the effective potential *vs.* r from Eqn. (9). For a fixed energy the plots represent the indicated impact parameters b. Turning points occur where the horizontal dashed line intersects a $U(r)$ plot. A metastable circular orbit of radius r_0 (Eqn. (12)) occurs when b equals b_0 (Eqn. (13)).

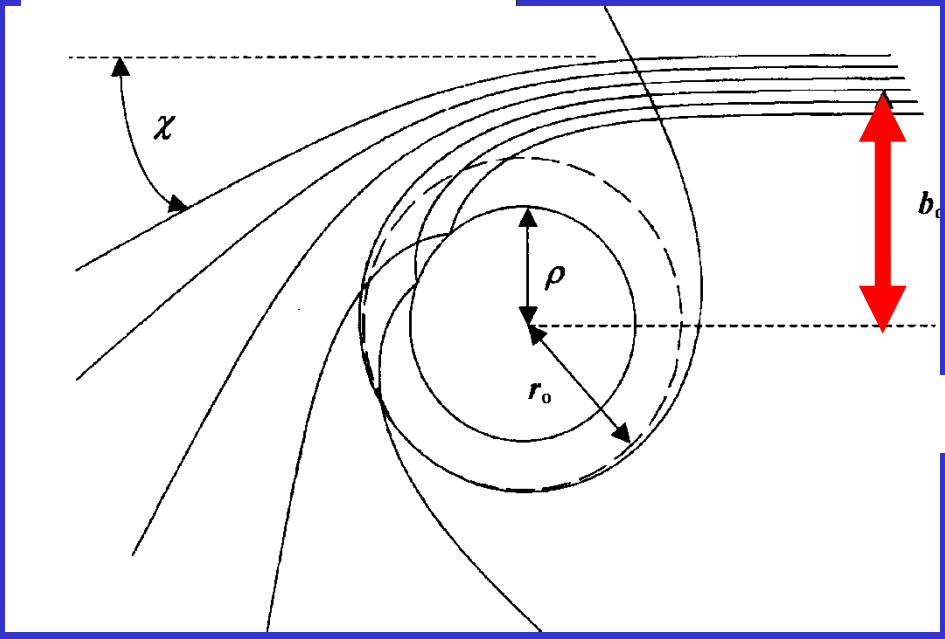

Figure 2
Trajectories for ion–induced dipole collisions in the scattering center system calculated from Eqn. (7) with b/b_0 equal to 1.1500, 1.1000, 1.0500, 1.0001, 1.0000, 0.9500, and 0.9000 corresponding to deflection angles χ equal to −28.6°, −40.2°, −61.2°, −299.9°, −infinity (dashed circle), −139.4°, and −80.1°, respectively. A hard sphere of radius ρ represents the structure of the ion–molecule pair.

For ion induced dipole force

$$r_0 = \left(\frac{\alpha e^2}{(4\pi\varepsilon_0)^2 \mu v_0^2}\right)^{1/4}$$

$$b_0 = \sqrt{2} r_0$$

$$\sigma_0 = \pi b_0^2 = \frac{2\pi e}{v_0(4\pi\varepsilon_0)}\sqrt{\frac{\alpha}{\mu}}$$

Collision rate coefficient -Langevin rate coefficient

$$\sigma_0 = \pi\rho_0^2 = \frac{2\pi e}{v_0(4\pi\varepsilon_0)}\sqrt{\frac{\alpha}{\mu}}$$

$$\sigma_{coll} = \sigma_L = const\,\frac{1}{v}\sqrt{\frac{\alpha}{\mu}} \sim \sigma_0\,\frac{v_0}{v}\,cm^2$$

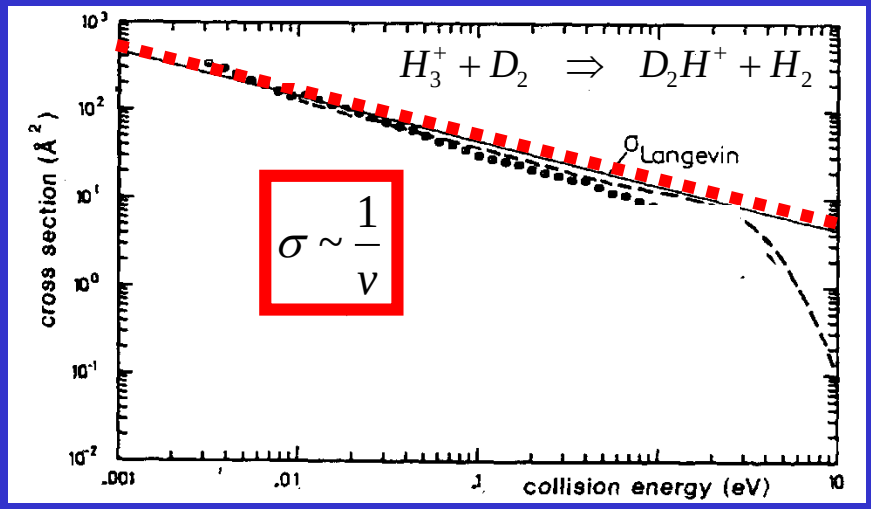

$$k_{coll}(T) = <\sigma v> \sim <\sigma_0\,\frac{v_0}{v}\,v> \sim const$$

$$k_{coll} = k_{coll} = const\sqrt{\frac{\alpha}{\mu}} \sim 3.34x10^{-9}\sqrt{\frac{\alpha}{\mu}}\,cm^3s^{-1};$$

α *in* *Debye*
μ *in* *atomic units*

	α
H	~0.666793
He	~0.204956
Li	~24.3
C	~1.76
Ar	~1.64
CO	~1.95
H_2	~0.8
C_2H_4	~4.5

Ind. dipole d=αe/r^2➔[α]=[dr^2/e]=[err^2/e]=[r^3]
α~dr^2/e➔if r~A and d~eA➔ α~A^3

$k_L \sim 10^{-9} cm^3 s^{-1}$

IMR thermal

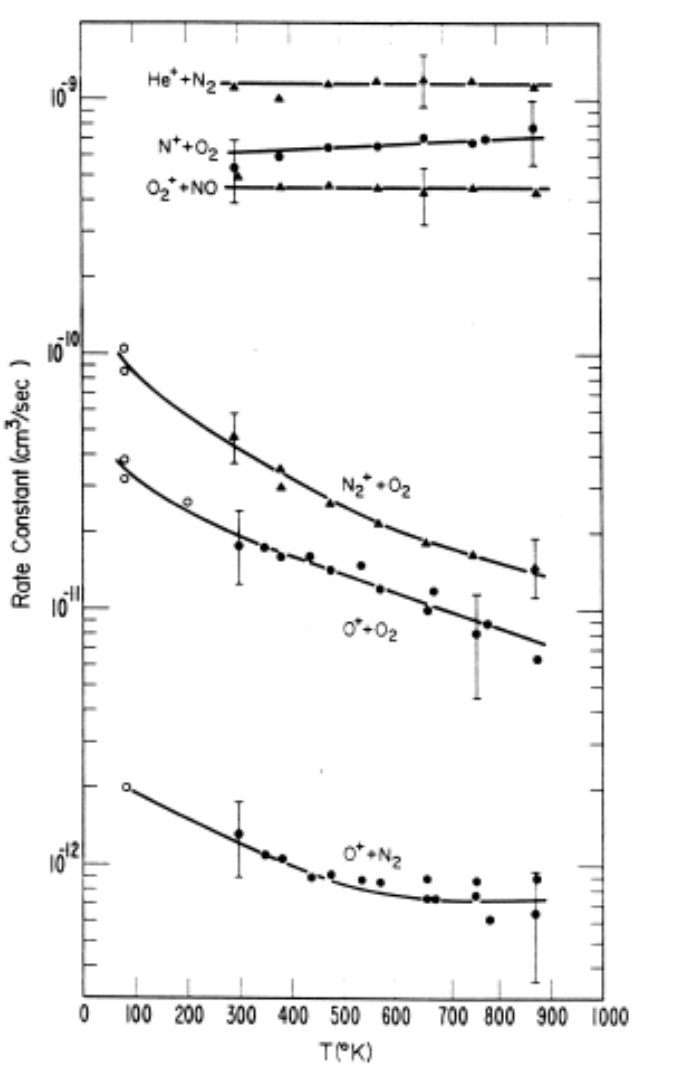

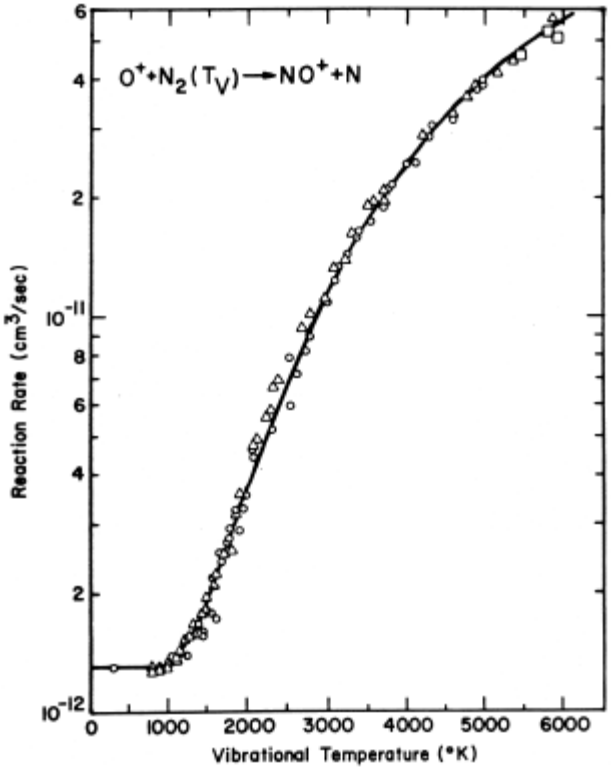

Fig. 12. Measurements of the variation of the rate coefficient for the reaction of $O^+ + N_2 \rightarrow NO^+ + N$ with the vibrational temperature of N_2 [16].

Ionic composition of the atmosphere

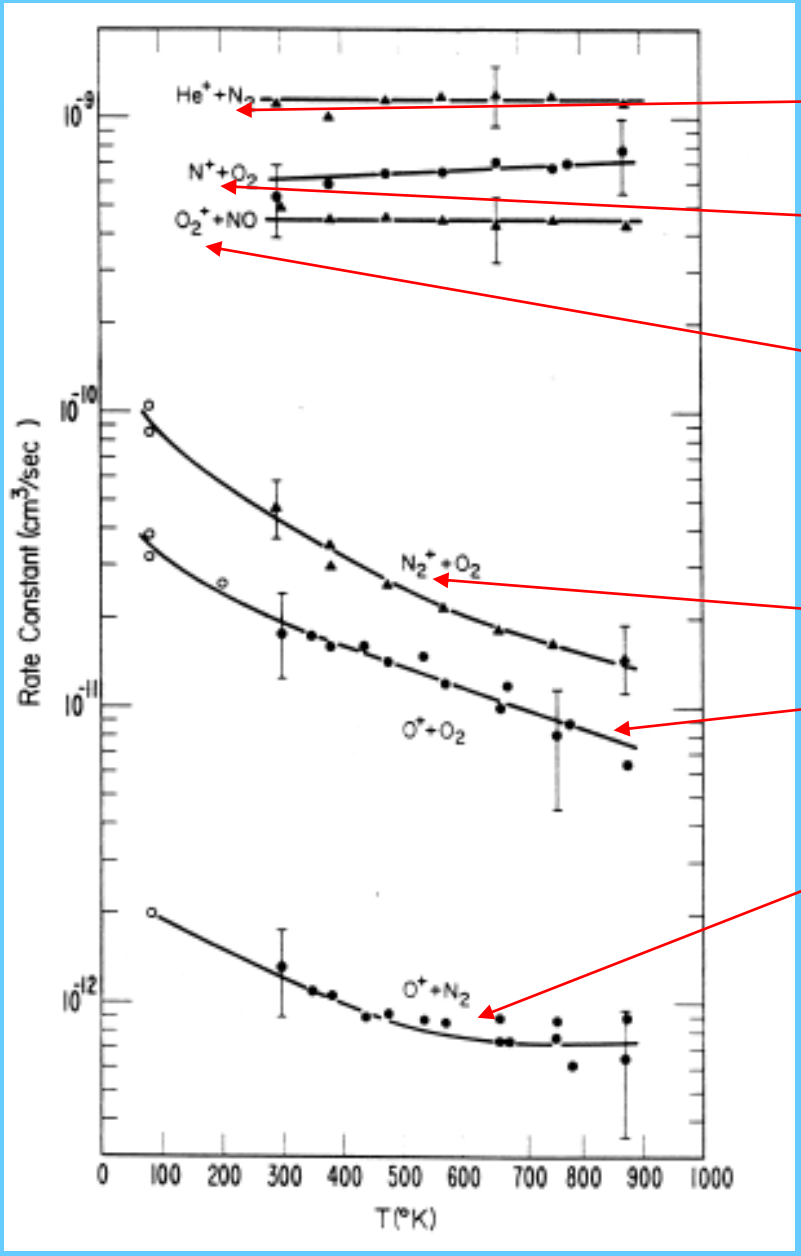

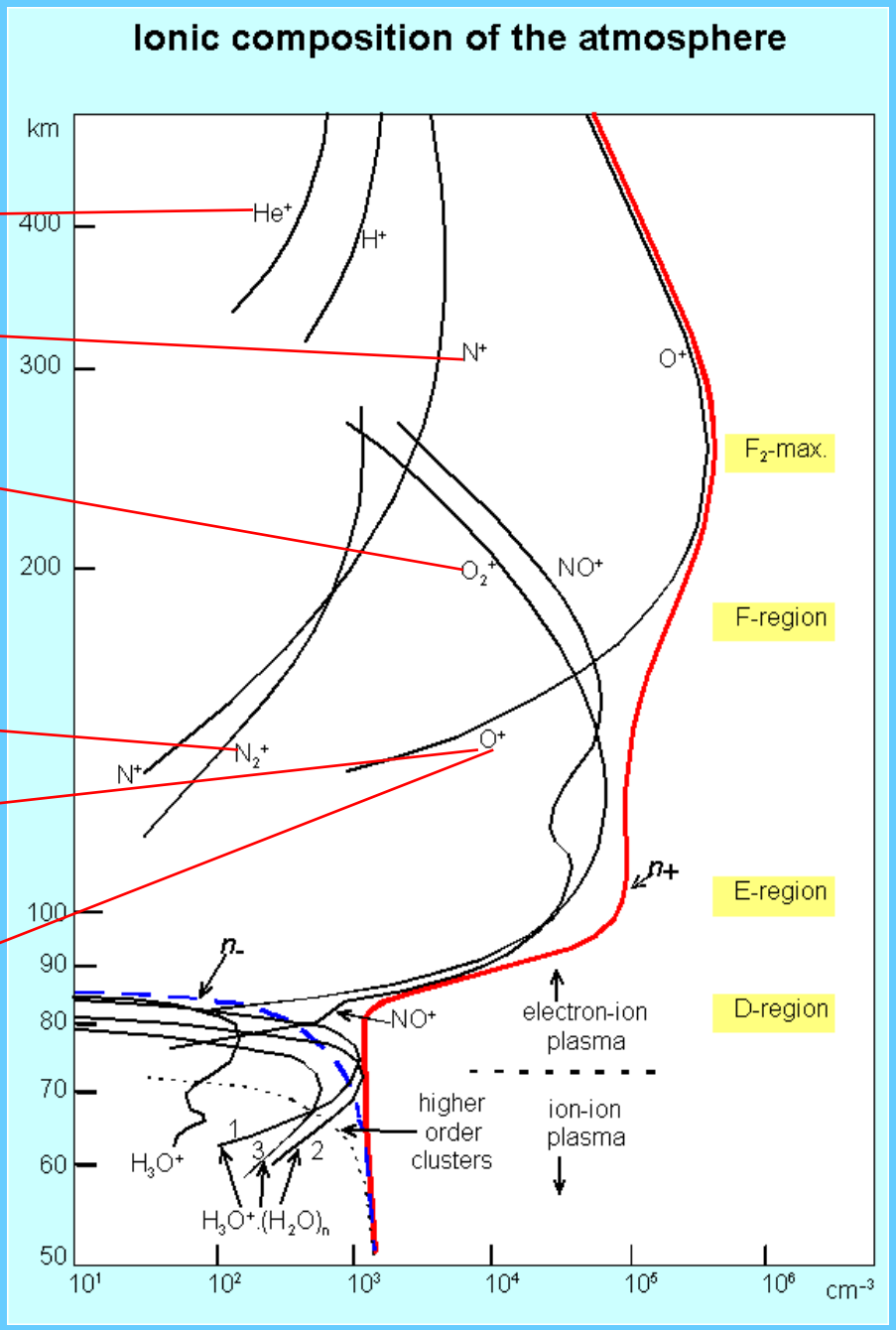

Reaction Rate of IMR relevant for ionosphere

k_{IMR}

$k_{coll} \sim 10^{-9} cm^3 s^{-1}$

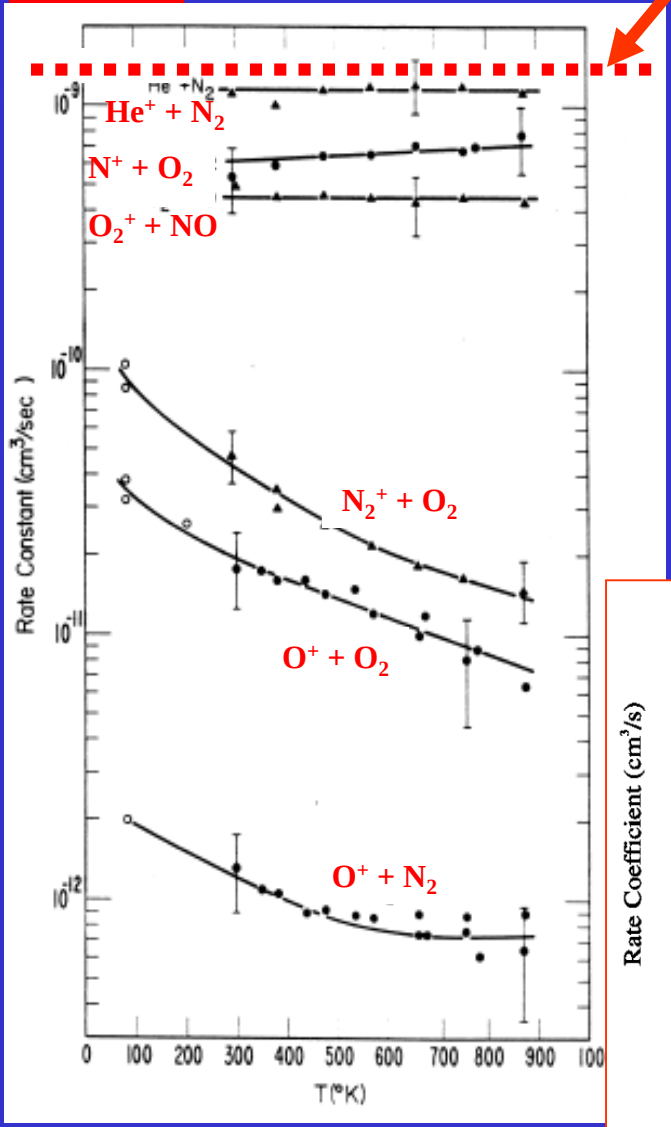

1975-90

1990-00

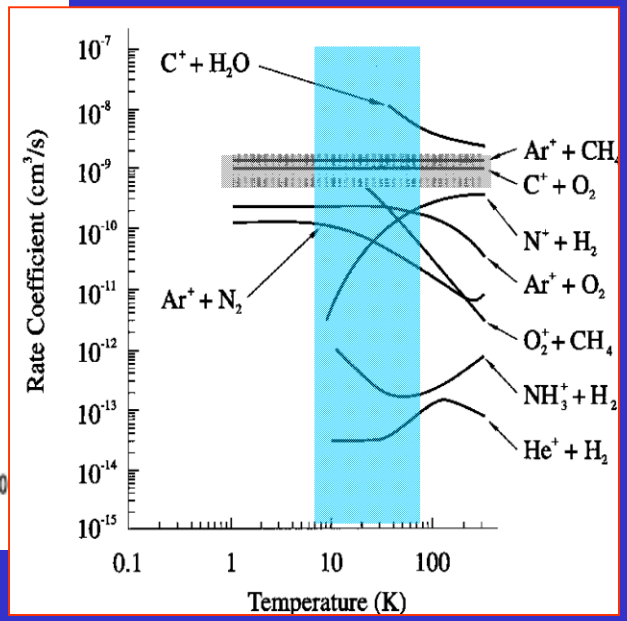

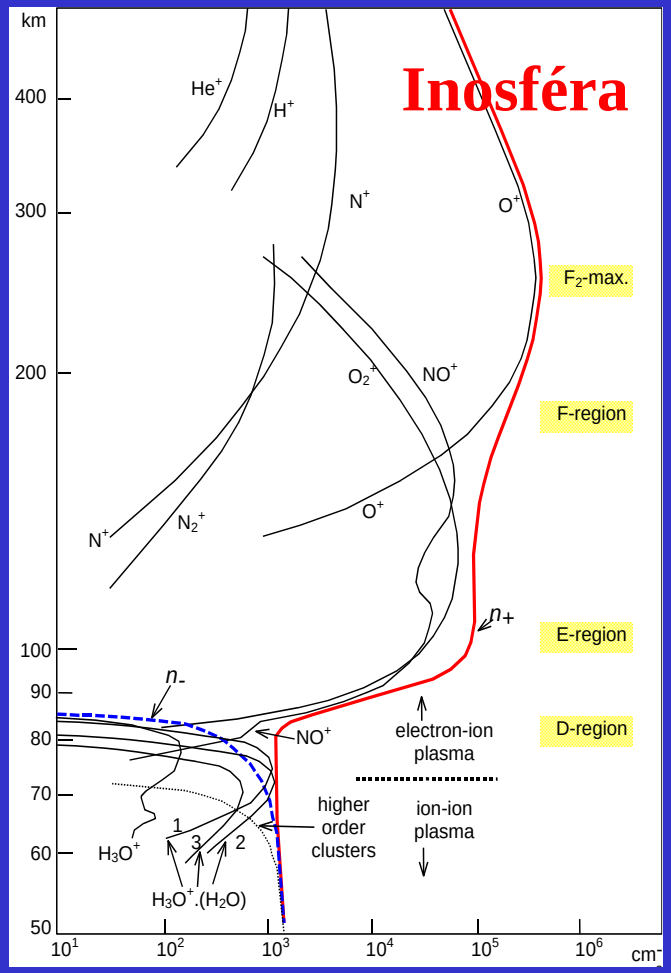

The ion chemistry of the lower atmosphere

Binary reactions

Ternary reactions

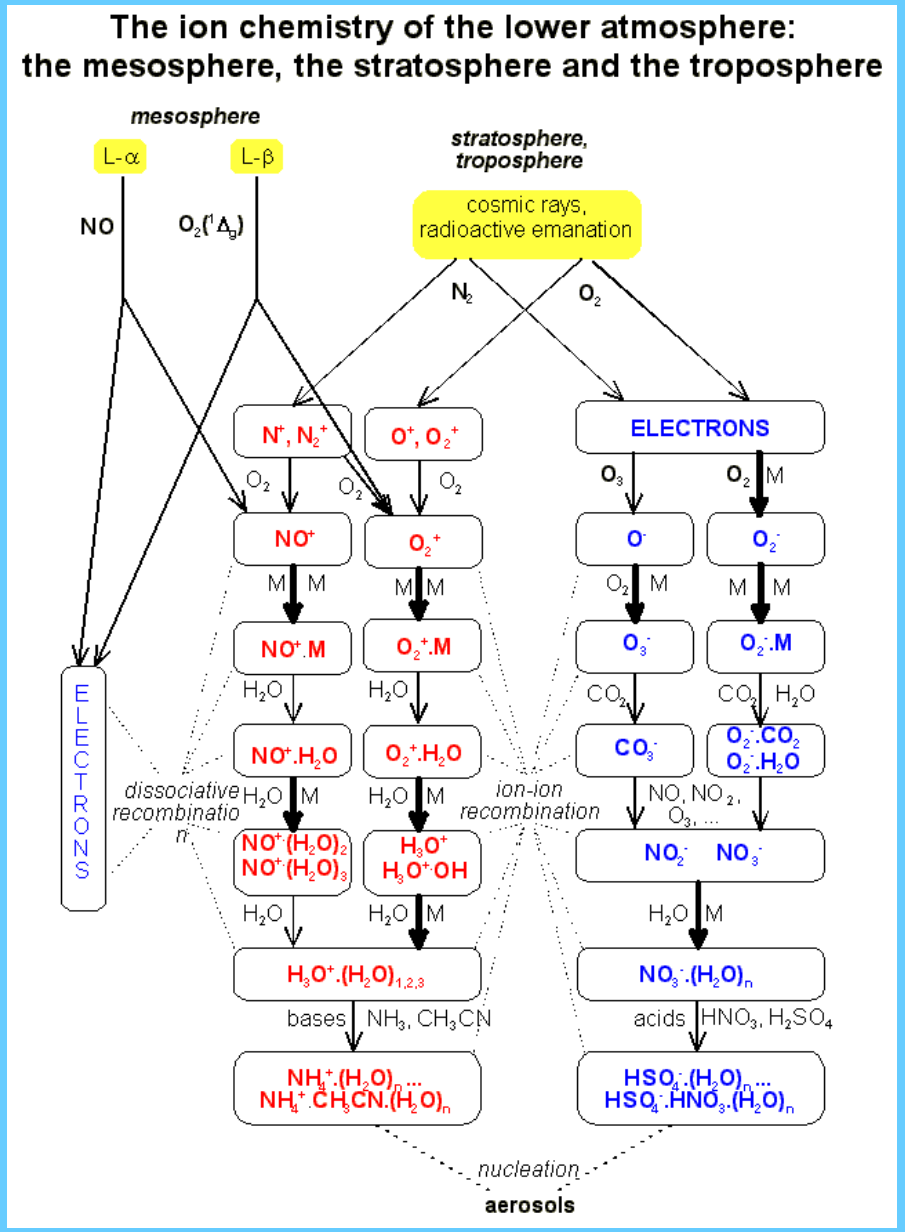

Branching ratio of IMR

$$AB^+ + C \underset{\tau_{-1}}{\overset{k_1}{\leftrightarrow}} (A.BC^+)^{\#} \xrightarrow{\tau_2} AB + C^+$$

$$\xrightarrow{\tau_3} AC + B^+$$

$$\xrightarrow{\tau_4} AC^+ + B$$

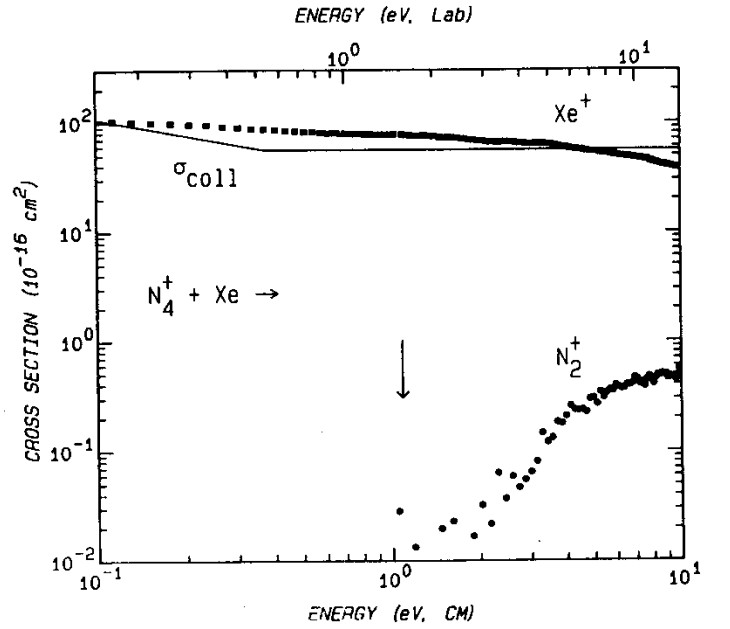

Fig. 4. Cross-sections for reaction of N_4^+ with Xe as a function of relative kinetic energy (lower x-axis) and laboratory energy (upper x-axis). Cross-sections are normalized to 100% isotopic abundance as described in the text. Circles are CID (reaction 4); squares, CT (reaction 5); and triangles, ligand exchange (reaction 6). The vertical arrow shows the N_2^+–N_2 bond strength of 1.09 eV. The solid line represents the LGS collision cross-section, Eq. 7, at low energy and the hard sphere collision cross-section of 54 Å^2 at higher energy.

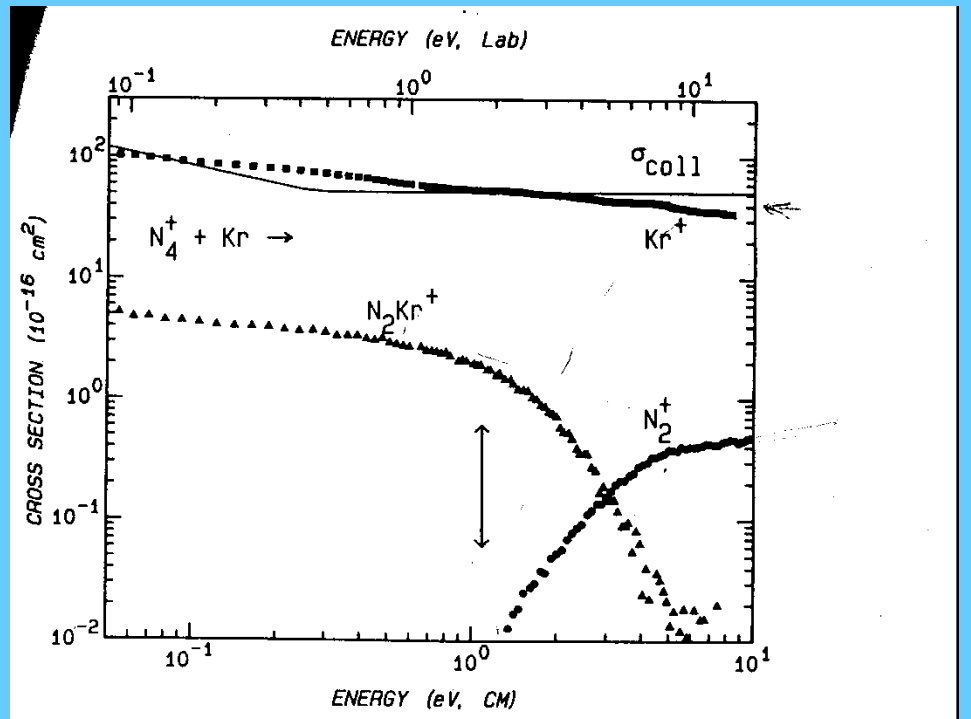

Fig. 3. Cross-sections for reaction of N_4^+ with Kr as a function of relative kinetic energy (lower x-axis) and laboratory energy (upper x-axis). The cross-sections are normalized to 100% isotopic abundance as described in the text. Circles are CID (reaction 4); squares, CT (reaction 5); and triangles, ligand exchange (reaction 6). The vertical arrow shows the N_2^+–N_2 bond strength of 1.09 eV. The solid line represents the LGS collision cross-section, Eq. 7, at low energy and the hard sphere collision cross-section of 51 Å^2 at higher energy.

Reaction rate coefficients

Typical values of at 300K (approximate values)

	reactants		products	rate coefficient
• Electron atomic ion rec.	$A^+ + e^-$	➔	$A + h\nu$	$\sim 10^{-11} cm^3 s^{-1}$
• Electron - ion recomb.	$O_2^+ + e^-$	➔	$O + O$	$2x10^{-7} cm^3 s^{-1}$
• Electron – cluster ion recomb.	$H_5^+ + e^-$	➔	products	$3.5x10^{-6} cm^3 s^{-1}$
• Ion – ion recombination	$Ar^+ + Cl^-$	➔	$Ar + Cl$	$2x10^{-8} cm^3 s^{-1}$
• Ion – molecule reactions	**$H_2^+ + H_2$,**	➔	**$H_3^+ + H$**	**$2x10^{-9} cm^3 s^{-1}$**
	$H_3^+ + H_2 + He$	➔	**$H_5^+ + He$**	**$k_{eff\ BIN} = k_3 x[He]$**
				$k_3 < 2x10^{-29} cm^6 s^{-1}$
• Attachment	$CCl_4 + e^-$		$Cl^- + CCl_3$	$\sim 10^{-7} cm^3 s^{-1}$
• Penning ionization	$He^* + Ar$		$Ar^+ + e^- + He$	$7x10^{-11} c$.

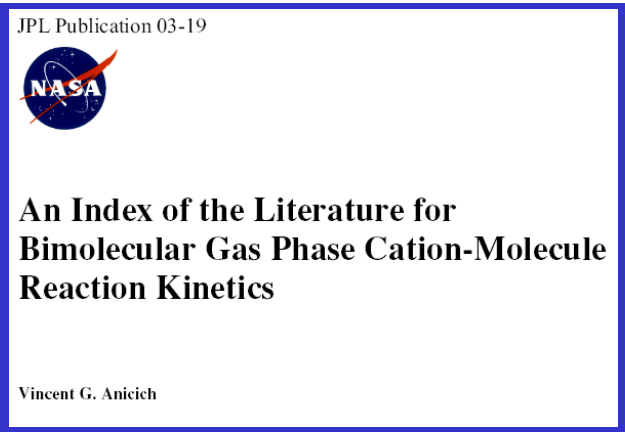

Rate coefficients

National Aeronautics and Space Administration

Jet Propulsion Laboratory
California Institute of Technology
Pasadena, California

2003

November 2003

A^+		B		products			%	k[cm^3s^{-1}]	T		
C^+	+	C_2H_6	→	Products					300	MS	6406
C^+	+	CH_2CCH_2	→	$C_4H_2^+$	+	H_2	0.40	1.40×10^{-9} ±20	300	SIFT	8207
				$C_3H_3^+$	+	CH	0.25				
				$C_2H_2^+$	+	C_2H_2	0.20				
				$C_3H_4^+$	+	C	0.15				
C^+	+	CH_3CCH	→	$C_4H_2^+$	+	H_2	0.30	1.90×10^{-9} ±25	300	SIFT	8207
				$C_3H_4^+$	+	C	0.30				
				$C_3H_3^+$	+	CH	0.20				
				$C_2H_2^+$	+	C_2H_2	0.10				
				$C_2H_3^+$	+	CCH	0.10				
C^+	+	CH_3CHCH_2	→	$C_2H_3^+$	+	$CHCH_2$	0.30	2.00×10^{-9} ±25	300	SIFT	8207
				$C_3H_3^+$	+	CH	0.20				
				$C_3H_3^+$	+	CH_3	0.15				
				$C_2H_2^+$	+	C_2H_4	0.15				
				$C_3H_6^+$	+	C	0.10				
				$C_4H_3^+$	+	H_2 + H	0.10				

Decay of plasma – change of plasma composition

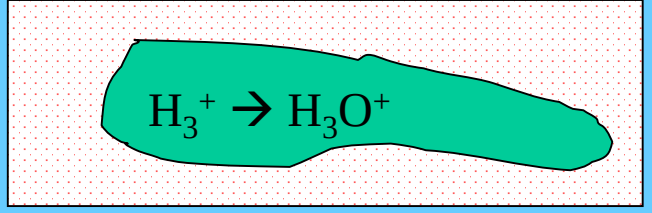

$H_3^+ + H_2O \rightarrow H_3O^+ + H_2$

Ion density in low temperature plasma, e.g. DC discharge $[H_3^+] \sim 10^{10} cm^{-3}$

"Pure He" … grade 5 …. 99.999% ….0.001 % of impurities

Water impurities $\sim 10^{-5}$ Torr $\rightarrow 3 \times 10^{11} cm^{-3}$

$$\frac{dH_3^+}{dt} = -k[H_3^+].[H_2O] = -[H_3^+]/\tau_{H2O}$$

$$[H_3^+] = [H_3^+]_0 . \exp(-k[H_2O]t) = [H_3^+]_0 . \exp(-t/\tau_{H2O})$$

$$\tau = \frac{1}{k[H_2O]} \sim \frac{1}{(2.10^{-9})x(3.10^{11})} \sim 0.0017s \sim 1.7ms$$

Dynamic of IMR

Reaction coordinate

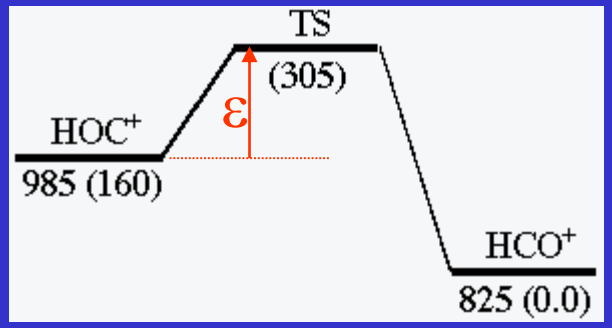

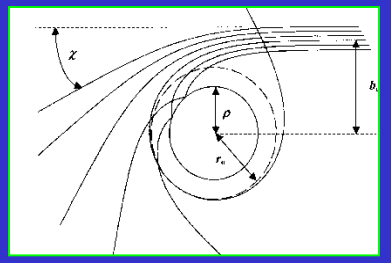

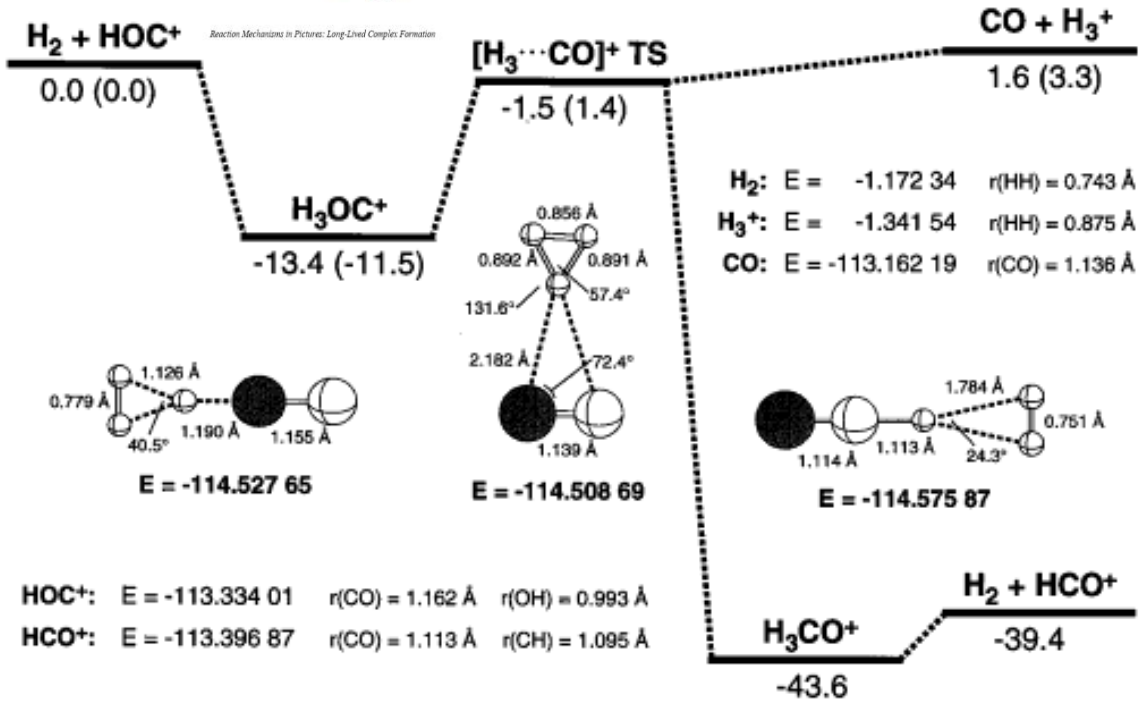

FIG. 1.—The minimum energy potential pathway from $HOC^+ + H_2$ reactants to two sets of products: $HCO^+ + H_2$ and $CO + H_3^+$. The computed relative energies (kcal mol^{-1}) listed for the stationary points (reactants, complexes, transition state, and products) are given without and with zero-point energy corrections. Corrected values are in parentheses. The structures of the two complexes and transition state are shown with bond lengths in angstroms (Å) and bond angles in degrees. Calculated absolute energies are in hartrees (1 H = 3.16×10^5 K).

Potential energy 3D

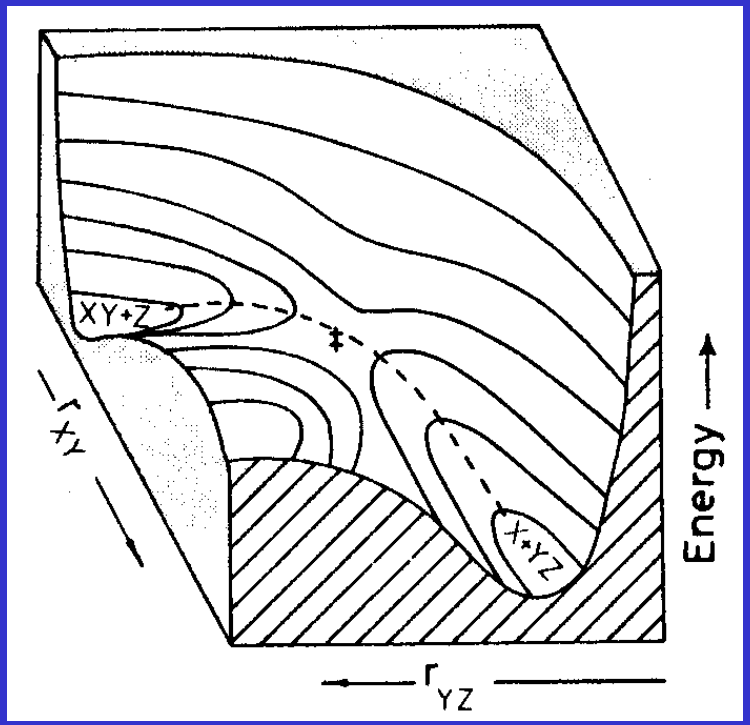

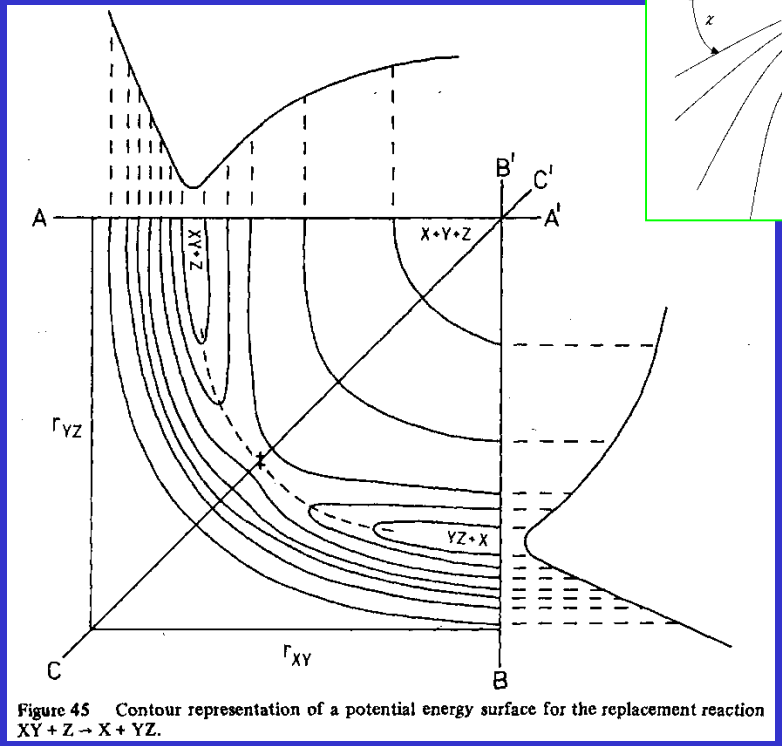

Figure 45 Contour representation of a potential energy surface for the replacement reaction XY + Z → X + YZ.

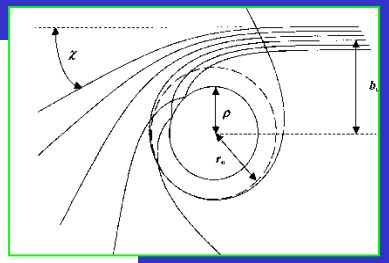

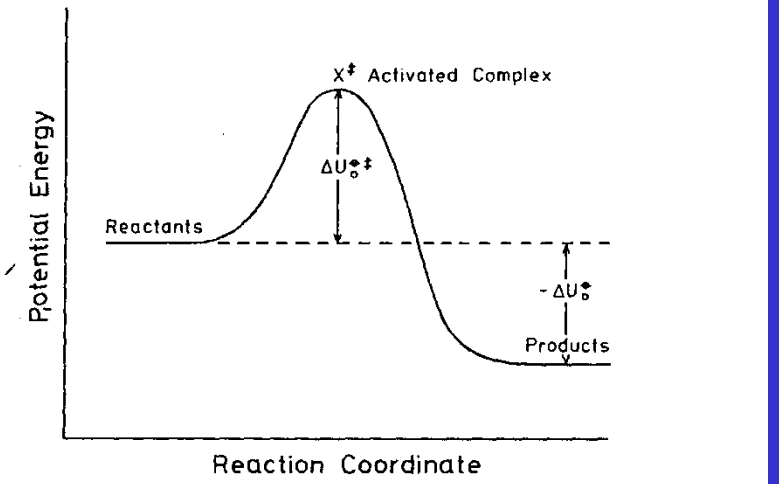

Figure 46 Variation in potential energy along the reaction coordinate for any elementary reaction at zero Ke

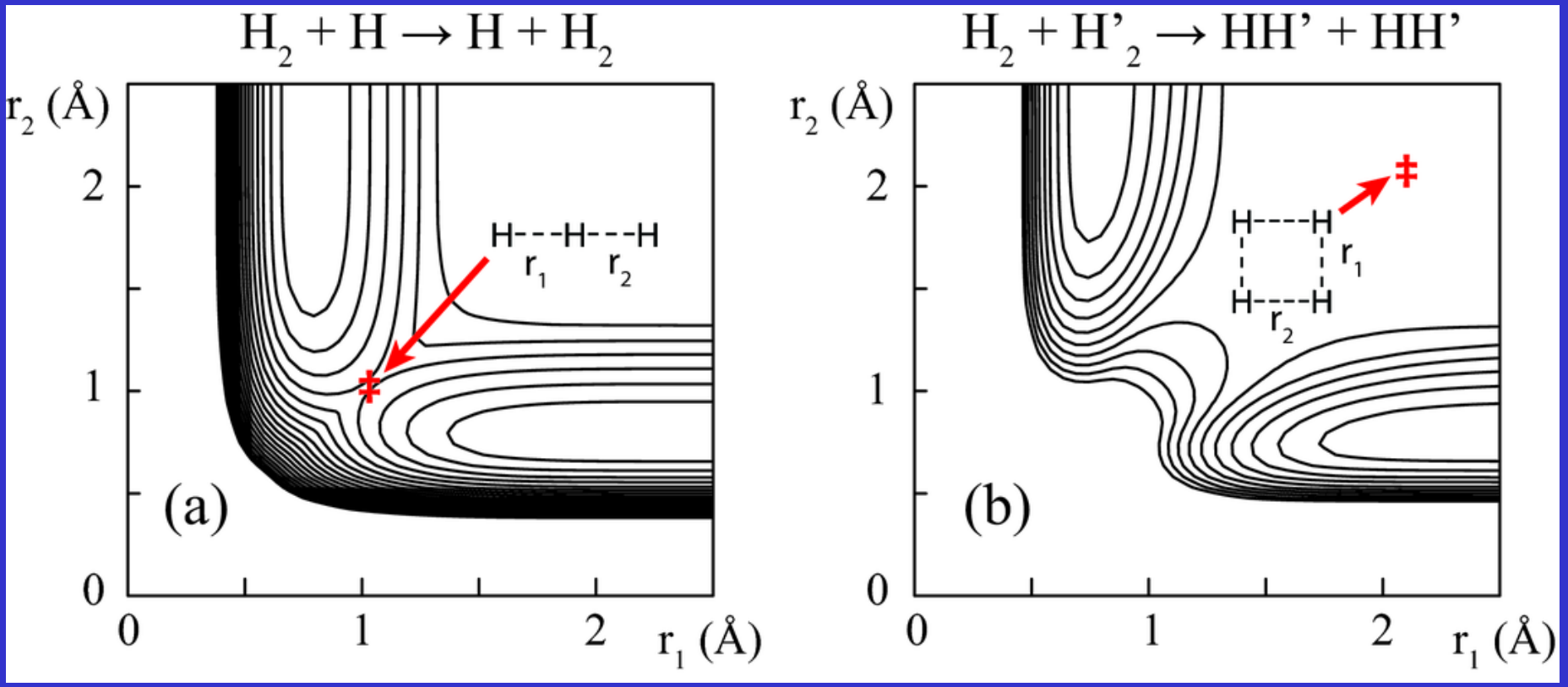
H2 + H → H + H2
r2 (Å)
2
1
0
H---H---H
r1
r2
‡
(a)
0
1
2
r1 (Å)
H2 + H'2 → HH' + HH'
r2 (Å)
2
1
0
H----H
H----H
r1
r2
‡
(b)
0
1
2
r1 (Å)

Guided Ion Beam

Electron and isotope transfer in $^{14}N^+ + {}^{15}N_2$ collisions

$$N^+ + N_2 \rightarrow products$$

$$^{14}N^+ + {}^{15}N_2 \rightarrow {}^{15}N^+ + {}^{14}N^{15}N$$
$$\rightarrow {}^{15}N_2^+ + {}^{14}N$$
$$\rightarrow {}^{14}N^{15}N^+ + {}^{15}N$$

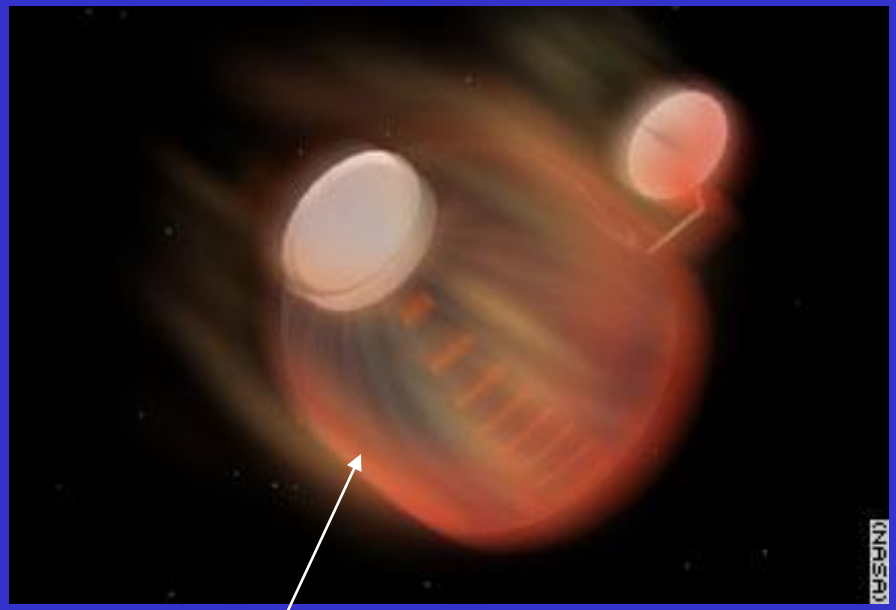

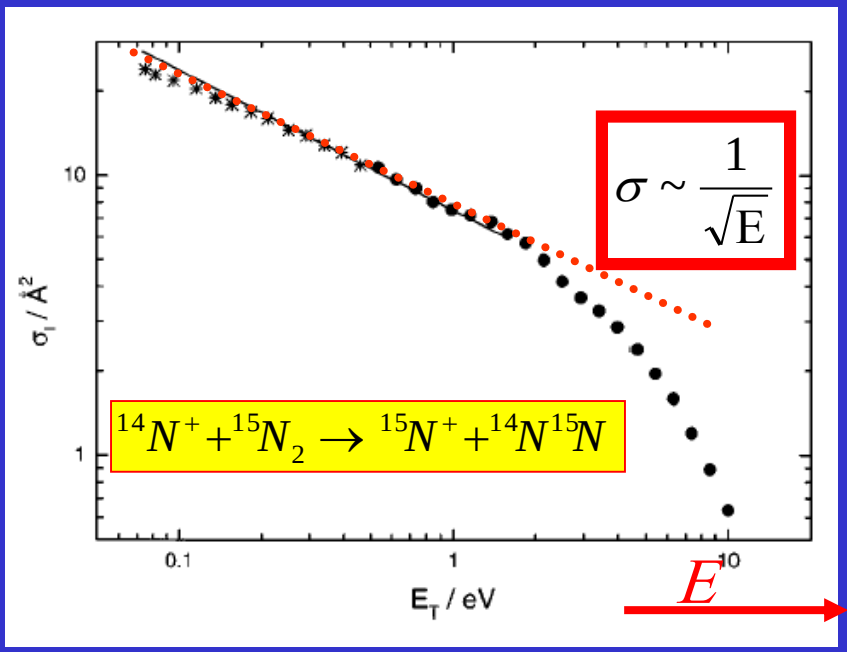

Energy transfer ????? Where is energy going

Dynamic of IMR

$$^{14}N^{+} + {}^{15}N_2 \rightarrow {}^{15}N^{+} + {}^{14}N^{15}N$$

$$\rightarrow {}^{15}N_2^{+} + {}^{14}N$$

$$\rightarrow {}^{14}N^{15}N^{+} + {}^{15}N$$

Dynamic of IMR

$$N^+ + N_2 \rightarrow products$$

$$^{14}N^+ + {}^{15}N_2 \rightarrow {}^{15}N^+ + {}^{14}N^{15}N$$
$$\rightarrow {}^{15}N_2^+ + {}^{14}N$$
$$\rightarrow {}^{14}N^{15}N^+ + {}^{15}N$$

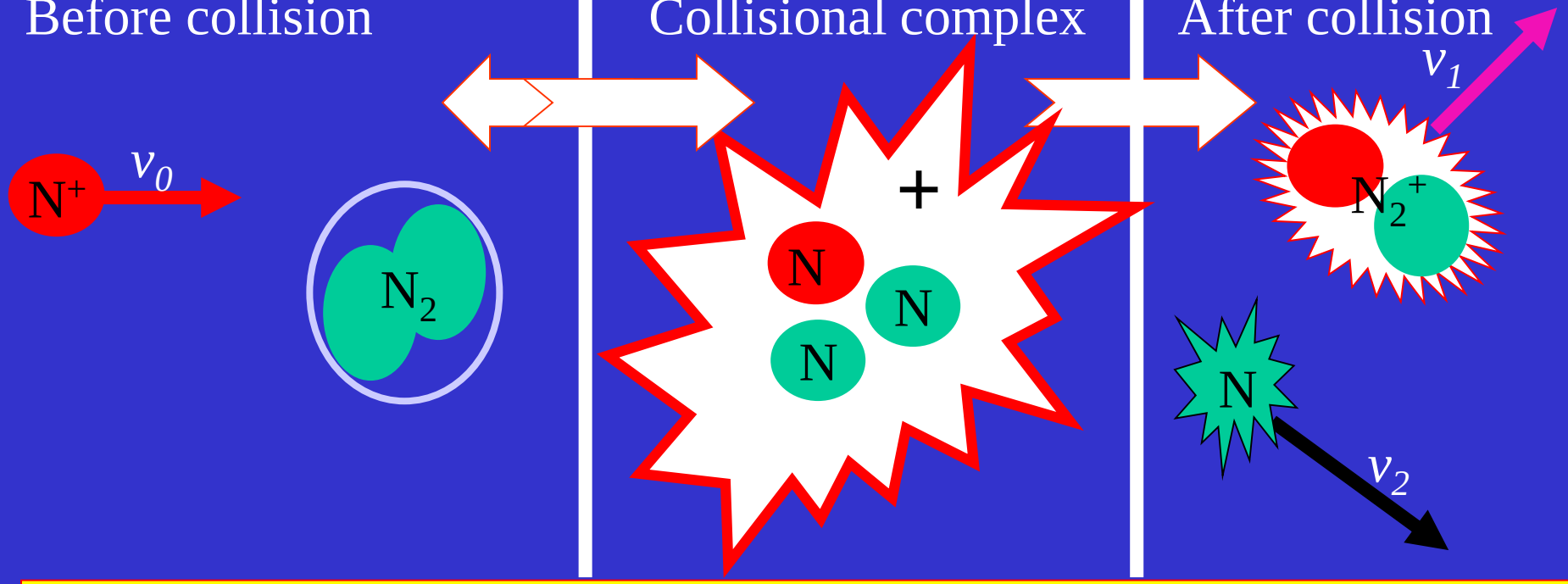

$$N^+ + N_2 \leftrightarrow (N_3)^{*+} \rightarrow N_2^+ + N$$

$$\sigma_{coll} = \pi\rho_0^2 = \frac{2\pi e}{v_0(4\pi\varepsilon_0)}\sqrt{\frac{\alpha}{\mu}}$$

Dynamic of IMR

$$N^+ + N_2 \leftarrow (N_3)^{*+} \rightarrow N_2^+ + N$$

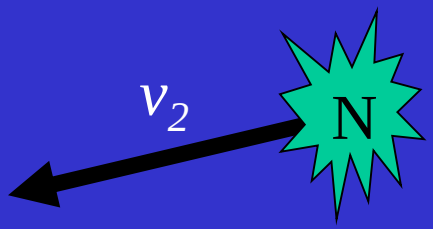

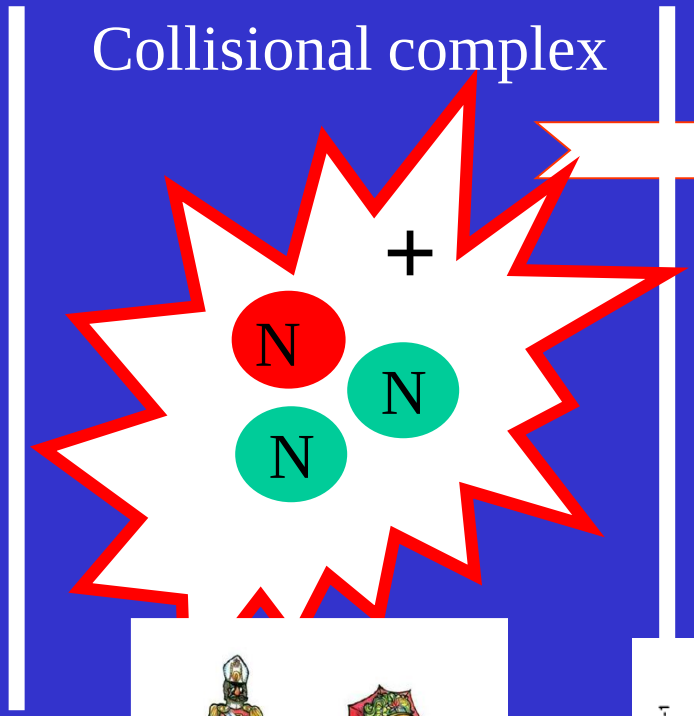

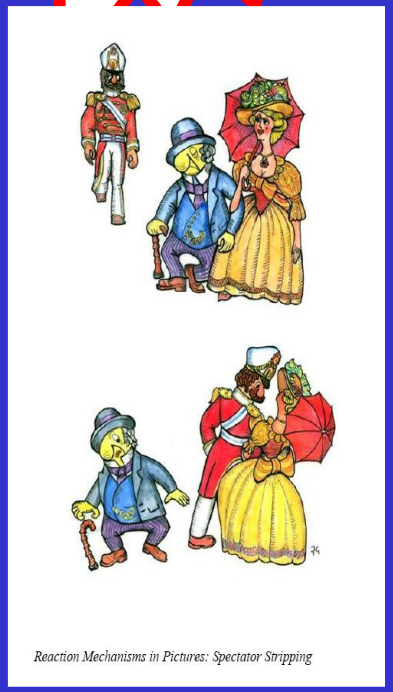

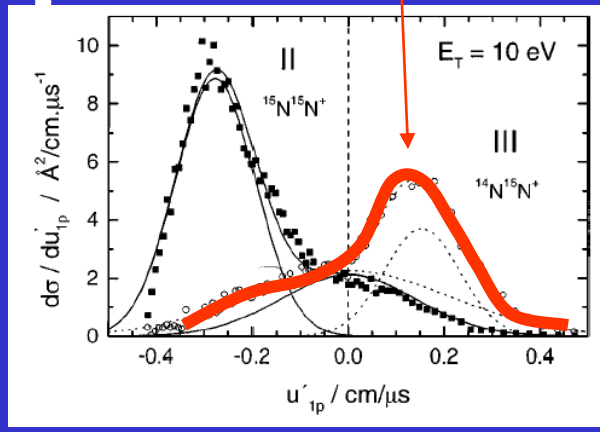

Dynamic of IMR

$$N^+ + N_2 \leftarrow (N_3)^{*+} \rightarrow N_2^+ + N$$

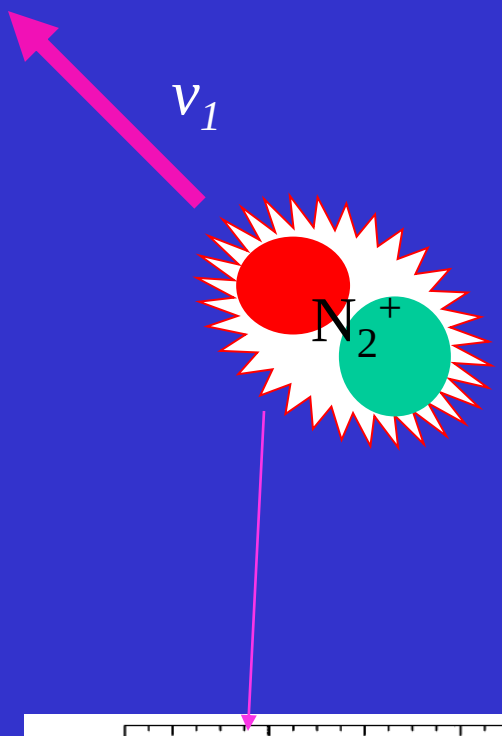

Collisional complex

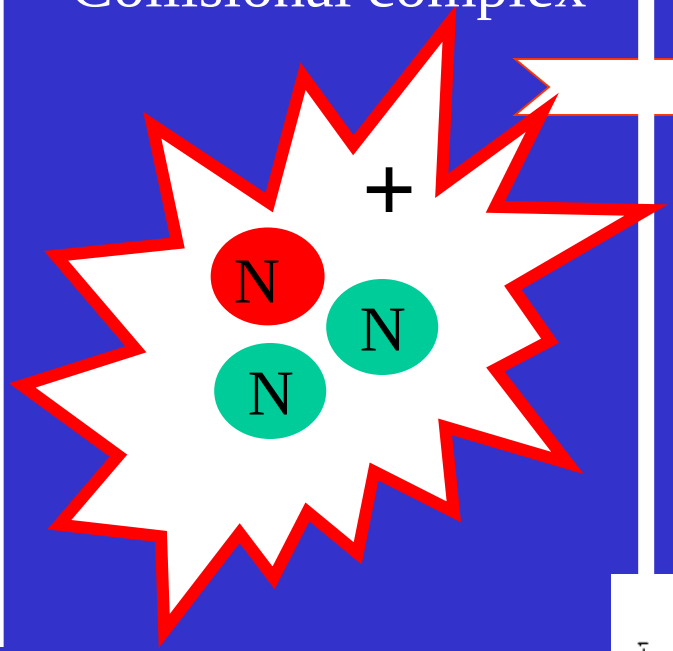

After collision

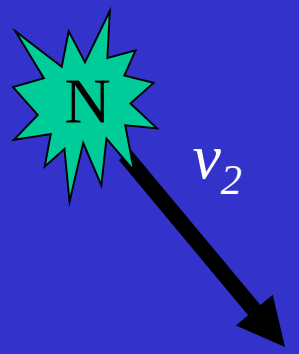

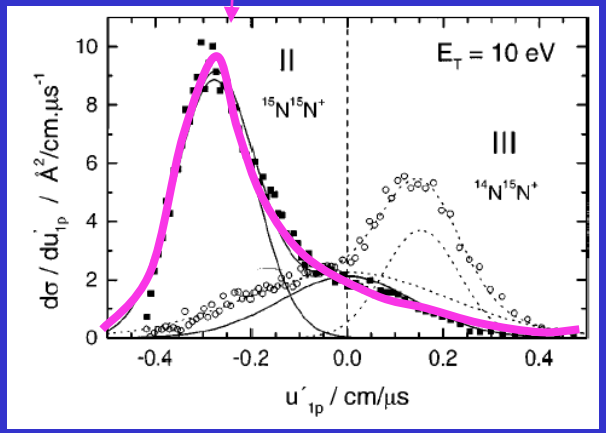

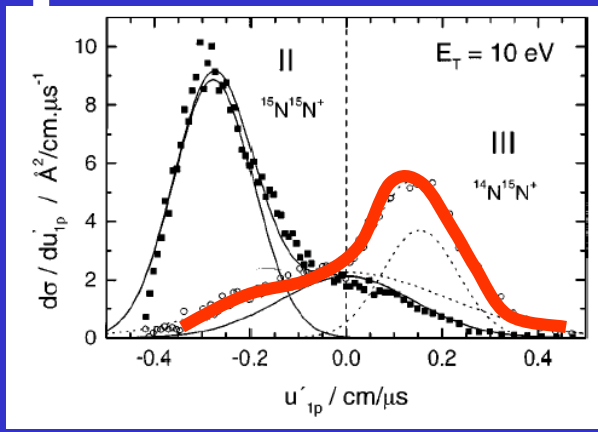

Dynamic of IMR $N^+ \quad + \quad N_2 \quad \leftarrow \quad (N_3)^{*+} \quad \rightarrow N_2^+ \quad + \quad N$

Collisional complex | After collision

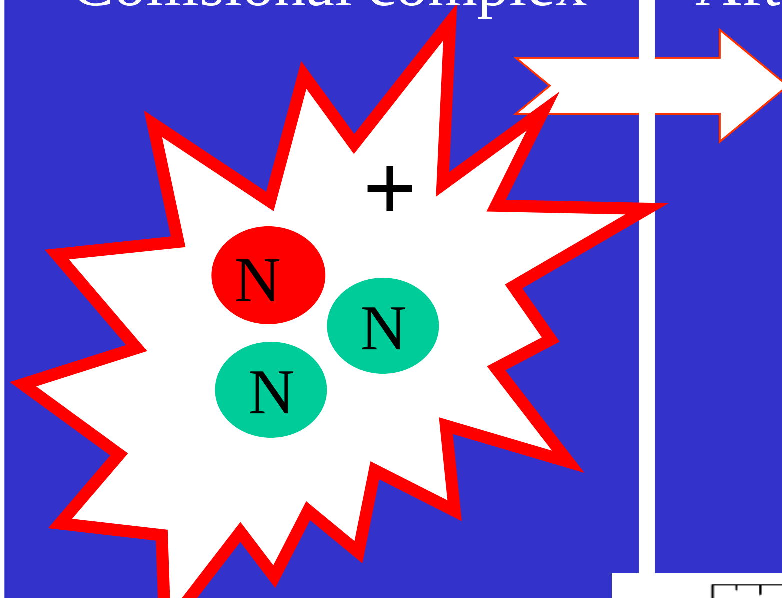

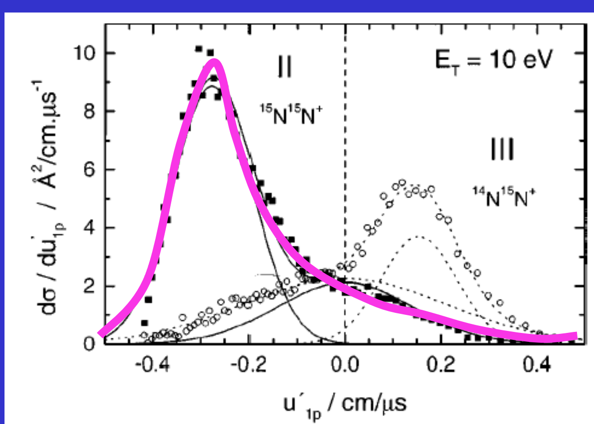

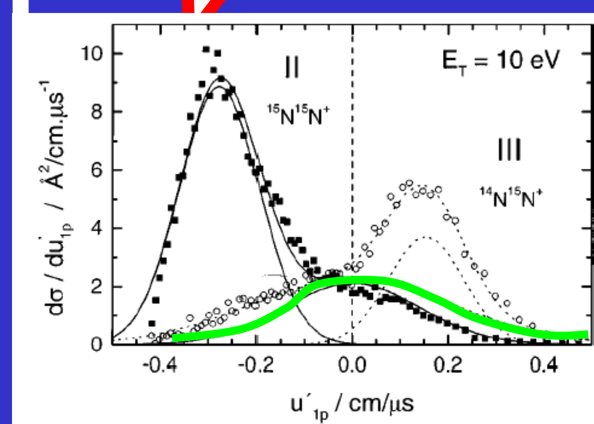

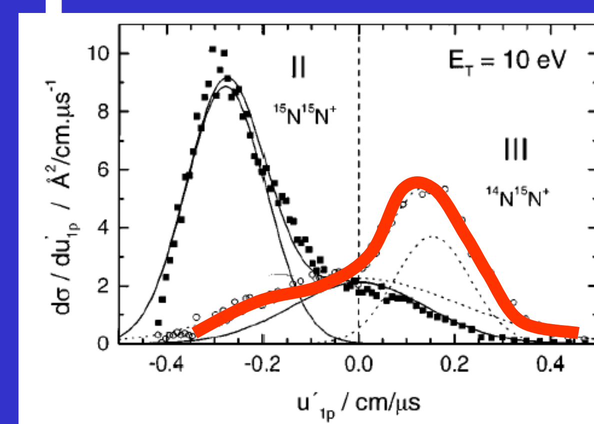

Reaction mechanism

Reaction Mechanisms in Pictures: Spectator Stripping

Reaction Mechanisms in Pictures: Long-Lived Complex Formation

Guided Ion Beam

Electron and isotope transfer in $^{14}N^+ + {}^{15}N_2$ collisions

$$N^+ + N_2 \rightarrow products$$

$$^{14}N^+ + {}^{15}N_2 \rightarrow {}^{15}N^+ + {}^{14}N^{15}N$$
$$\rightarrow {}^{15}N_2^+ + {}^{14}N$$
$$\rightarrow {}^{14}N^{15}N^+ + {}^{15}N$$

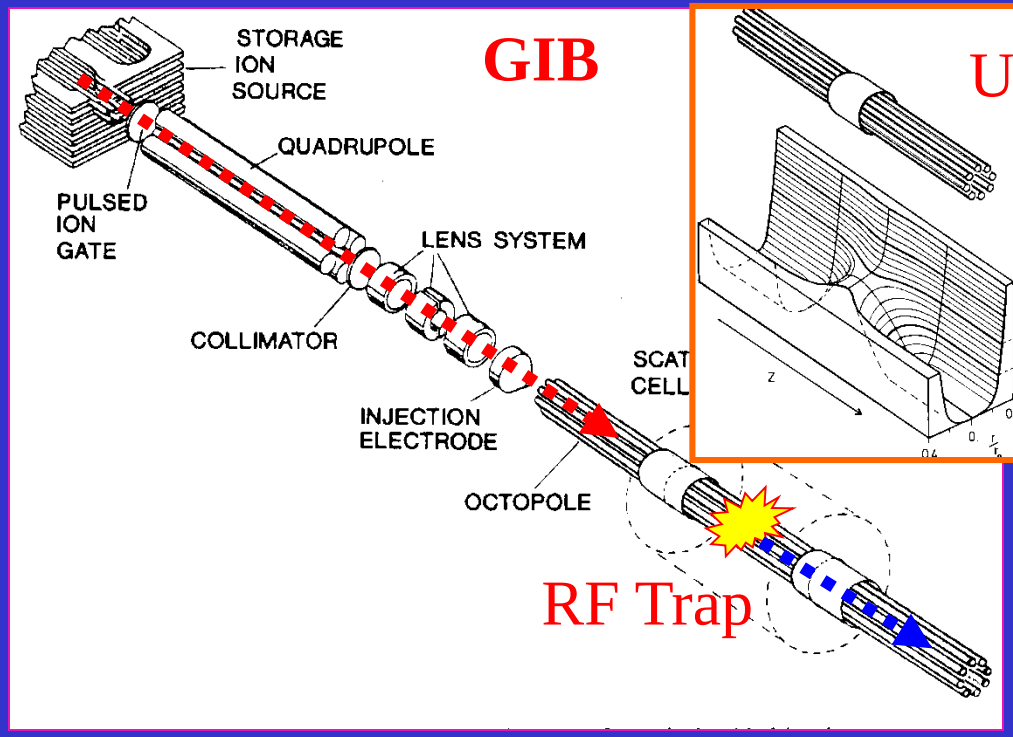

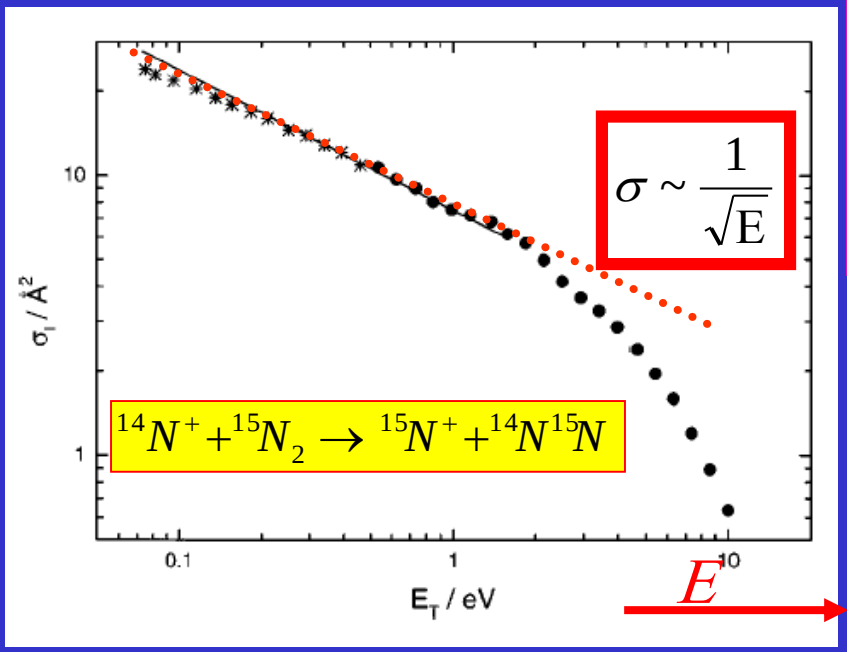

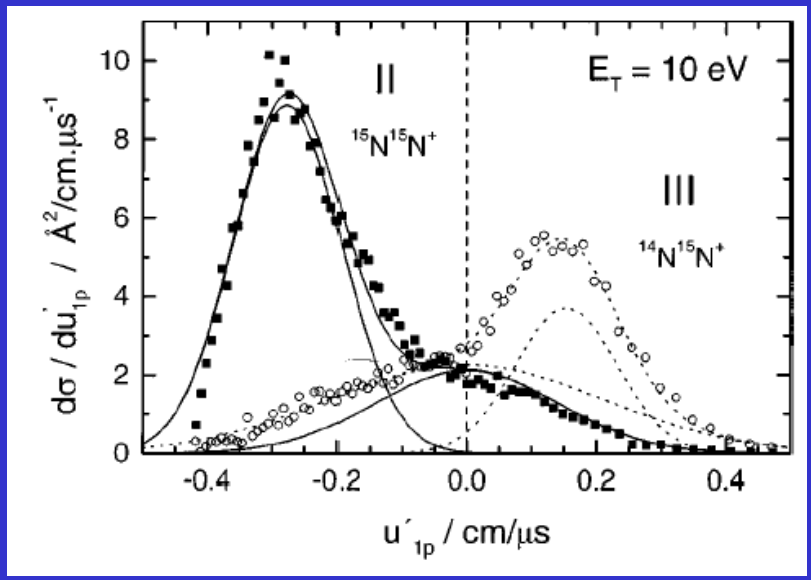

$$\sigma_{coll} = \pi\rho_0^2 = \frac{2\pi e}{v_0(4\pi\varepsilon_0)}\sqrt{\frac{\alpha}{\mu}}$$

Reaction proceeding via intermediate states

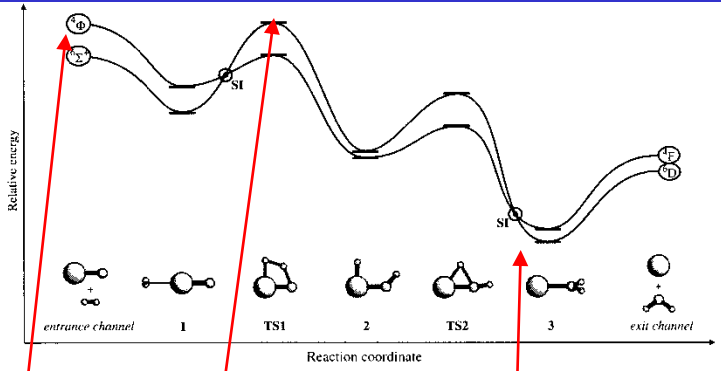

Figure 3
Reaction pathways on the sextet and quartet potential energy surfaces for the gas-phase reaction $H_2 - FeO^+ \rightarrow Fe^+ + H_2O$ (reproduced by permission of Wiley-VCH from (*31*)).

Table 5
Computed energies (kJ mol^{-1}) of stationary points for the activation of H_2 by FeO^+ (D_0 relative to separated FeO^- ($^6\Sigma^+$) + H_2).

	BP86[a]	B3LYP[a]	B3LYP[b]	CCSD(T)[b]	CASPT2[c]
$FeO^+(^4\Phi) + H_2$	53	33	31	52	80
^{6}1	−68	−64	−53	−50	−22
^{4}1	−68	−28	−23	1	15
^{6}TS1	29	35	40	53	77
^{4}TS1	0	3	4	31	24
^{6}2	−139	159	142	−130	−61
^{4}2	170	−171	−160	−124	−121
^{6}TS2	−28	−54	−48	27	
^{4}TS2	128	−141	−124	−91	
^{6}3	−226	−307	−276	291	280
^{4}3	260	330	312	−280	
$Fe^+(^6D) + H_2O$	−16	−161	−139	−133	−151
$Fe^+(^4D) + H_2O$	−34	−171	−157	156	

[a]Wachters basis for Fe, Dunning TZ2P basis for H and O (*64*). [b]Modified Ahlrichs TZVP basis for Fe, 6-311 + + G(2df,2p) for H and O (*65*). [c]ANO [8s7p6d4f2 g] basis for Fe, [3s2p1d] and [5s4p3d2f] for H and O, respectively (*63*).

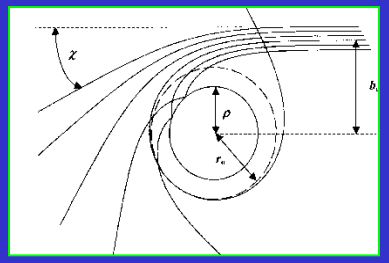

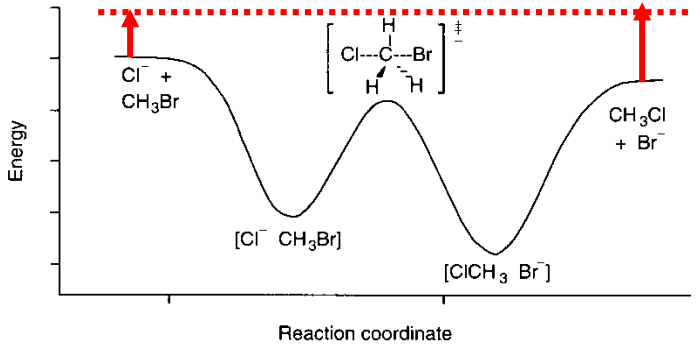

Figure 1
Double-well potential energy surface for the reaction of Cl^- with CH_3Br (after Olmstead and Brauman (*3*)).

Reaction mechanism

Reaction Mechanisms in Pictures: Spectator Stripping

Reaction Mechanisms in Pictures: Long-Lived Complex Formation

Endothermic ion-molecule reactions

Implications of a barrier along reaction path

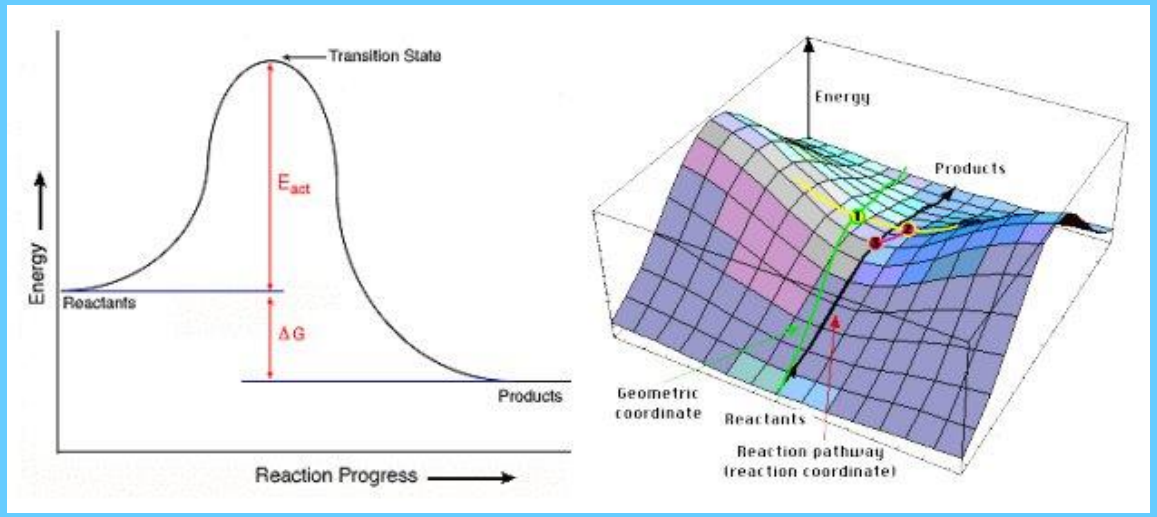

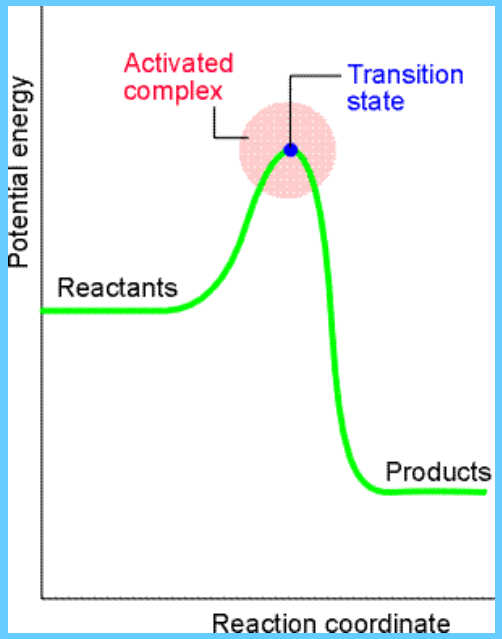

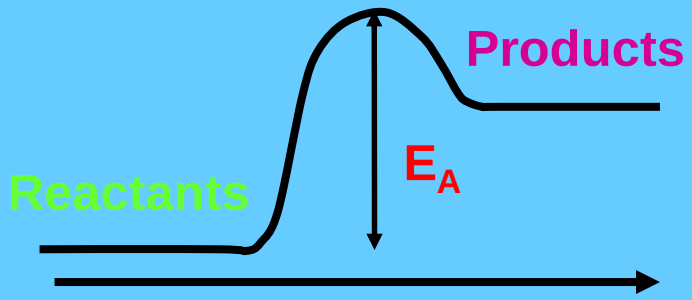

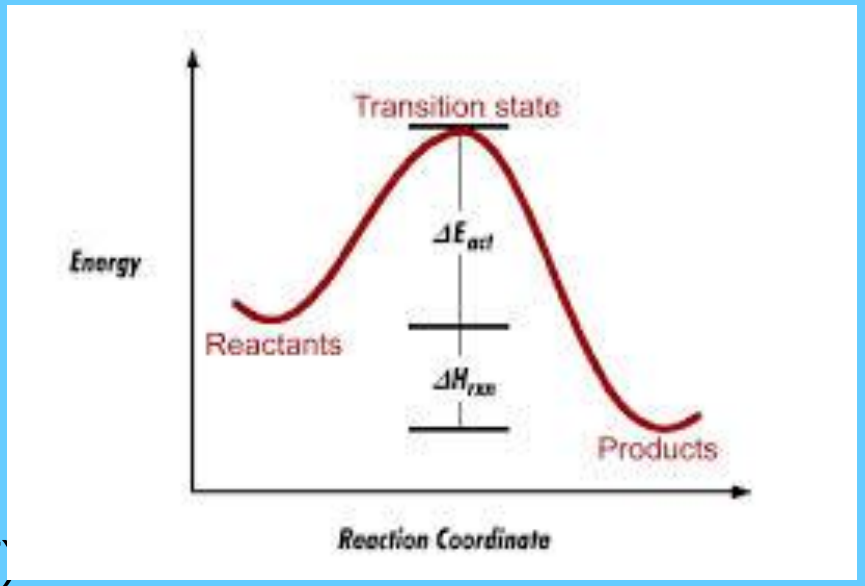

Arrhenius:

$$k(T) = \langle \sigma v \rangle = A \exp(-E_A/kT)$$

The excitation function quantifies the dependence of the reaction cross section on collision energy. It is the microscopic equivalent of the temperature dependence of the rate constant. Broadly speaking, there are two different types of excitation function, shown below, with the type exhibited by a particular reaction depending on whether or not the reaction has an activation barrier.

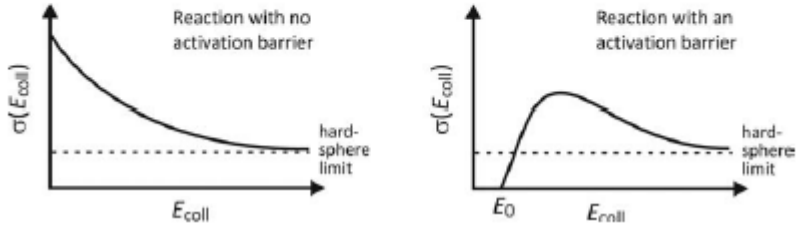

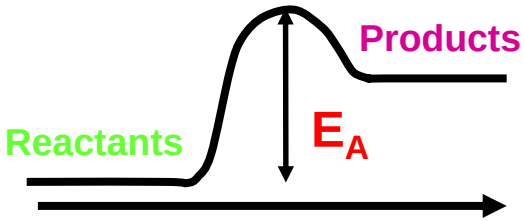

1. *Exoergic with no barrier*

This type of excitation function is typical of many exoergic[1] processes, e.g. ion-molecule reactions. At low energies there is enough time for long-range attractive interactions (van der Waals interactions, dipole interactions etc). to act on the particles and the cross section is large. If the long-range interactions are strong, even particles with large impact parameters can be pulled together by the attractive interactions and undergo a collision. As the collision energy increases, the particles fly past each other faster and their trajectories are deviated by a smaller amount by the attractive interactions. The cross section therefore reduces, until eventually there is no time for any attractive forces to act and the so-called 'hard-sphere limit' is reached. At this point the cross section is given by $\sigma = \pi d^2$, where $d=r_A+r_B$ is the sum of the particle radii. For many reactions the hard-sphere limit is very small, and the excitation function essentially tends to zero at very high energies.

2. *Endoergic or exoergic with a barrier.*

When the reaction has a barrier, no reaction occurs until there is enough energy available to surmount the barrier and the cross section is zero. The cross section then increases to a maximum in the region where attractive forces can act (c.f. Arrhenius equation for macroscopic rate constants), before decreasing again to the hard sphere limit at high energies for the same reasons as described above. The excitation function is the product of the decreasing ' barrierless' excitation function described above and an 'Arrhenius-type' function which rises once the activation barrier is surmounted.

Once we know the excitation function, expressed as a function of collision energy or relative velocity, the thermal rate constant may be recovered. From simple collision theory, the rate constant for a given relative velocity is simply $k(v) = v\,\sigma_r(v)$. Integrating over the velocity distribution $P(v)$ of the molecules present in the sample yields the thermal rate constant.

$$k(T) = \int_0^\infty v\,\sigma_r(v)P(v)\,dv \qquad (1.10)$$

Implications of a barrier along reaction path

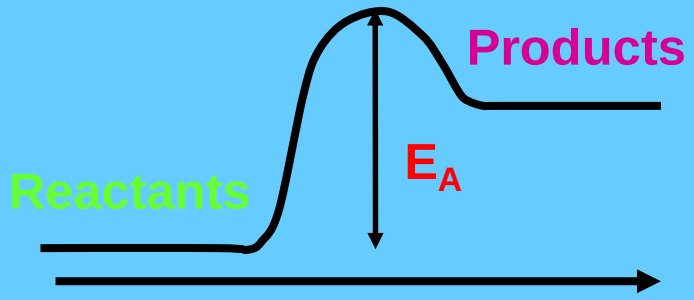

Arrhenius:

$$k(T) = \langle \sigma v \rangle = A \exp(-E_A/kT)$$

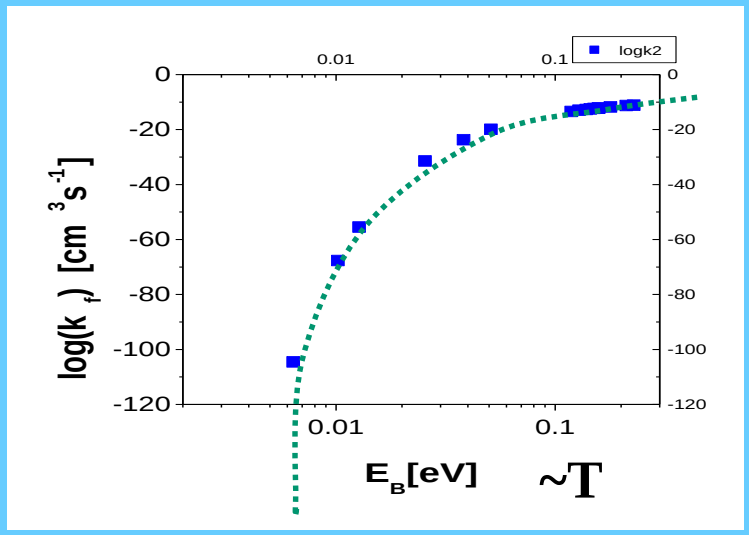

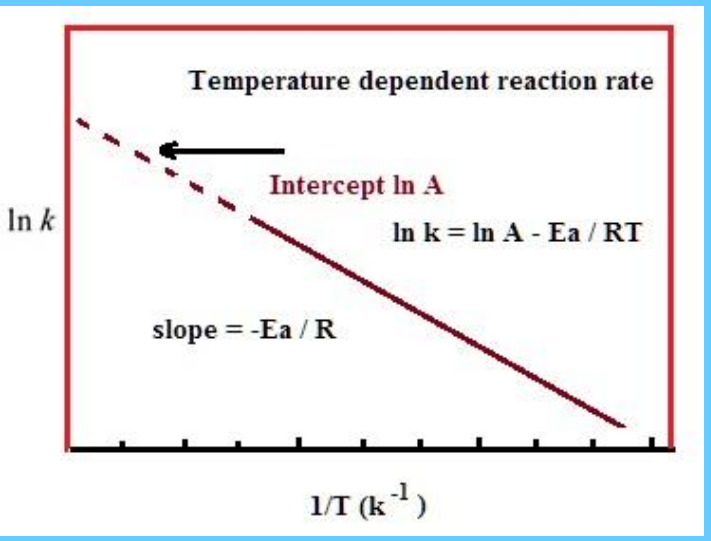

$$N_4^+ + He \rightarrow N_2^+ + N_2 + He$$

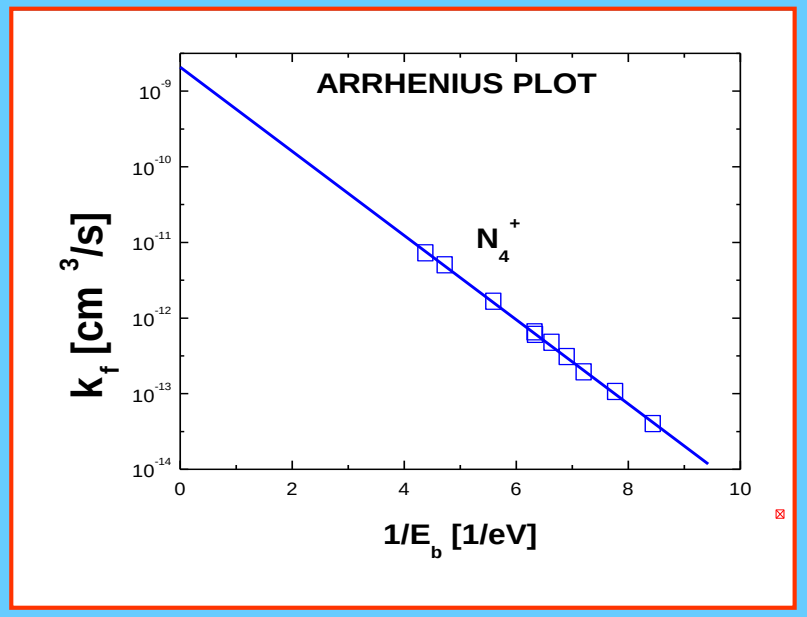

IMR Energy dependence eV region

Endothermic IMR

$$N_4^+ + He \rightarrow N_2^+ + N_2 + He$$

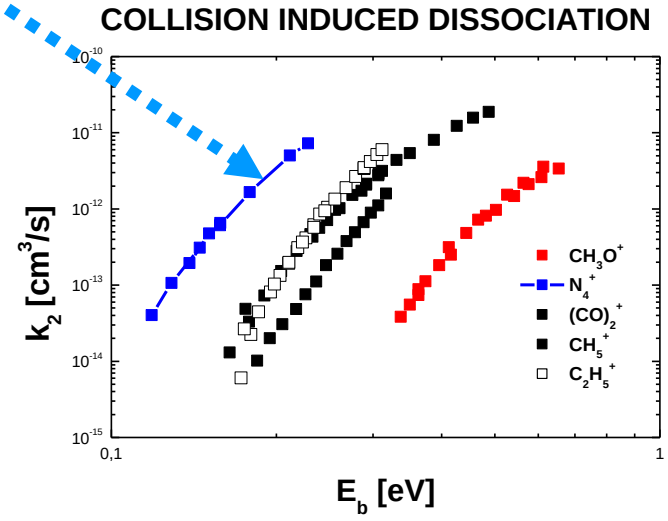

$k(T) = \langle \sigma v \rangle = A \exp(-E_A/kT)$

$\ln(k(T)) \sim (-E_A/kT)$

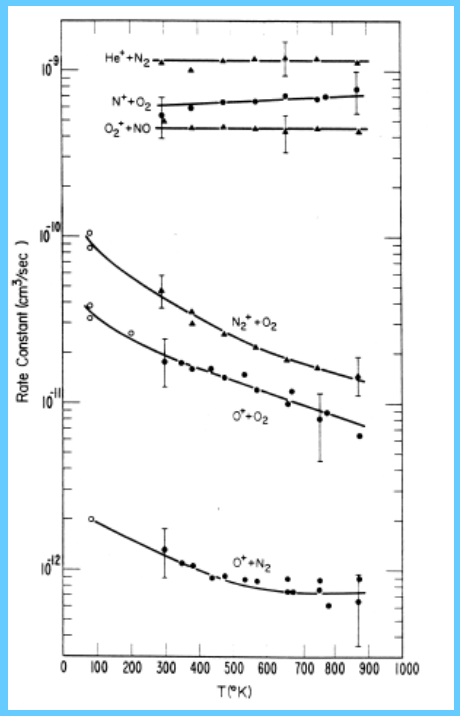

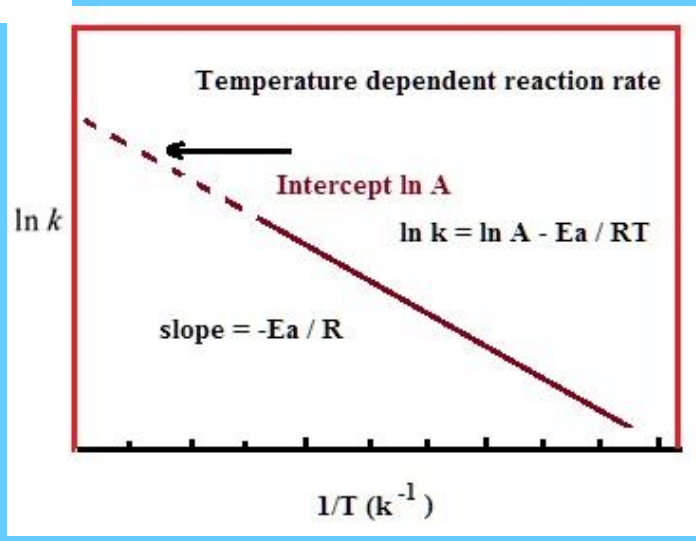

Collision induced dissociation

$$N_4^+ + He \underset{k_r}{\overset{k_f}{\rightleftharpoons}} N_2^+ + N_2 + He$$

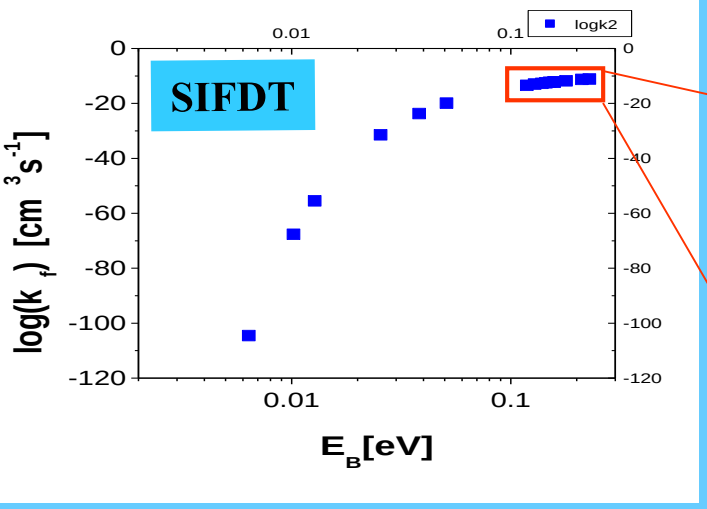

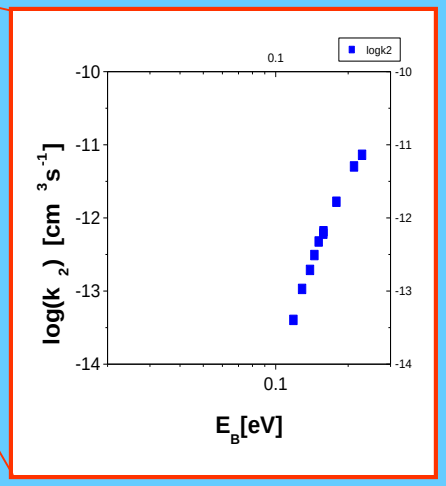

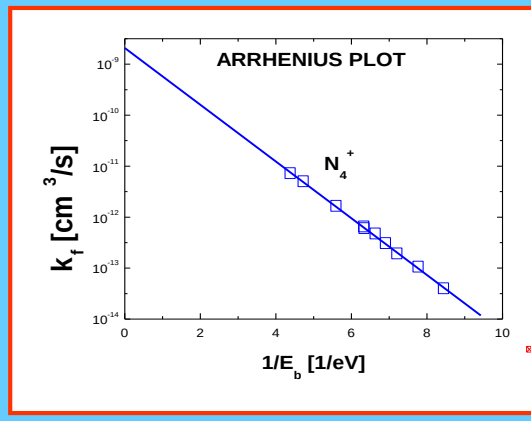

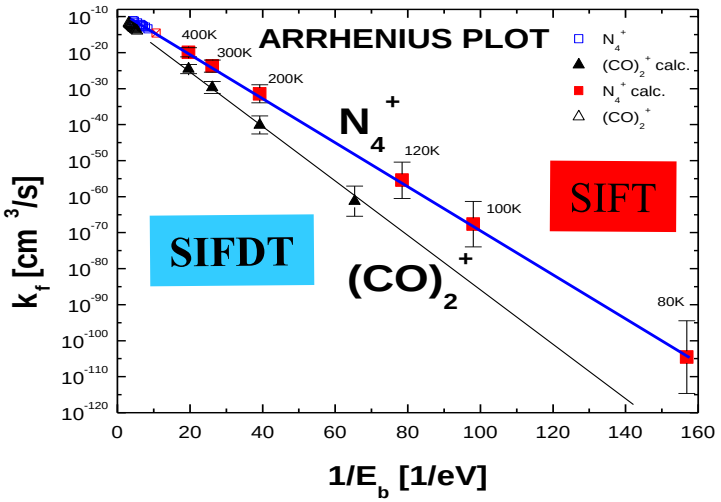

$$k_f \sim k_{coll} \exp(-\Delta H / kT)$$

$$\ln(k_f) \sim -\Delta H / kT$$

Equilibrium

$$N_4^+ + He \underset{k_r}{\overset{k_f}{\rightleftharpoons}} N_2^+ + N_2 + He$$

The equilibrium between reactant A and product B: $A \rightleftarrows B$

$$N_4^+ \rightleftharpoons N_2^+$$

$$N_4^+ + He \underset{k_r}{\overset{k_f}{\rightleftharpoons}} N_2^+ + N_2 + He$$

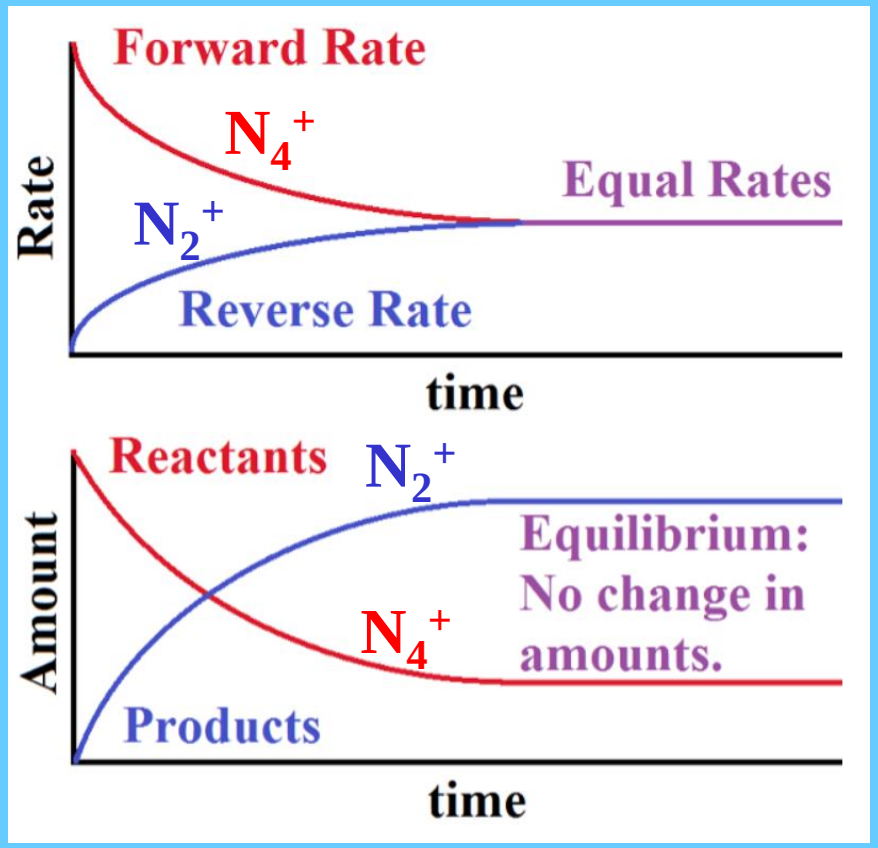

Van’t Hoff equation

For a system undergoing a reversible reaction described by the general chemical equation

$$\alpha\,\mathrm{A} + \beta\,\mathrm{B} + \cdots \rightleftharpoons \rho\,\mathrm{R} + \sigma\,\mathrm{S} + \cdots$$

a thermodynamic equilibrium constant, denoted by $K^\ominus$, is defined to be the value of the reaction quotient Q_t when forward and reverse reactions occur at the same rate. At chemical equilibrium, the chemical composition of the mixture does not change with time and the Gibbs free energy change ΔG for the reaction is zero. If the composition of a mixture at equilibrium is changed by addition of some reagent, a new equilibrium position will be reached, given enough time. An equilibrium constant is related to the composition of the mixture at equilibrium by [1][2]

$$K^\ominus = \frac{\{\mathrm{R}\}^\rho\{\mathrm{S}\}^\sigma\cdots}{\{\mathrm{A}\}^\alpha\{\mathrm{B}\}^\beta\cdots} = \frac{[\mathrm{R}]^\rho[\mathrm{S}]^\sigma\cdots}{[\mathrm{A}]^\alpha[\mathrm{B}]^\beta\cdots} \times \Gamma,$$

$$\Gamma = \frac{\gamma_R^\rho\gamma_S^\sigma\cdots}{\gamma_A^\alpha\gamma_B^\beta\cdots},$$

where {X} denotes the thermodynamic activity of reagent X at equilibrium, [X] the corresponding concentration, and γ the corresponding activity coefficient. If it can be assumed that the quotient of activity coefficients, Γ, is constant over a range of experimental conditions, such as pH, then an equilibrium constant can be derived as a quotient of concentrations.

$$K_c = K^\ominus/\Gamma = \frac{[\mathrm{R}]^\rho[\mathrm{S}]^\sigma\cdots}{[\mathrm{A}]^\alpha[\mathrm{B}]^\beta\cdots}.$$

An equilibrium constant is related to the standard Gibbs free energy change of reaction $\Delta G^\ominus$ by

$$\Delta G^\ominus = -RT\ln K^\ominus,$$

where R is the universal gas constant, T is the absolute temperature (in kelvins), and $\ln$ is the natural logarithm. This expression implies that $K^\ominus$ must be a pure number and cannot have a dimension, since logarithms can only be taken of pure numbers. K_c must also be a pure number. On the other hand, the reaction quotient at equilibrium

$$\frac{[\mathrm{R}]^\rho[\mathrm{S}]^\sigma\cdots}{[\mathrm{A}]^\alpha[\mathrm{B}]^\beta\cdots}(eq)$$

does have the dimension of concentration raised to some power (see § Dimensionality, below). Such reaction quotients are often referred to, in the biochemical literature, as equilibrium constants.

For an equilibrium mixture of gases, an equilibrium constant can be defined in terms of partial pressure or fugacity.

An equilibrium constant is related to the forward and backward rate constants, k_f and k_r of the reactions involved in reaching equilibrium:

$$K^\ominus = \frac{k_\mathrm{f}}{k_\mathrm{r}}.$$

The Arrhenius Equation

Experimental observation : $k=Aexp(-B/T)$

1889 Arrhenius sugested expression:

$k=Aexp(-E_a/RT)$ Arrhenius equation

A - pre exponential factor or Frequency factor

E_a – activation energy

Better definition is $\ln k = (-E_a/RT) + \ln A$

Dependence of lnk versus 1/T will have a slope equal $-E_a/R$

Boltzmann's Distribution Law

Boltzmann distribution law

$N_i/N = [\exp(-\varepsilon_\iota /kT)]/[\Sigma \exp(-\varepsilon_\iota /kT)]$

$N_2/N_1 = \exp(-(\varepsilon_2-\varepsilon_1)/kT)$

$N_i/N = g_i [\exp(-\varepsilon_\iota /kT)]/g$

g – molecular partition function

Van't Hoff equation

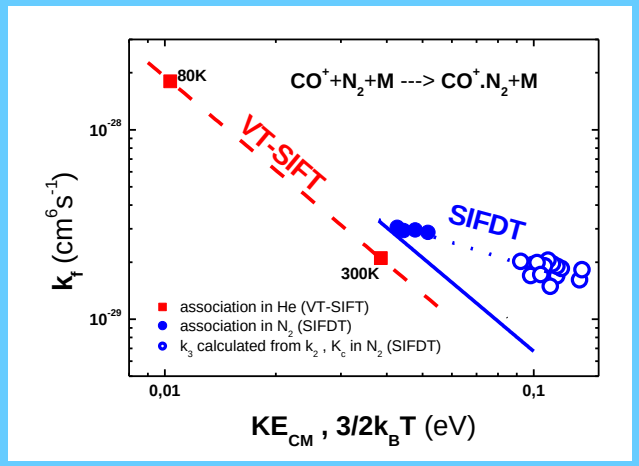

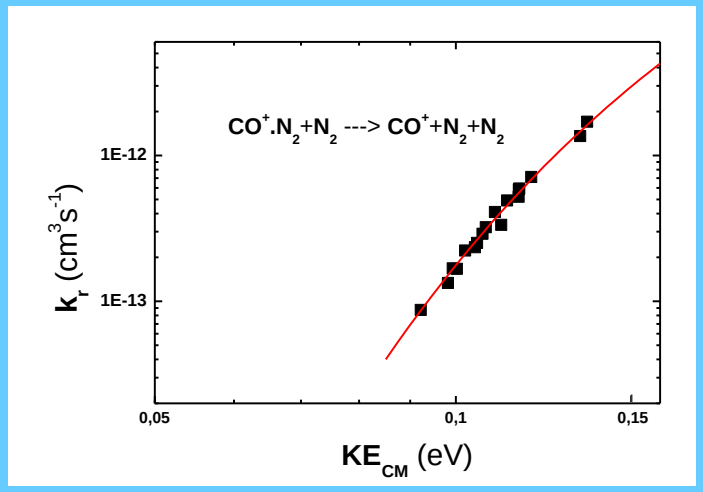

$RTlnK_P = -\Delta G_P = -\Delta H_P + T\Delta S_P$ van't Hoff equation

$lnK_P = -\Delta H_P/RT + \Delta S_P/R$

$\Delta H_P^0 =$ -17,1 kcalmol^{-1} a
$\Delta S_P^0 =$ -10,2 kcalmol^{-1} K^{-1}

The Arrhenius Equation

$k = Aexp(-E_a/RT)$

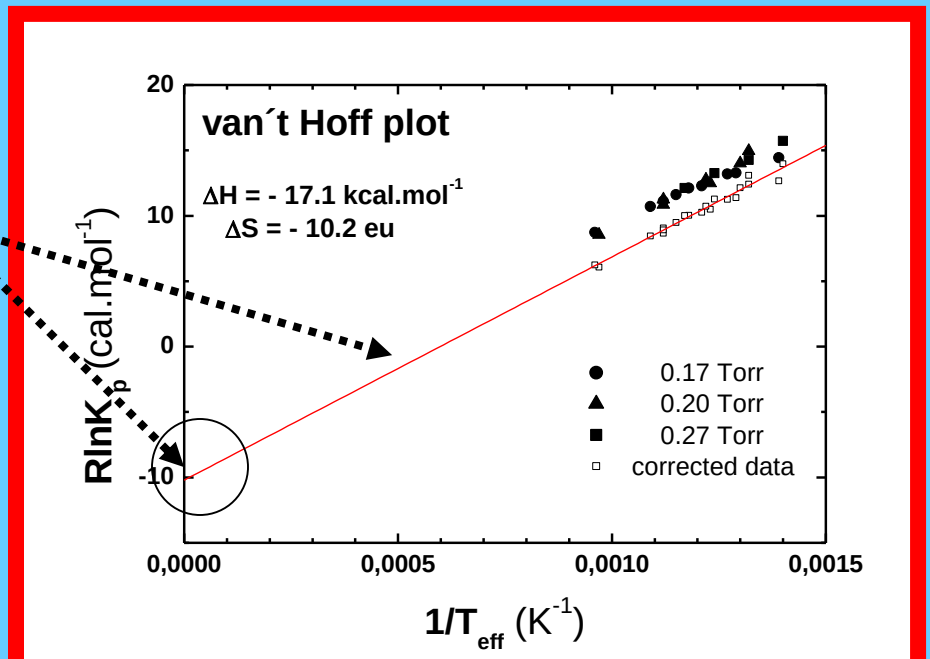

Van't Hoff equation and thermodynamic parameters

$RTlnK_P=-\Delta G_P=-\Delta H_P + T\Delta S_P$ van't Hoff equation

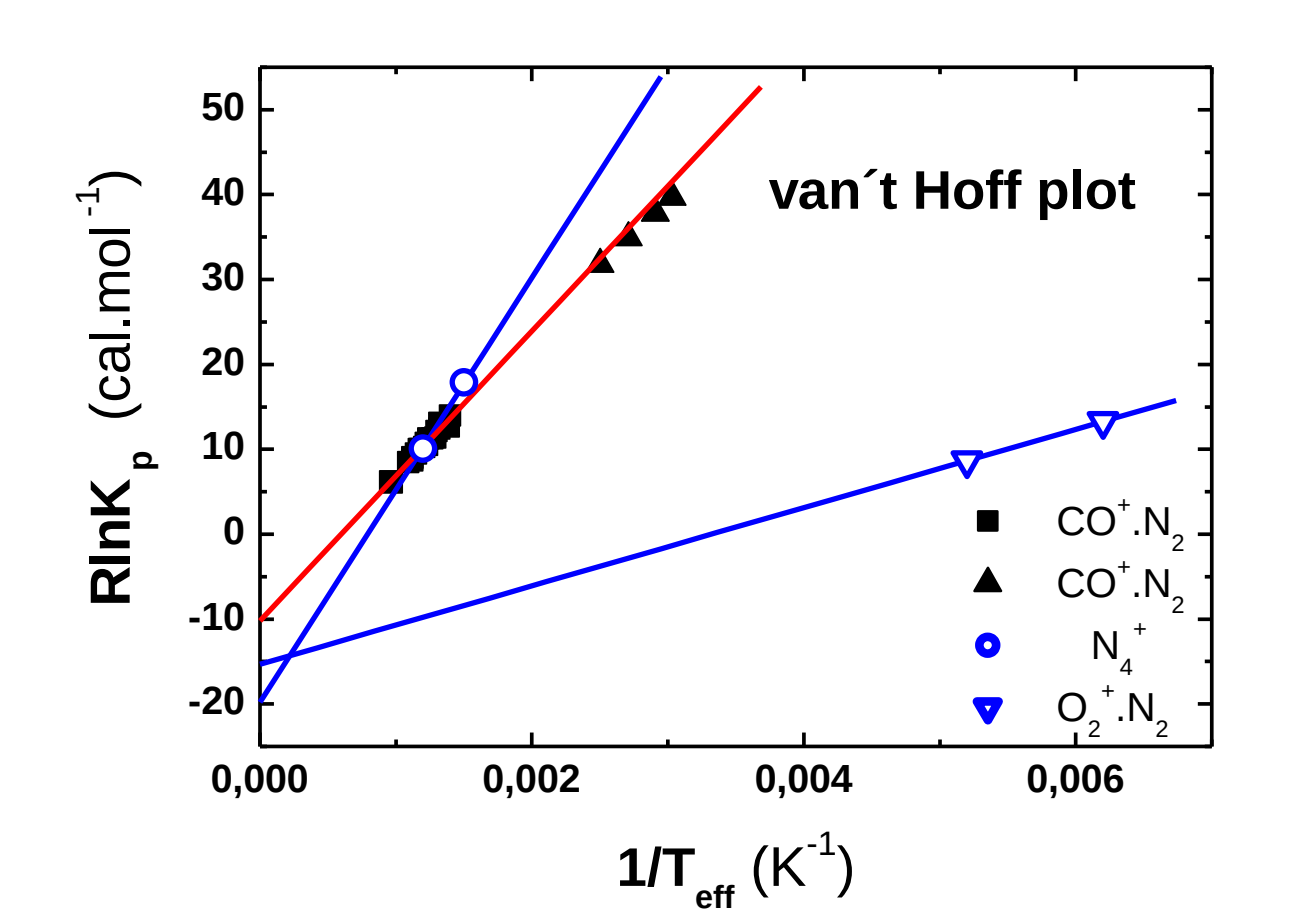

$lnK_P=-\Delta H_P/RT + \Delta S_P/R$ van't Hoff plot

Ion – molecule reactions

$$AB^+ + CD \xrightarrow{k} AC^+ + BD$$

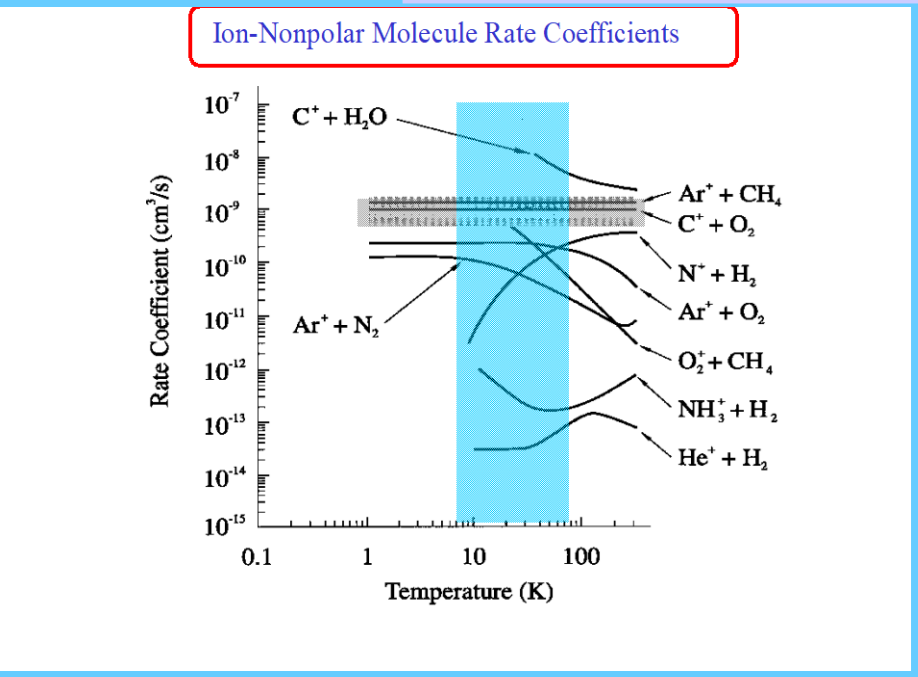

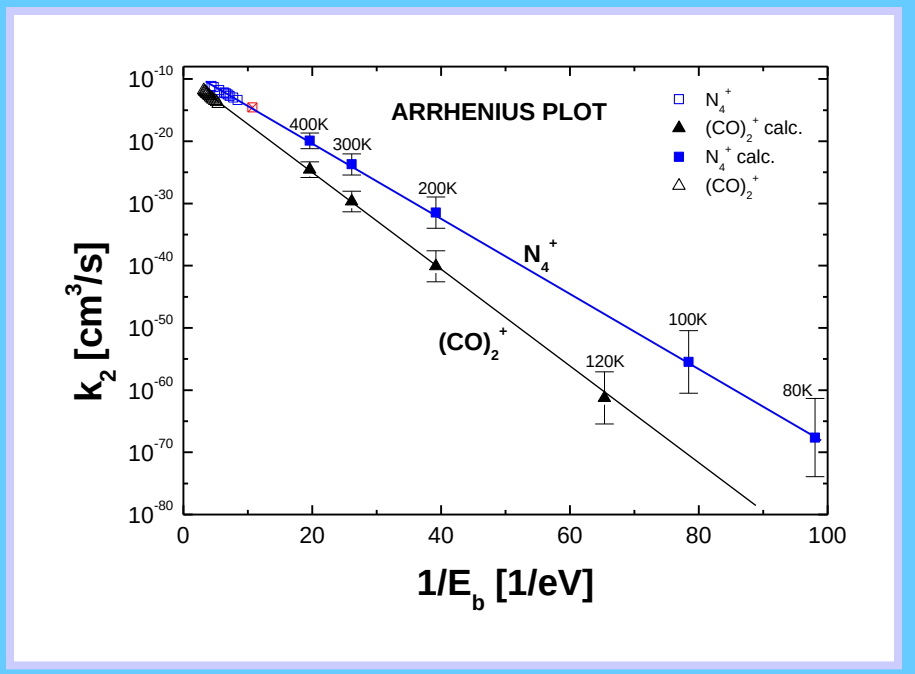

Proton transfer: $H_3O^+ + NH_3 \xrightarrow{k} NH_4^+ + H_2O$

CID – collision induced dissociation:

$$N_4^+ + He \xrightarrow{k_{BIN}} N_2^+ + N_2 + He$$

$$N_4^+ \xrightarrow{k_{UNI}} N_2^+ + N_2$$

Collision induced dissociation

$$N_4^+ + He \underset{k_r}{\overset{k_f}{\rightleftharpoons}} N_2^+ + N_2 + He$$

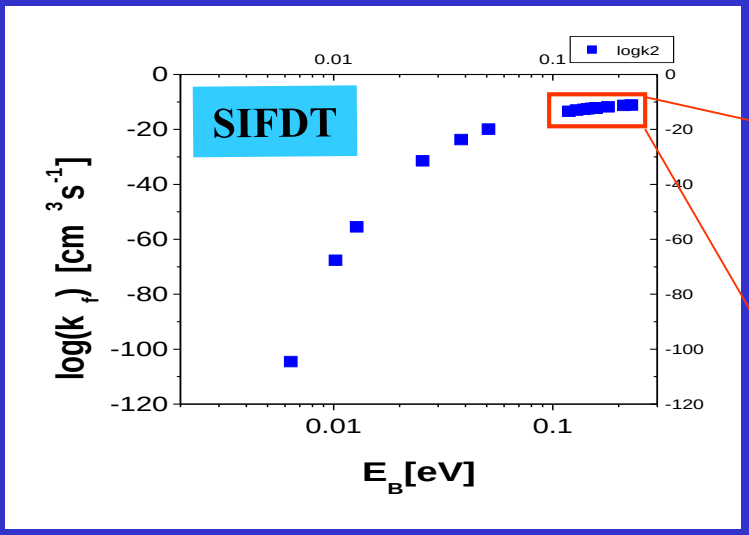

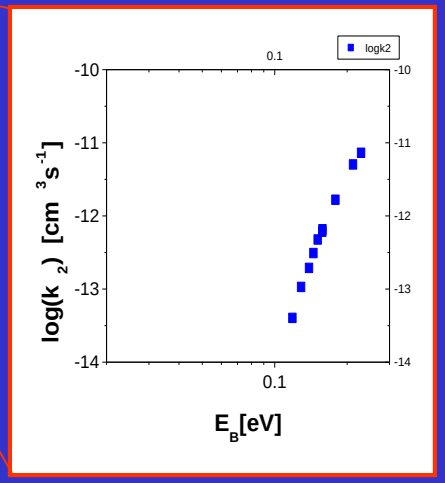

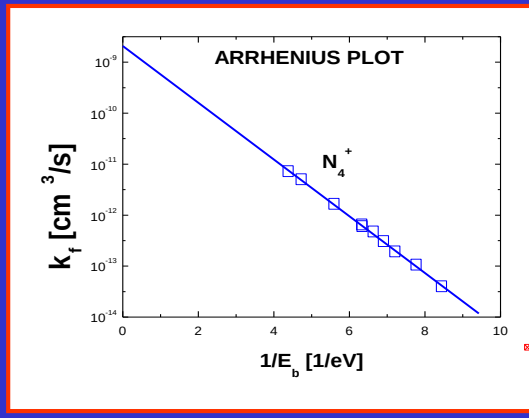

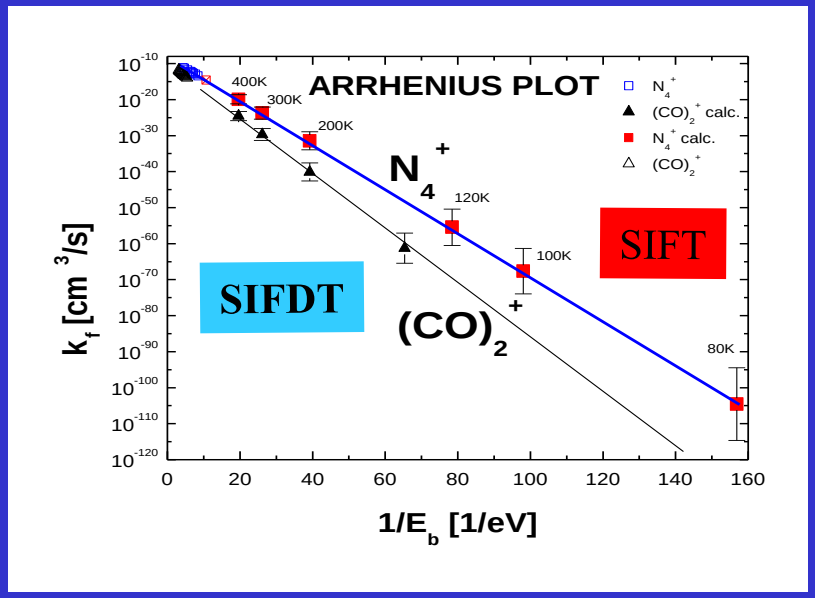

$$k_f \sim k_{coll} \exp(-\Delta H / kT)$$

$$\ln(k_f) \sim -\Delta H / kT$$

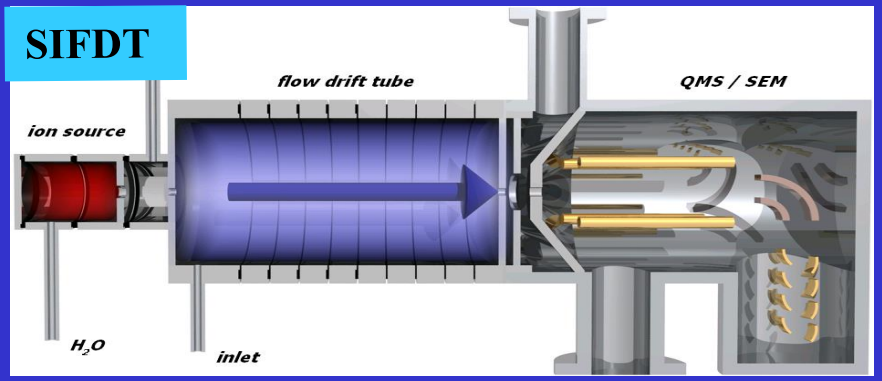

$Ar^+ + e^- + e^-$

$k=\sim 4\times10^{-6} cm^3 s^{-1}$ $H_5^+ + e^-$

$k=\langle v\sigma\rangle \sim 4\times10^{-7} cm^3 s^{-1}$ SF_6

k_{rec} $H_3^+ + e^-$

Ar_2^+

rotation

$Ar^+ + e^- \rightarrow Ar + h\nu$

k ($cm^3 s^{-1}$)

10^{-5} 10^{-6} 10^{-7} 10^{-8} 10^{-9} 10^{-10} 10^{-11} 10^{-12} 10^{-13} 10^{-14} 10^{-15}

0.1 1 10 100 1000 10000 10000

T (K)

0.1 eV 1 eV 10 eV

$\tau \sim 1/n_{xxx}k$

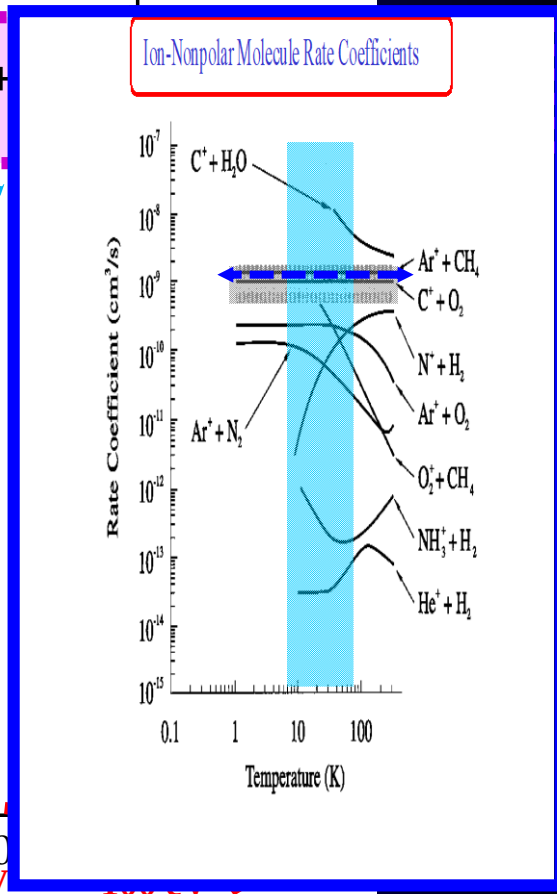

$Ar^+ + e^- + e^-$

$n_e = 10^{10}\ cm^{-3}$

$k = \langle v\sigma \rangle \sim 4 \times 10^{-7} cm^3 s^{-1}$ SF_6

k=~4x

$\alpha_{CRR} = 3.8 \times 10^{-9} T_e^{-4.5} 10^{10} \sim 38 \times T_e^{-4.5} cm^3 s^{-1}$

k_{rec} $H_3^+ + e^-$

$Ar_2^+ + e^- \rightarrow Ar + Ar$

rotation

k_{O4}

IMR

$\rightarrow Ar + h\nu$

ionization Ar

k_{O2}

O^-

$O^- + D_2 \rightarrow$

$k\ (cm^3\ s^{-1})$

T (K)

0.1 eV 1 eV 10 eV 100 eV

$\tau \sim 1/n_{xxx}k$

Rate coefficient of IMR - $C_2H_2^+ + H_2$

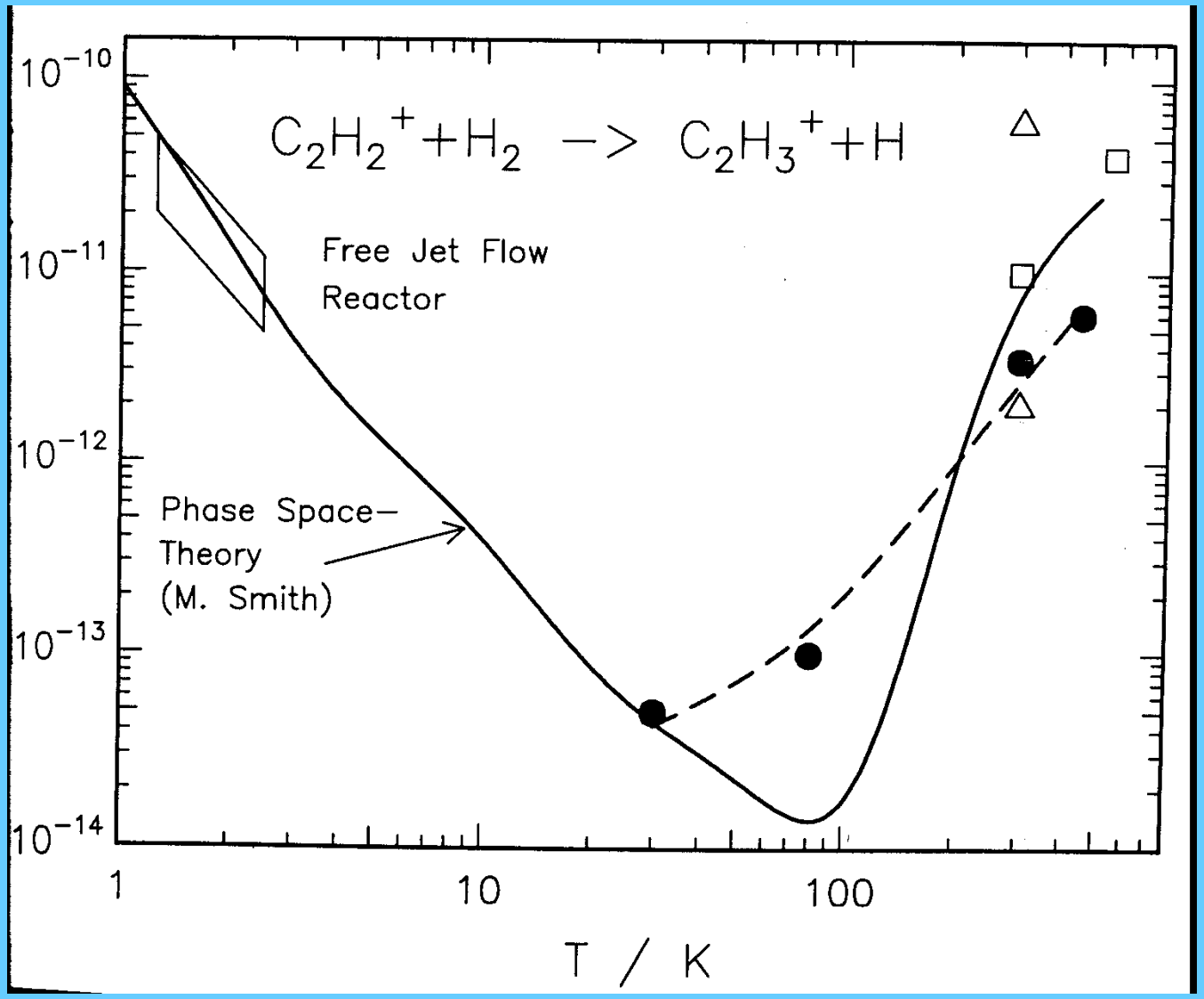

Unimolecular reactions

Reaction rate coefficient

$$A^+ \rightarrow product$$

$$\frac{dA^+}{dt} = -k_{UNI} A^+ = -A^+ / \tau_{UNI}$$

Unimolecular reactions

Reaction rate coefficient

$$A^+ \rightarrow product \qquad \frac{dA^+}{dt} = -k_{UNI} A^+ = -A^+ / \tau_{UNI}$$

$$[A^+]_t = [A^+]_{t=0} \cdot e^{-k_{UNI} t} = [A^+]_{t=0} \cdot e^{-t/\tau_{UNI}}$$

$$k_{UNI} = 1/\tau_{UNI}$$

$$[k_{UNI}] = s^{-1}$$

$$A^+ \rightarrow B^+ \rightarrow C^+$$

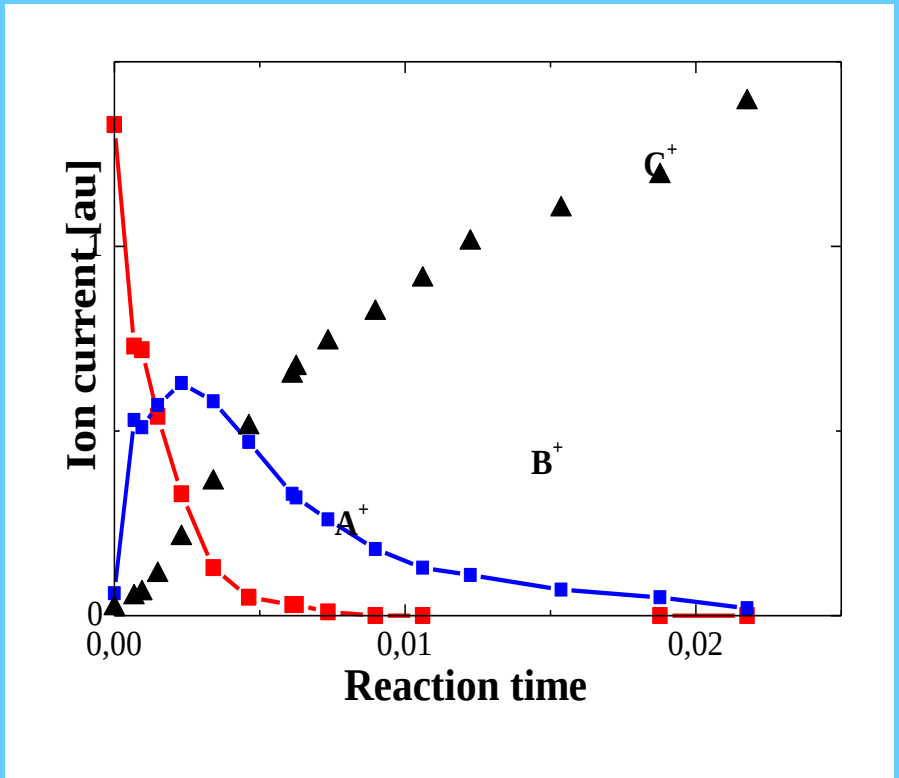

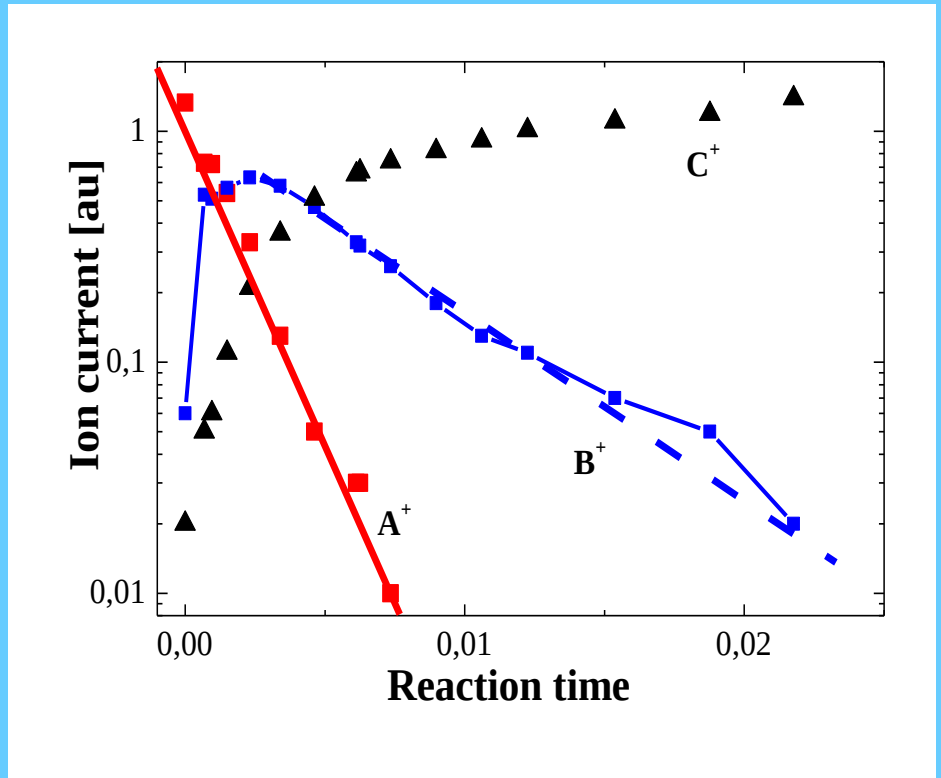

Unimolecular reactions

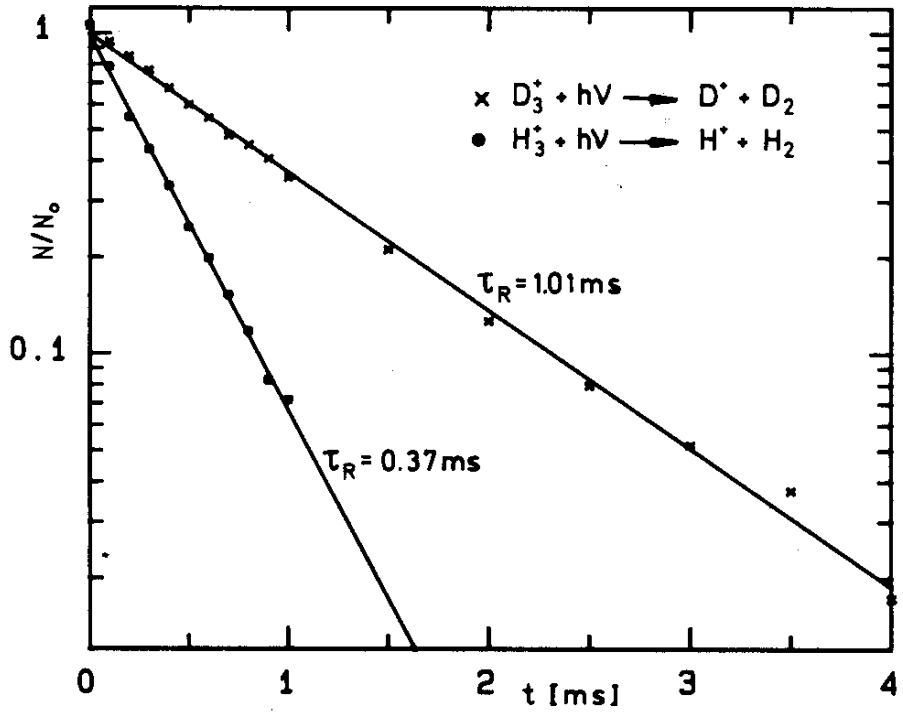

Figure 87. Direct determination of radiative lifetimes of highly exited H_3^+ and D_3^+ ions. Externally created ions were injected into the ring electrode trap, and their spontaneous radiative decay was probed by delayed CO_2 laser-induced fragmentation. Loss by processes other than radiative decay is excluded on the depicted time scale and at the low pressure ($<10^{-9}$ mbar).

Radiative lifetimes

$$[A^+]_t = [A^+]_{t=0} \cdot e^{-k_{UNI} t} = [A^+]_{t=0} \cdot e^{-t/\tau_{UNI}}$$

$$k_{UNI} = 1/\tau_{UNI}$$

Three body reactions

$$A^+ + B + M \rightarrow C^+ + D + M$$

$$\frac{d[A^+]}{dt} = -k_{BINeff}[A^+][B] = -k_3[A^+][B][M]$$

$$[k_3] = cm^6 s^{-1}$$

For $[A^+] \ll [B],[M]$ $$[A^+]_t = [A^+]_{t=0} \cdot e^{-k_3[B][M]t}$$

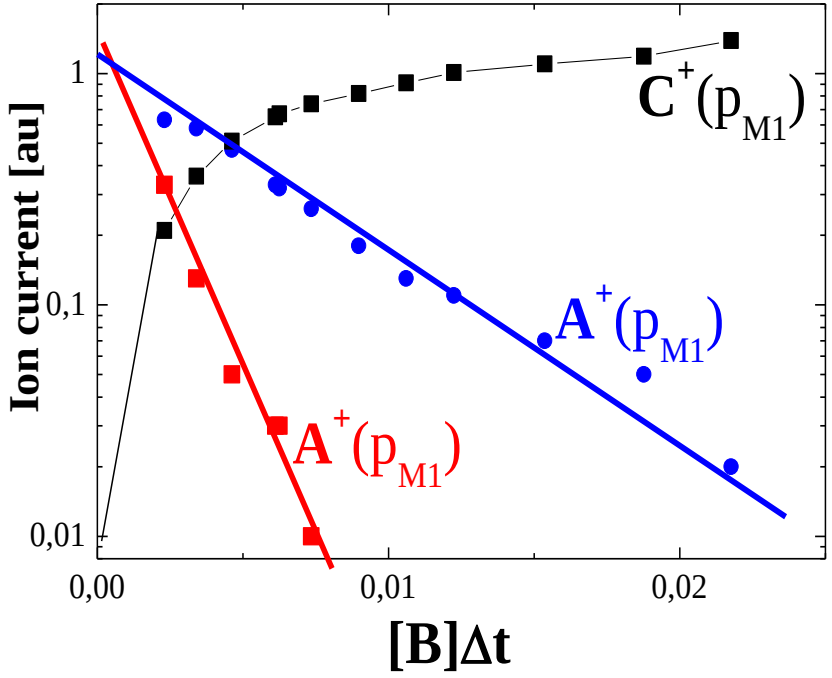

Three body reactions

$$He^+ + 2\,He \rightarrow He_2^+ + He$$

$$\frac{d[A^+]}{dt} = -k_{BINeff}[A^+][B] = -k_3[A^+][B][M]$$

$$[k_3] = cm^6 s^{-1}$$

For [A⁺]<<[B],[M] $$[A^+]_t = [A^+]_{t=0} \cdot e^{-k_3[B][M]t}$$

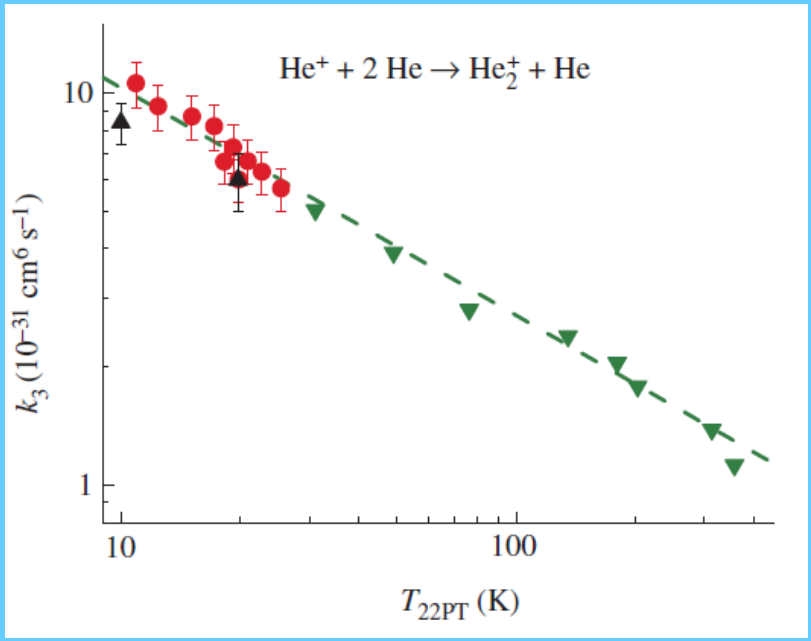

He

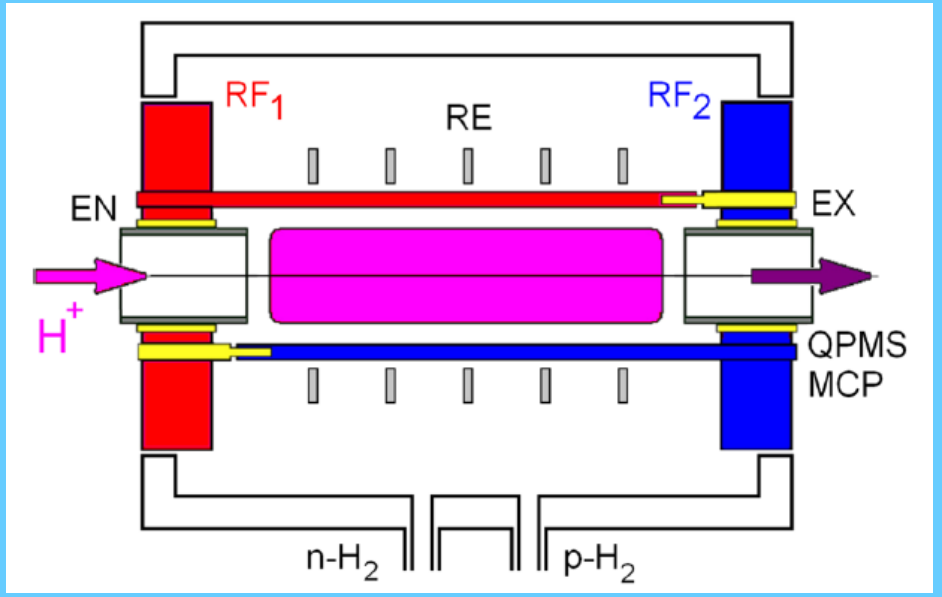

Radiative lifetime

PHILOSOPHICAL TRANSACTIONS OF THE ROYAL SOCIETY A MATHEMATICAL, PHYSICAL & ENGINEERING SCIENCES

Stabilization of H_+–H_2 collision complexes between 11 and 28K

Radek Plasil, Illia Zymak, Pavol Jusko, Dmytro Mulin, Dieter Gerlich and Juraj Glosík

Phil. Trans. R. Soc. A 2012 **370**, 5066-5073
doi: 10.1098/rsta.2012.0098

2012

$$H^+ + H_2 \xrightarrow{k_r} H_3^+ + h\nu,$$

$$H^+ + 2H_2 \xrightarrow{k_3} H_3^+ + H_2,$$

$$k^* = k_r + k_3[H_2]$$

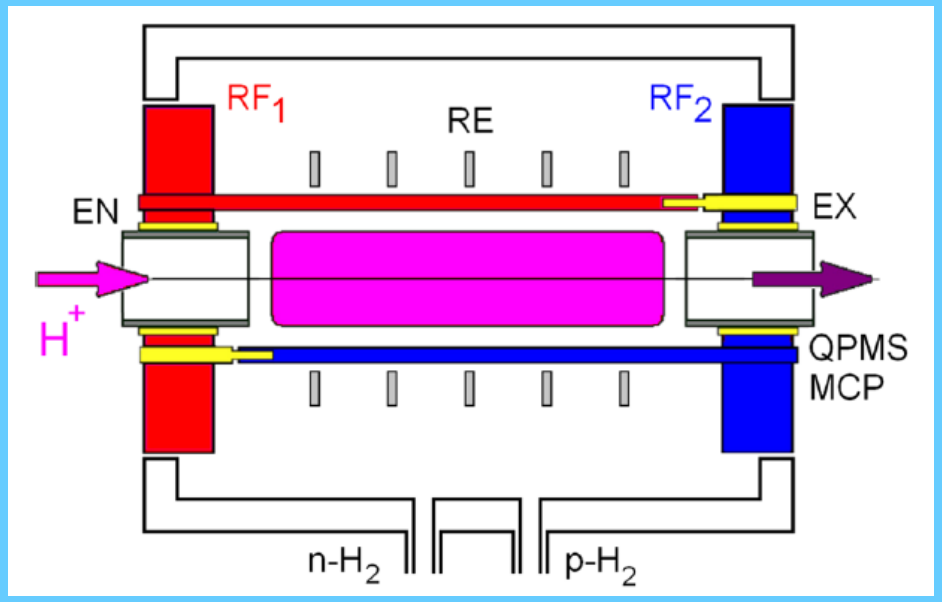

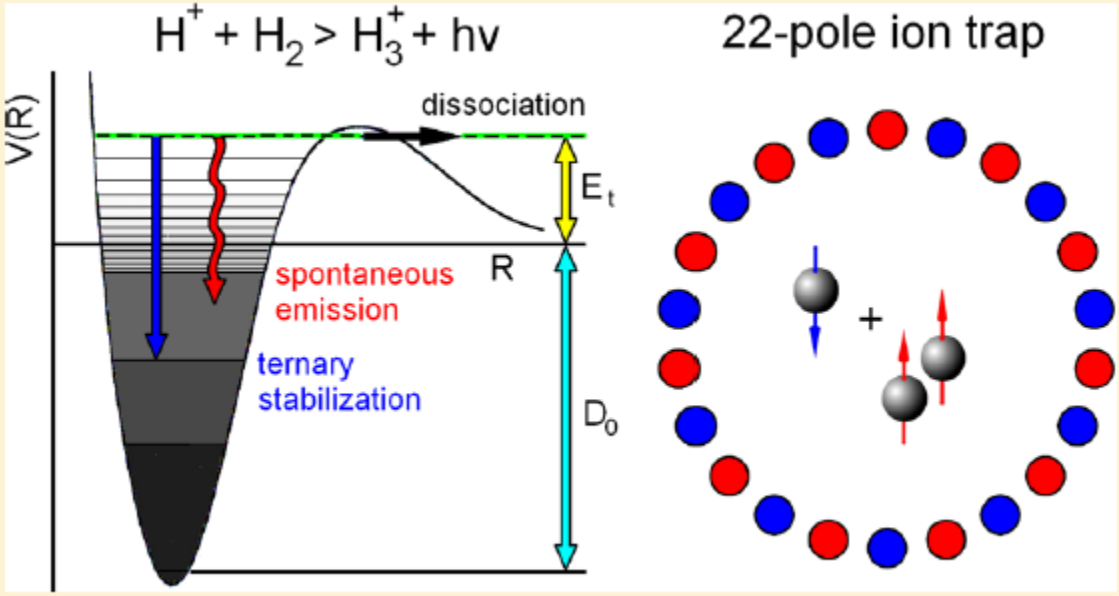

k_r

Stabilization of $H^+–H_2$ collision complexes between 11 and 28 K

$$H^+ + H_2 \xrightarrow{k_r} H_3^+ + h\nu,$$

$$H^+ + 2H_2 \xrightarrow{k_3} H_3^+ + H_2,$$

$$k^* = k_r + k_3[H_2].$$

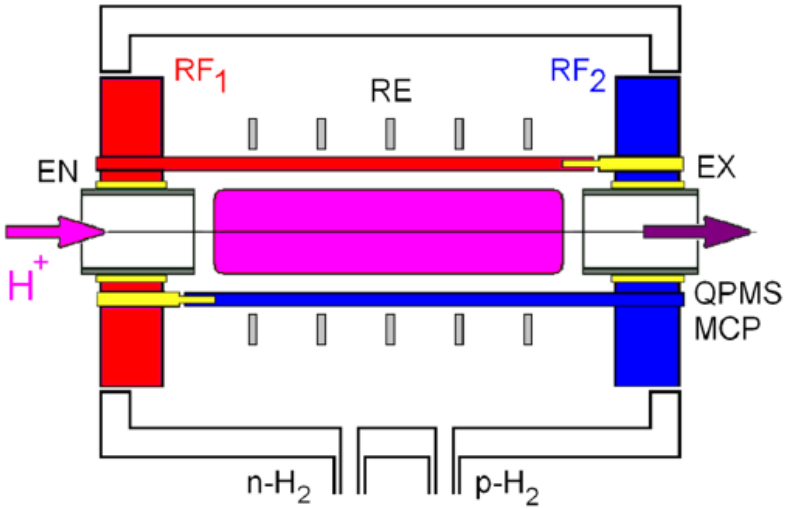

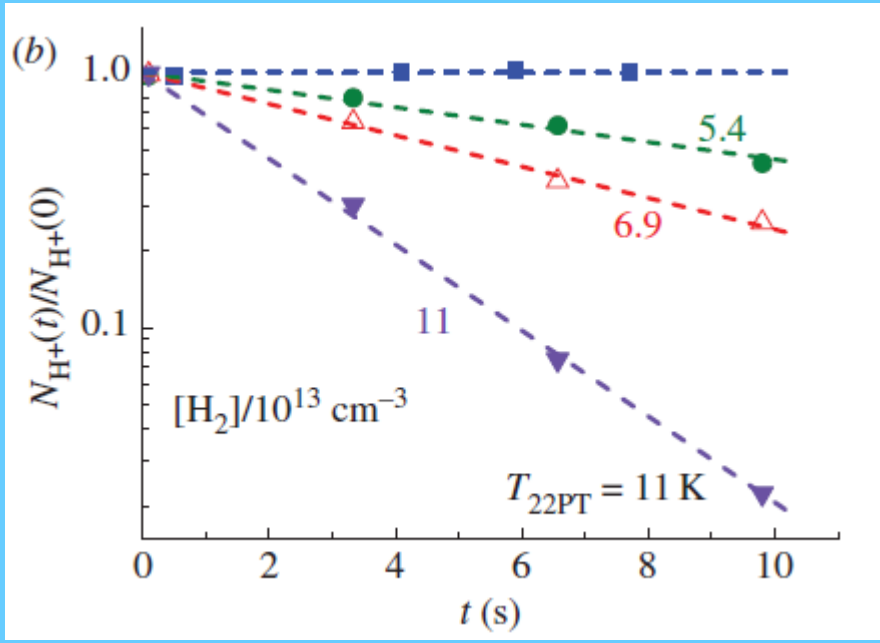

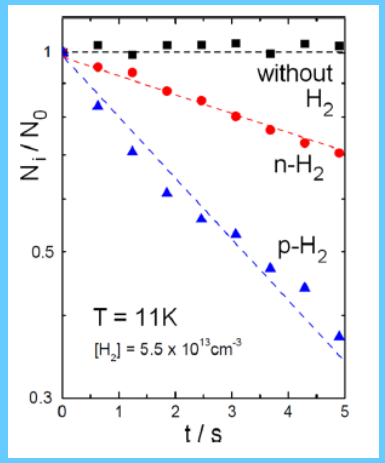

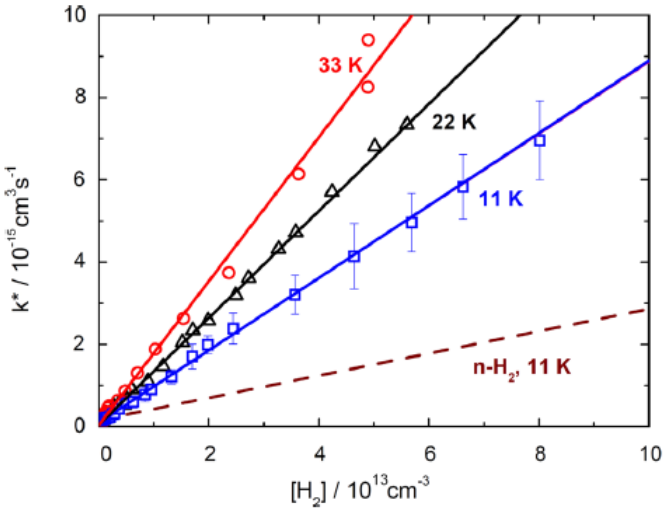

Figure 2. Apparent binary association rate coefficient k^* for T_{22PT} = 11, 22, and 33 K as a function of the p-H_2 number density. The data have been averaged over many iterations. For emphasizing the ternary rate coefficients, the results are plotted on a linear scale. The data are fitted with $k^* = k_r + k_3[H_2]$. The resulting parameters are in Table 1. The surprising result is that ternary association gets faster with increasing temperature. Concerning $k_r(T)$, see the text and Figure 3.

$$k^* = k_r + k_3[H_2].$$

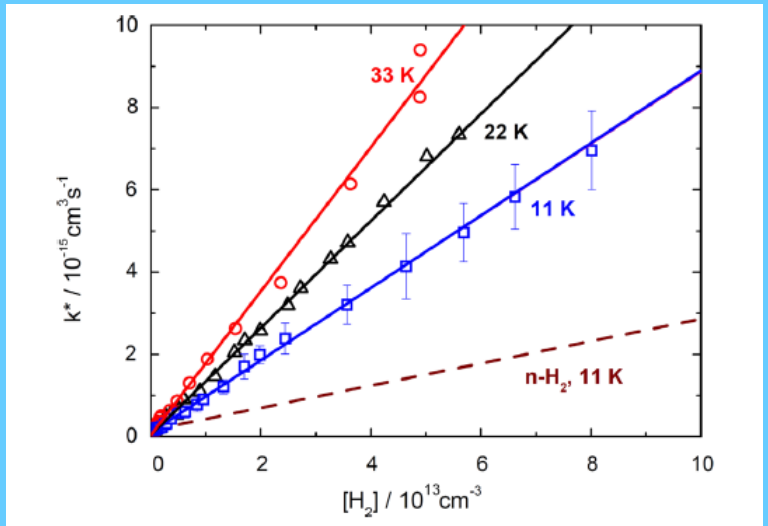

Figure 2. Apparent binary association rate coefficient k^* for T_{22PT} = 11, 22, and 33 K as a function of the p-H_2 number density. The data have been averaged over many iterations. For emphasizing the ternary rate coefficients, the results are plotted on a linear scale. The data are fitted with $k^* = k_r + k_3[H_2]$. The resulting parameters are in Table 1. The surprising result is that ternary association gets faster with increasing temperature. Concerning $k_r(T)$, see the text and Figure 3.

$$k^* = k_r + k_3[H_2].$$

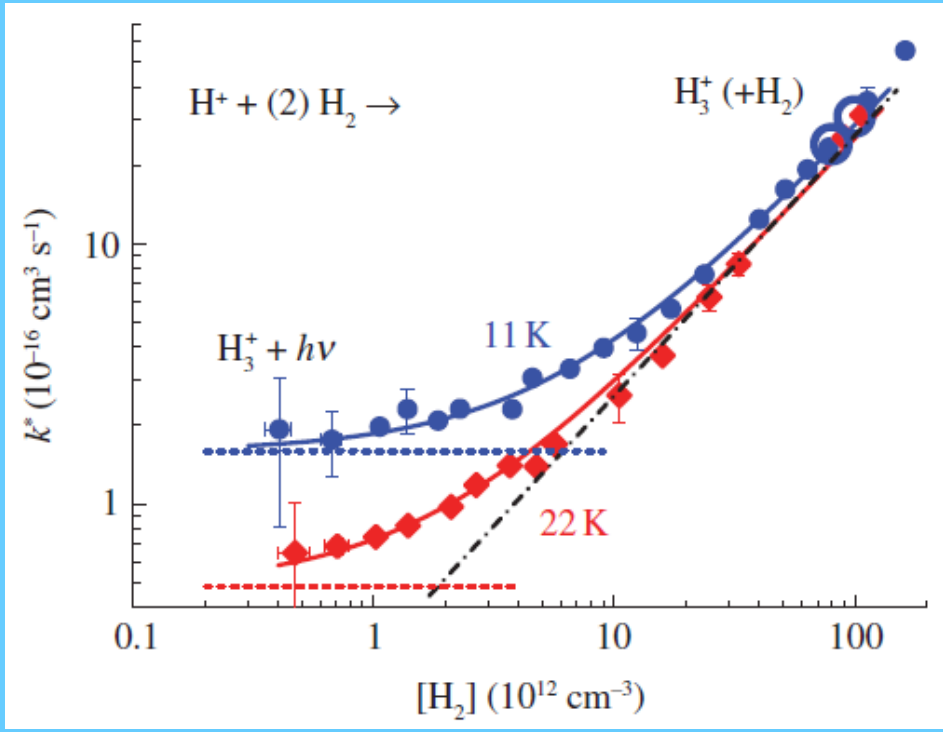

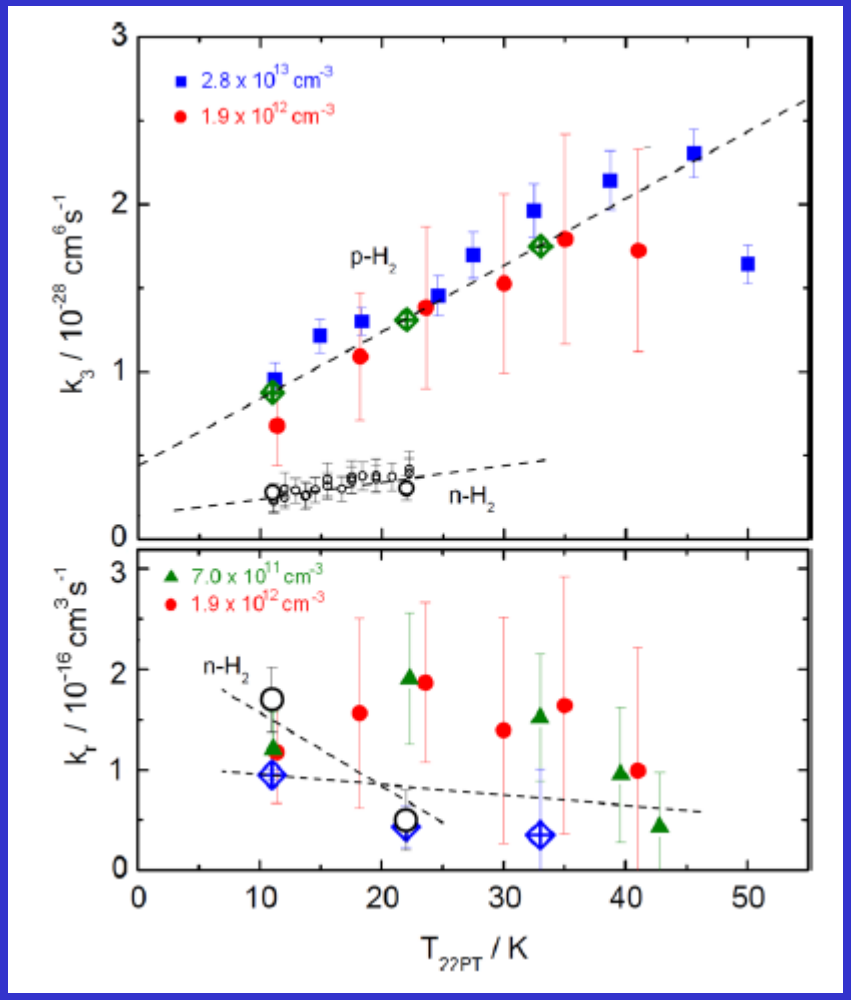
2.8 x 10^13 cm^-3
1.9 x 10^12 cm^-3
p-H2
n-H2
k3 / 10^-28 cm^6 s^-1
7.0 x 10^11 cm^-3
1.9 x 10^12 cm^-3
n-H2
kr / 10^-16 cm^3 s^-1
T??PT / K

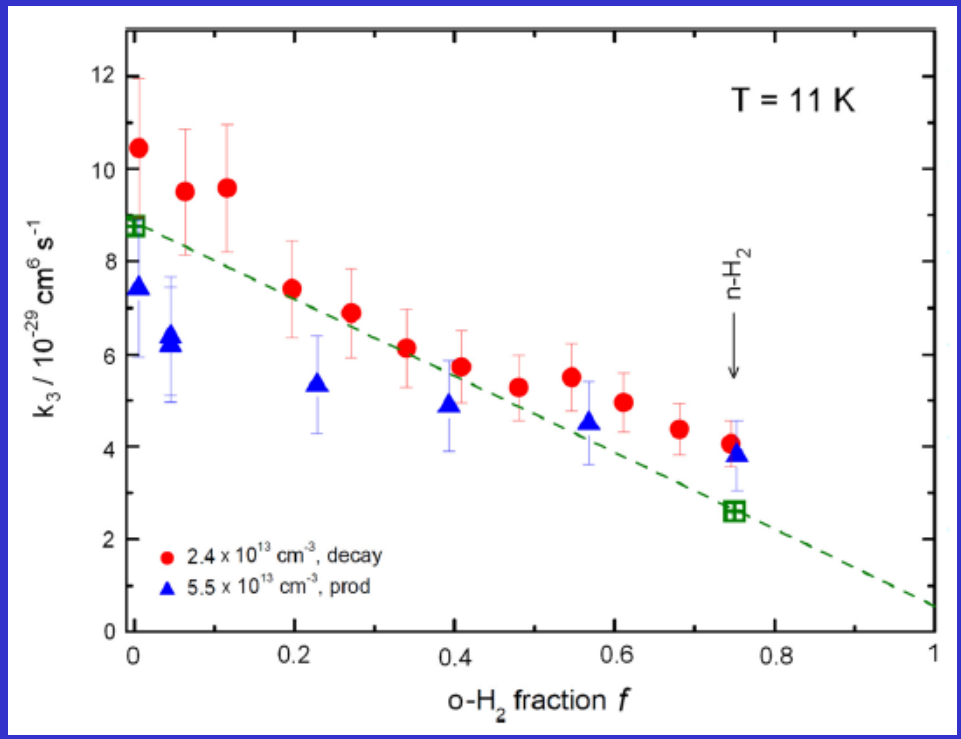
T = 11 K
n-H2
k3 / 10^-29 cm^6 s^-1
2.4 x 10^13 cm^-3, decay
5.5 x 10^13 cm^-3, prod
o-H2 fraction f

Radiative association and ternary association

$$k^* = k_r + k_3[H_2]$$

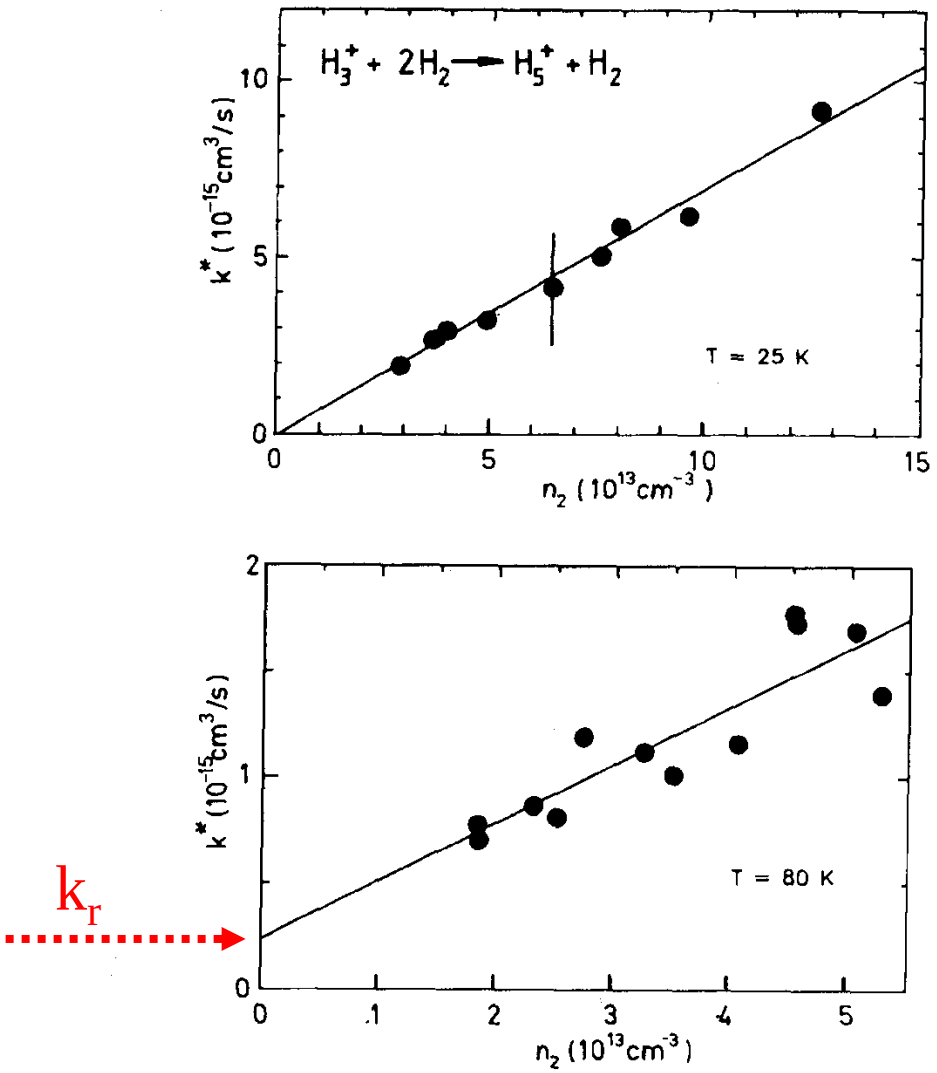

Figure 59. Apparent binary rate coefficient k^* for the ternary association reaction $H_3^+ + 2H_2 \rightarrow H_5^+ + H_2$, plotted as a function of the H_2 density n_2 (Paul, 1990). Increasing the nominal temperature of the ring electrode trap from 25 K to 80 K leads to a decrease of the ternary rate coefficient from 7×10^{-29} cm^6/s to 2.8×10^{-29} cm^6/s.

Kinetics of IMR

Techniques for study of IMR – reality

Flow tubes

FA– Flowing Afterglow principle

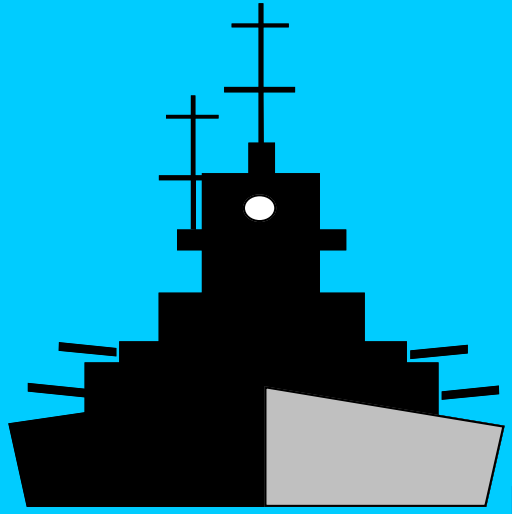

RECOMBINATION

FLOWING AFTERGLOW

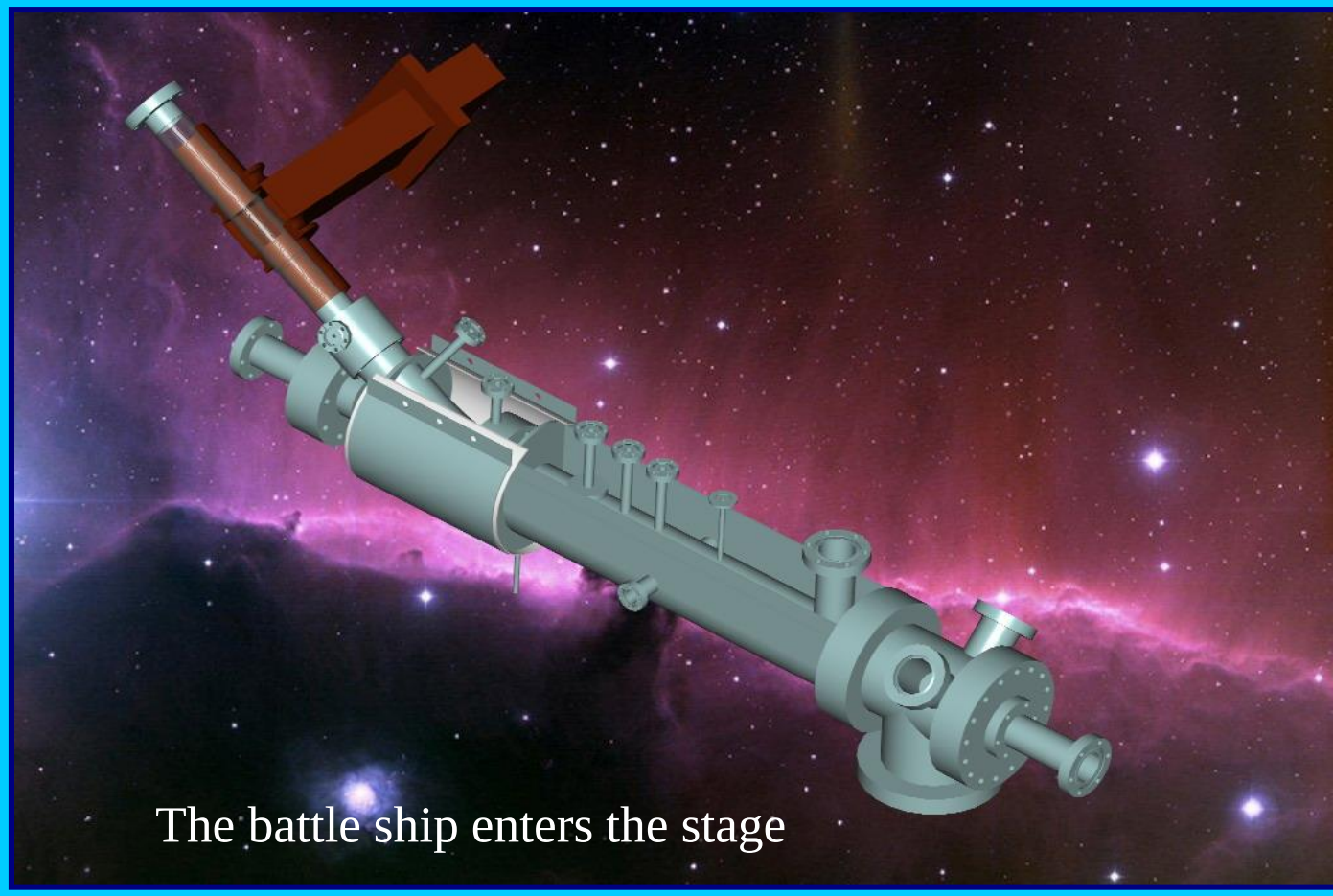

Single collision cross section $I=I_0 \exp(-\sigma n_i x)$

Plasma in Thermodynamic Equilibrium (T =80-350K ~ 10-40meV) $T_{rot}=T_{vib}=T_{kin}=T_e=T$

AISA - **Advanced Integrated Stationary Afterglow**

FALP - **Flowing Afterglow Langmuir Probe**

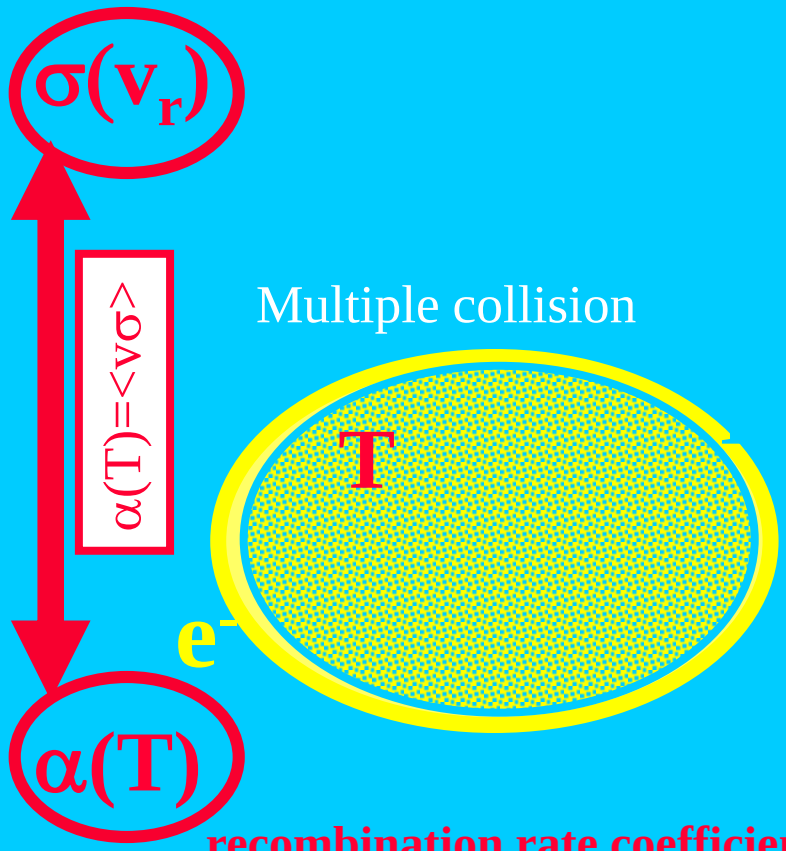

Multiple collision

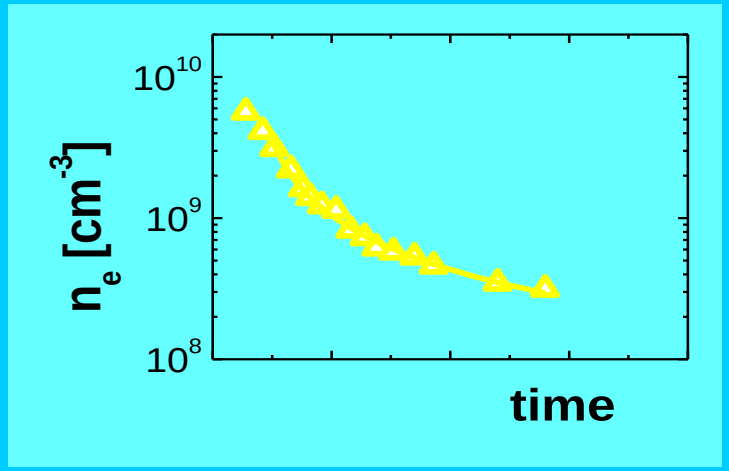

recombination rate coefficient

$dn_i/dt=-\alpha n_i n_e$

Recombination in a plasma (one ion species only, quasi-neutral)

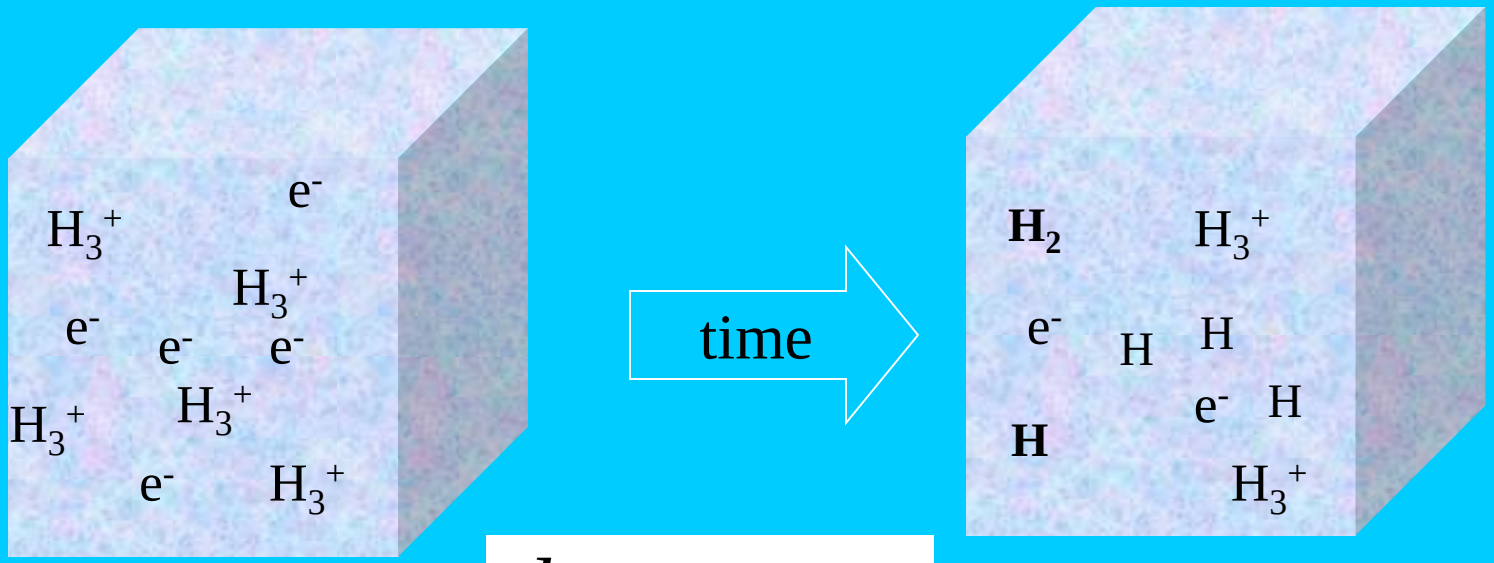

$$\frac{dn_e}{dt} = -\alpha n_e^{\,2}$$

The recombination coefficient $\alpha(T_e)$ varies with electron temperature typically as:

$$\alpha = 10^{-7}\left(\frac{T}{300}\right)^{-1/2} \quad [cm^3/s]$$

Pulsed (stationary) afterglow

SA

Discharge pulse

microwave, UV, x-ray, e-beam

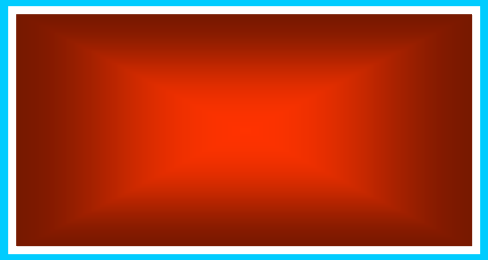

Plasma chamber
He: ~ 1 –20 Torr
Ar: 0,10 to 30 %
+ molecules

Measure $n_e(t)$

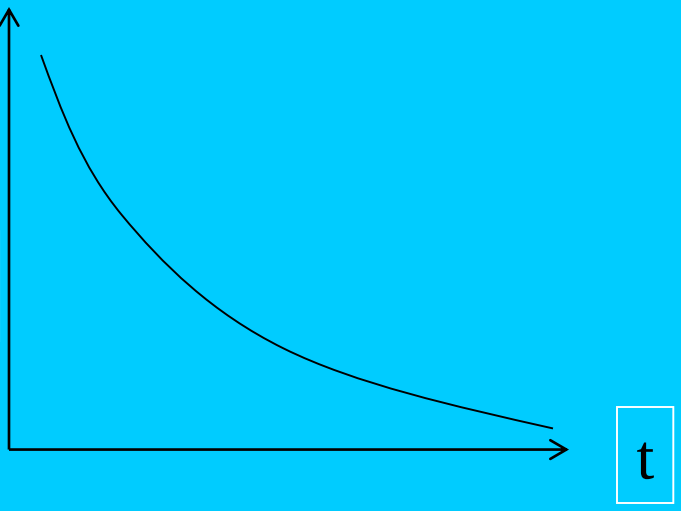

Get:

$$\frac{dn_e}{dt} = -\alpha n_e^{\,2} + (diffusion)$$

$$n_e(t) = \frac{n_{e0}}{1+\alpha n_{e0} t}$$

Formation of H_3^+ in He/Ar/H_2

T_e~2eV

($10^{17}/10^{14}/10^{11-14}$)

microwave discharge

He^+
He^m
e^-
Ar^+
Ar^m
H_2^+
H^+

He → He_2^+ → Ar → Ar^+ → H_2 → ArH^+, H_2^+ → H_2 → $H_3^+ + e^-$

Ar → Ar^+

$+e^-(300K)$ → hν

HeH^+ +He+He

After 10 ms

Recombination of H_3^+

Ion composition

AISA

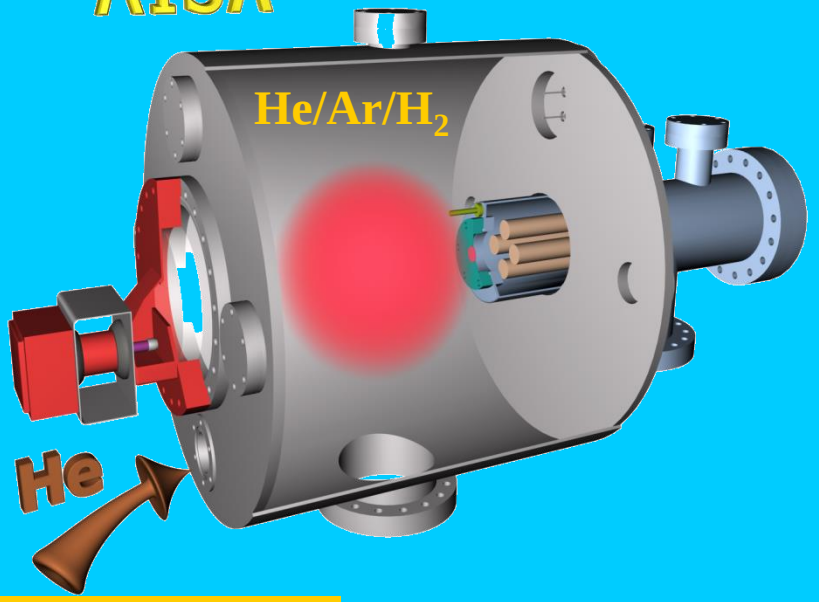

Time resolved mass spectra

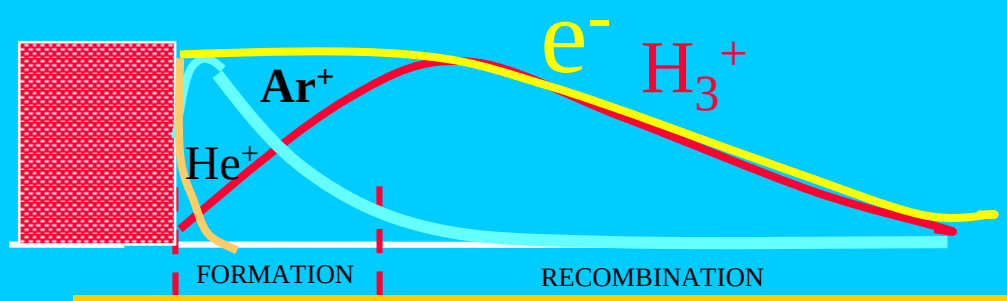

AISA –all gases are exposed to microwaves during active discharge !!!

Time resolved mass spectra

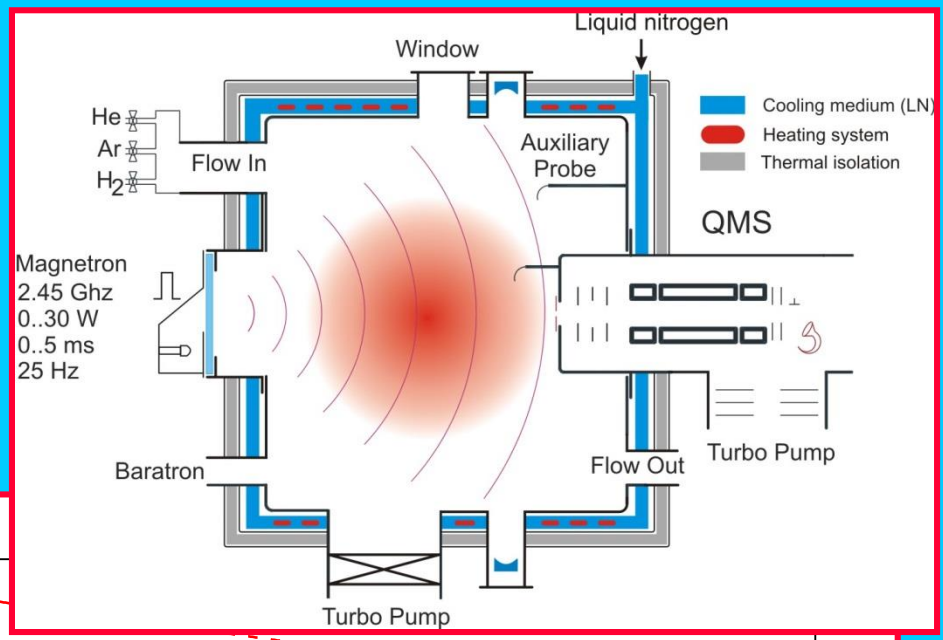

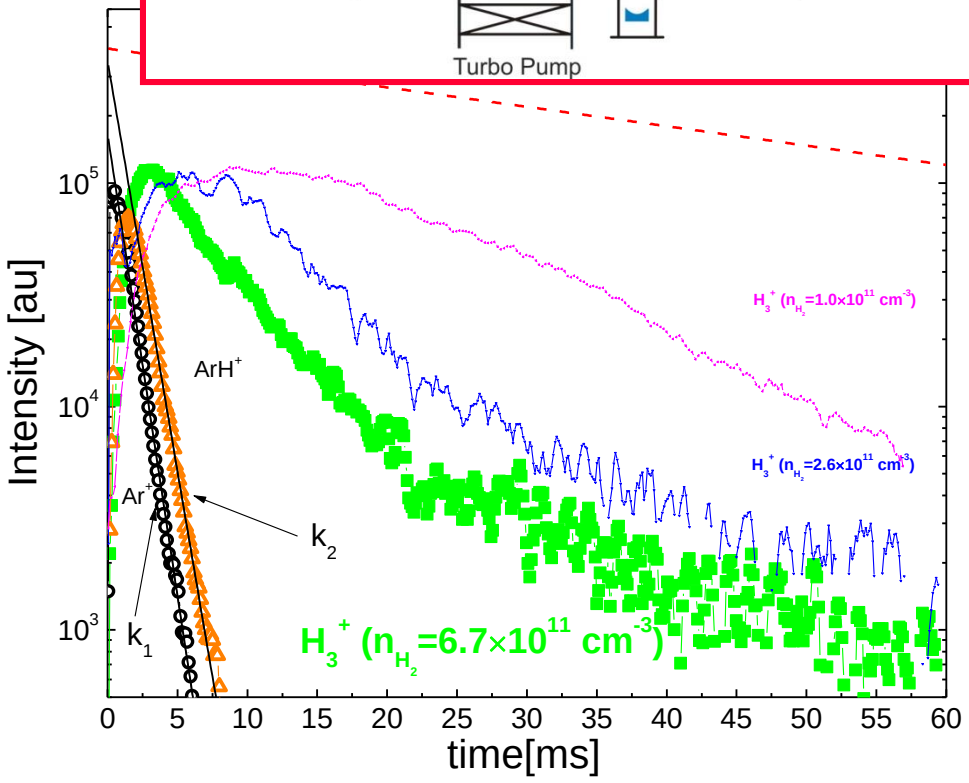

Flow techniques

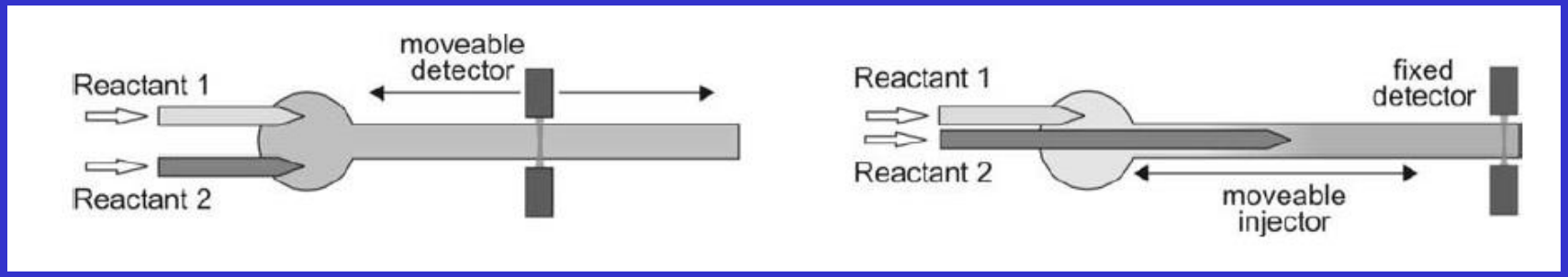

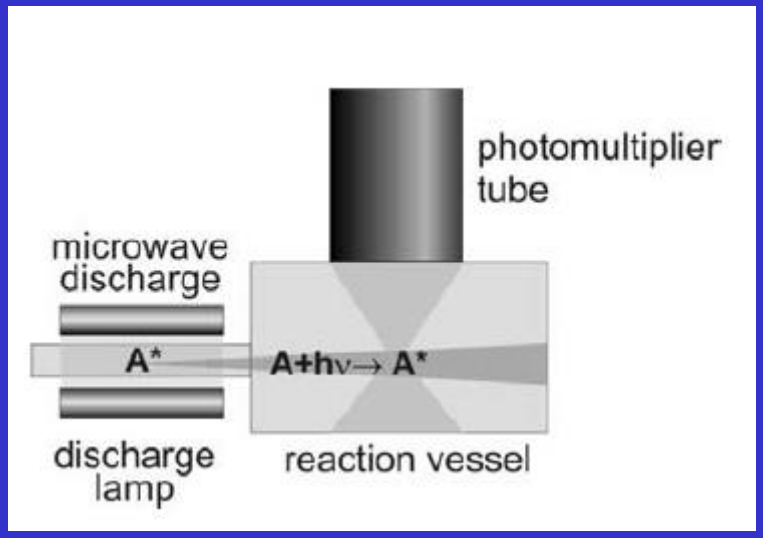

Rate Law

- **rate = $k[A]^x[B]^y$**
- **rate order = x + y**
- **knowledge of order can help control reaction**
- **rate must be experimentally determined**

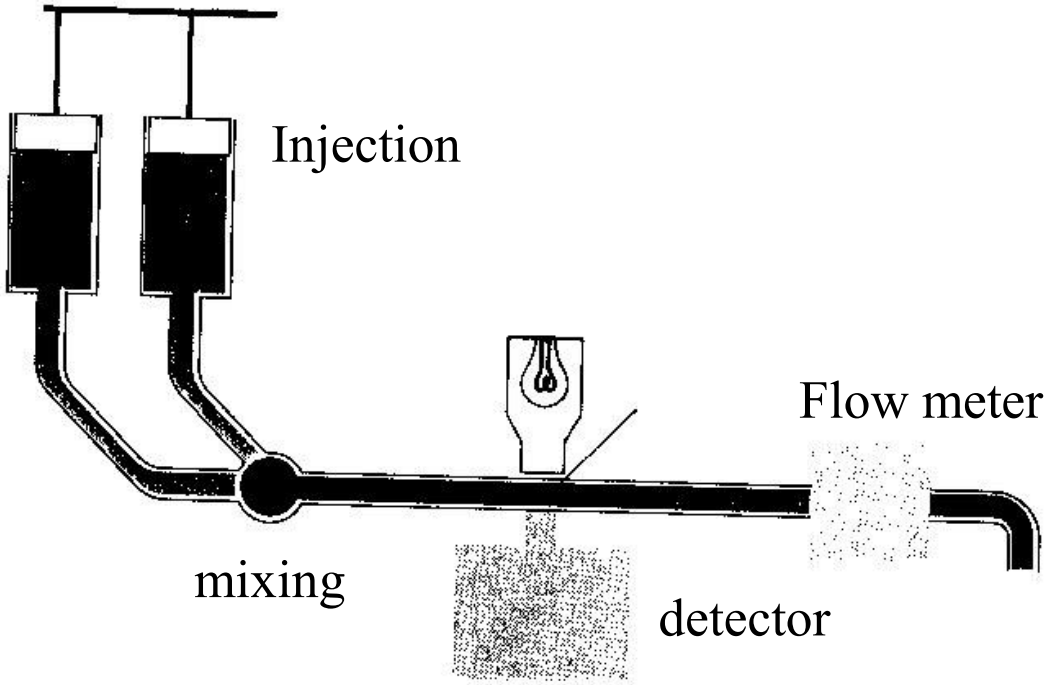

FA– Flowing Afterglow principle

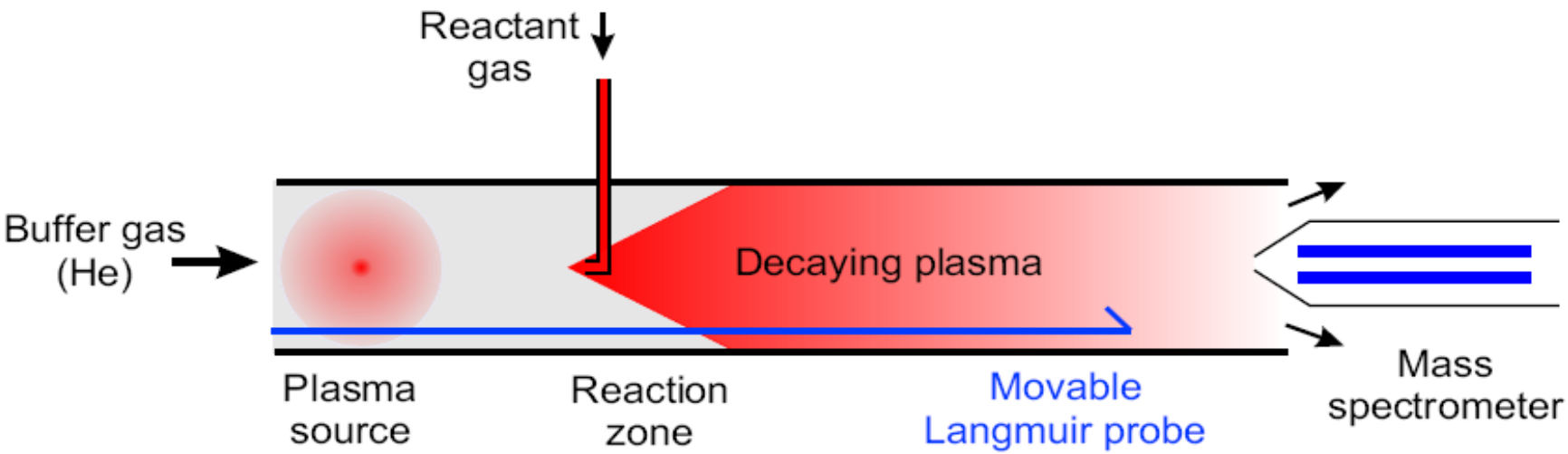

Figure 1.1: The basic principle of FA and FALP techniques.

Flowing afterglow - IMR and recombination

FA FALP

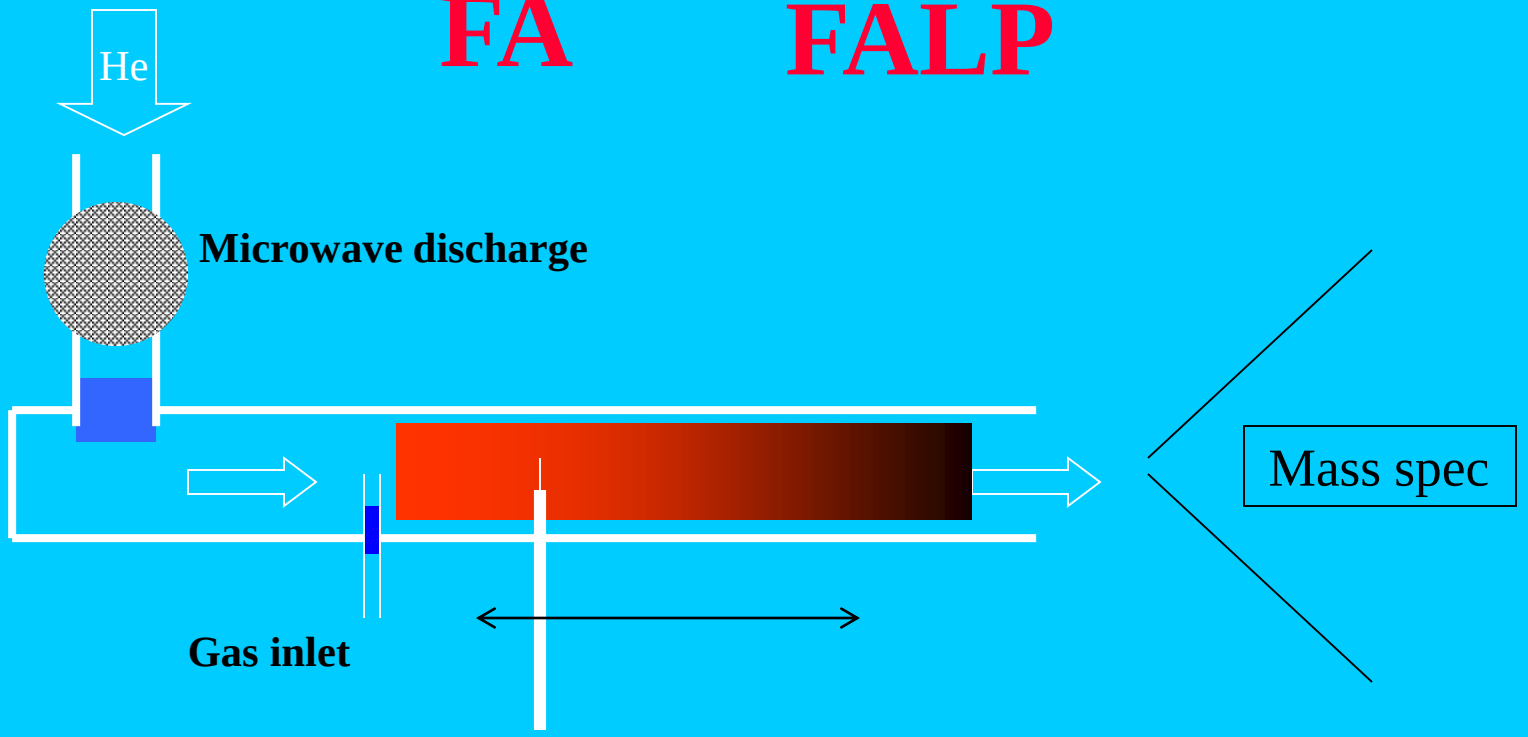

Langmuir probe measures $n_e(z)$

$z \sim v_{flow} t$

Techniques for study of IMR – FALP 1965

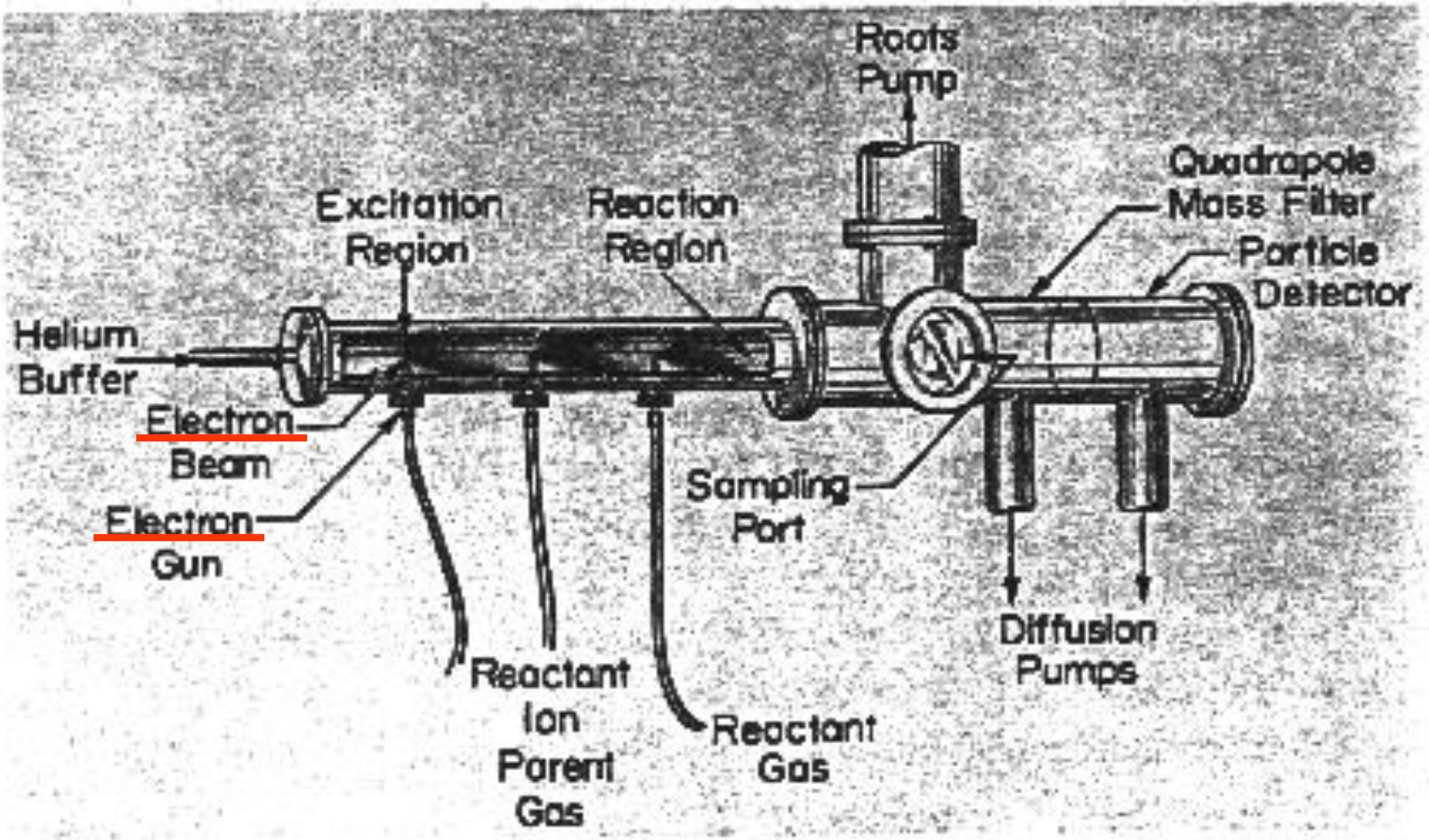

FIG. 1. Pictorial representation of the flowing afterglow tube.

Experimental studies of IMR ➔FA

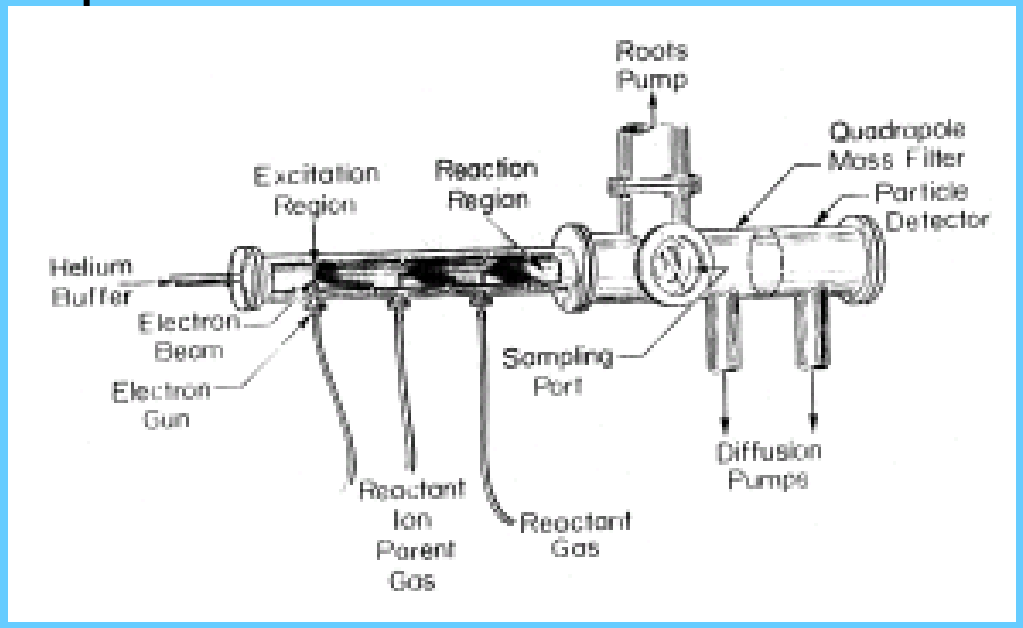

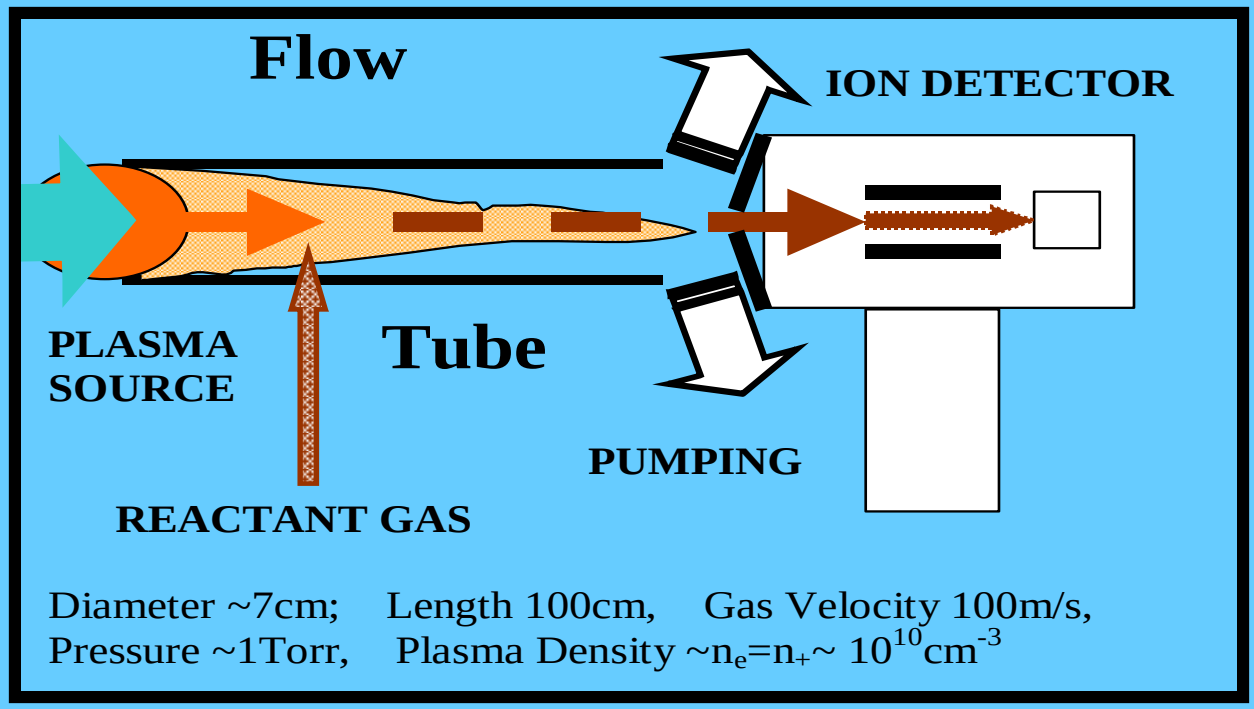

FLOWING AFTERGLOW

Ion-molecule reactions

FA

FA **E.E.Ferguson, Fehsenfeld, ~1965**
FALP **J. Hasted, D. Smith, N. Adams, ….**

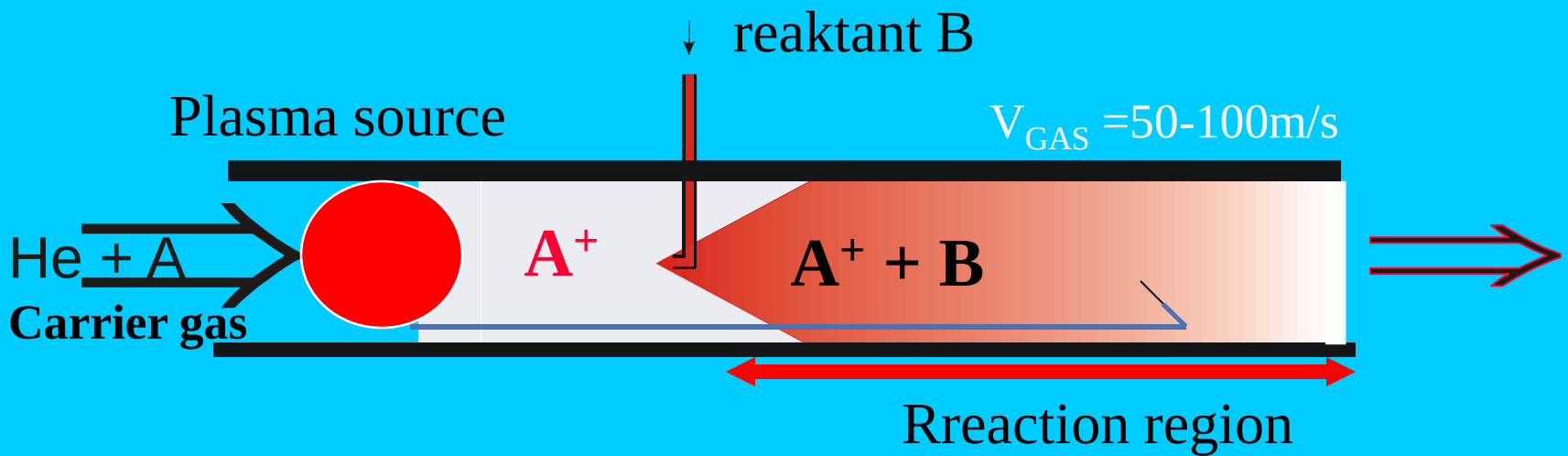

$$A^+ + B \xrightarrow{k} products,$$

$$d[A^+]/dt = -k[B][A^+], \qquad at\ [A^+] << [B]$$

$$[A^+] = [A^+]_0 \exp(-k[B]t) = [A^+]_0 \exp(-k[B]L_0/v)$$

SIFT

, D. Smith, N. Adams, ….

Flowing Afterglow 1968

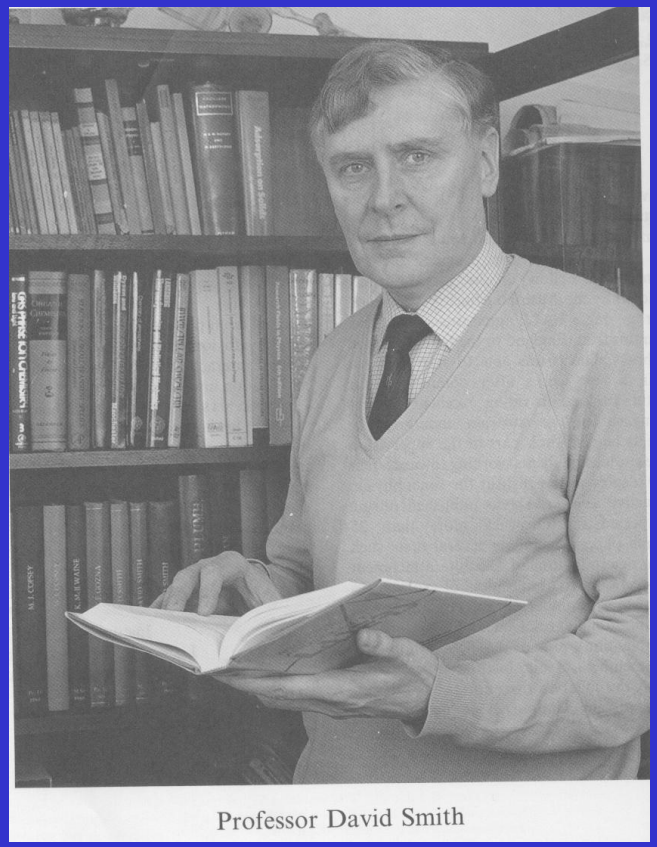
Professor David Smith

microwave discharge

μw

Ar

Reactant

He

He

He^+

Ar^+

Afterglow

T_e ~2eV

$T_e = T_i = T_G$ = 170 - 260K

FA– Flowing Afterglow

100-700 K

$$H_3^+ + CO \Rightarrow HCO^+ + H$$

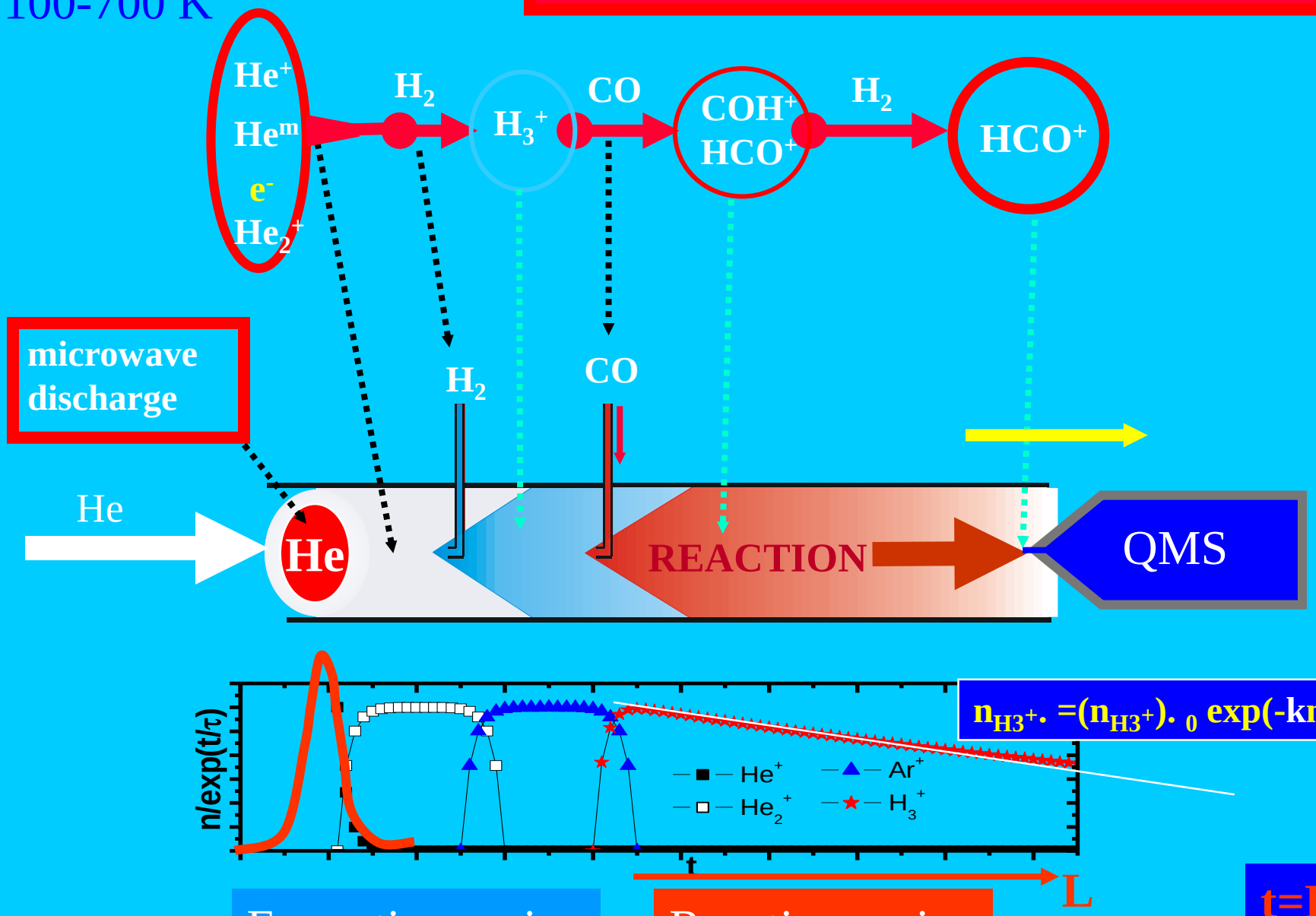

Principle of Flowing Afterglow Langmuir Probe - FALP

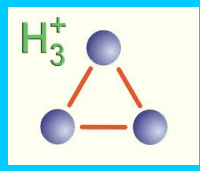

microwave discharge

T_e~ 2eV

Formation of H_3^+ in He/Ar/H_2 mixture (10 Torr)

He^+
He^m
e^-
He_2^+

Ar

Ar^+

H_2

ArH^+, H_2^+

H_2

$H_3^+ + e^-$

H_2

$H_5^+ + e^-$

μw

Ar

H_2

He

He

RECOMBINATION

2eV

T_e

$T_e = T_i = T_G$ = 170 - 260K

Table 1. Table of reactions taking place in He/Ar plasma. The values in the middle column are calculated for 80 K if temperature dependence was known.

N	Reaction	Rate coef. [cm^3s^{-1}], [cm^6s^{-1}]	Ref.
1	$He^+ + He + He \rightarrow He_2^+ + He$	1×10^{-31}	[*Ikezoe et al.*, 1987]
2	$He^m + He^m \rightarrow He^+ + He + e^-$	5×10^{-9}	[*Deloche et al.*, 1976]
3	$\rightarrow He_2^+ + e^-$	5×10^{-9}	[*Urbain et al.*, 1999]
4	$He_2^+ + e^- \rightarrow 2He$	$<5\times10^{-10}$	[*Deloche et al.*,1976]
Ar+ formation and destruction			
5	$He^+ + Ar \rightarrow Ar^+ + He$	$<1\times10^{-13}$	[*Johnsen et al.,* 1973]
6	$He^m + Ar \rightarrow Ar^+ + He + e^-$	7×10^{-11}	[*Glosík et al.*, 1999]
7	$He_2^+ + Ar \rightarrow Ar^+ + 2He$	2×10^{-10}	[*Ikezoe et al.*, 1987]
8	$Ar^+ + e^- + e^- \rightarrow Ar + e^-$	1.1×10^{-17}	[*Kotrík et al.*, 2011]
9	$Ar^+ + e^- + He \rightarrow Ar + He$	2.7×10^{-26}	[*Bates et al.*, 1965]
Ar_n^+ formation and destruction			
10	$Ar^+ + Ar + He \rightarrow Ar_2^+ + He$	1.3×10^{-31}	[*Smirnov*, 1977]
11	$Ar_2^+ + e^- \rightarrow 2Ar$	8×10^{-7}	[*Okada et al.*, 1993]
12	$Ar_2^+ + Ar + Ar \rightarrow Ar_3^+ + Ar$	3.2×10^{-30}	[*Hiraoka et al.*, 1989]
13	$Ar_2^+ + Ar + He \rightarrow Ar_3^+ + He$	5.5×10^{-31}	[*Smirnov*, 1977]
14	$Ar_3^+ + e^- \rightarrow 3Ar$	3.6×10^{-5}	Estimate
15	$Ar_3^+ + Ar + He \rightarrow Ar_4^+ + He$	5.5×10^{-31}	Estimate
16	$Ar_4^+ + e^- \rightarrow 4Ar$	3.6×10^{-5}	Estimate

Techniques for study of IMR

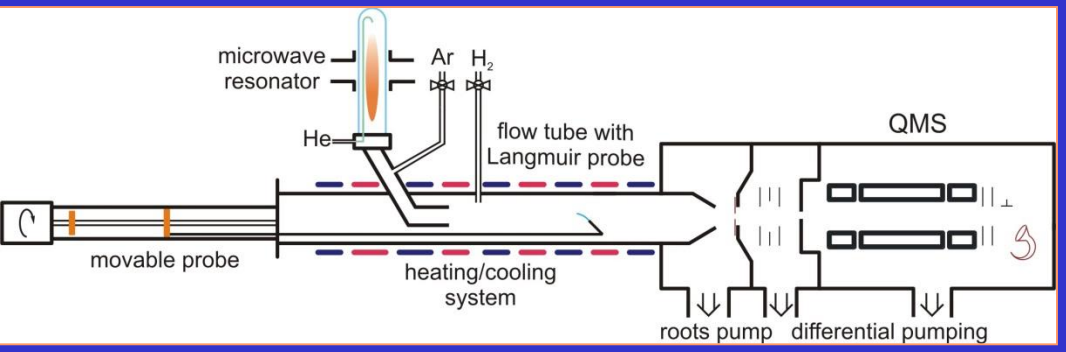

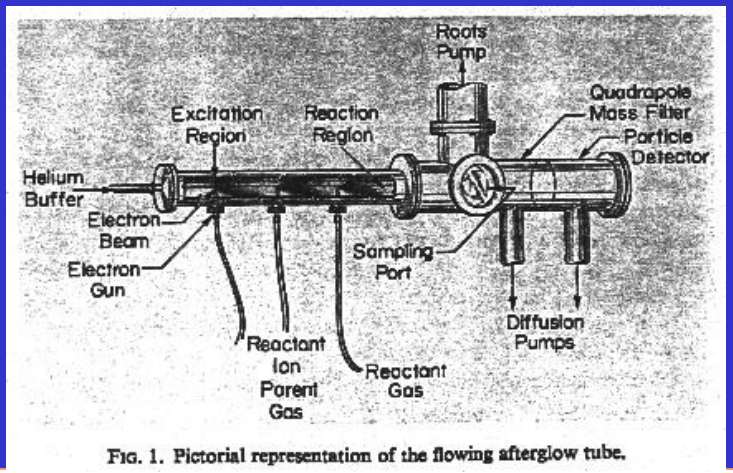

FIG. 1. Pictorial representation of the flowing afterglow tube.

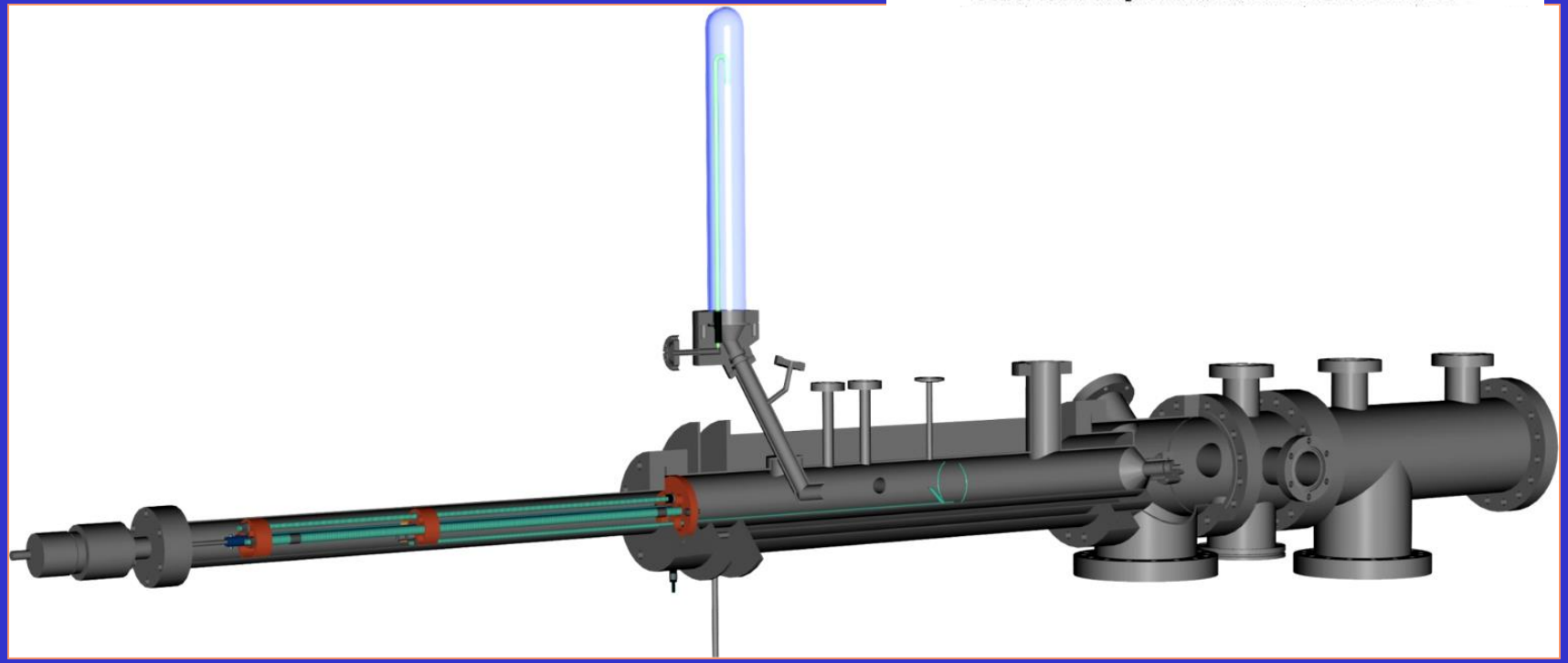

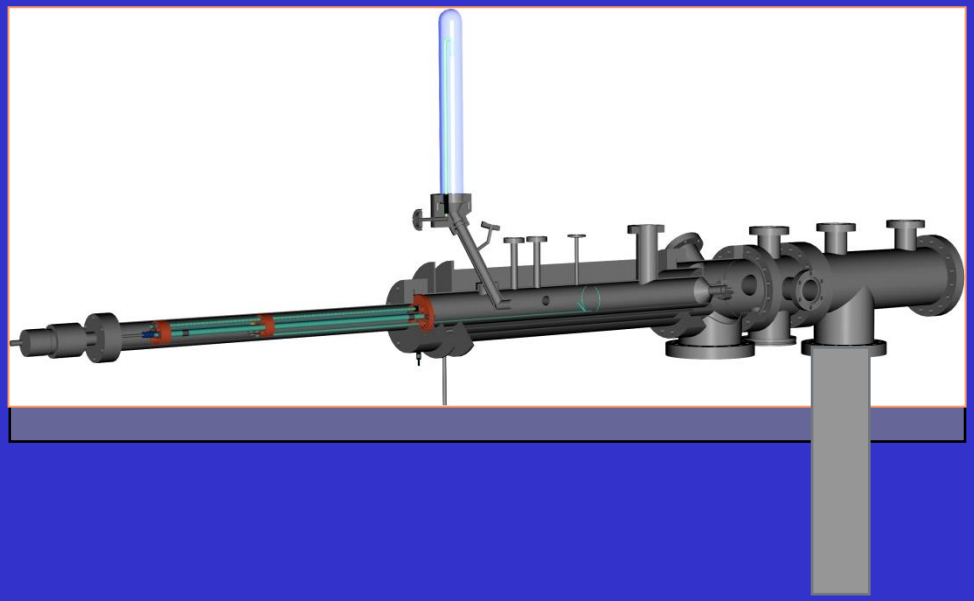

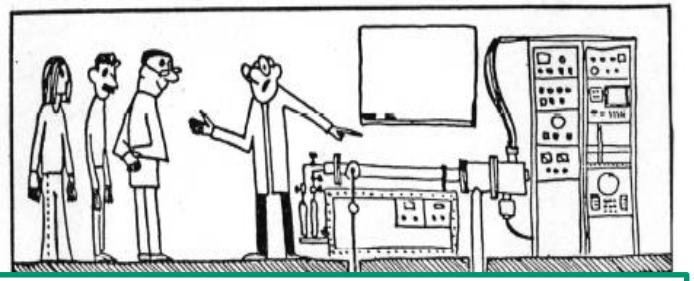

Two faces of a flowing afterglow.

(Opening picture to a seminar in Boulder, 1980)

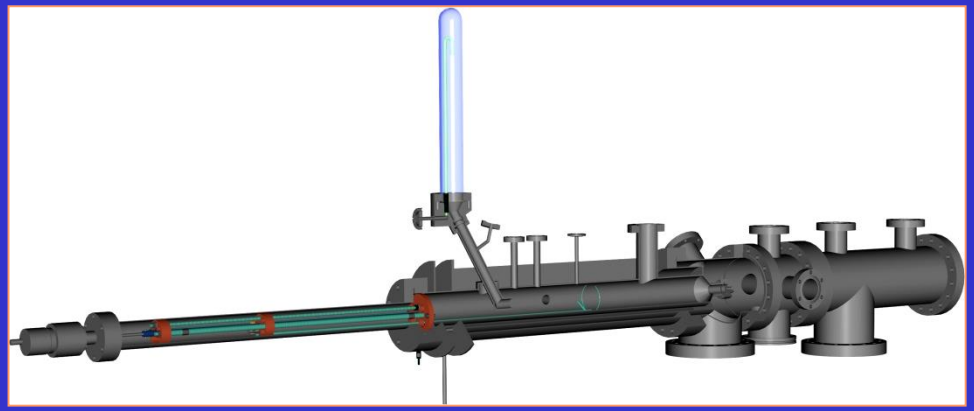

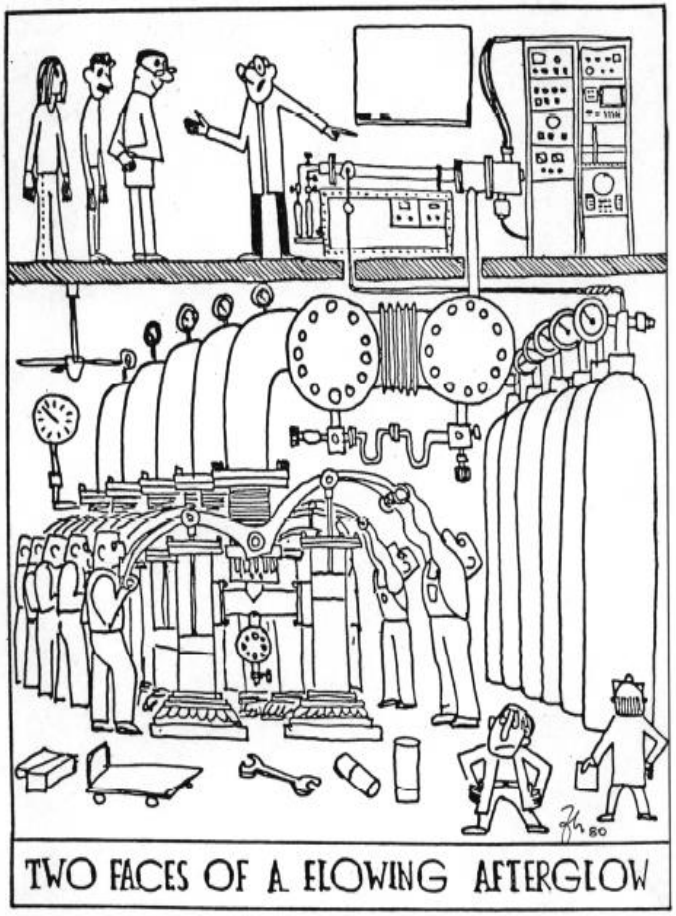

Two faces of a flowing afterglow.

(Opening picture to a seminar in Boulder, 1980)

Techniques for study of IMR – reality

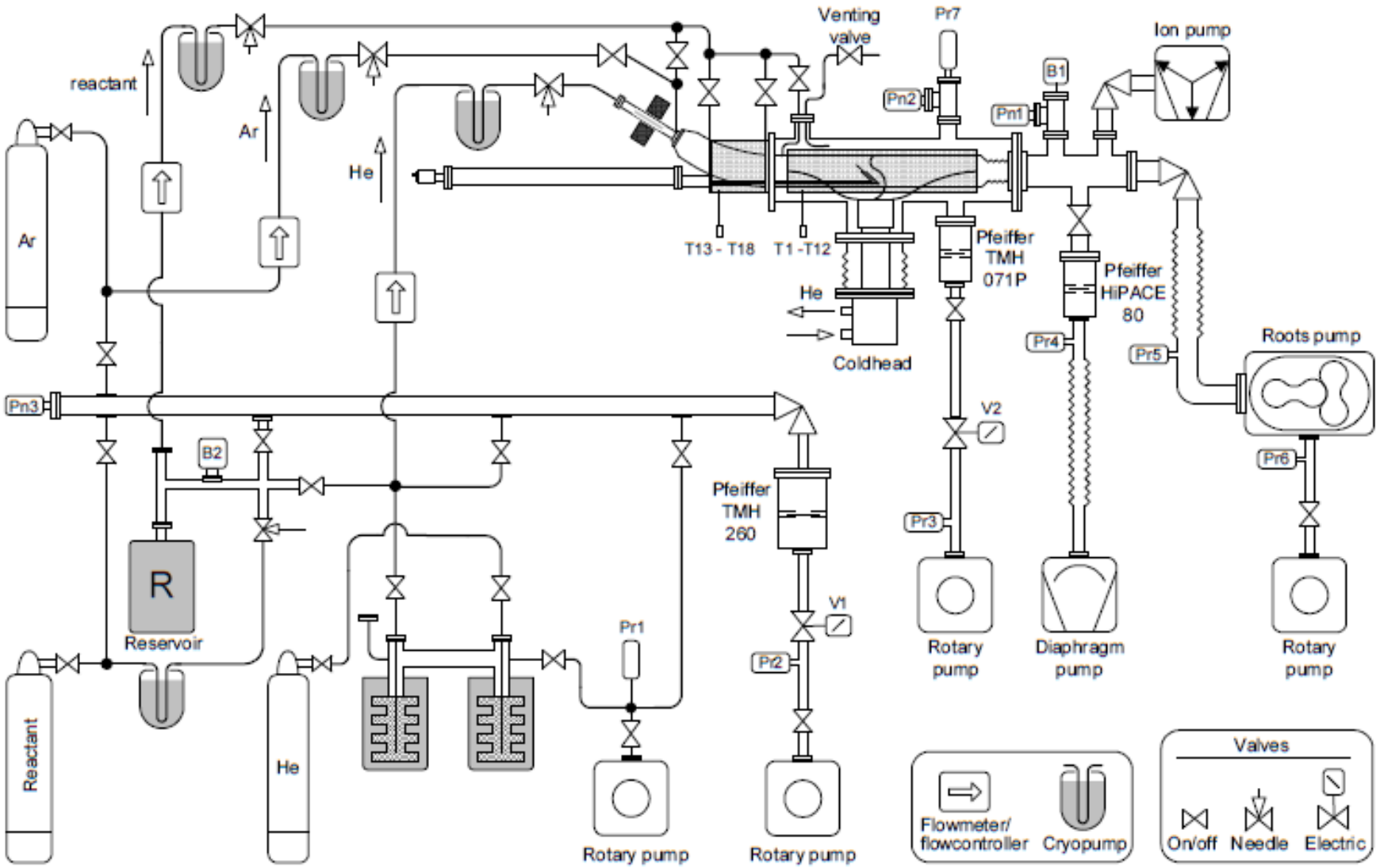

Figure 2.4 Vacuum scheme of the Cryo-FALP II apparatus.

FA– Flowing Afterglow

100-700 K

$$H_3^+ + CO \Rightarrow HCO^+ + H$$

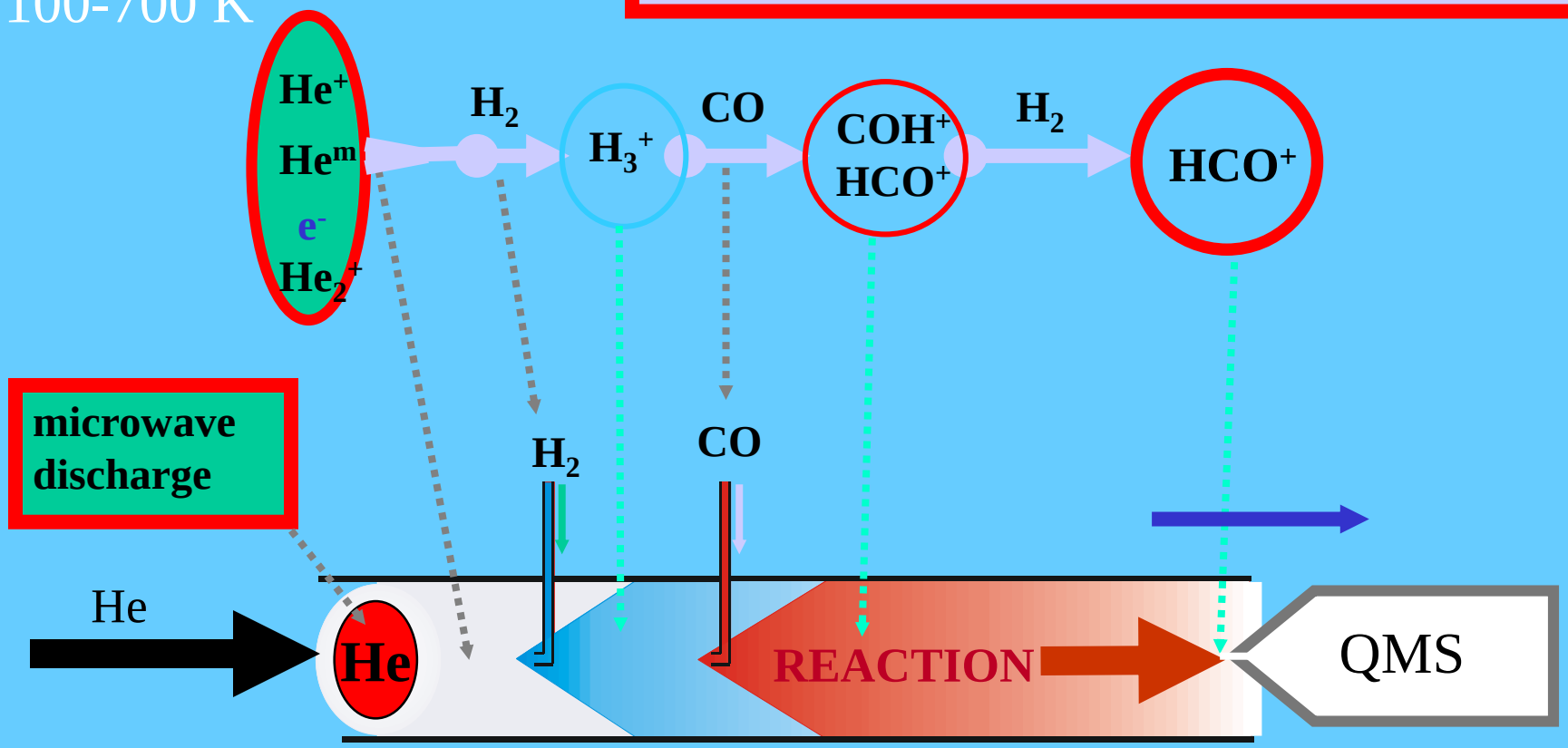

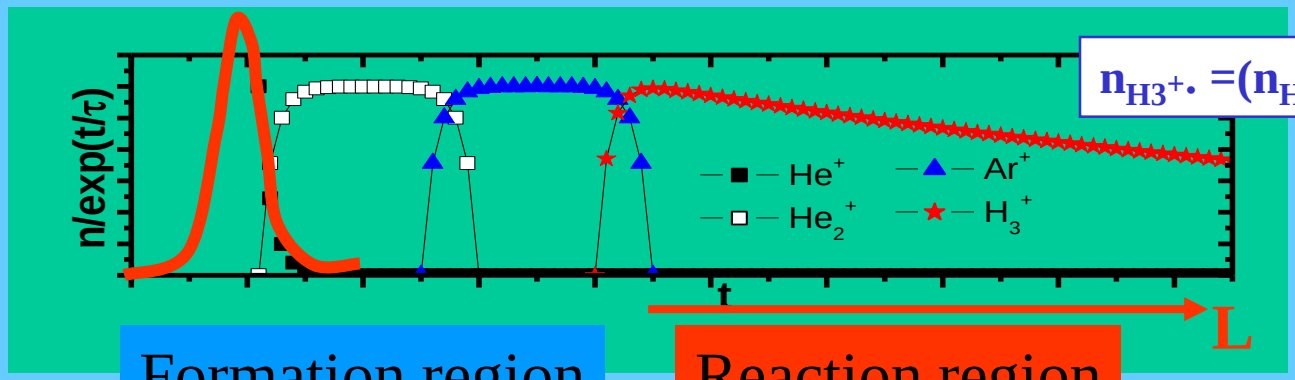

$n_{H3^+}. = (n_{H3^+})._0 \exp(-k n_{Ar} t)$

$t = L/v$

Formation region

Reaction region

FA – Flowing Afterglow

100-700 K

$$H_3^+ + CO \Rightarrow HCO^+ + H$$

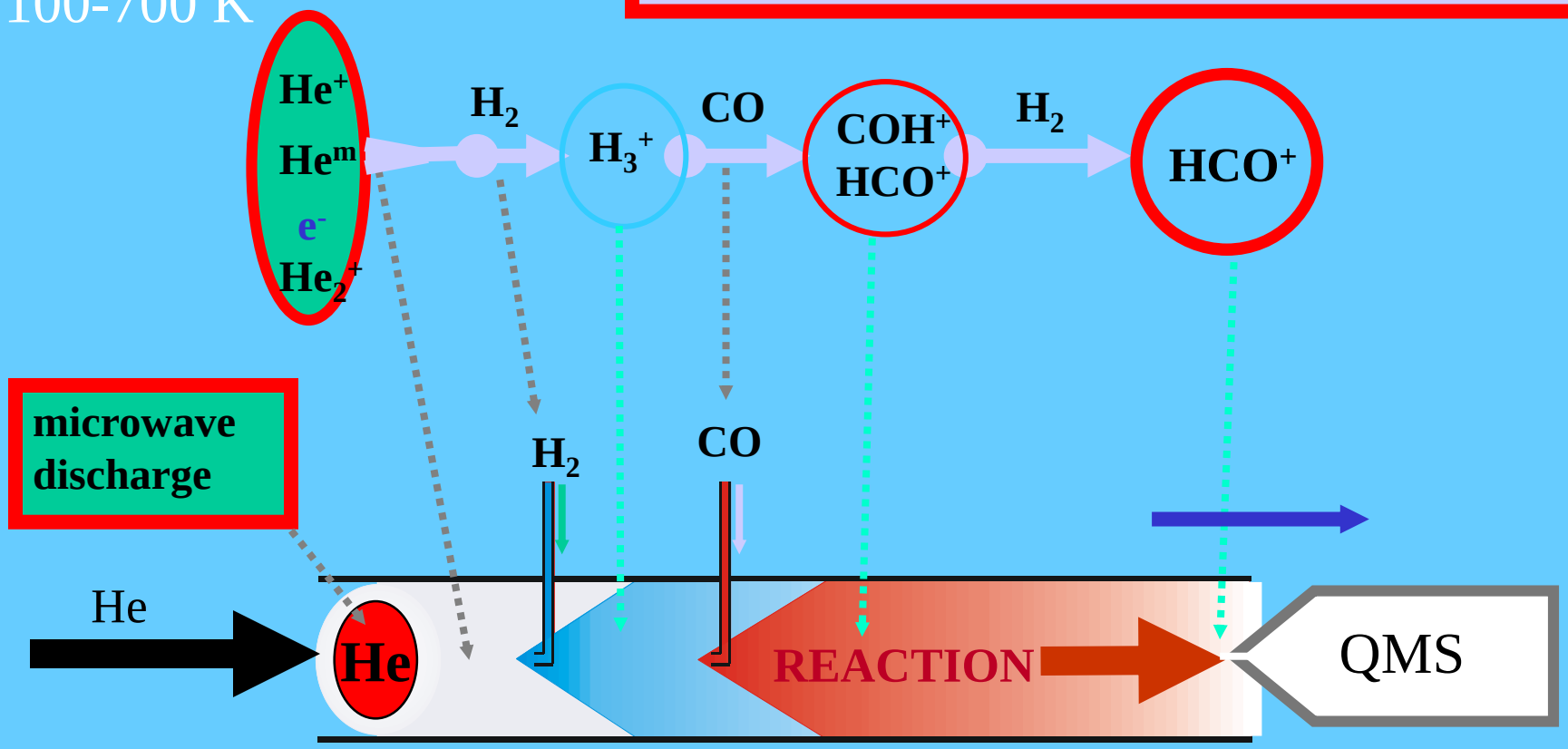

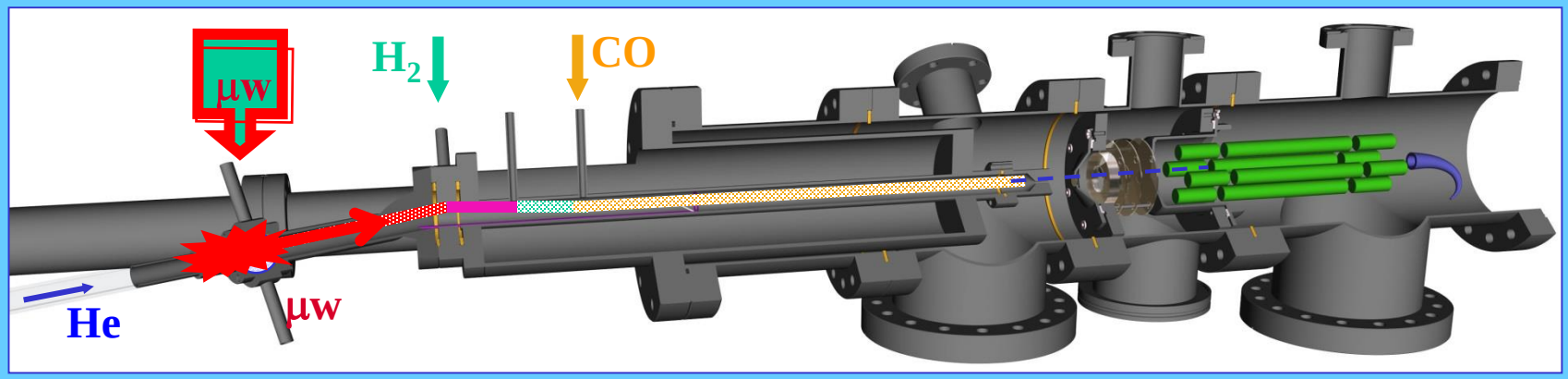

Evolution along the flow tube

$$[A^+]_L = [A^+]_{L=0} \cdot e^{-DL/\lambda^2 v}$$

$$[A^+]_L = [A^+]_{L=0} \cdot e^{-const_1 . D_0 p_0 L/Q} = [A^+]_{L=0} \cdot e^{-const_2 . L/Q}$$

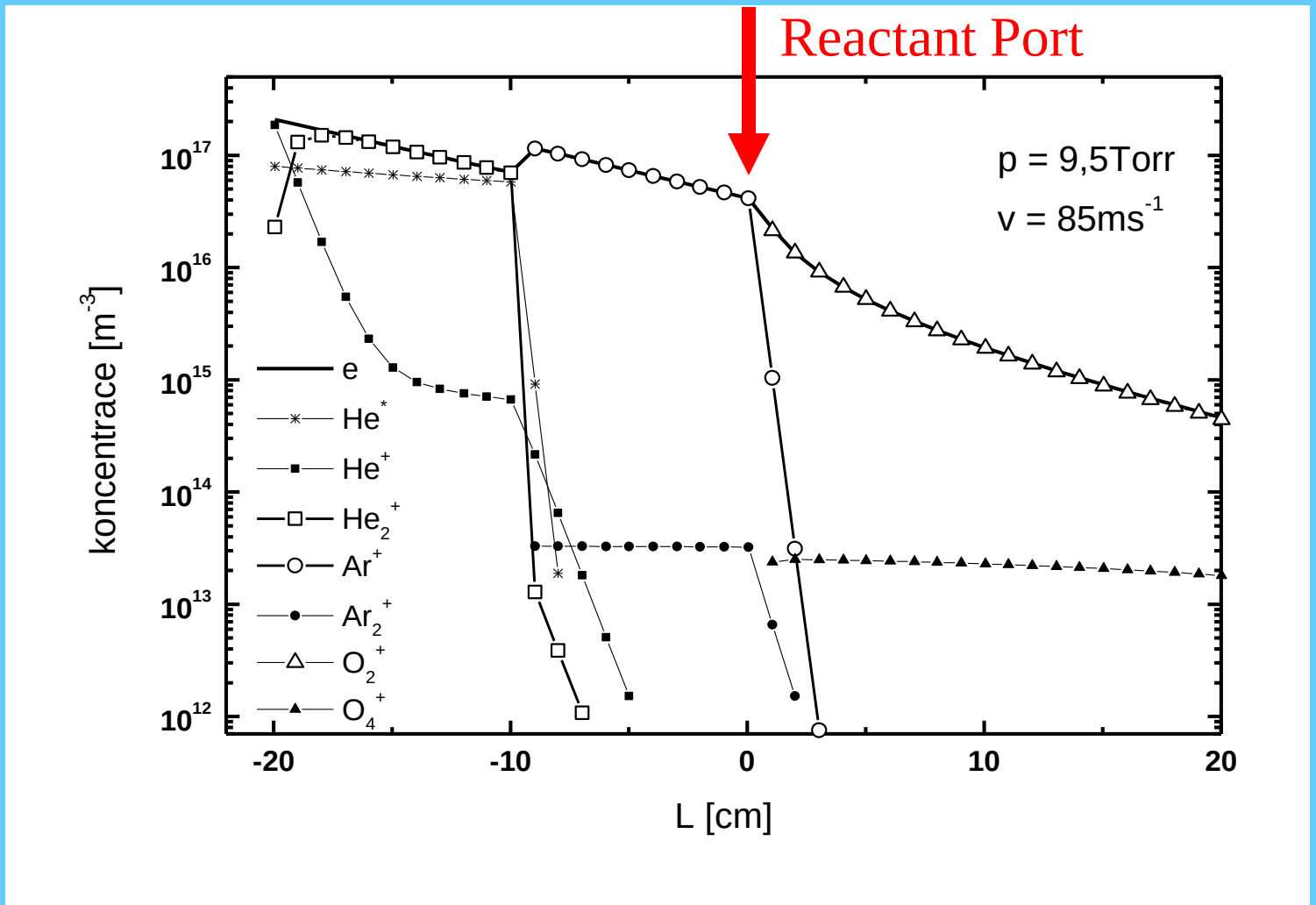

High temperature study

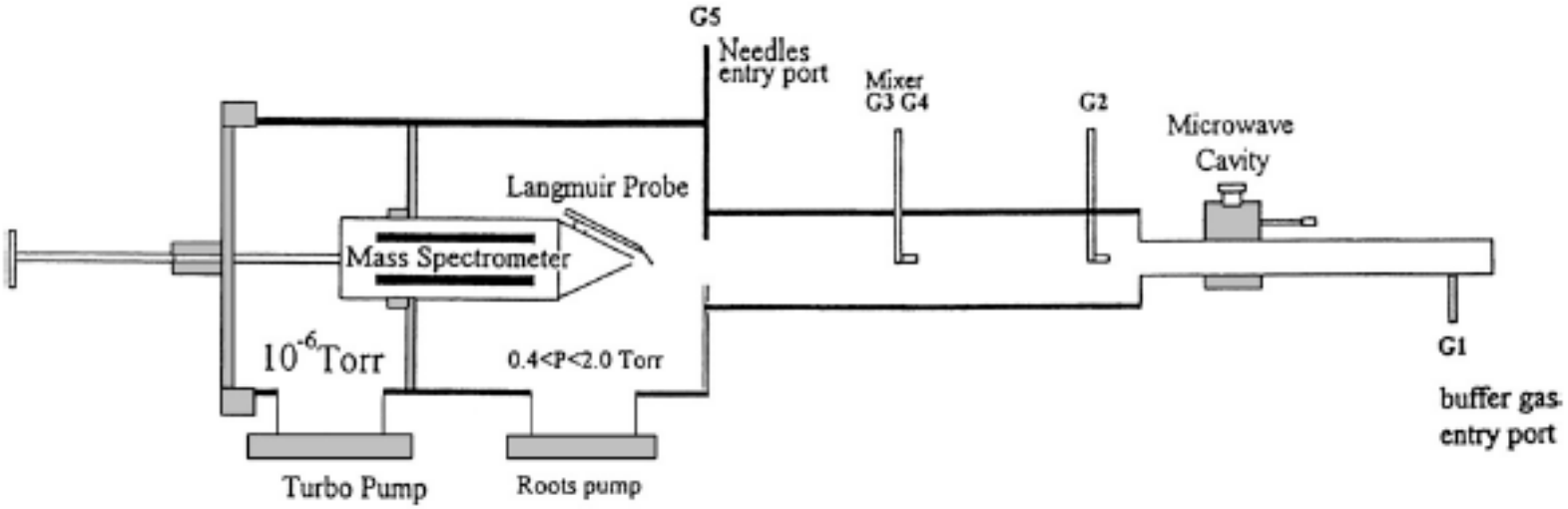

Fig. 12. Schematic view of the Rennes FALP-MS [164]

RENNES MS - FALP

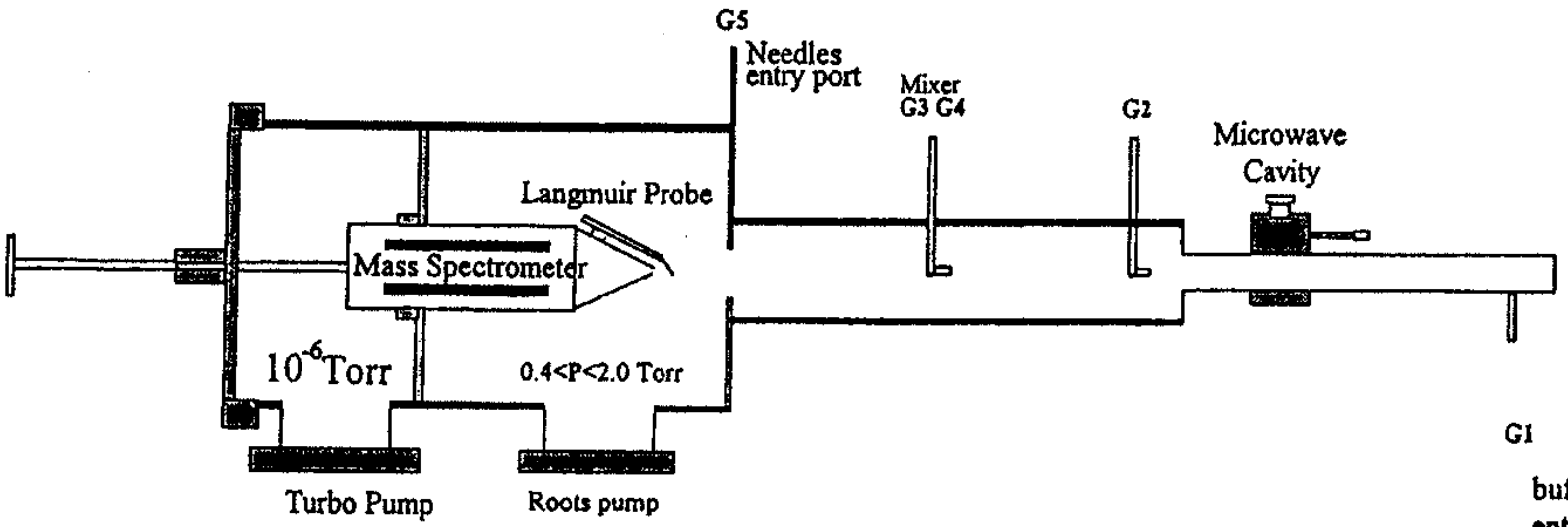

Figure 1. Sketch of the FALP apparatus.

RENNES absorption studies

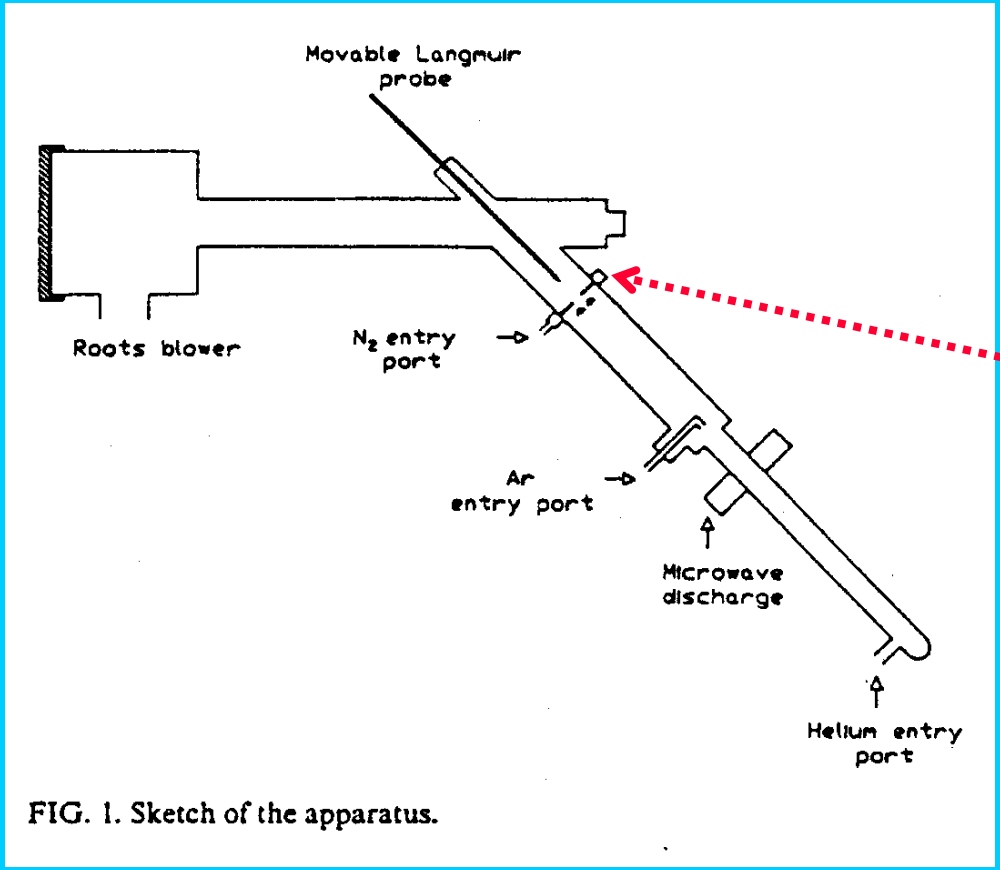

FIG. 1. Sketch of the apparatus.

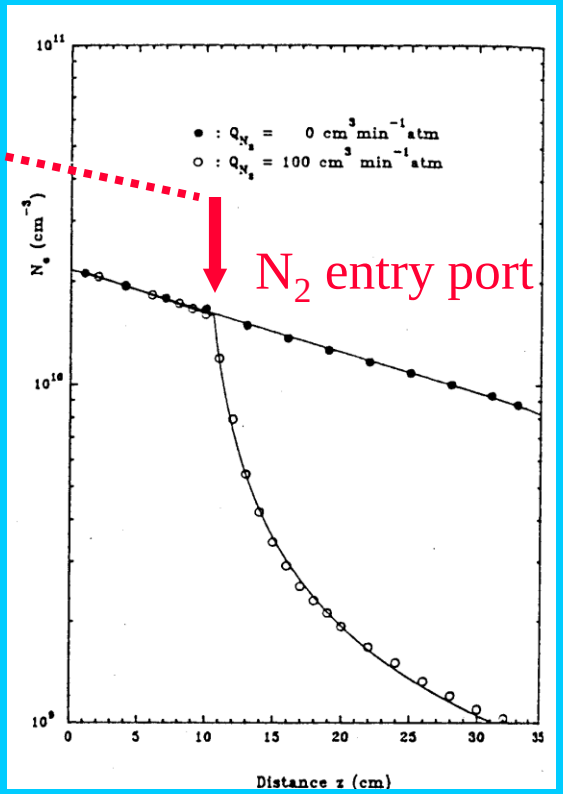

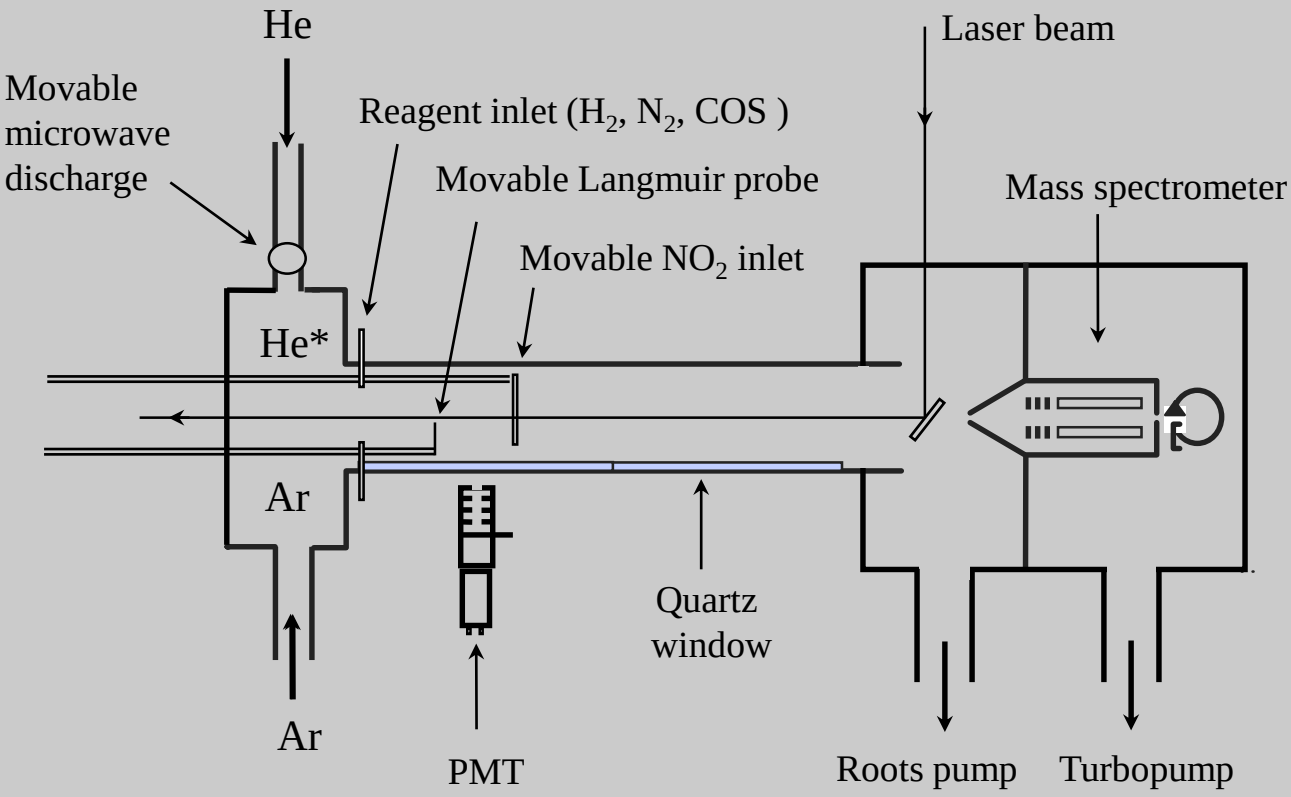
He
Movable
microwave
discharge
Reagent inlet (H_2, N_2, COS)
Movable Langmuir probe
Movable NO_2 inlet
Laser beam
Mass spectrometer
He*
Ar
Ar
PMT
Quartz
window
Roots pump
Turbopump

Pittsburg Rainer Johnsen FALP

Emission spectroscopy for identification products of recombination

collisional radiative recombination of argon ions

$Ar^+ + e^- + e^- \rightarrow Ar + e^-$

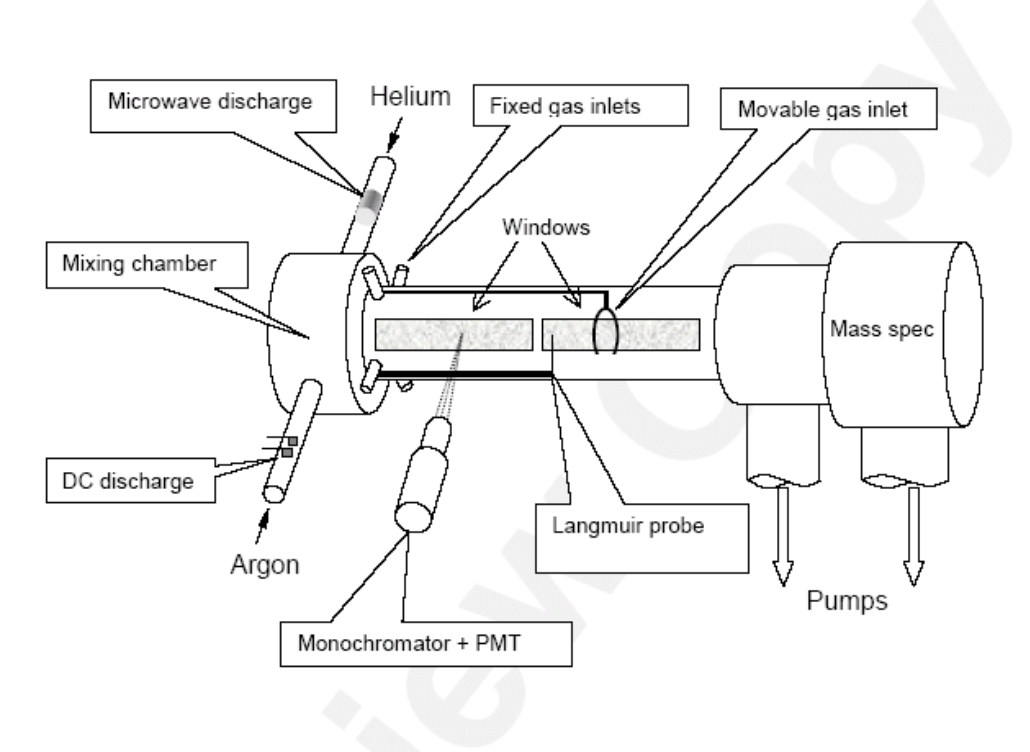

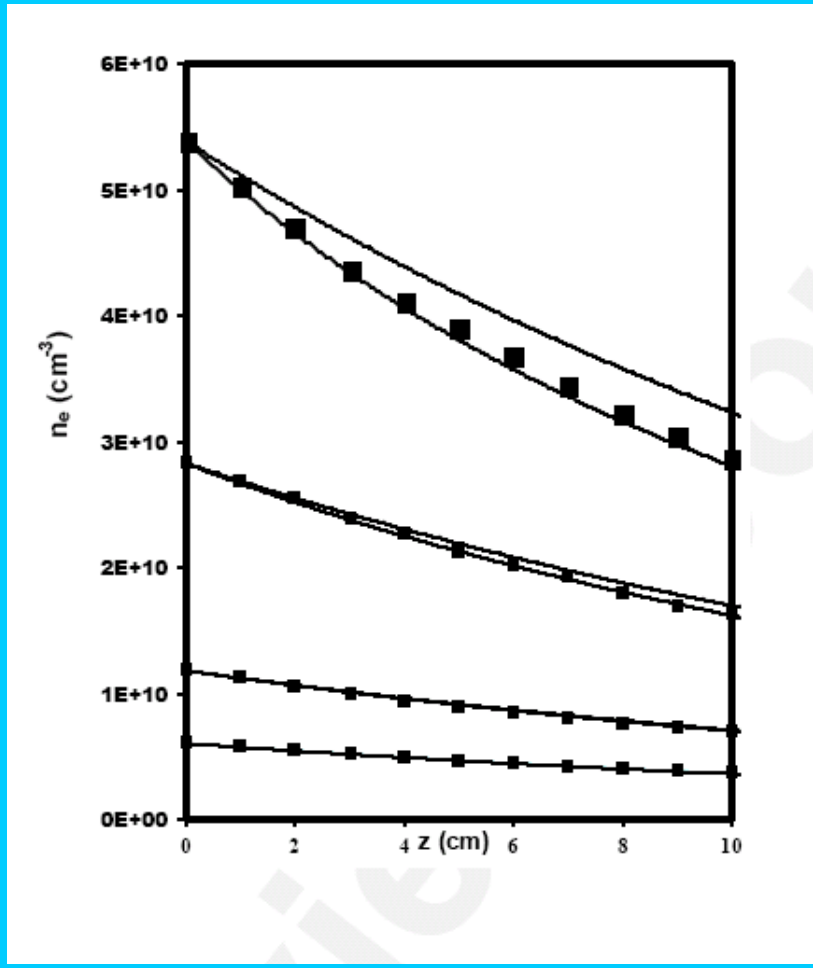

The Pittsburgh flow tube

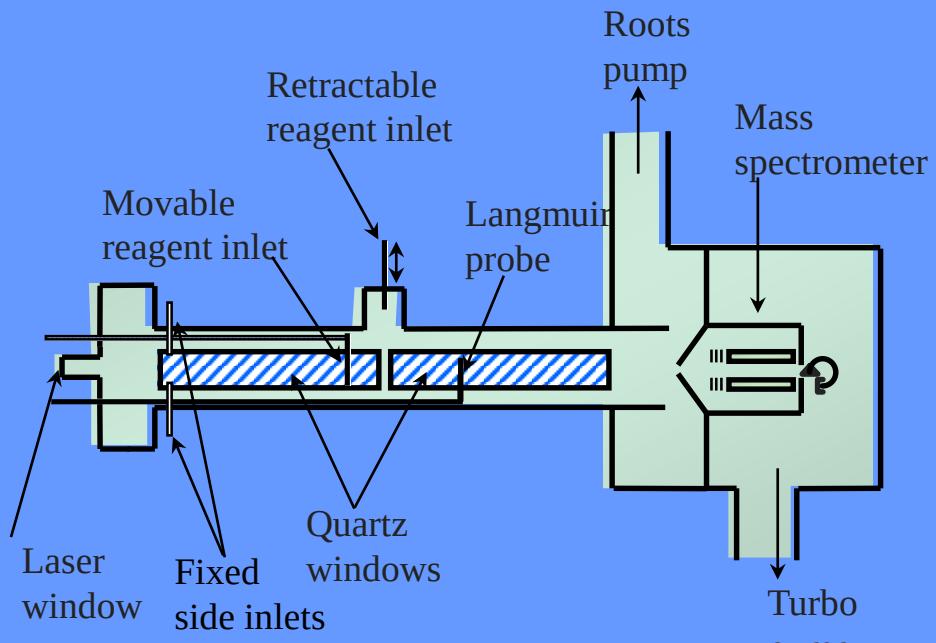

FLOW TUBE (side view)

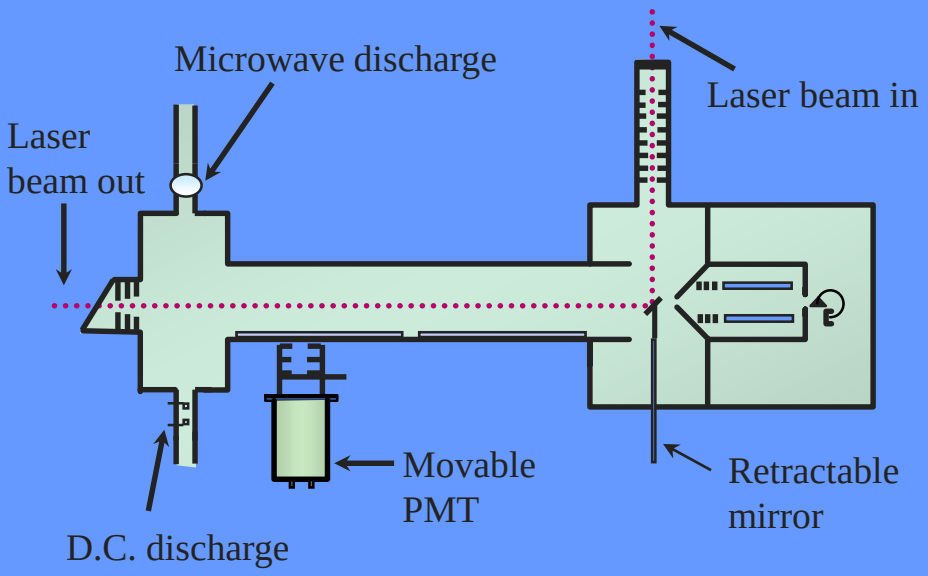

FLOW TUBE (top view)

$$Ar^+ + H_2 \rightarrow ArH^+ + H \quad (+ 1.53eV)$$

$$ArH^+ + H_2 \rightarrow Ar + H_3^+ \quad (+ 0.57\ eV)$$

N.G.ADAMS University of Georgia, Viktoria Poterya

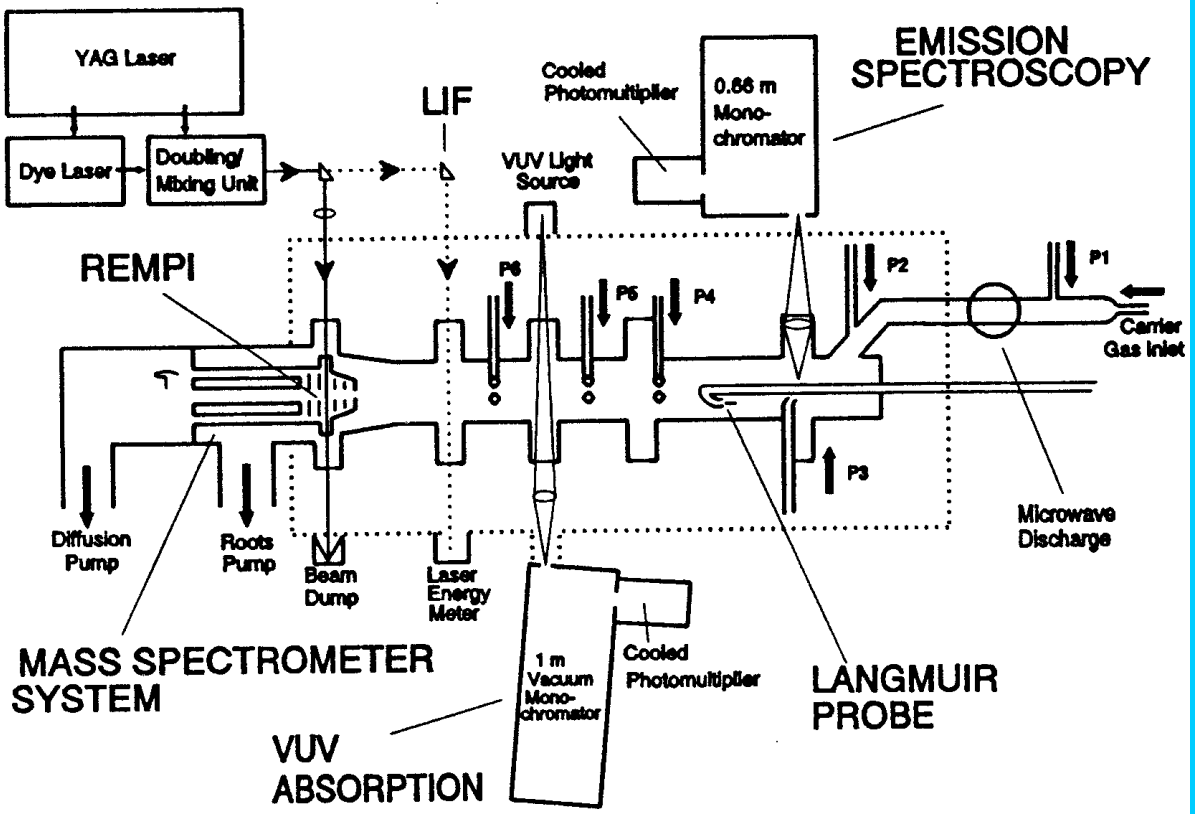

Figure 1. A schematic of the University of Georgia flowing afterglow. Illustrated are the axially movable Langmuir probe, the downstream mass spectrometer, a 0.66 m monochromator with red sensitive photomultiplier for emission studies, a vuv light source and 1 m vacuum monochromator with uv enhanced photomultiplier for detection of atoms and a YAG pumped dye laser with doubling and mixing capabilities for detection of radical species by LIF and REMPI. All photomultipliers are cooled to reduce the background noise and photon counting is used throughout. Further details of this apparatus are described in a separate review.[27]

FA– Flowing Afterglow 2005

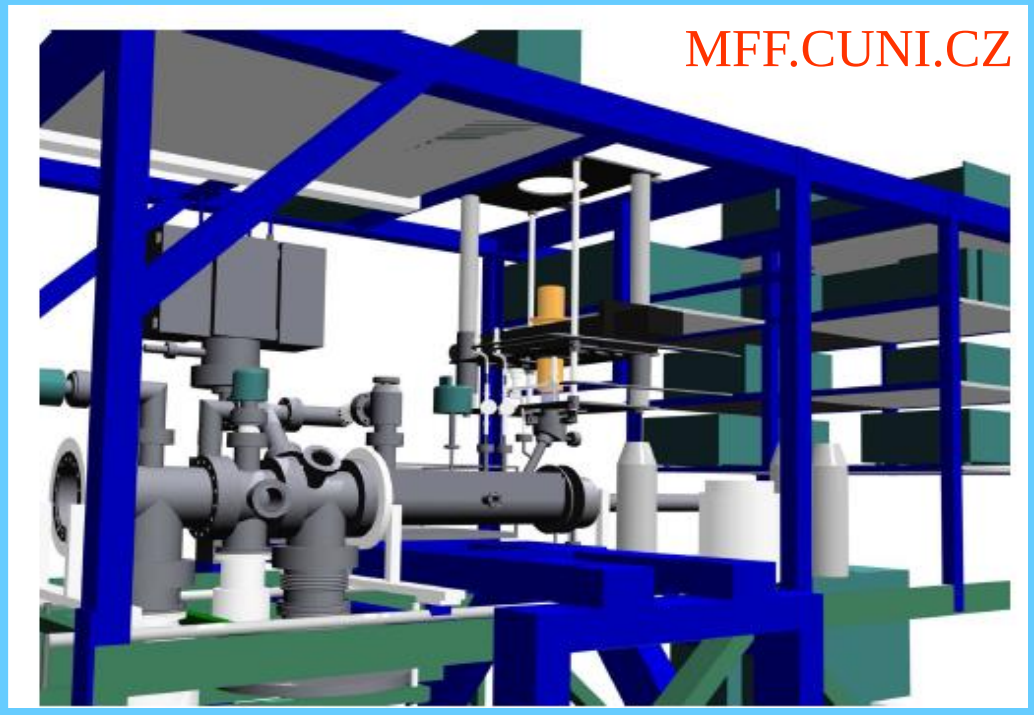

FA– Flowing Afterglow 2005

MFF.CUNI.CZ

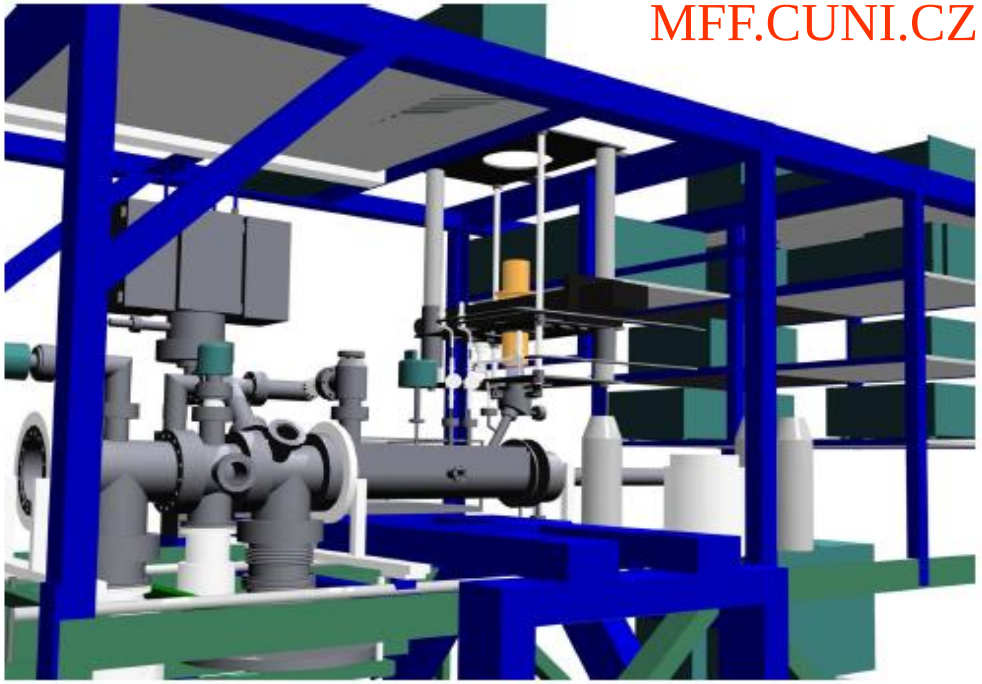

FA– Flowing Afterglow 1965 -2006

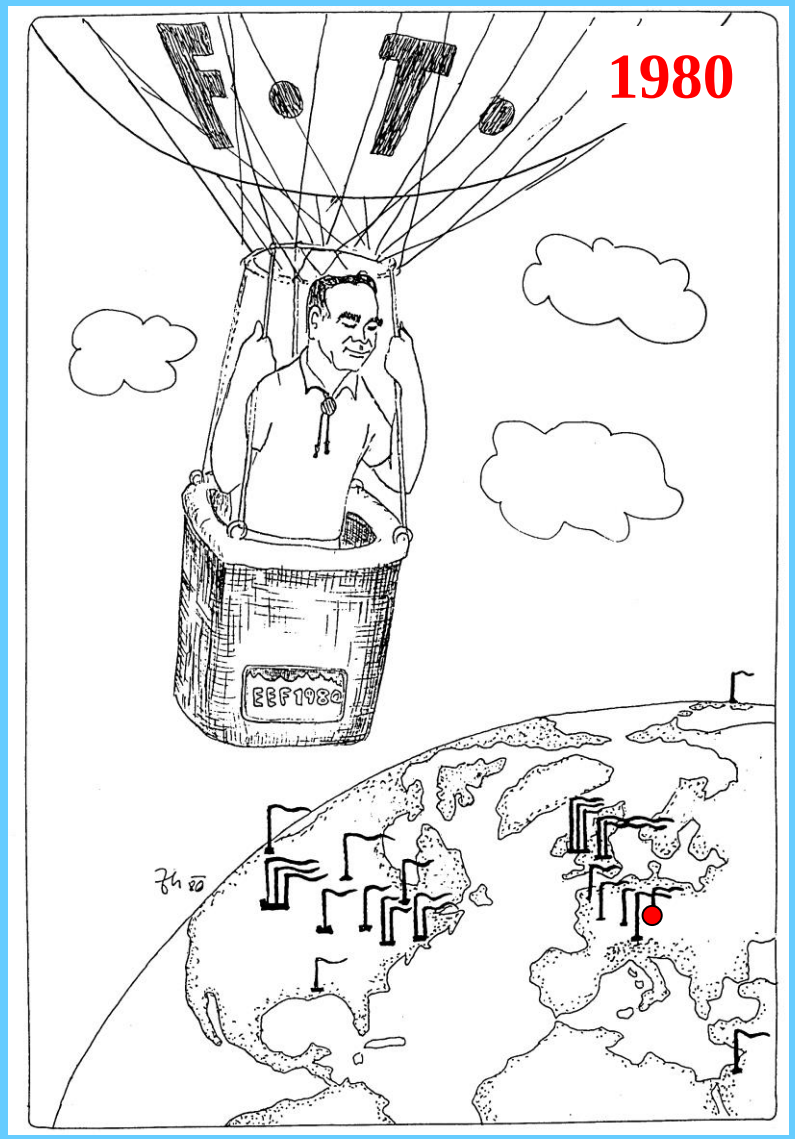

CU – Chemistry 1980:
Eldon Ferguson watching the flow-tube centers

MFF.CUNI.CZ

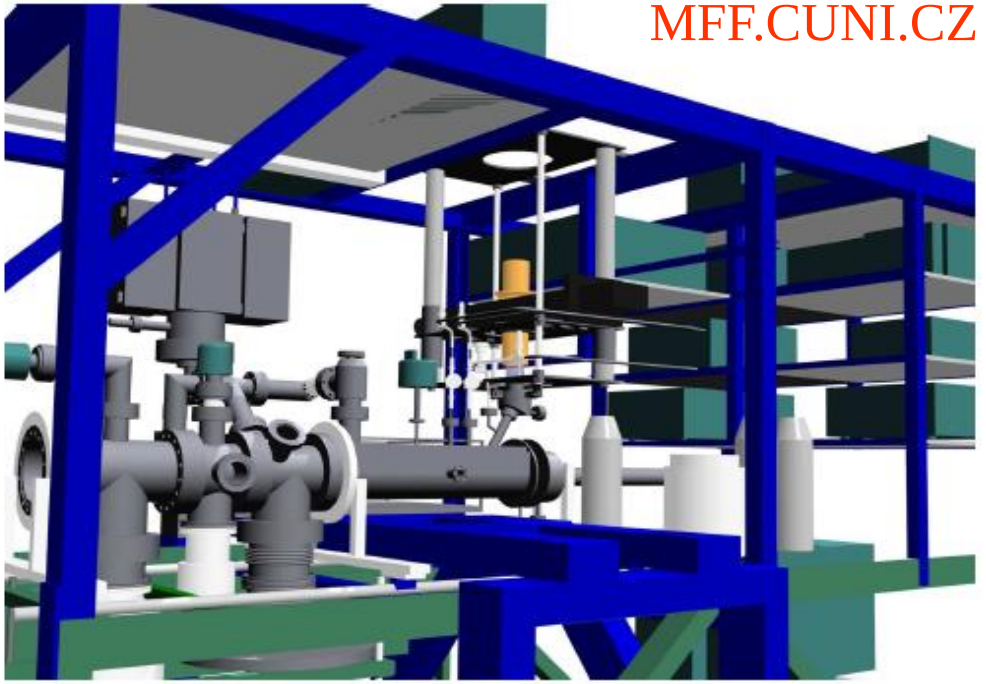

FALP – MFF.CUNI.CZ

Plasma, IMR, Recombination Diagnostics

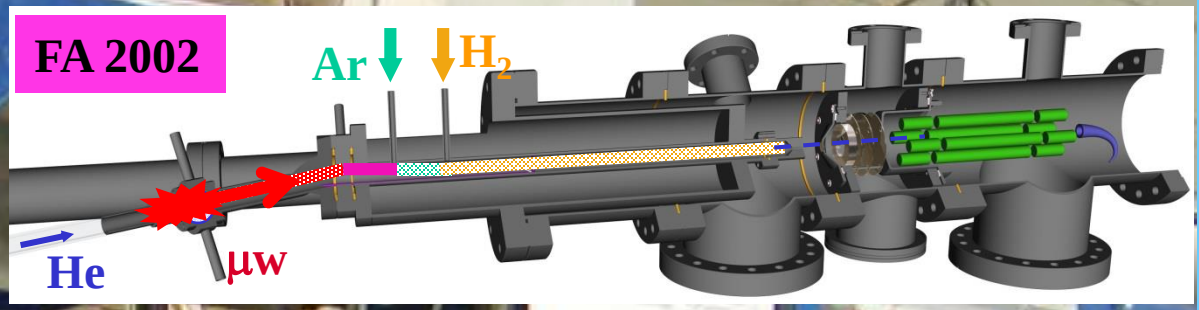

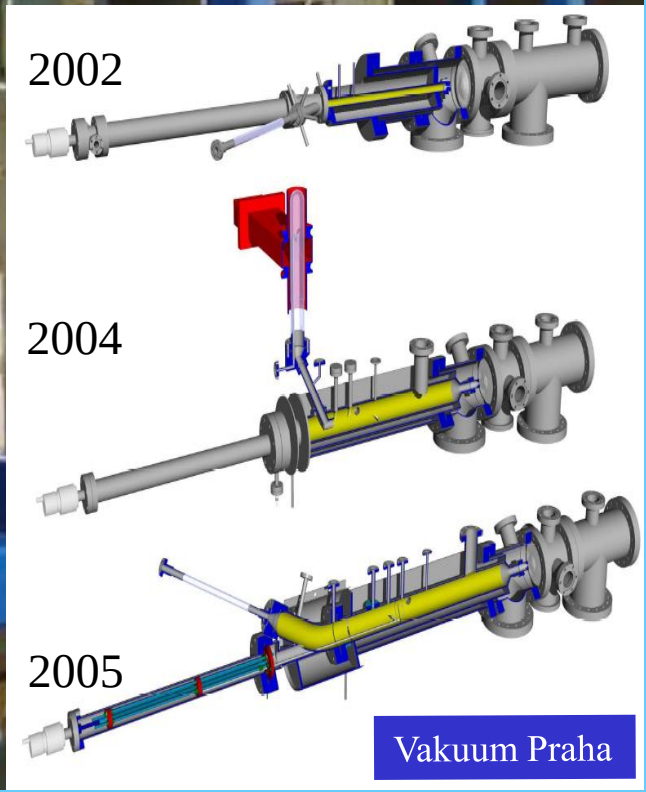

Vakuum Praha

O.Novotný

14th August 2002

Our LAB

FACULTY OF MATHEMATICS AND PHYSICS

TROJA, Praha 8

2002 - 2004

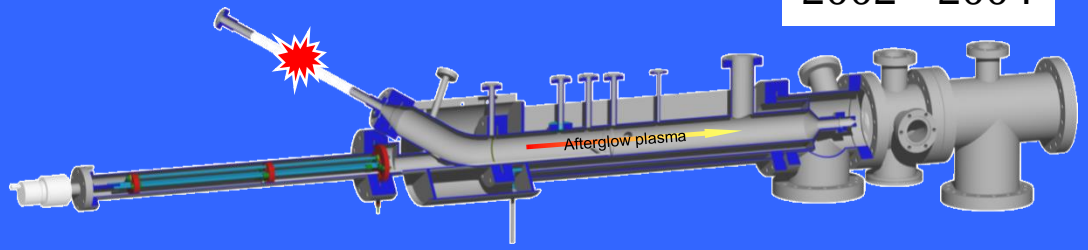

Principle of Flowing Afterglow Langmuir Probe - FALP

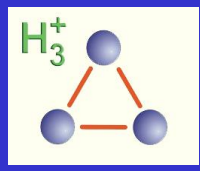

microwave discharge

Formation of H_3^+ in He/Ar/H_2 mixture (10 Torr)

He^+
He^m
e^-
He_2^+

Ar → Ar^+ → H_2 → ArH^+, H_2^+ → H_2 → H_3^+ +

H_2 → H_5^+ +

μw

Ar

H_2

He → **He** → **RECOMBINATION**

T_e ~2eV

$T_e = T_i = T_G$ = 170 - 260K

Apparatus -FALP

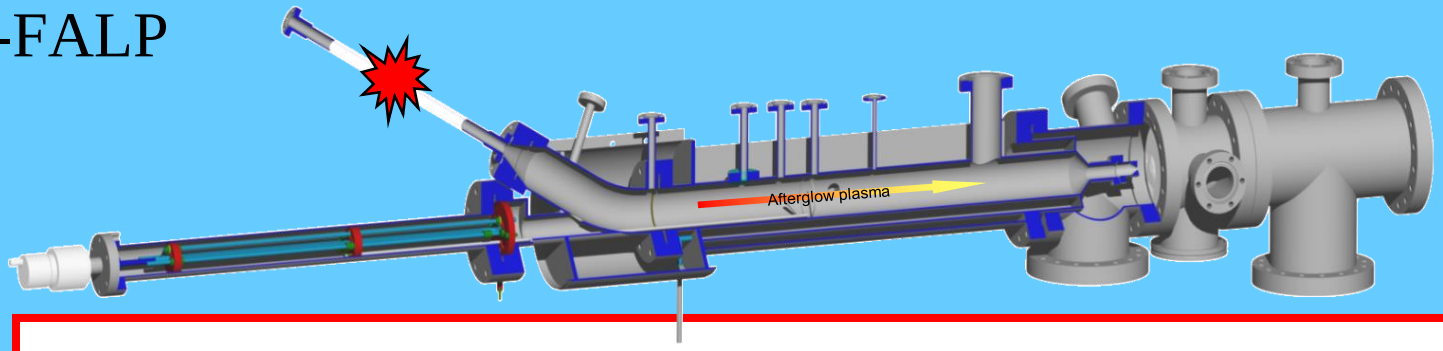

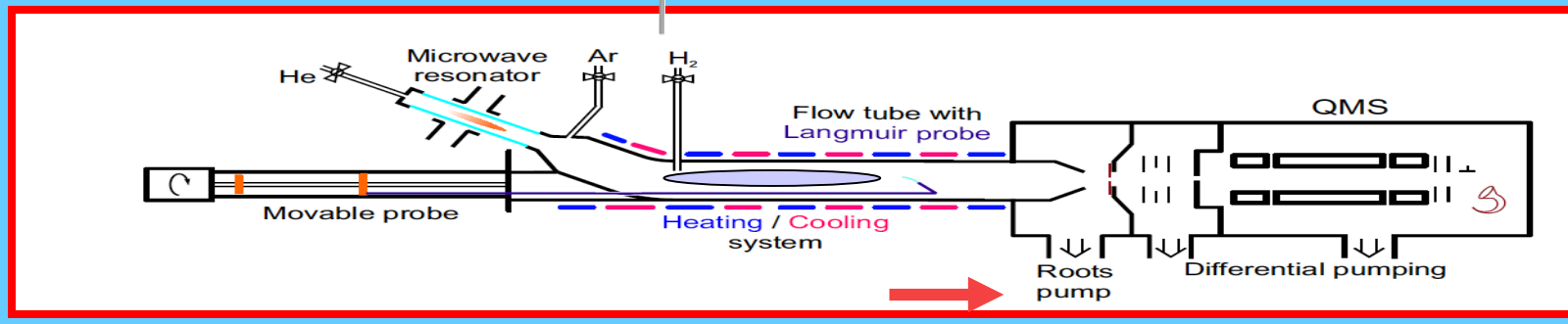

Kinetics

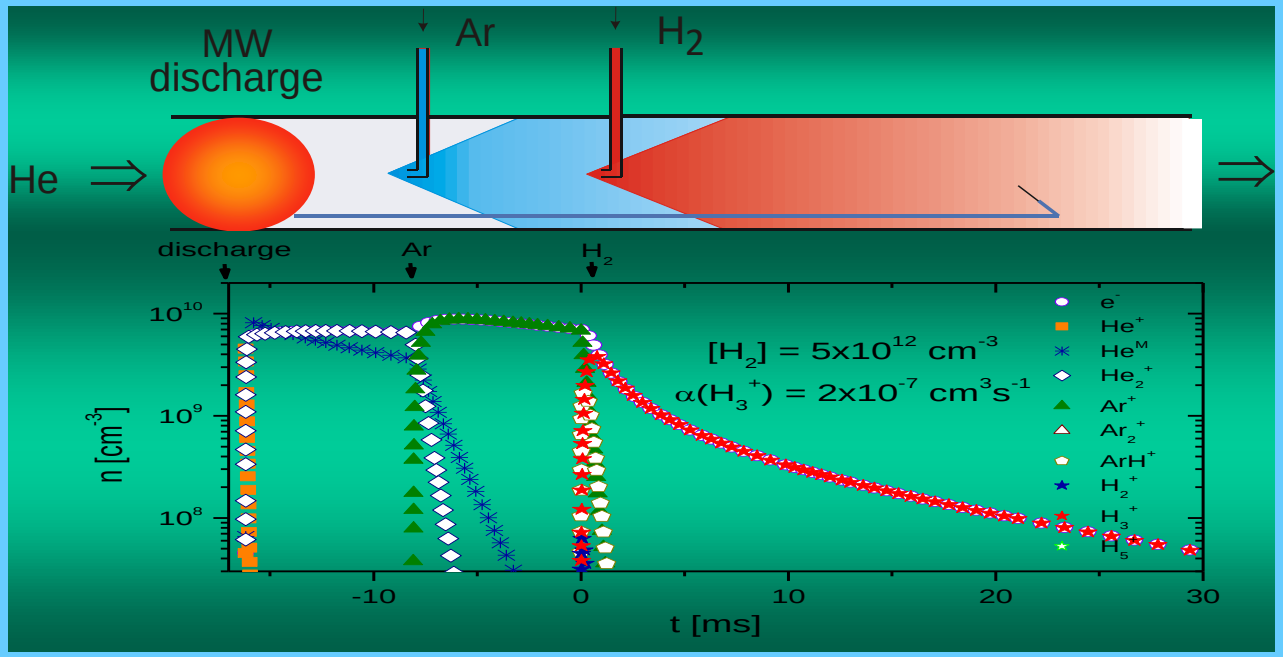

$\alpha \sim 5x10^{-9}$ cm^{3}s^{-1}

Plasma decay can be monitored up to 35 cm ➔ 65 ms, Temperature – 130 - 300 K Pressure up to 12 Torr

Evolution along the flow tube

$$[A^+]_L = [A^+]_{L=0} \cdot e^{-DL/\lambda^2 v}$$

$$[A^+]_L = [A^+]_{L=0} \cdot e^{-const_1 . D_0 p_0 L/Q} = [A^+]_{L=0} \cdot e^{-const_2 . L/Q}$$

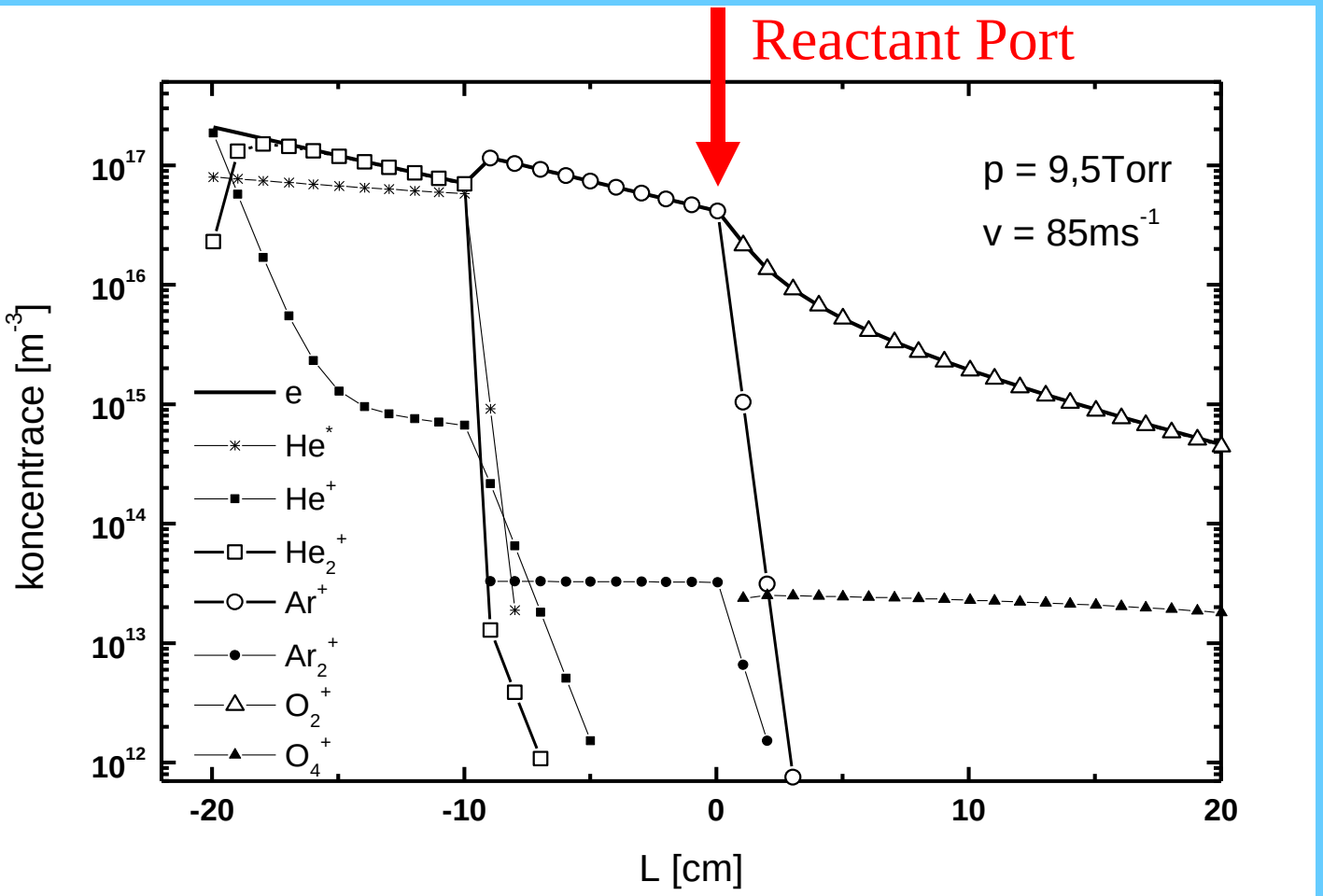

Ion-molecule reactions

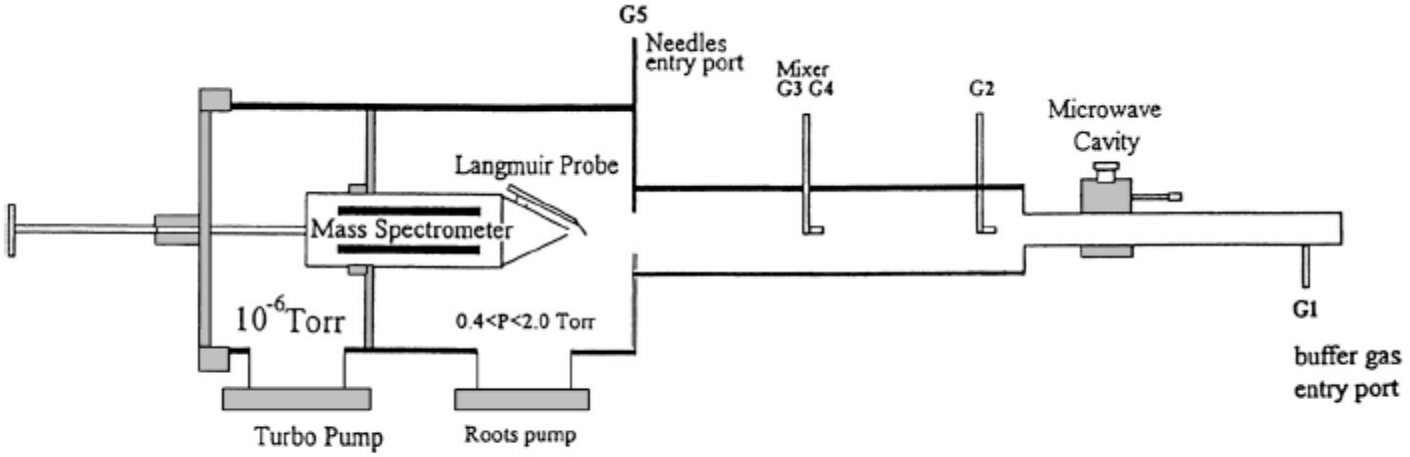

Fig. 12. Schematic view of the Rennes FALP-MS [164]

2. EXPERIMENTAL TECHNIQUE

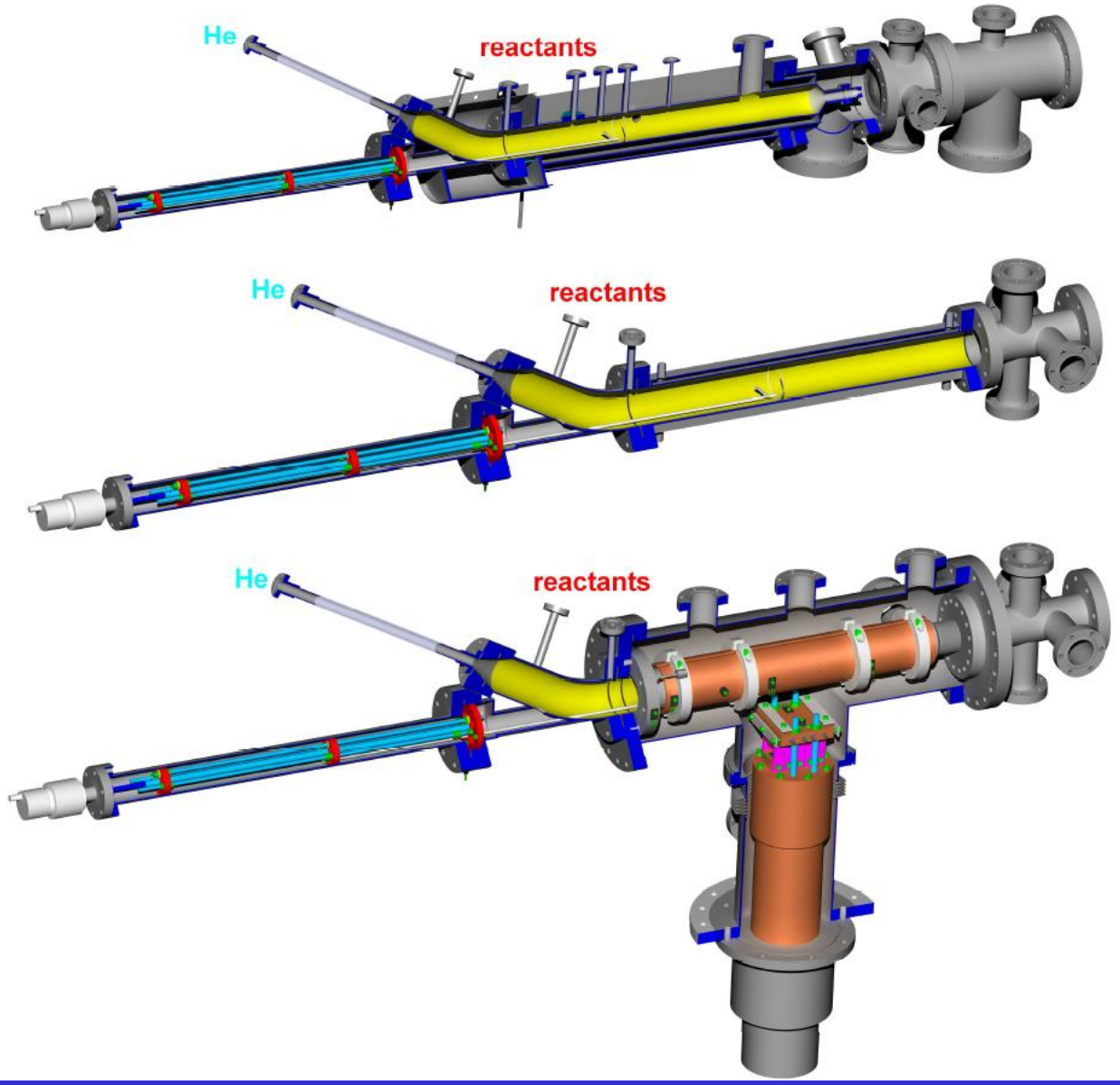

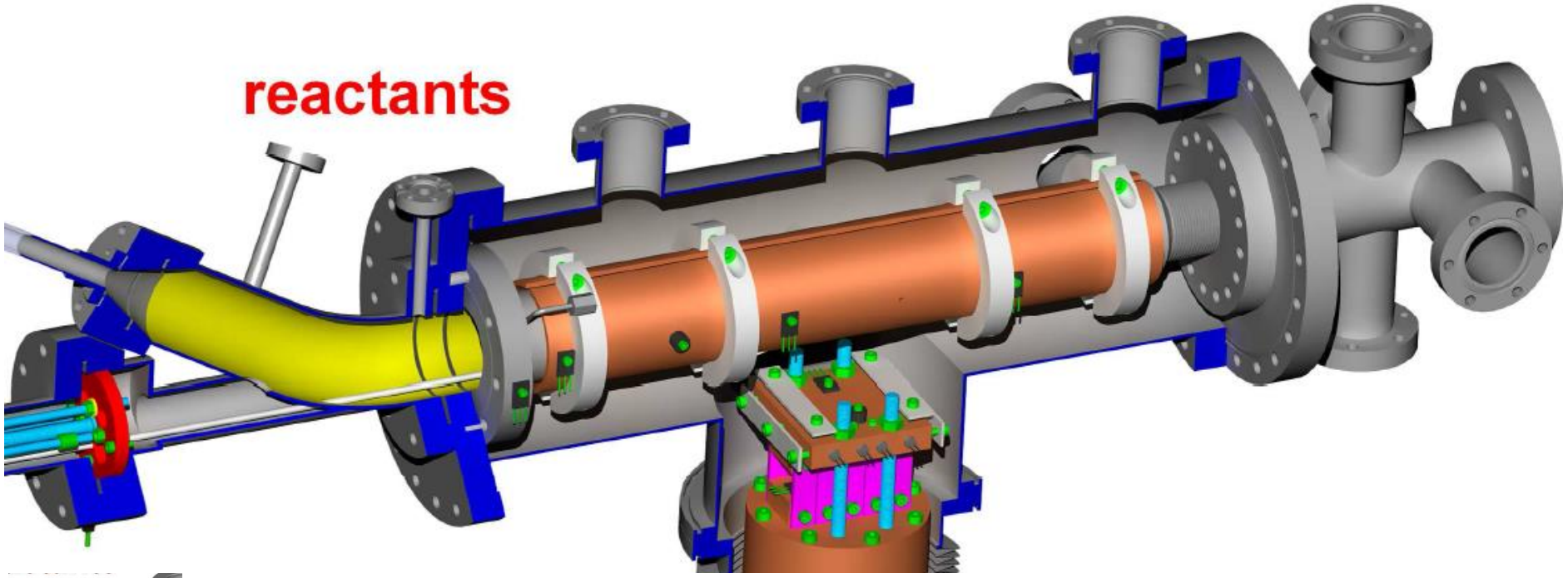
reactants

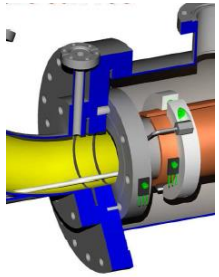

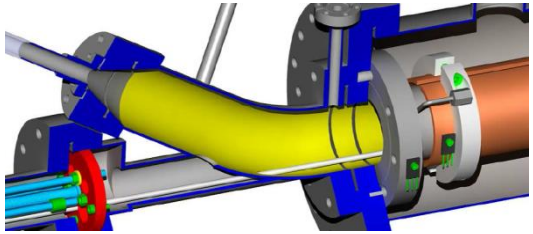

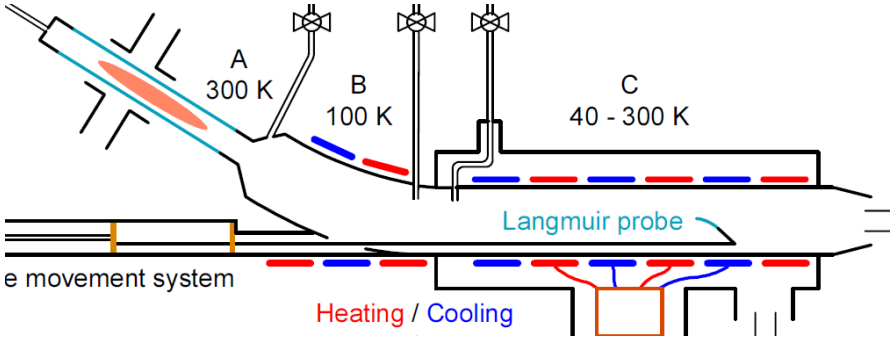
A
300 K
B
100 K
C
40 - 300 K
Langmuir probe
e movement system
Heating / Cooling

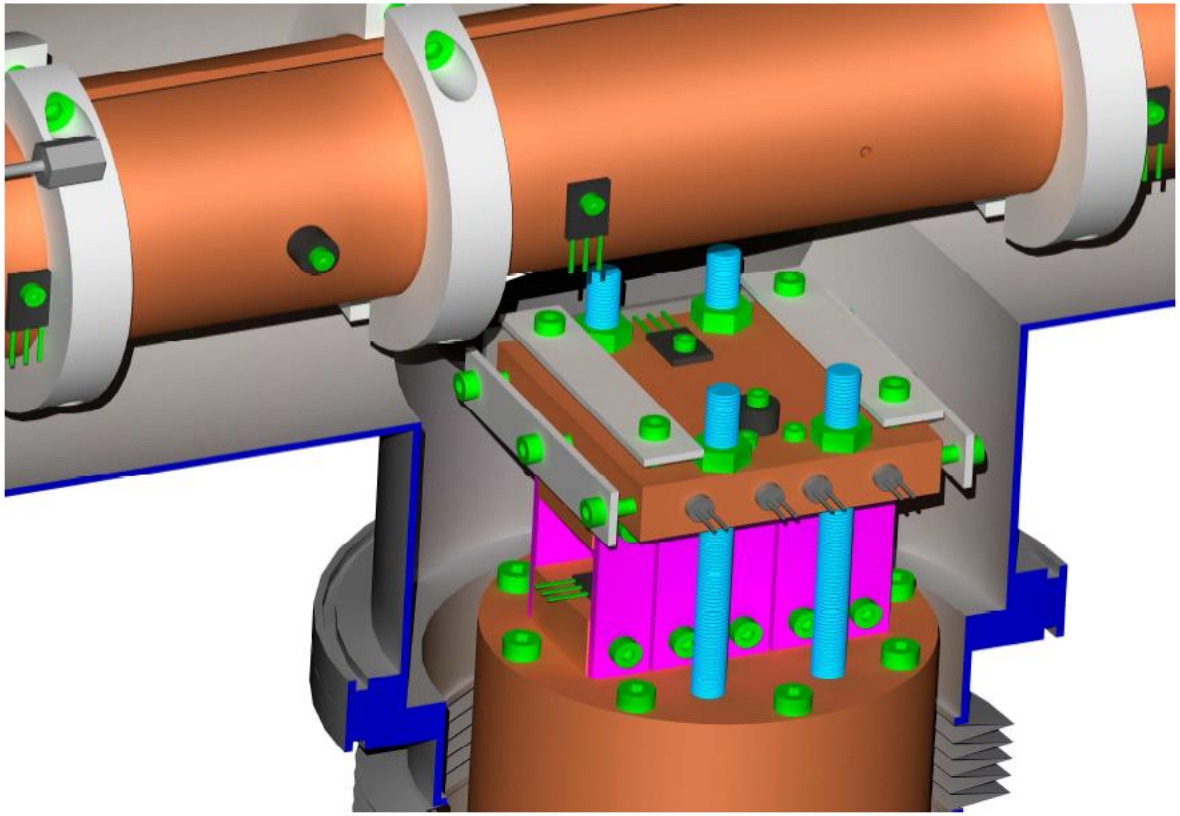

Figure 2.6 The detail of a 3D model of the Cryo-FALP II cooling system. The main copper parts are coldhead, platform and two half-cylinders pressing the copper braids (not shown in the figure) wound on the flow tube against the flow tube wall. The interconnecting removable copper blocks are colored magenta, the temperature sensors are black and the heating elements are dark grey cylinders embedded in the platform block. Other construction elements are colored green and cyan.

Techniques for study of IMR – reality

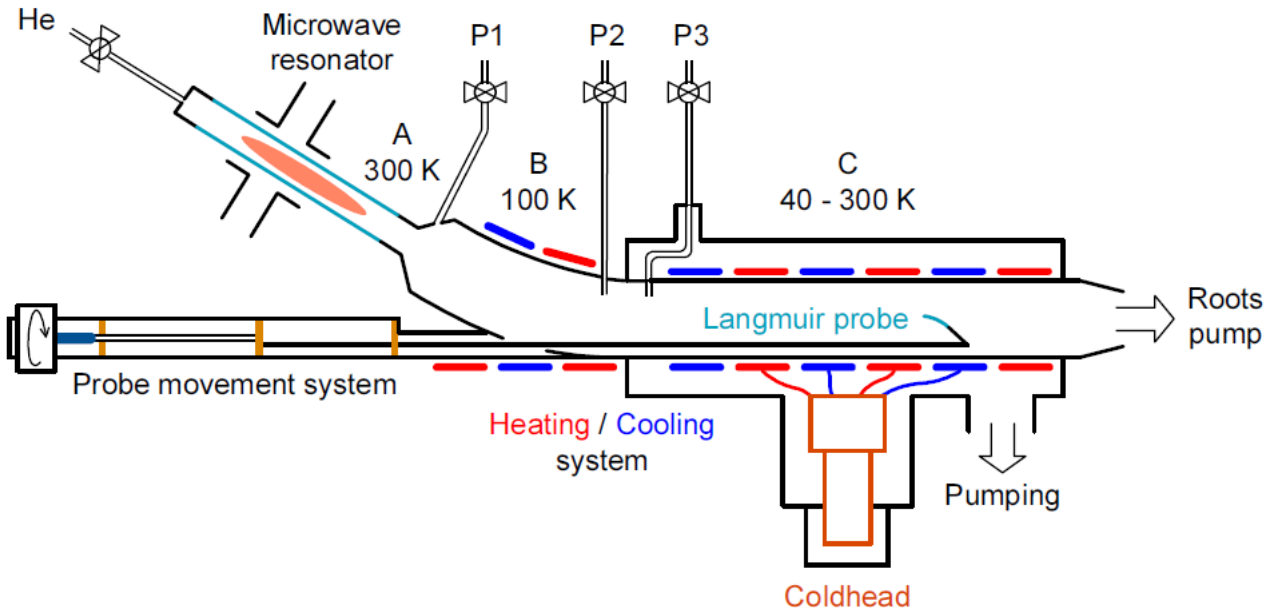

Figure 2.3 The scheme of the novel Cryo-FALP II apparatus.

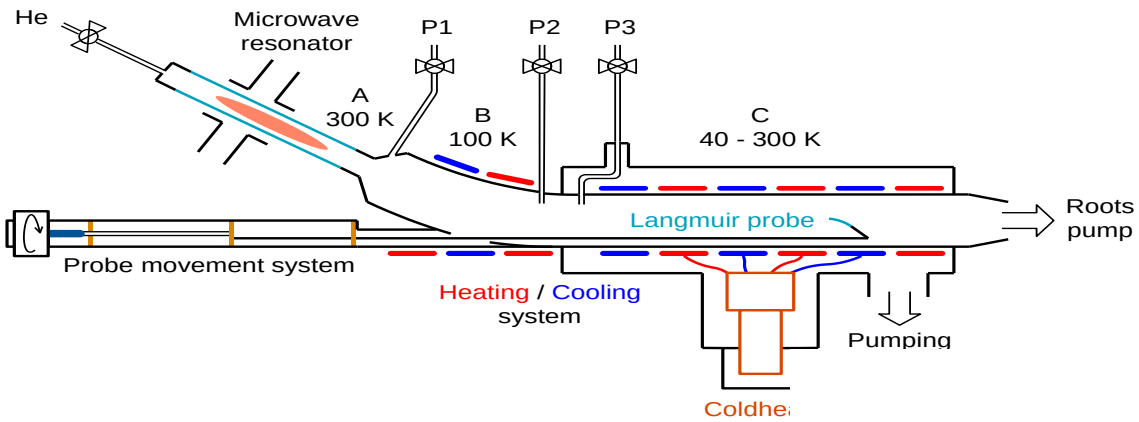
He
Microwave resonator
P1
P2
P3
A
300 K
B
100 K
C
40 - 300 K
Roots pump
Langmuir probe
Probe movement system
Heating / Cooling system
Pumping
Coldhe

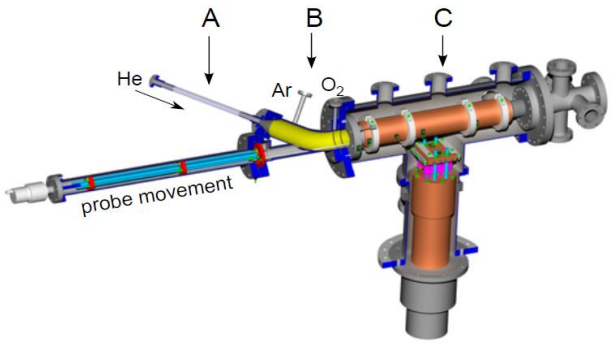
A
B
C
He
Ar
O_2
probe movement

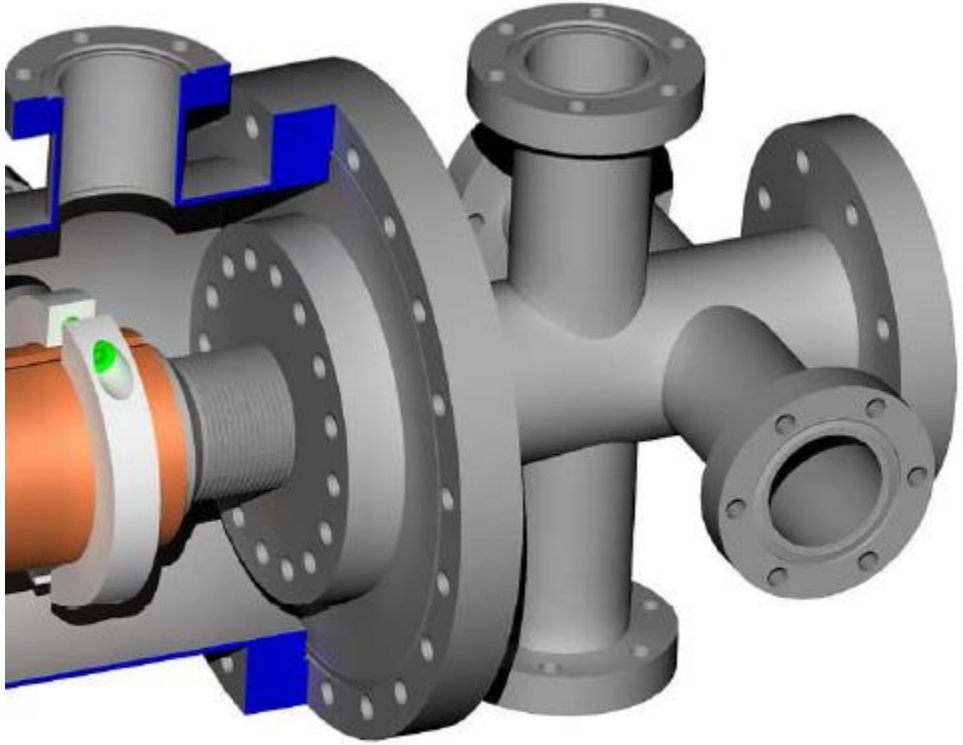

Fig. 1

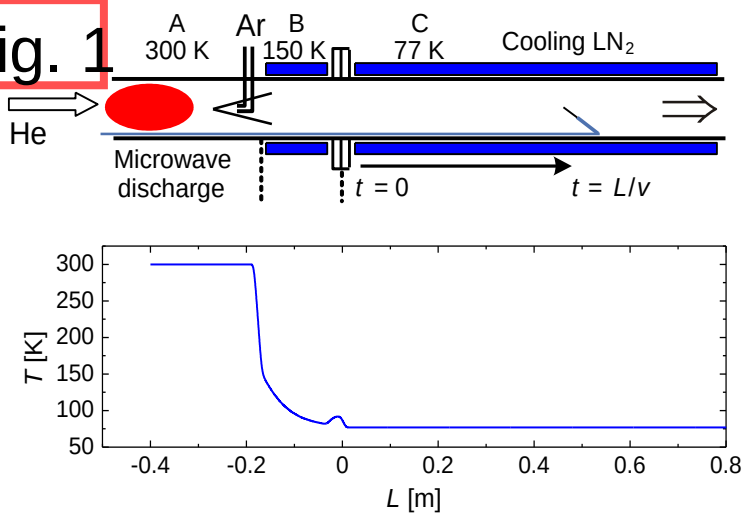
A
300 K
Ar
B
150 K
C
77 K
Cooling LN2
He
Microwave
discharge
t = 0
t = L/v
T [K]
300
250
200
150
100
50
-0.4
-0.2
0
0.2
0.4
0.6
0.8
L [m]

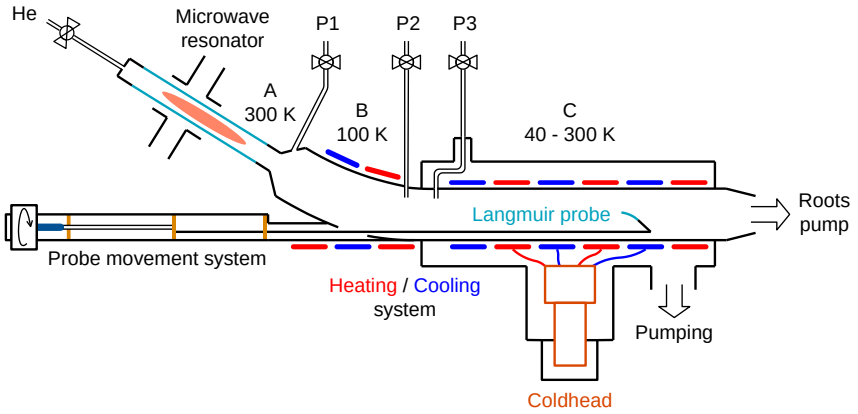
He
Microwave
resonator
P1
P2
P3
A
300 K
B
100 K
C
40 - 300 K
Roots
pump
Langmuir probe
Probe movement system
Heating / Cooling
system
Pumping
Coldhead

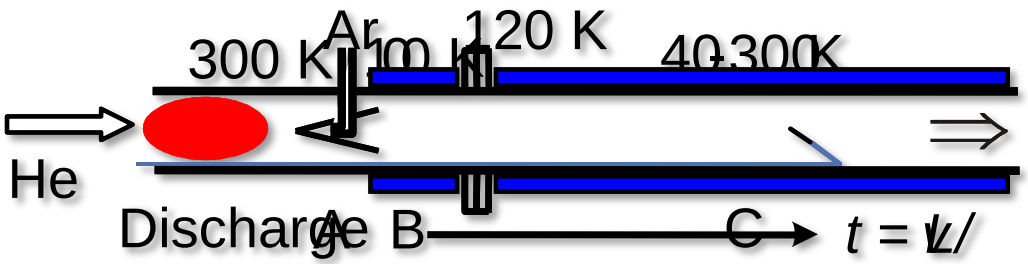
300 K
Ar
120 K
40-300K
He
Discharge
A
B
C
t = L/v

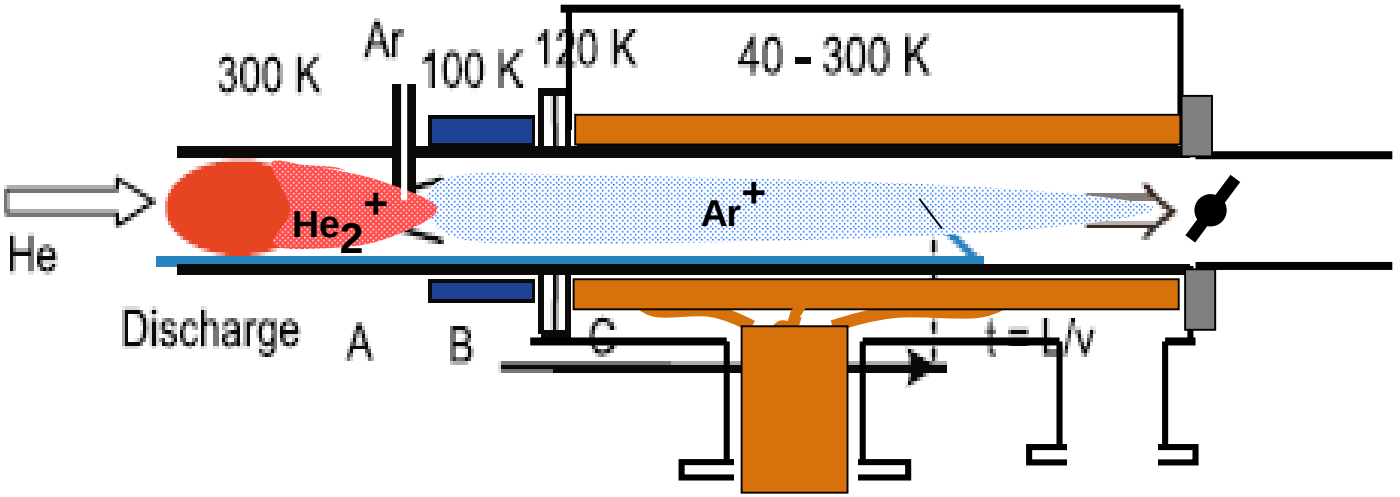
300 K
Ar
100 K
120 K
40 - 300 K
He
He2+
Ar+
Discharge
A
B
C
t = L/v

Recombination in He/Ar Afterglow Plasma at Low Temperatures

P. Dohnal, P. Rubovič, T. Kotrík, R. Plašil, and J. Glosík

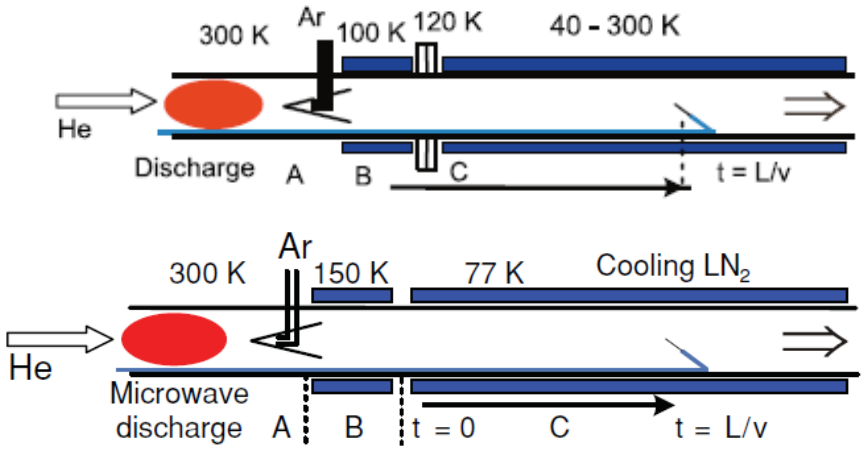

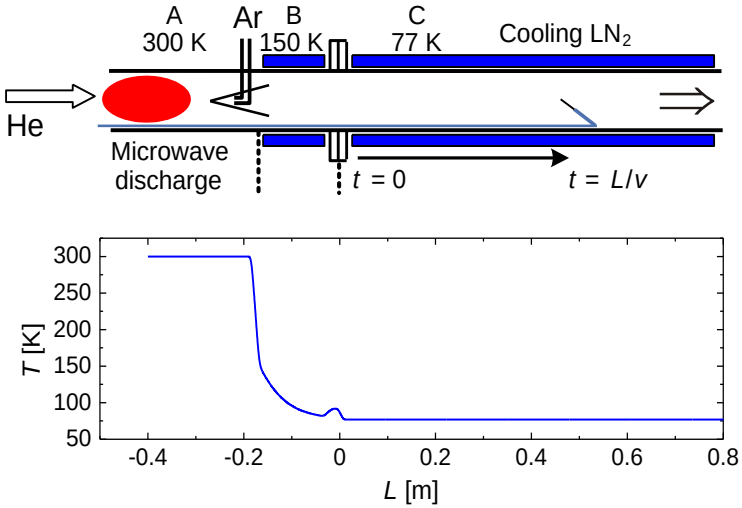

FIG. 1. (Color online) Simplified diagram of the Cryo-FALP apparatus (see text in Sec. II).

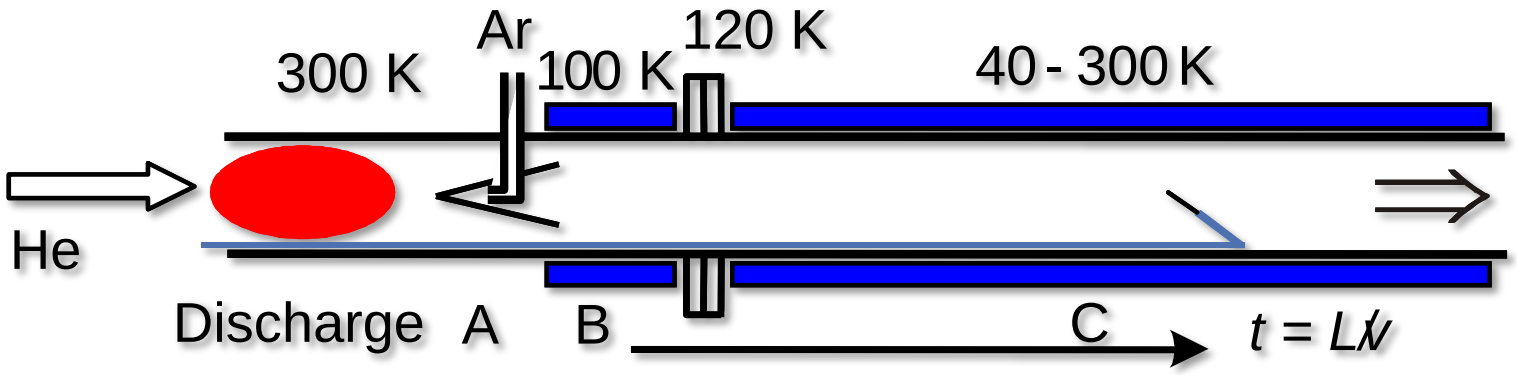

Techniques for study of IMR – reality

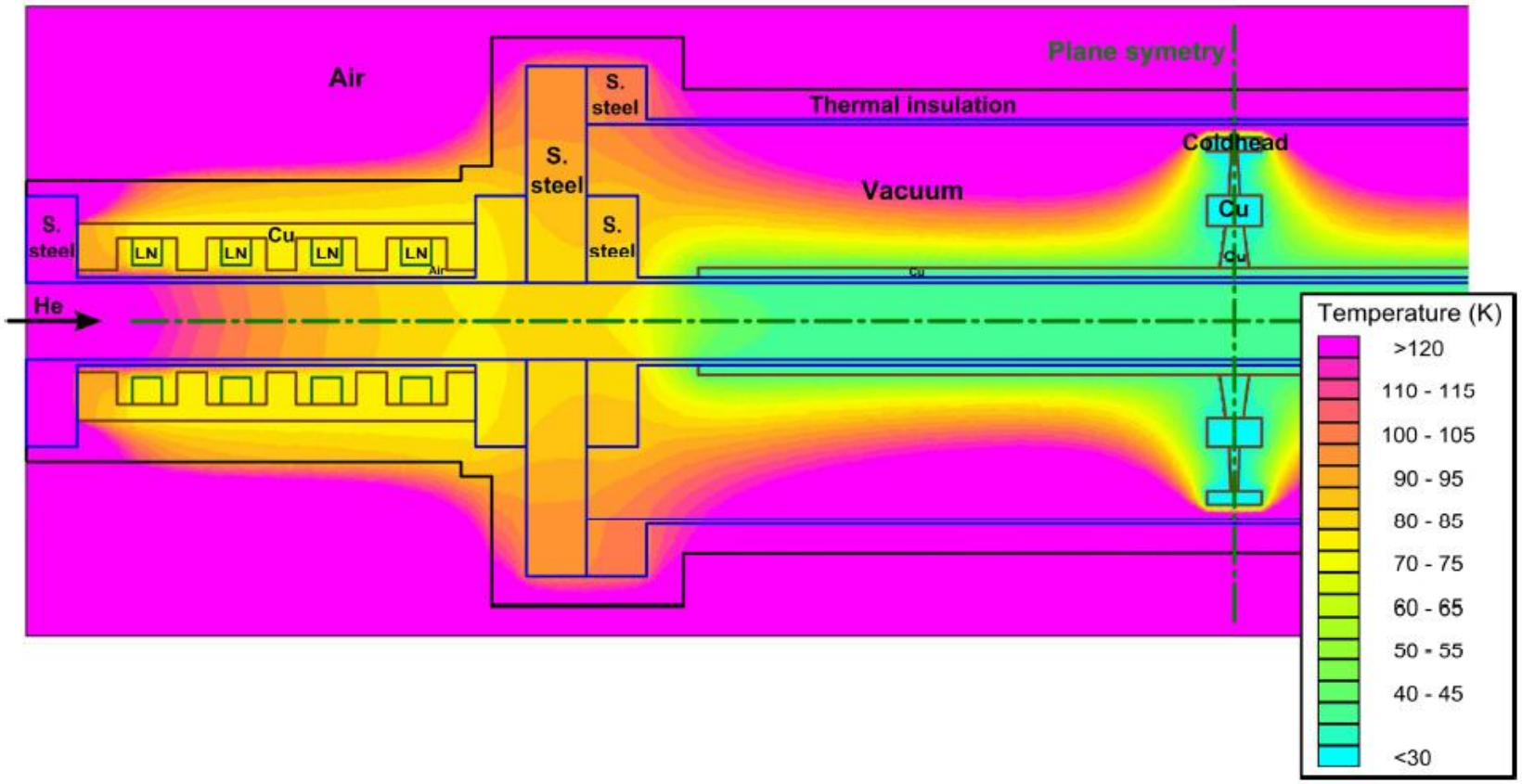

CRYO-FALP

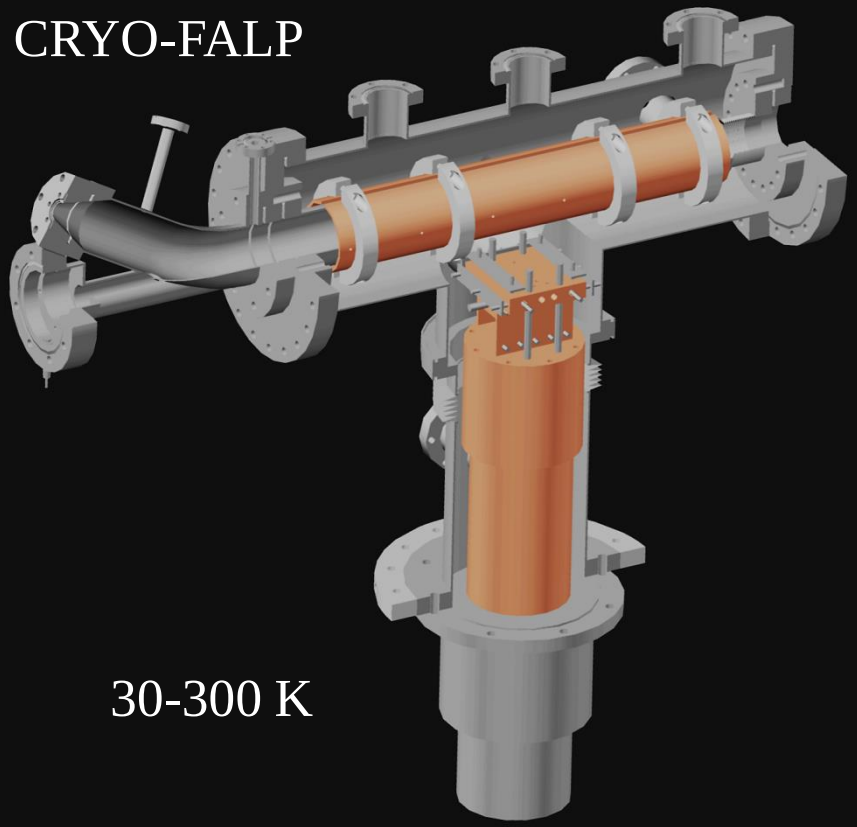

30-300 K

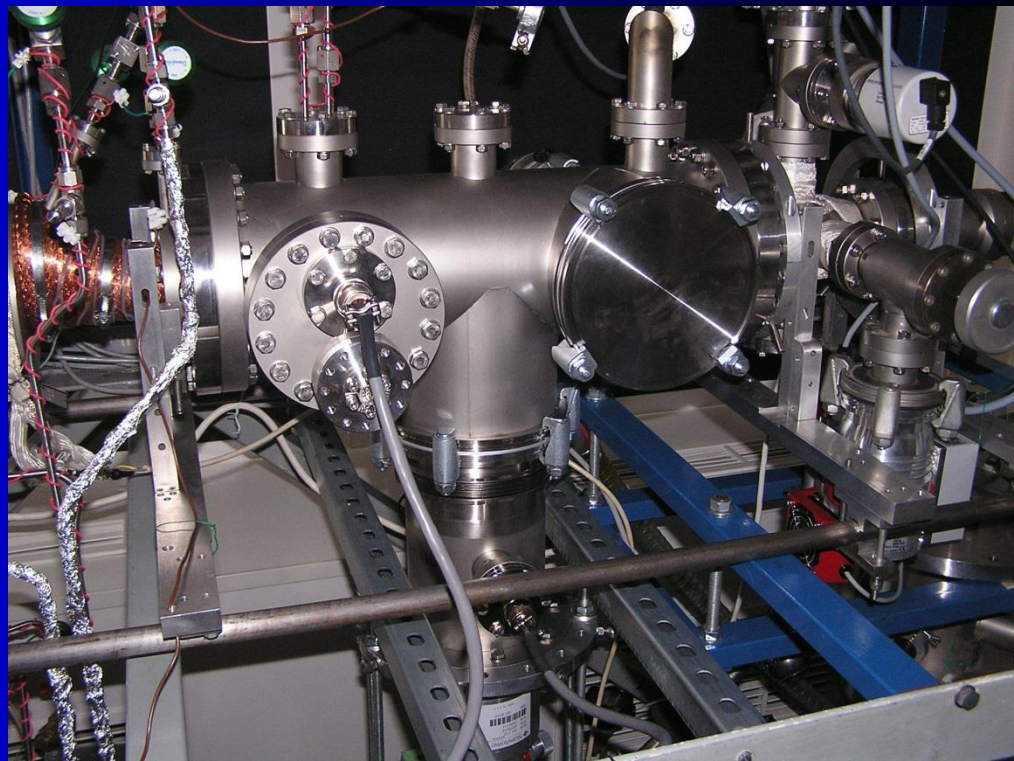

CRESU (*cinétique de réaction en ecoulement supersonique uniforme* or reaction kinetics in uniform supersonic flow)

Low Temperature Collisions in Flow Systems and Traps

(state-of-the-art experiments)

Pulsed Uniform Supersonic Expansion

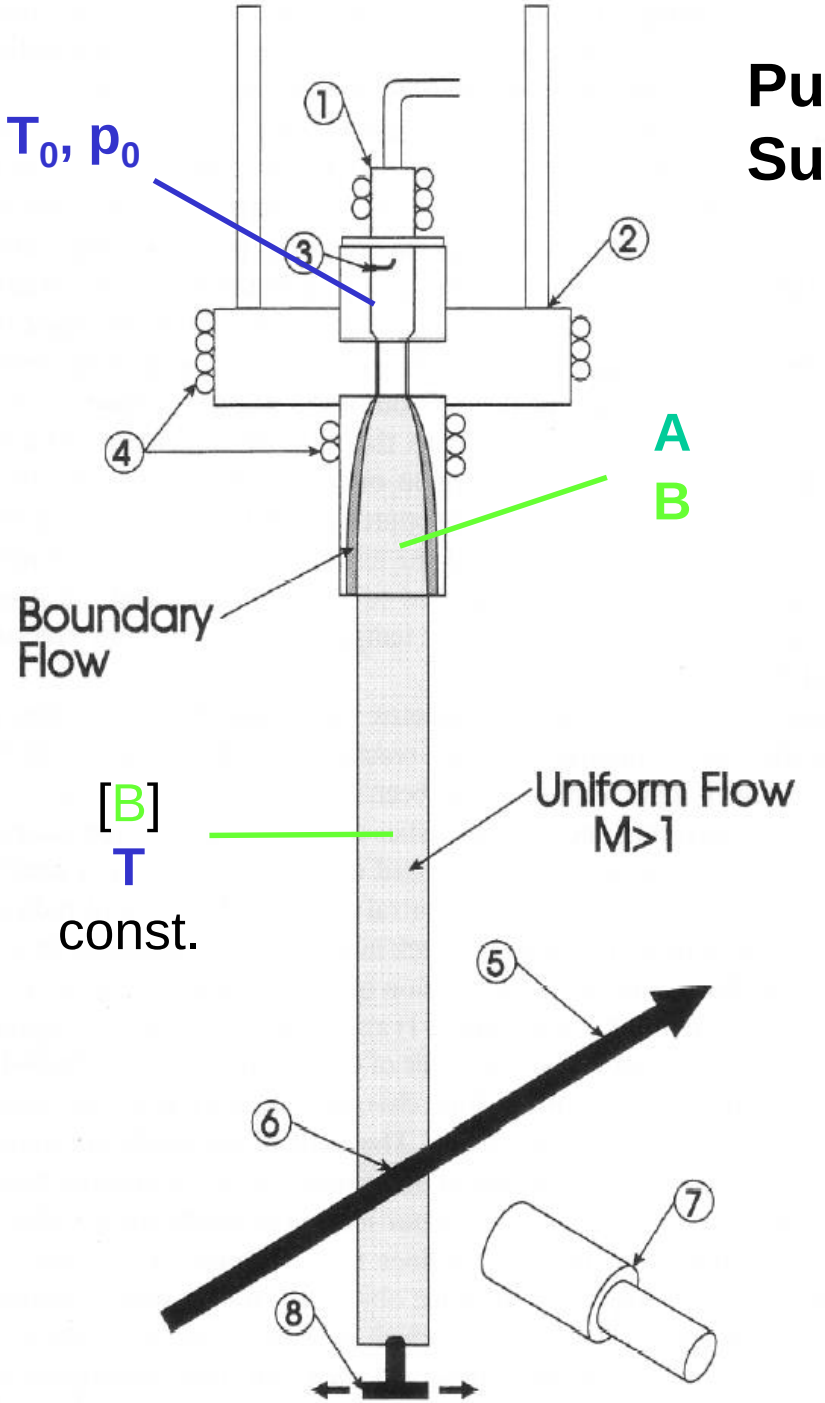

k(T)

$A + B \rightarrow Products$

$k = (\tau [B])^{-1}$

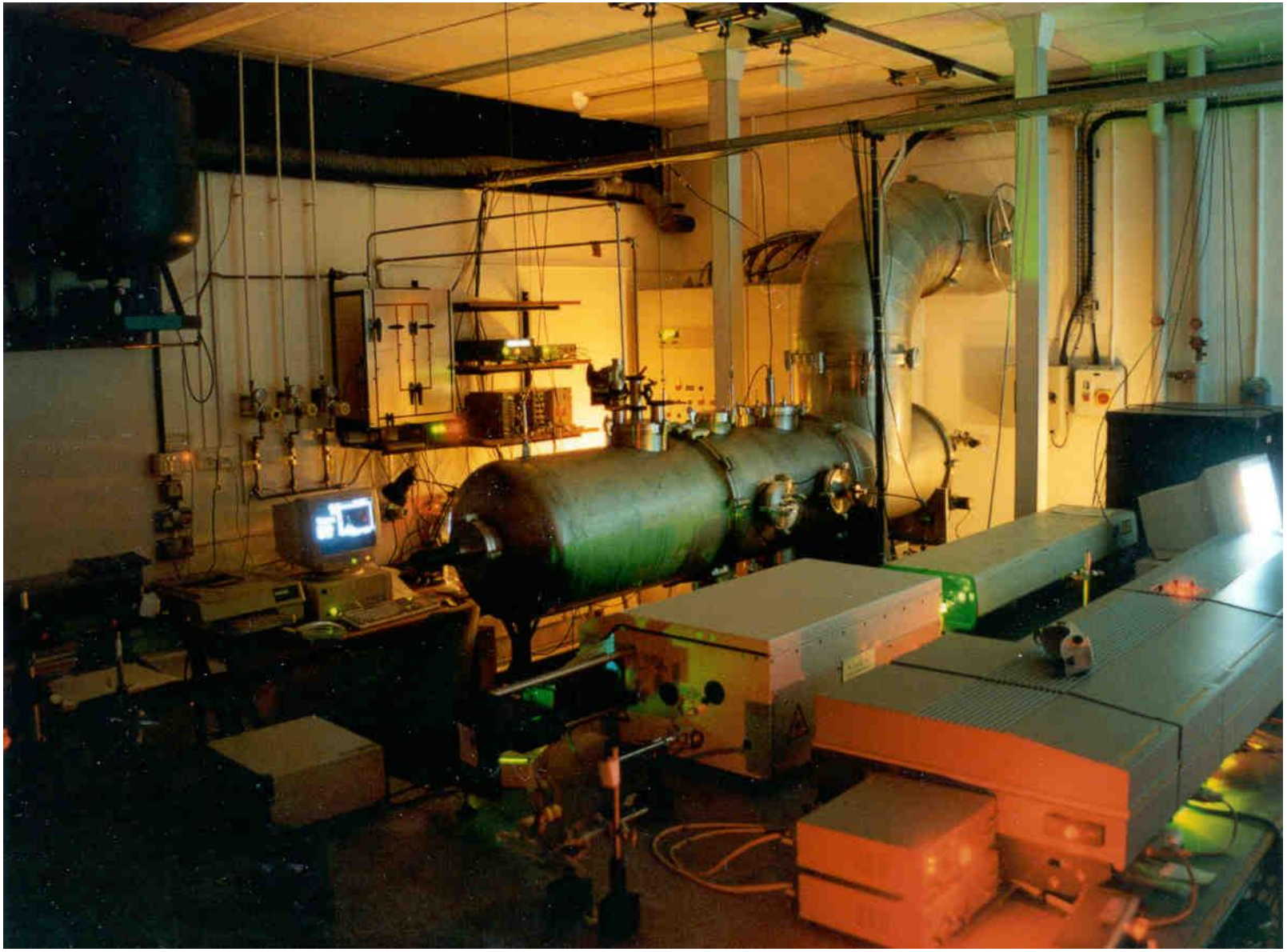

Schematic of the CRESU apparatus devoted to the measurement of ion/molecule reactions at low temperatures

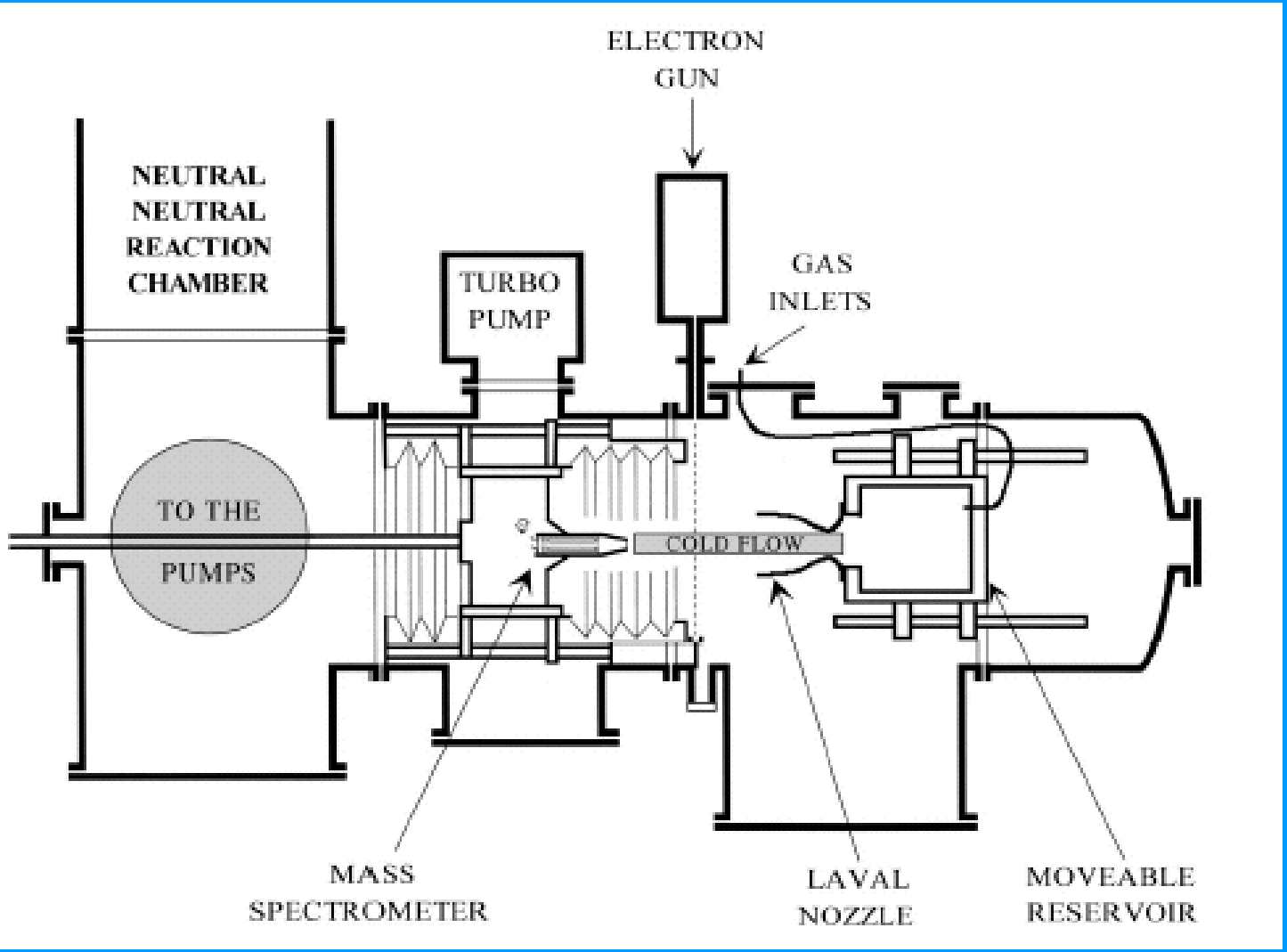

CRESU apparatus
Variation of the rate coefficient with temperature
N+ NH_3

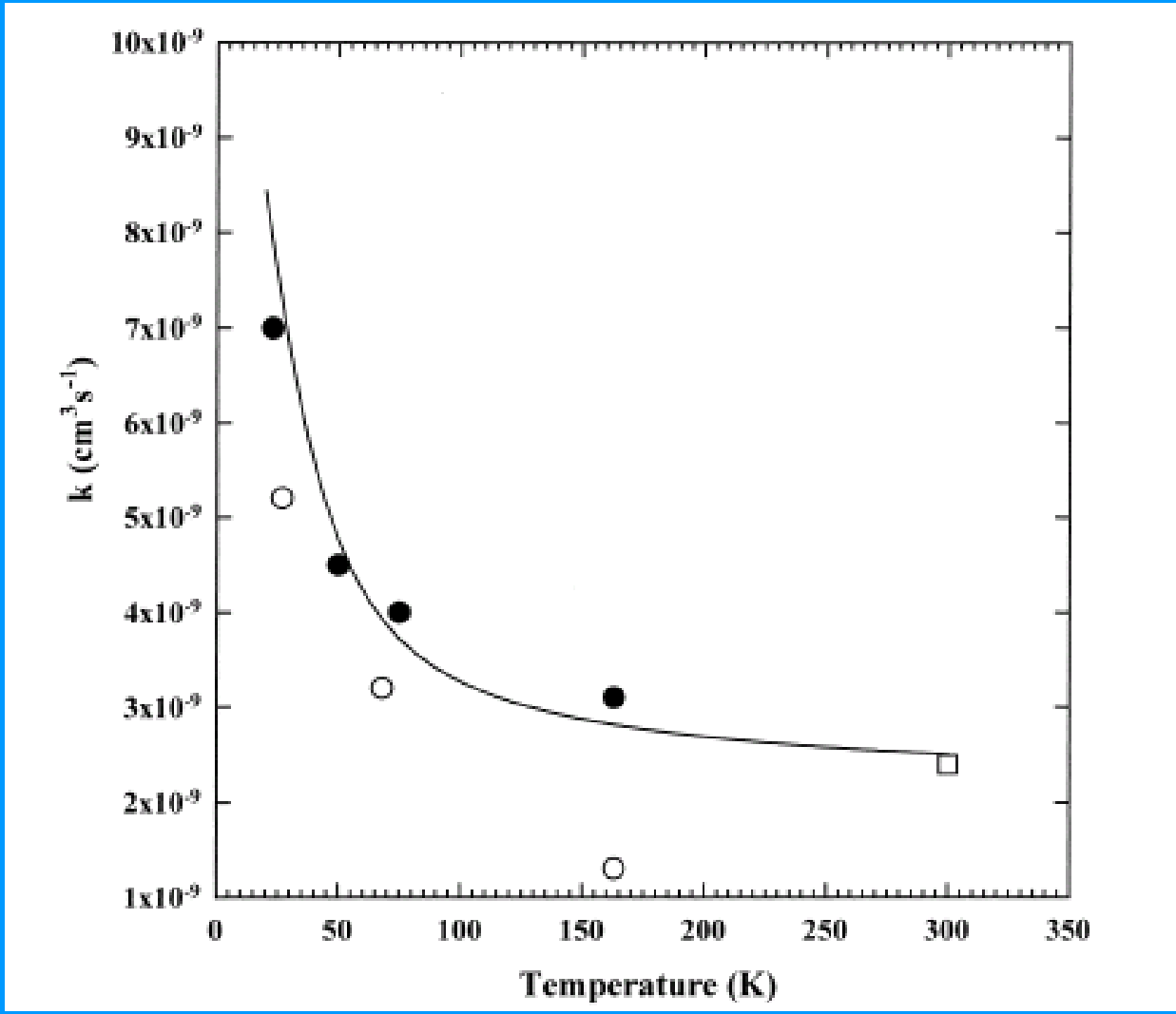

Free jet flow reactor

Mark Smith

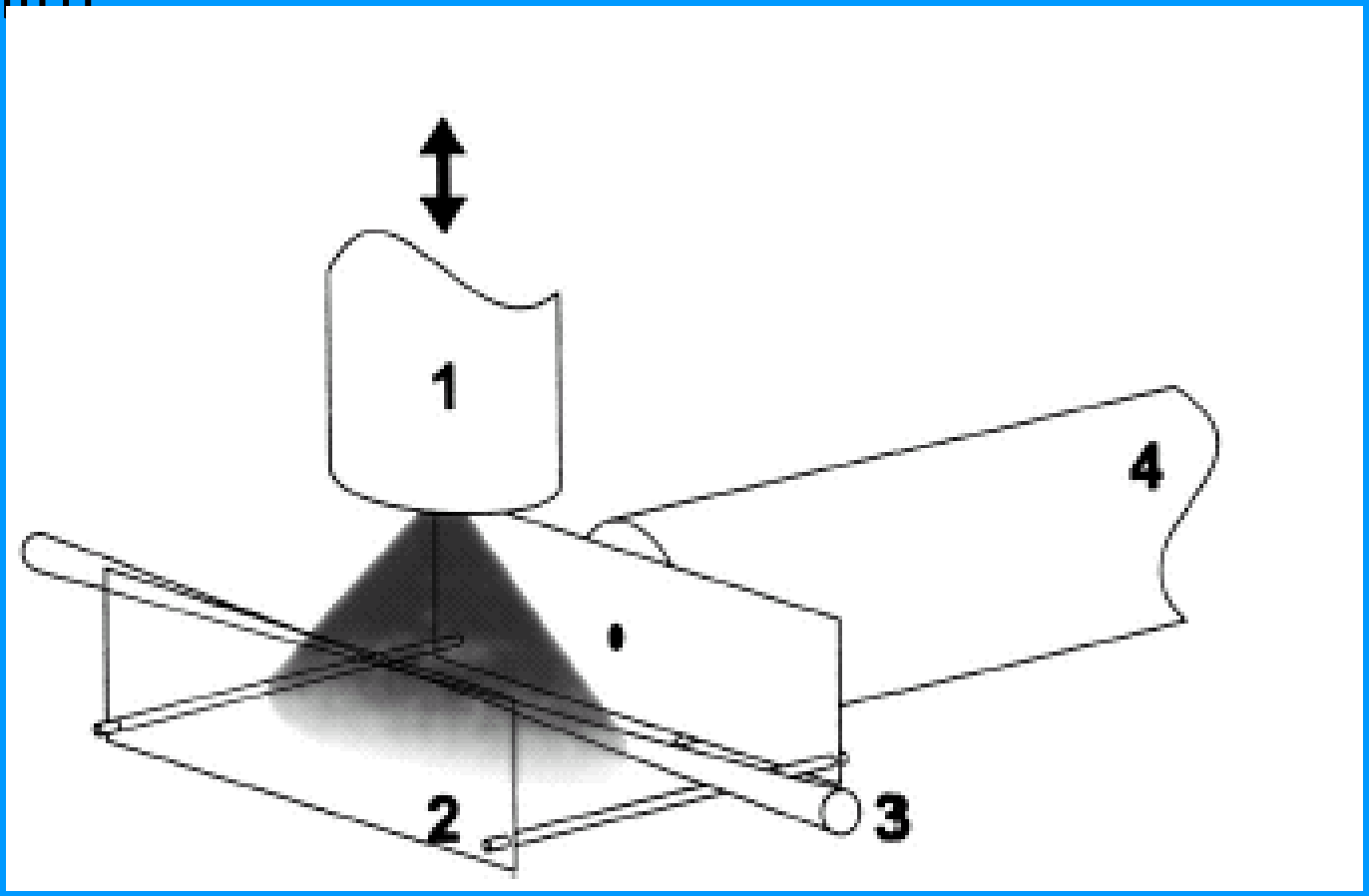

The jet originates from a pulsed beam valve **1**, and ions are produced by REMPI using a focused pulsed laser. The reaction zone is bounded by a repeller plate **2** and an endplate **3**:
ions are propelled, by a pulsed voltage on the repeller, towards a sampling aperture in the endplate which leads to a TOF-MS **4**

Flowing Afterglow 1968

microwave discharge

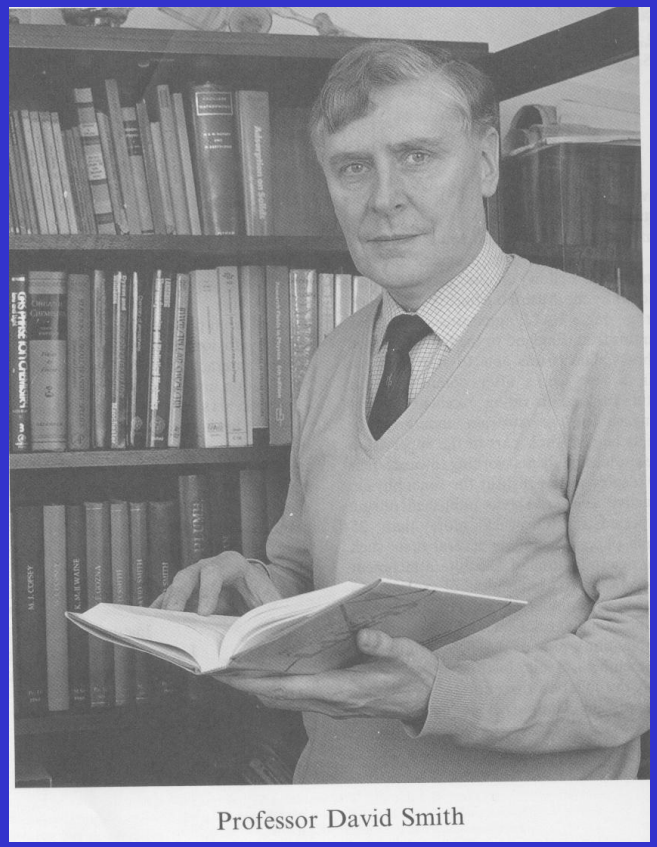

Professor David Smith

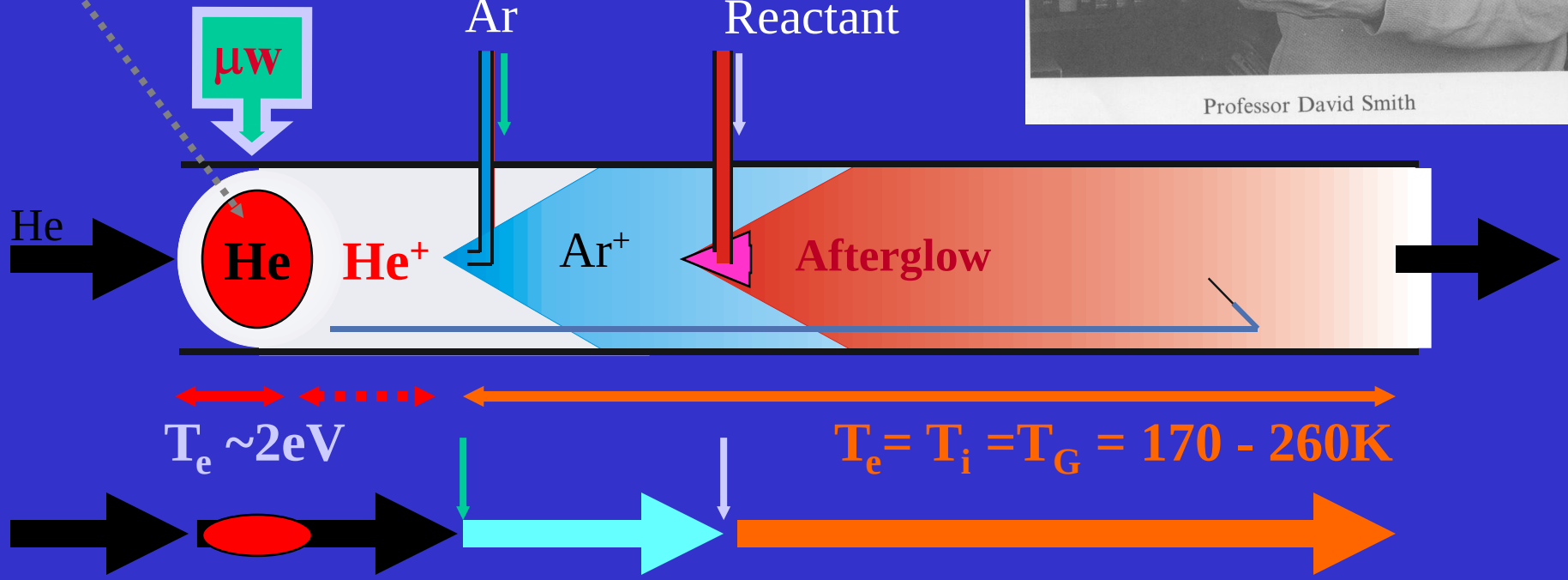

Selected Ion Flow Tube - SIFT

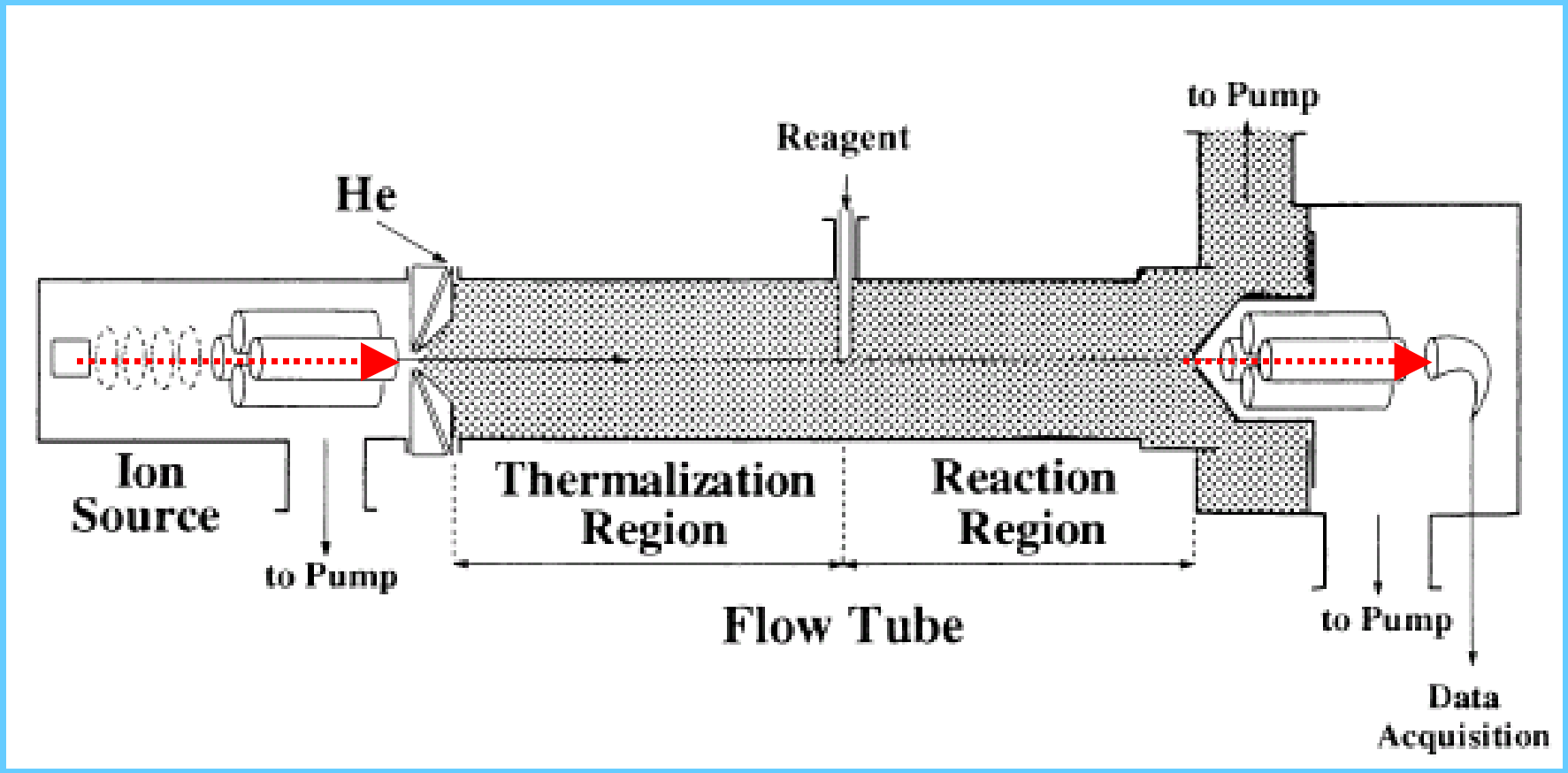

Ion-molecule reactions

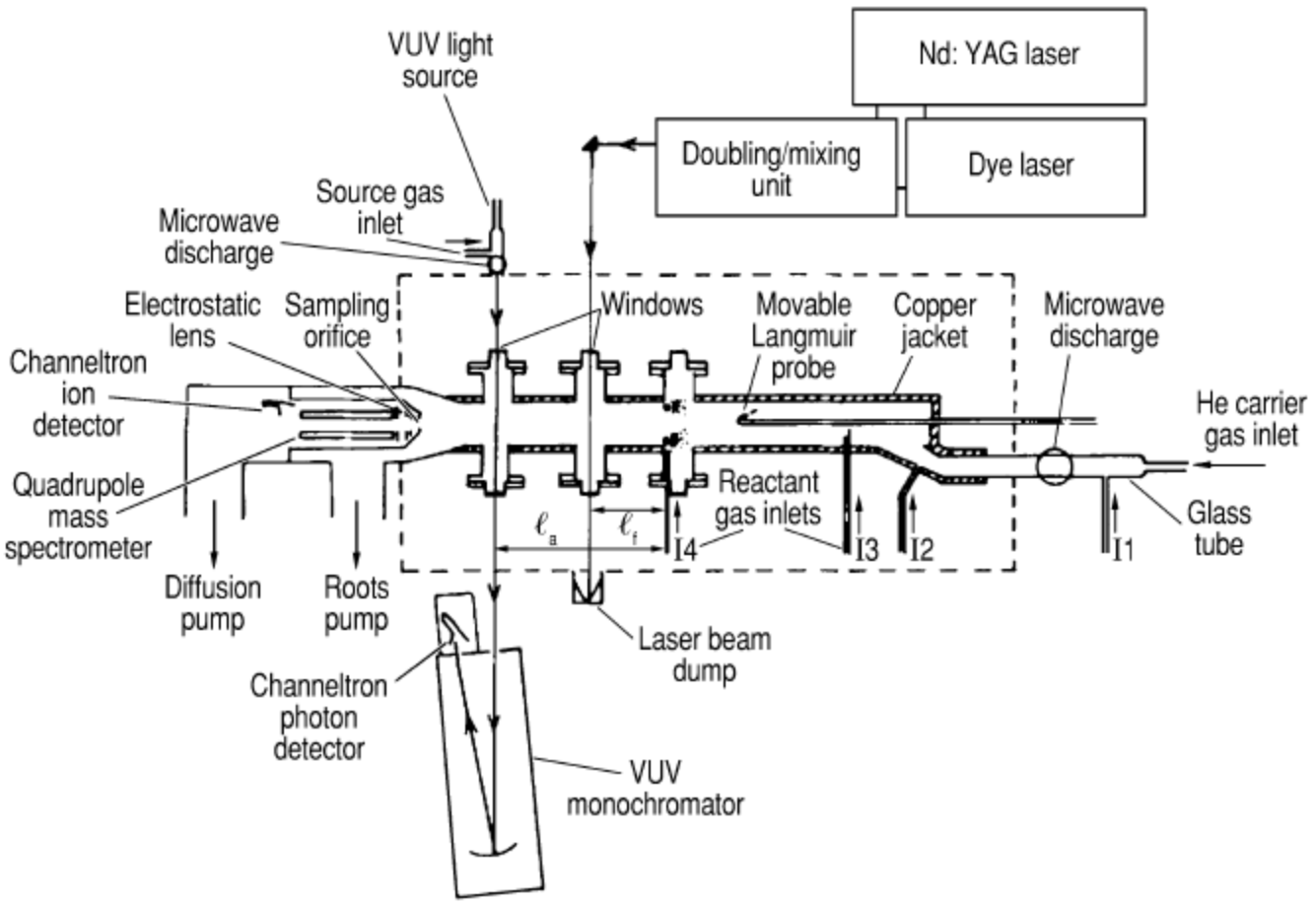

Fig. 13. Schematic diagram of the FALP-LIF/VUV apparatus used, in various configurations, since 1989 by Adams et al. [161] in their characterization of DR neutral products. The *dotted line* encasing the central flow tube represents a vacuum jacket facilitating operation at a broad range of temperatures

SIFDT

100 K – 3eV

$$N_4^+ + He \rightarrow N_2^+ + N_2 + He$$

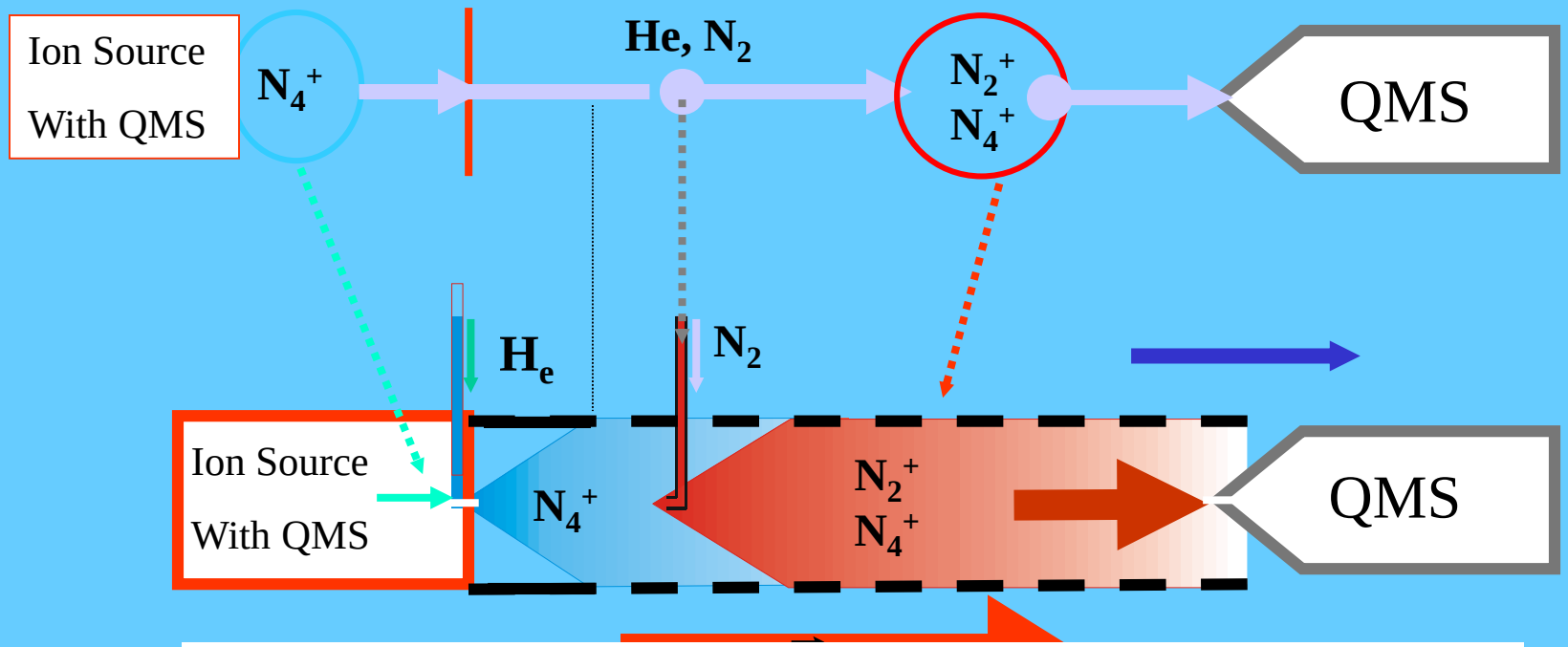

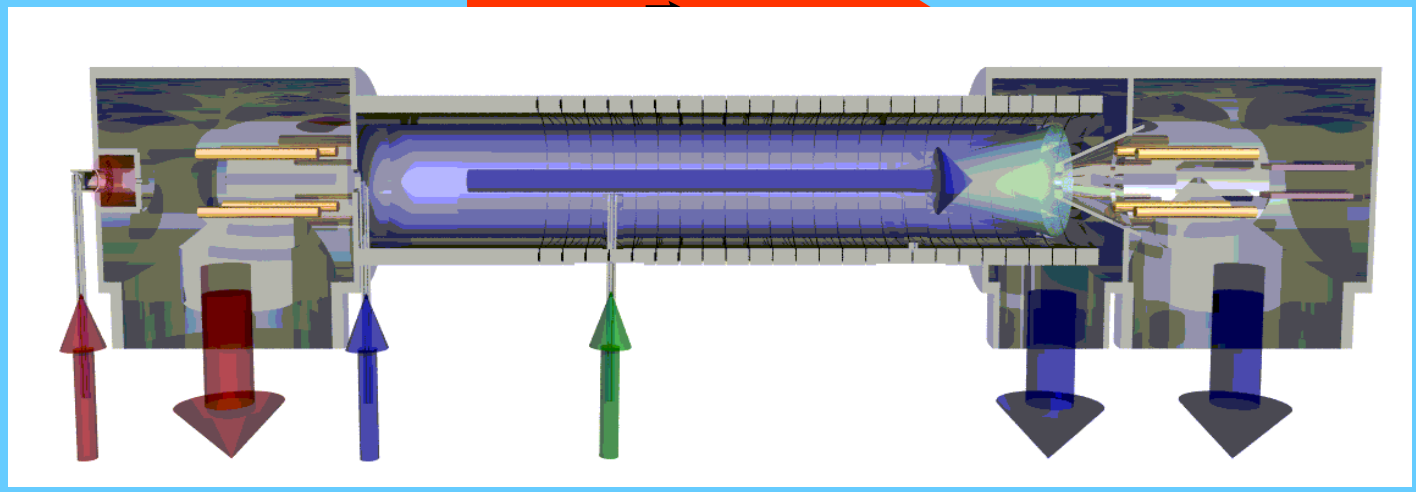

SIFDT experiment

Selected Ion Flow Drift Tube – SIFDT

$$v_d' = \mu \cdot E$$

$$\mu_0 = \mu \cdot \frac{p}{760} \cdot \frac{273}{T}$$

$$KE_{ion} = \frac{3}{2} k_b T_g + (m_c + m_i) \frac{v_d^2}{2}$$

$$KE_r = \frac{3}{2} k_b T_g + \frac{1}{2} m_r v_d^2 \left(\frac{m_i + m_c}{m_i + m_r}\right)$$

$$KE_c = \frac{3}{2} k_b T_g + \frac{1}{2} m_c v_d^2$$

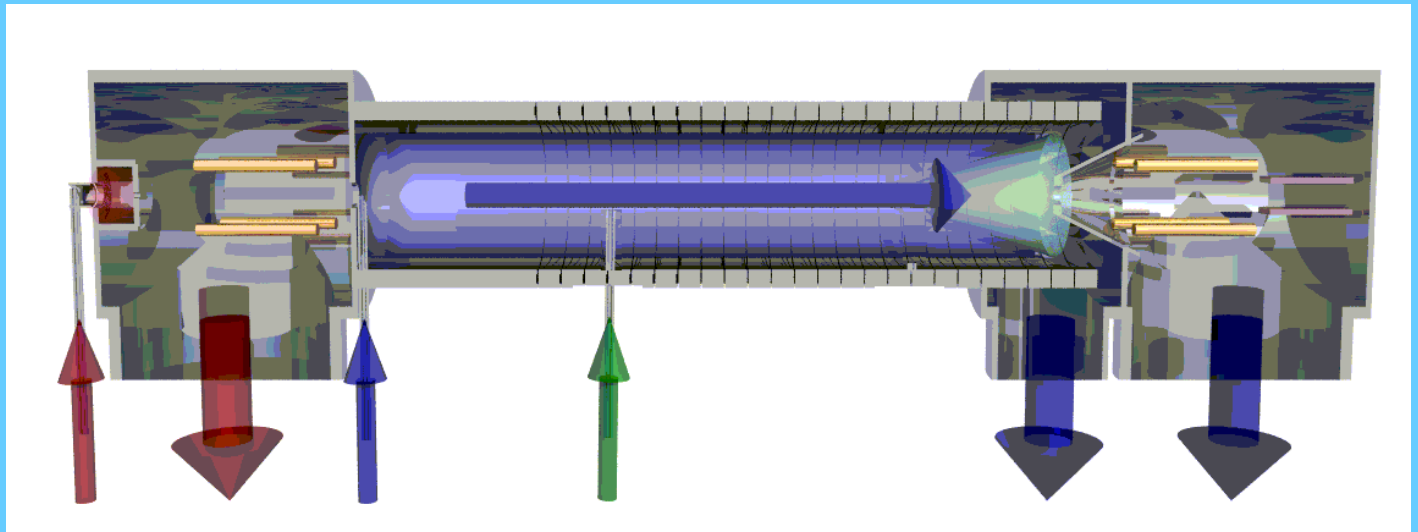

Proton transfer mass spectroscopy - Innsbruck

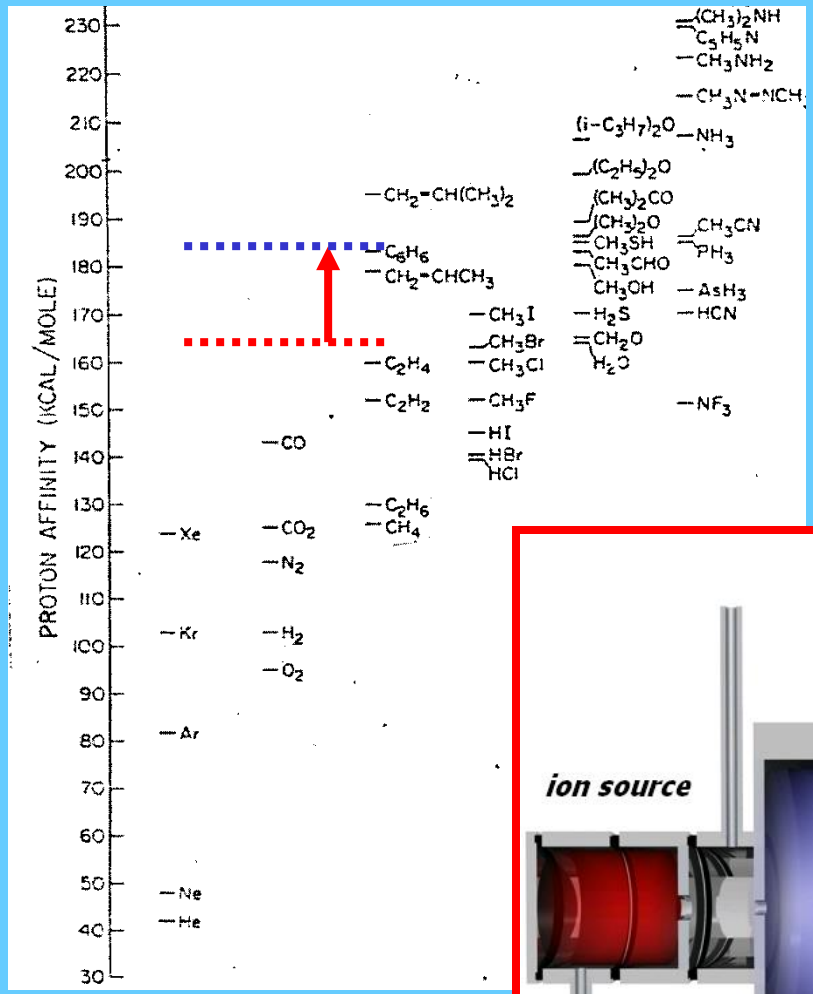

$$H_3O^+ + C_6H_6 \rightarrow C_6H_7^+ + H_2O$$